

JAERI - M  
86-195

TWO-DIMENSIONAL THERMAL-HYDRAULIC  
BEHAVIOR IN CORE IN SCTF CORE-II FORCED  
FEED REFLOOD TESTS  
(EFFECTS OF RADIAL POWER AND TEMPERATURE  
DISTRIBUTIONS)

January 1987

Takamichi IWAMURA, Makoto SOBAJIMA, Tsutomu OKUBO  
Akira OHNUKI, Yutaka ABE and Hiromichi ADACHI

日本原子力研究所  
Japan Atomic Energy Research Institute

JAERI-M レポートは、日本原子力研究所が不定期に公刊している研究報告書です。  
入手の問合せは、日本原子力研究所技術情報部情報資料課（〒319-11茨城県那珂郡東海村）  
あて、お申しこしください。なお、このほかに財團法人原子力弘済会資料センター（〒319-11茨城  
県那珂郡東海村日本原子力研究所内）で複写による実費領布をおこなっております。

JAERI-M reports are issued irregularly.

Inquiries about availability of the reports should be addressed to Information Division, Department  
of Technical Information, Japan Atomic Energy Research Institute, Tokai-mura, Naka-gun,  
Ibaraki-ken 319-11, Japan.

© Japan Atomic Energy Research Institute, 1987

---

編集兼発行 日本原子力研究所  
印 刷 日立高速印刷株式会社

Two-Dimensional Thermal-Hydraulic Behavior in Core  
in SCTF Core-II Forced Feed Reflood Tests  
(Effects of Radial Power and Temperature Distributions)

Takamichi IWAMURA, Makoto SOBAJIMA, Tsutomu OKUBO

Akira OHNUKI, Yutaka ABE and Hiromichi ADACHI

Department of Reactor Safety Research,

Tokai Research Establishment,

Japan Atomic Energy Research Institute

Tokai-mura, Naka-gun, Ibaraki-ken

(Received December 25, 1986)

Major purpose of the Slab Core Test Program is to investigate the two-dimensional thermal-hydraulic behavior in the core during the reflood phase of a PWR-LOCA. It was revealed in the previous Slab Core Test Facility (SCTF) Core-II test results that the heat transfer was enhanced in the higher power bundles and degraded in the lower power bundles in the non-uniform radial power profile tests. In order to separately evaluate the effect of the radial power( $Q$ ) distribution itself and the effect of the radial temperature ( $T$ ) distribution, four tests were performed with steep  $Q$  and  $T$ , flat  $Q$  and  $T$ , steep  $Q$  and flat  $T$ , and flat  $Q$  and steep  $T$ . Based on the test results, it was concluded that the radial temperature distribution which accompanied the radial power distribution was the dominant factor of the two-dimensional thermal-hydraulic behavior in the core during the initial period.

Selected data from these four tests are also presented in this report. Some data from Test S2-12 (steep  $Q$ ,  $T$ ) were compared with TRAC post-test calculations performed by the Los Alamos National Laboratory.

Keywords: Reflood, LOCA, ECCS, PWR, Reactor Safety, Two-Phase Flow, Chimney Effect, Cross Flow, Quench, Heat Transfer

---

The work was performed under contract with the Atomic Energy Bureau of Science and Technology Agency of Japan.

S C T F 第 2 次炉心強制注入再冠水試験における炉心内 2 次元熱水力挙動  
(出力及び温度の半径方向分布効果)

日本原子力研究所東海研究所原子炉安全工学部

岩村 公道・傍島 真・大久保 努

大貫 晃・阿部 豊・安達 公道

(1986年12月25日受理)

平板炉心試験計画の主目的は、PWR - LOCA時再冠水過程における炉心内 2 次元熱水力挙動を調べることである。既に実施した平板炉心試験装置 (SCTF) 第 2 次炉心試験結果により、不均一半径方向出力分布が存在すると、高出力バンドルでは熱伝達が促進され、低出力バンドルでは熱伝達が劣化することが明らかとなった。半径方向出力 (Q) 分布自体と半径方向温度 (T) 分布の効果を分離して評価するため、急峻 Q かつ急峻 T、平坦 Q かつ平坦 T、急峻 Q かつ平坦 T、および平坦 Q かつ急峻 T の 4 試験を実施した。本試験結果により、半径方向出力分布に付随して生じる半径方向温度分布が、再冠水初期の炉心内 2 次元熱水力挙動にとって重要な原因であることが明らかとなった。

これら 4 試験のデータの一部も本報告書に収録されている。また、急峻 Q, T 試験 S 2 - 12 の一部データと、ロスアラモス研究所で実施された TRAC 試験後計算結果との比較も行った。

## Contents

1. Introduction .....	1
2. Test Description .....	3
2.1 Test Facility .....	3
2.2 Test Conditions .....	3
2.3 Test Procedure .....	5
3. Test Results and Discussions .....	9
3.1 Overall Fluid Behavior .....	9
3.1.1 Boundary Conditions .....	9
3.1.2 Fluid Behavior in Upper Plenum and around End Box Tie Plate .....	10
3.1.3 Water Accumulation Behavior in Core .....	11
3.1.4 Total Steam Generation Rate in Core and Steam Outflow Rate from Pressure Vessel .....	11
3.1.5 Fluid Behavior in Primary Loops .....	12
3.2 Effects of Radial Power and Temperature Distribution on Two- Dimensional Hydraulic Behavior in Core .....	12
3.2.1 Pressure Distribution .....	12
3.2.2 Void Fraction Distribution .....	13
3.2.3 Horizontal Differential Pressure .....	15
3.3 Effects of Radial Power and Temperature Distribution on Two- Dimensional Thermal Behavior in Core .....	15
3.3.1 Heater Rod Temperature Behavior .....	15
3.3.2 Heat Transfer Characteristics .....	16
3.3.3 Radial Distribution of Steam Generation Rate .....	18
4. Conclusions .....	59
Acknowledgment .....	60
References .....	60
Appendix A Slab Core Test Facility Core-II .....	62
A.1 Test Facility .....	62
A.2 Instrumentation .....	66
Appendix B Selected Data of Test S2-12 .....	100
Appendix C Selected Data of Test S2-14 .....	113
Appendix D Selected Data of Test S2-15 .....	126
Appendix E Selected Data of Test S2-21 .....	140
Appendix F Comparison between TRAC Post-Test Analysis and Test Data of Test S2-12 .....	154

## 目 次

1. 序 論 .....	1
2. 試 験 .....	3
2.1 試験装置 .....	3
2.2 試験条件 .....	3
2.3 試験手順 .....	5
3. 試験結果と検討 .....	9
3.1 全体的な流体挙動 .....	9
3.1.1 境界条件 .....	9
3.1.2 上部プレナム内及びエンドボックスタイプレート周辺の流体挙動 .....	10
3.1.3 炉心内蓄水挙動 .....	11
3.1.4 炉心内全蒸気発生量及び圧力容器からの蒸気流出量 .....	11
3.1.5 一次系内流体挙動 .....	12
3.2 半径方向出力／温度分布が炉心内二次元流体挙動に与える影響 .....	12
3.2.1 圧力分布 .....	12
3.2.2 ポイド率分布 .....	13
3.2.3 水平差圧 .....	15
3.3 半径方向出力／温度分布が炉心内二次元熱的挙動に与える影響 .....	15
3.3.1 燃料棒温度挙動 .....	15
3.3.2 熱伝達特性 .....	16
3.3.3 蒸気発生量の半径方向分布 .....	18
4. 結 論 .....	59
謝 辞 .....	60
参考文献 .....	60
付 錄 A 平板炉心試験装置第2次炉心 .....	62
A.1 試験装置 .....	62
A.2 計 測 .....	66
付 錄 B 試験S 2 - 12のデータ .....	100
付 錄 C " S 2 - 14 " .....	113
付 錄 D " S 2 - 15 " .....	126
付 錄 E " S 2 - 21 " .....	140
付 錄 F TRAC試験後解析と試験S 2 - 12のデータとの比較 .....	154

## List of Tables

- Table 2.1 Test Conditions for Tests S2-12, S2-14, S2-15 and S2-21  
 Table 3.1 Chronologies of major events for Tests S2-12, S2-14, S2-15 and S2-21

## List of Figures

- Fig. 2.1 Schematic diagram of SCTF  
 Fig. 2.2 Vertical cross section of pressure vessel  
 Fig. 3.1 Comparison of ECC injection rates into lower plenum  
 Fig. 3.2 Comparison of core inlet mass flow rates obtained by mass balance  
 Fig. 3.3 Comparison of integrated core inlet water mass  
 Fig. 3.4 Comparison of core inlet water temperatures  
 Fig. 3.5 Comparison of core heating powers  
 Fig. 3.6 Comparison of pressures at core center  
 Fig. 3.7 Comparison of pressures at top of containment tank-II  
 Fig. 3.8 Comparison of liquid levels in upper plenum  
 Fig. 3.9 Comparison of differential pressures across end box tie plate  
 Fig. 3.10 Comparison of differential pressures across core full height among Bundles 2, 4, 6 and 8 in Test S2-12  
 Fig. 3.11 Comparison of differential pressures across core full height in Bundle 4 among Tests S2-12, S2-14, S2-15 and S2-21  
 Fig. 3.12 Comparison of steam generation rates obtained by heat balance  
 Fig. 3.13 Comparison of steam outflow rates from pressure vessel obtained by mass balance  
 Fig. 3.14 Mass flow rates in 4 regions of hot leg in Test S2-14  
 Fig. 3.15 Comparison of differential pressures across hot leg  
 Fig. 3.16 Comparison of differential pressures across intact cold leg  
 Fig. 3.17 Comparison of differential pressures across broken cold leg steam/water separator side  
 Fig. 3.18 Comparison of differential pressures across broken cold leg pressure vessel side  
 Fig. 3.19 (a) through (f)  
 Comparisons of equal pressure lines in core and bottom quench front distributions

- Fig. 3.20 (a) through (c)  
Comparisons of void fractions in core at three elevations
- Fig. 3.21 Comparisons of liquid fractions vs. distance from bottom quench front at 2.33 m among Bundles 2, 4 and 8
- Fig. 3.22 (a) and (b)  
Comparisons of horizontal differential pressures at 1.905 m
- Fig. 3.23 (a) and (b)  
Comparisons of horizontal differential pressures at 3.235 m
- Fig. 3.24 Comparisons of heater rod surface temperatures at 2.33 m in Bundles 4 and 8
- Fig. 3.25 Comparisons of average heater rod surface temperatures among Bundles 2, 4, 6 and 8
- Fig. 3.26 Comparisons of radial temperature distribution at 2.33 m among Tests S2-12, S2-14 and S2-15
- Fig. 3.27 Comparisons of radial temperature distribution at 2.33 m among Tests S2-12, S2-14 and S2-21
- Fig. 3.28 Comparisons of quench front propagation profiles among Bundles 2, 4, 6 and 8 for each of Test S2-12, S2-14, S2-15 and S2-21
- Fig. 3.29 Comparison of average heat transfer coefficients at 2.33 m in Bundle 4
- Fig. 3.30 Comparison of average heat fluxes at 2.33 m in Bundle 4
- Fig. 3.31 Comparisons of non-heated rod surface temperatures at 0.95, 1.905 and 2.76 m in Bundle 4
- Fig. 3.32 Comparisons of side wall surface temperatures at 1.838 and 2.191 m in Bundle 3
- Fig. 3.33 Comparisons of fluid temperatures in core at 1.735 and 2.33 m in Bundle 4
- Fig. 3.34 Comparison of average heat transfer coefficient vs. time
- Fig. 3.35 Comparison of average heat transfer coefficient vs. distance from bottom quench front
- Fig. 3.36 (a) through (d)  
Comparisons between steam generation rates and heating powers divided by latent heat of evaporation in Bundles 2, 4, 6 and 8

## 1. INTRODUCTION

The Slab Core Test Facility (SCTF) test program is a part of the large scale reflood test program under contract with Atomic Energy Bureau of Science and Technology Agency of Japan together with the Cylindrical Core Test Facility (CCTF) test program. One of the major objectives of the SCTF program is to investigate the two-dimensional thermal-hydraulic behavior in the core during the reflood phase of a loss-of coolant accident (LOCA) of a pressurized water reactor (PWR)<sup>(1)-(7)</sup>. In order to meet this objective, SCTF simulates a full radius slab section of a PWR with 8 bundles arranged in a row and the heating power can be independently controlled for each bundle. Therefore, the effects of radial core power and temperature distributions can be investigated with SCTF. On the other hand, the major objective of the CCTF test program is to investigate system characteristics during the reflood phase of a PWR-LOCA using a 1/4.5 scaled core.

Based on the previous SCTF test results<sup>(7),(8)</sup>, the two-dimensional effect during the reflood phase are classified into the following two individual effects :

### (1) Effect of radial core power/temperature distribution

The heat transfer above the quench front is enhanced in the higher power/temperature bundles and degraded in the lower power/temperature bundles and resultantly the turnaround temperature is reduced in the higher power/temperature bundles.

### (2) Effect of non-uniform water accumulation in the upper plenum

As the collapsed water level in the upper plenum becomes higher in the hot leg side on the periphery than in the radial center side, the bottom-up quench velocity in the upper half of the core is reduced in the peripheral bundles due to a degradation of heat transfer in these bundles.

In the SCTF tests, the radial core power/temperature distribution has more significant effect on the reduction of peak cladding temperature than the non-uniform water accumulation in the upper plenum. When the radial core power distribution is given, the radial rod temperature distribution is induced in the previous tests and therefore the effects of core power and rod temperature distributions could not be distinguished from each other.

In order to separately evaluate these two effects, four tests were

performed with various combinations of radial core power and rod temperature distributions as follows :

Test number	S2-12	S2-14	S2-15	S2-21
Core heating power distribution	Steep	Flat	Steep	Flat
Initial rod temperature distribution	Steep	Flat	Flat	Steep

These tests were performed under the forced flooding condition to make the core inlet flow rate the same. The water in the upper plenum was extracted in these tests so as to avoid the effect of non-uniform water accumulation in the upper plenum.

The present report describes the results of these four tests, focusing on the effects of radial core power distribution itself and the effects of radial temperature distribution on the two-dimensional thermal-hydraulic behavior in the core.

Presented in Appendix A are a brief description of SCTF Core-II. Some selected data obtained in Tests S2-12, S2-14, S2-15 and S2-21 are presented in Appendixes B, C, D and E, respectively. Additionally, in order to evaluate the predictability of the two-dimensional behavior observed in the SCTF tests by the Transient Reactor Analysis Code (TRAC)<sup>(14)</sup>, some data from Test S2-12 were compared with TRAC post-test calculation performed by the Los Alamos National Laboratory in Appendix F.

## 2. Test Description

### 2.1 Test Facility

A schematic diagram of SCTF is shown in Fig. 2.1. The primary coolant loops consist of a hot leg equivalent to four actual hot legs, a steam/water separator corresponding to four actual steam generators, an intact cold leg equivalent to three intact cold legs, a broken cold leg on the pressure vessel side, and a broken cold leg on the steam/water separator side. These two broken cold legs are connected to two containment tanks one by one which are connected to each other by the pressure equalizing pipe.

The flow area scaling ratio is 1/21 of a 1,100 MWe PWR, whereas the heights of each component are preserved.

Figure 2.2 shows a vertical cross section of the pressure vessel. The pressure vessel includes a simulated core, an upper plenum with internals, a lower plenum, a core baffle and downcomer. The SCTF pressure vessel simulates a full radius slab section of a 1,100 MWe PWR.

The simulated core consists of 8 bundles arranged in a row with full radial width. Each bundle consists of 234 heater rods and 22 non-heated rods arranged in a 16x16 array. The outer diameter and the heated length of the heater rod are 10.7 mm and 3660 mm, respectively. The dimensions and arrangement pitch of the rod are based on those for a 15x15 fuel rod bundle of a Westinghouse type PWR.

The core and the upper plenum are enveloped by honeycomb thermal insulators with wall plates to minimize the wall thermal effects.

More detailed information on SCTF Core-II is available in reference (9) and a brief description is presented in Appendix A.

### 2.2 Test Conditions

The tests referred to in this report are Tests S2-12, S2-14, S2-15 and S2-21. Major test conditions for these four tests are listed in Table 2.1. The BOCREC (bottom of core recovery) in Table 2.1 represents the time when the ECC water reaches the bottom of heated part.

These four tests were performed under almost the same conditions

except the radial core power distribution and the initial rod temperature distribution. The normalized power ratio in Test S2-12 was 1.0 (Bundles 1 & 2), 1.2 (Bundles 3 & 4), 1.0 (Bundles 5 & 6) and 0.8 (Bundles 7 & 8). This is called the steep radial power distribution because the radial peaking factor was set to be larger than that expected in the initial loading core of a 1,100 MWe Westinghouse type PWR. The radial temperature distribution in this test was also steep. On the other hand, both the radial core power and temperature distributions were flat in Test S2-14. In Tests S2-15 and S2-21, the radial power distribution was steep and flat, respectively. However, the radial distribution of initial temperature was set to be flat and steep in Test S2-15 and S2-21, respectively, based on the test procedure described in Section 2.3. The initial stored energy in the core was set to be the same for these four tests as well as the total core heating power.

In order to specify the core inlet water flow rate during test period, the present four tests were performed under the forced flooding condition. That is, the downcomer was isolated from the lower plenum by inserting a blocking plate at the bottom of downcomer and emergency core cooling (ECC) water was directly injected into the lower plenum. In the previous CCTF Core-II tests<sup>(10)</sup>, the ECC water was injected into the lower plenum during the accumulator injection period and then into the intact cold leg during the low pressure coolant injection (LPCI) period. This ECC injection mode is called the gravity feed because the core flooding is driven by the water head in the downcomer as in the case of an actual PWR. By comparing the test results under these two ECC injection modes, it was found that the ECC injection mode, irrespective of forced feed or gravity feed, has little effect on the two-dimensional thermal-hydraulic behavior<sup>(11)</sup> for the flow rate range in this report.

The injection rate and temperature of ECC water were varied to make the core inlet flow rate and water temperature as equal as possible to those in CCTF Test C2-06<sup>(12)</sup>, which was the flat radial power distribution test with CCTF Core-II. The maximum ECC water injection rate was 25.7 kg/s corresponding to 8.5 cm/s of nominal flooding velocity. The injection rate for the LPCI period was 4.8 kg/s corresponding to 1.6 cm/s of nominal flooding velocity.

The water in the upper plenum was extracted in these four tests so as to avoid the effect of non-uniform water accumulation in the upper plenum because the major purpose of these four tests was to separately evaluate

the effects of radial core power and temperature distribution on the two-dimensional thermal-hydraulic behavior in the core.

The system pressure in the containment tanks was controlled to be 0.2 MPa.

### 2.3 Test Procedure

In Tests S2-15 and S2-21, the core was initially heated up with the flat and steep radial power distributions, respectively, so as to establish the flat and steep radial temperature distributions. After the maximum temperature reaches to just below the temperature for the ECC injection initiation, the radial power distribution was changed to steep and flat for Tests S2-15 and S2-21, respectively, and the core heating started again. In this way, the radial temperature distribution at the BOCREC could be established independent of the radial power distribution in these two tests. In Tests S2-12 and S2-14, the core heating was initiated after setting the initial pressure and temperature conditions as in the cases of the other SCTF tests.

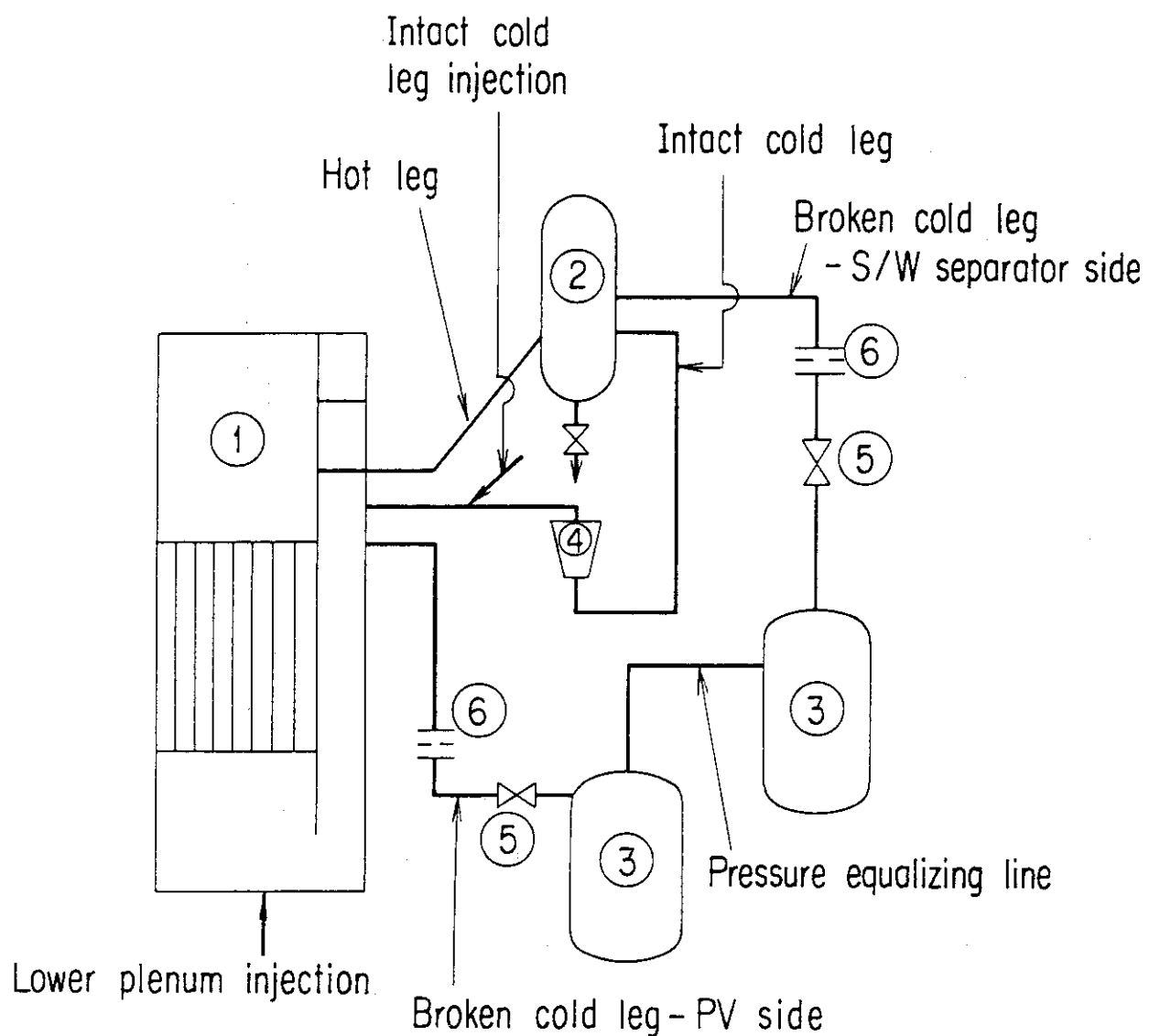
In Test S2-15, the period from the end of the initial core heating to the initiation of the second core heating was so long that the initial core heat transfer behavior was affected by the superheating of the walls and the non-heated rods as will be discussed in Section 3.3.2. In Test S2-21, on the other hand, this unfavorable effect could be minimized by shortening the time required for the change of radial power distribution to approximately zero.

The ECC injection into the lower plenum was initiated when four cladding temperatures exceeded 1016 K for Test S2-12 and S2-21 and 910 K for Tests S2-14 and S2-15, respectively, so as to make the initial core stored energy the same. At the same time as the ECC injection initiation, the core power decay started simulating the reactor power from 40s after shutdown. The decay curve was based on the 1.02 x (ANS standard + Actinides).

In order to investigate the thermal-hydraulic behavior in a large core under no ECC flow rate in Test S2-21, the ECC injection into the lower plenum was terminated after the quench of whole core at 409 s while the core heating continued along the specified decay curve.

Table 2.1 Test conditions for Tests S2-12, S2-14,  
S2-15 and S2-21

Test No.	S2-12	S2-14	S2-15	S2-21
Initial pressure	0.2 MPa	0.2 MPa	0.2 MPa	0.2 MPa
Initial total power	7.11 MW	7.11 MW	7.11 MW	7.11 MW
Maximum Acc injection rate	25.8 kg/s	24.5 kg/s	26.1 kg/s	26.5 kg/s
LPCI injection rate	4.7 kg/s	4.8 kg/s (oscillated)	5.2 kg/s	4.7 kg/s
Maximum core inlet subcooling	16 K	16 K	20 K	18 K
Radial power ratio				
Bundles 1 & 2	1.0	1.0	1.0	1.0
" 3 & 4	1.2	1.0	1.2	1.0
" 5 & 6	1.0	1.0	1.0	1.0
" 7 & 8	0.8	1.0	0.8	1.0
Maximum rod temperature at BOCREC				
Bundles 1 & 2	940 K	907 K	922 K	934 K
" 3 & 4	1046 K	927 K	931 K	1045 K
" 5 & 6	961 K	921 K	892 K	969 K
" 7 & 8	857 K	935 K	895 K	865 K
UCSP extraction				
start	98 s	77 s	79 s	99 s
end	398 s	377 s	379 s	399 s



- |                             |                                |
|-----------------------------|--------------------------------|
| (1) Pressure vessel         | (5) Break valves               |
| (2) Steam / water separator | (6) Flow resistance simulators |
| (3) Containment tanks       |                                |
| (4) Pump simulator          |                                |

Fig. 2.1 Schematic diagram of SCTF

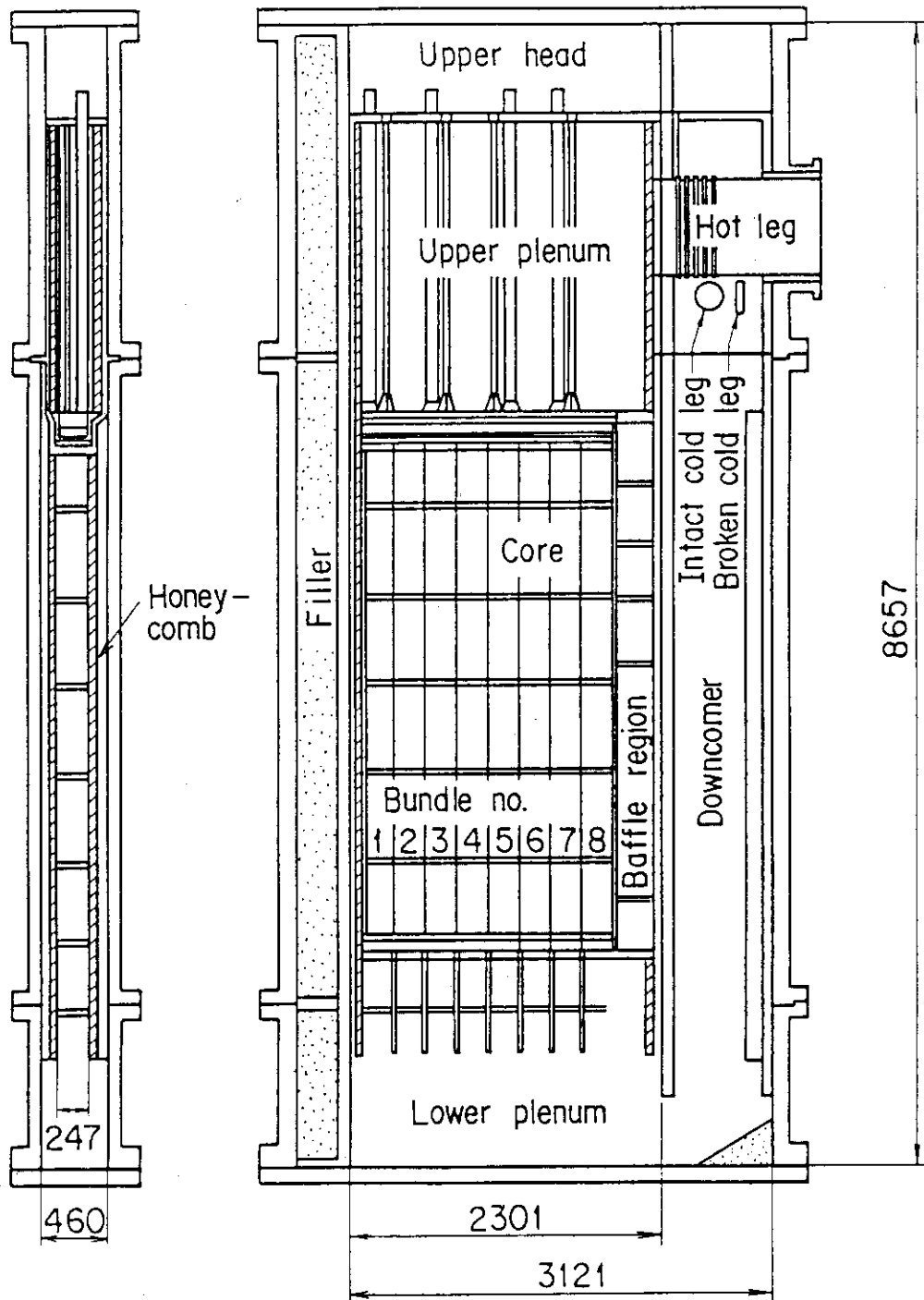


Fig. 2.2 Vertical cross section of pressure vessel

### 3. Test Results and Discussions

#### 3.1 Overall Fluid Behavior

##### 3.1.1 Boundary Conditions

Figure 3.1 shows the comparison of ECC injection rates into the lower plenum for Tests S2-12, S2-14, S2-15 and S2-21. The ECC injection rate is in good agreement with each other except the oscillation in Test S2-14 after 240s. Figure 3.2 shows the estimated core inlet mass flow rate obtained by a mass balance method<sup>(7)</sup>. As shown in Fig. 3.2, the core inlet mass flow rate during the initial 30s is lower than the ECC injection rate because a part of the injected water flows into the core baffle region during this period. After 30s, the core inlet mass flow rate agrees with the ECC injection rate because the water accumulation rate in the core baffle becomes much lower than the ECC injection rate. The difference of the core inlet mass flow rate among these four tests is also small except during the initial 20s for all of these four tests and after 240s for Tests S2-14.

Figure 3.3 compares the integrated core inlet water mass. The integrated core inlet water mass agrees approximately for these four tests except that the integrated mass in Test S2-14 is slightly lower than in the other three tests.

Figure 3.4 shows the comparison of core inlet water temperatures. The core inlet water temperature is the lowest in Test S2-15 and the highest in Test S2-14 and the difference between these two tests is about 10 K. The core inlet water temperarures in Tests S2-12 and S2-21 agree well with each other and are between those in Tests S2-14 and S2-15.

Figure 3.5 shows the transients of core heating power. The radial core power distribution is flat in Tests S2-14 and S2-21 and the power transients completely agree with each other for these two tests. In Tests S2-12 and S2-15, the radial core power distribution is steep and also the power transients completely agree with each other for these two tests. The total heating power at the BOCREC was set to be the same for these four tests.

As compared in Figs. 3.6 and 3.7, the pressures at the core center and at the top of the containment tank-II are in good agreement with each other for the present four tests. During the initial 100 s, the pressures at the core center in Tests S2-12 and S2-21 which have steep initial temperature disribution are slightly higher than the pressures in Tests S2-

14 and S2-15 which have flat initial temperature distribution.

The chronologies of major events for these four tests are summarized in Table 3.1.

### 3.1.2 Fluid Behavior in Upper Plenum and around End Box Tie Plate

Figure 3.8 shows the comparison of liquid level in the upper plenum above Bundles 2, 4, 6 and 8 in these four tests. In order to avoid the effect of non-uniform water accumulation in the upper plenum on the two-dimensional thermal-hydraulic behavior in the core, the water in the upper plenum was extracted through the eight extraction nozzles located just above the UCSP at each bundle. Therefore, the liquid levels in the upper plenum in these four tests were kept at lower level in comparison to those in Tests S2-SH2 and S2-06<sup>(7)</sup>. Although the water in the upper plenum was extracted, the liquid levels in the present four tests were slightly higher above the Bundle 8 side and lower above the Bundle 1 side as in the cases of Tests S2-SH2 and S2-06<sup>(7)</sup>. The ripples in the liquid levels indicate the intermittent actuation of the extraction system. The increase of liquid level after about 380 s in Tests S2-12, S2-14 and S2-15 is due to the end of water extraction. The decrease of liquid level after about 450 s in Test S2-21 is caused by the termination of water injection into the lower plenum.

Figure 3.9 shows the differential pressures across the end box tie plate above Bundles 2, 4, 6 and 8 in the present four tests. In general, the differential pressure is the lowest at Bundle 8 from 20 to 200 s in these four test, suggesting the lower steam up-flow rate above Bundle 8 during this period. This is explained by the fact that the liquid level in the upper plenum is higher at the Bundle 8 side as shown in Fig. 3.8 and resultantly the two-phase cross flow occurs from the Bundle 8 side to the Bundle 1 side at the upper part of the core due to the horizontal pressure gradient as will be discussed in Section 3.2.3 (Fig.3.23). After 450 s in Tests S2-12 and S2-15, the negative differential pressure above Bundle 8 which is the lowest power bundle indicates the water fall back into the core through the end box tie plate holes.

### 3.1.3 Water Accumulation Behavior in Core

Figure 3.10 shows the differential pressures across the core full height in Bundles 2, 4, 6 and 8 in Test S2-12. The total water accumulation behavior in the core is almost flat even for the steep radial power distribution test. The vertical differential pressures across the core full height in Bundle 4 in Tests S2-12, S2-14, S2-15 and S2-21 are compared in Fig.3.11. The difference in the differential pressures across the core full height among these four tests is relatively small except the lower differential pressure in Test S2-14 after 300 s which was due to the reduction of the core inlet water flow rate shown in Fig. 3.2 .

### 3.1.4 Total Steam Generation Rate in Core and Steam Outflow Rate from Pressure Vessel

Figures 3.12 and 3.13 show the comparison of steam generation rates in the core obtained by a heat balance method and the comparison of steam outflow rates from the pressure vessel obtained by the sum of the steam flow rates in the intact cold leg and in the broken cold leg steam-water separator side, respectively, for Tests S2-12, S2-14, S2-15 and S2-21. As shown in Fig. 3.13 , the steam outflow rates are in good agreement among these four tests after 100 s. During the initial 100 s, the steam outflow rates are divided into two groups ; Tests S2-12 and S2-21 and Tests S2-14 and S2-15, corresponding to the initial radial temperature distribution. On the other hand, the estimated steam generation rate in Test S2-15 is much lower than those in the other tests during the initial 160 s and after that time these four steam generation rates agree well with each other. The lower steam generation rate in Test S2-15 is corresponding to the fact that the water accumulation level is lower in this test as shown in Fig. 3.11.

It is indicated by comparing Fig. 3.12 with Fig. 3.13 that the steam generation rate are higher than the steam outflow rate during the initial 60 s except in Test S2-15. This discrepancy may be attributed to the following two reasons. One reason is that the generated steam is considered to be condensed because the temperature of the structure could not be in equilibrium with the saturation temperature during the pressure overshoot period. Another reason is that some amount of the generated

steam contributes to the pressurization of the system.

### 3.1.5 Fluid Behavior in Primary Loops

Figure 3.14 shows the comparisons of mass flow rates in 4 regions of the hot leg in Test S2-14. The top region comprises the upper 31 % of the pipe cross-sectional area, the second region comprises the next lower 27 %, the third region comprises the next lower 26 %, and the bottom region comprises the bottom 16 %. As shown in this figure, after 106 s, the mass flow rate in the bottom region is negative, indicating the flow reversal at the bottom part of the hot leg after 106 s. The same kind of flow reversal was also observed in Tests S2-12, S2-15 and S2-21.

Figures 3.15 through 3.18 show the comparisons of differential pressures across the hot leg, the intact cold leg, the broken cold leg steam/water separator side and the broken cold leg pressure vessel side, respectively. As shown in these figures, the transients of differential pressures in the primary loops in these four tests are in good agreement with each other after about 100 s. During the initial 100 s, the differential pressures in Tests S2-14 and S2-15 are slightly smaller than those in Tests S2-12 and S2-21, corresponding to the fact that the initial temperature distribution is flat in Tests S2-14 and S2-15 and steep in Tests S2-12 and S2-21. These differential pressure behaviors in the primary loops indicate that the total core heat transfer rate and resultant steam generation rate are increased by the steep radial temperature distribution under the same total core power and the same core stored energy. The agreement of the differential pressures for these four tests in the later period indicates that the radial power distribution has little effect on the fluid behavior in the primary loops.

## 3.2 Effects of Radial Power and Temperature Distribution on Two-Dimensional Hydraulic Behavior in Core

### 3.2.1 Pressure Distribution

In order to investigate the two-dimensional hydraulic behavior in the core, vertical and horizontal differential pressures were measured at

various locations in the core. By combining the measured horizontal and/or vertical differential pressures, horizontal differential pressures at other locations could be obtained. The absolute pressures at various points in the core were also obtained by combining the measured absolute pressure with the measured or calculated differential pressures. By vertically interpolating these calculated absolute pressures, equal pressure lines were obtained. Figures 3-19(a) through (f) show the comparisons of equal pressure lines in the core among Tests S2-12, S2-14, S2-15 and S2-21 at 25, 50, 100, 200, 300 and 400 s, respectively. The distribution of bottom quench front is also shown in these figures.

At 25 and 50 s, the pressure in the Bundle 8 side is lower than the pressure in the Bundle 1 side at the middle elevation of the core in Test S2-12 and S2-21, indicating the steam flow towards the Bundle 8 side, while almost flat distribution is observed in Tests S2-14 and S2-15. The quench front distribution is also approximately flat in Tests S2-14 and S2-15 at these times. In Tests S2-12 and S2-21, on the other hand, the quench front is lower in Bundles 3 and 4 and higher in Bundles 7 and 8. It is suggested from the above-mentioned pressure and quench front behaviors that the two-dimensional thermal-hydraulic behavior above the quench front is not so much affected by the radial power distribution itself but is mainly affected by the radial temperature distribution which accompanies the radial power distribution during the initial period.

As the radial temperature distributions in Tests S2-15 and S2-21 approach those in Tests S2-12 and S2-14, respectively, due to the radial power distribution, the radial pressure distribution and the radial quench front distribution become similar between Tests S2-12 and S2-15 and also between Tests S2-14 and S2-21 as shown in Figs. 19(c) through 19(e).

After the quench of the whole core, the pressure in the Bundle 1 side is slightly higher than the pressure in the Bundle 8 side at the middle elevation of the core for all of these four tests as shown in Fig. 19(f).

### 3.2.2 Void Fraction Distribution

Figures 3.20 (a) through 3.20 (c) show the comparisons of void fractions in Bundles 2, 4 and 8 at 3 elevations for Tests S2-12, S2-14, S2-15 and S2-21. These void fractions were calculated from the measured vertical differential pressures by neglecting the effects of frictional and accelerational pressure drops.

As shown in Fig.3.20 (a), for the elevation between 0.085 and 0.7 m, no significant difference in the void fractions among bundles is observed in Tests S2-14 and S2-15, whereas the void fraction in Bundle 8 is lower than that in Bundles 2 and 4 during the initial 40 s in Tests S2-12 and S2-21 because the quench front propagates faster in Bundle 8 than Bundles 2 and 4 in these two tests due to the radial temperature distribution.

As shown in Fig.3.20 (b), for the elevation between 2.03 and 2.57 m, the void fraction in Bundle 8 is the highest among these three bundles in Tests S2-12 and S2-15 until about 250 s and thereafter the lowest in this bundle, whereas the radial void fraction distribution is almost flat in Tests S2-14 and S2-21. The higher void fraction in Bundle 8 for the steep power distribution test indicates that the effect of radial power distribution on the radial void fraction distribution is more dominant than the effect of radial temperature distribution at the middle elevation of the core probably due to the radial distribution of steam generation rate. It is also observed in Fig. 3.20 (b) that the horizontal distribution of void fraction at this elevation is flat in these four tests during the initial 40 s which is corresponding to the period of high ECC injection rate.

As shown in Fig. 3.20 (c), at the top region of the core, the void fraction in Bundle 2 is the lowest and that in Bundle 8 is the highest among these three bundles and this behavior is common in the present four tests. This is probably attributed to the reduction of steam velocity at the Bundle 8 side because of the higher upper plenum liquid level at the Bundle 8 side as shown in Fig. 3.8 .

Figure 3.21 compares the relation between the liquid fraction at elevation of 2.33 m and the distance from the bottom quench front among Bundles 2, 4 and 8 in these four tests. In Tests S2-12 and S2-21, the liquid fraction is the highest in Bundle 4 and the lowest in Bundle 8 at the same distance from the bottom quench front except at about 1.7 m. As shown in Figs. 3.2 and 3.28, the time when the quench front was at the elevation of 0.63 m (the distance between the elevation of 2.33 and 0.63 is 1.7 m) is approximately corresponding to the time when the core inlet flow rate was reduced. Therefore, it is indicated that the horizontal difference of liquid fraction disappears temporarily when the core inlet flow rate is reduced from the accumulator flow rate to the LPCI flow rate.

### 3.2.3 Horizontal Differential Pressure

Figures 3.22 and 3.23 show the comparisons of horizontal differential pressures in the core at elevations of 1.905 and 3.235 m, respectively, among Tests S2-12, S2-14, S2-15 and S2-21.

As shown in Fig.3.22 (b), the horizontal differential pressure between Bundles 4 and 8 at 1.905 m in Test S2-15 is close to that in Test S2-14 during the initial 80 s and thereafter approaches that in Test S2-12. On the contrary, the horizontal differential pressure in Test S2-21 is close to that in Test S2-12 during the initial 40 s and thereafter approaches that in Test S2-14. It is indicated from the above-mentioned horizontal differential pressure behaviors that the cross flow across the rod bundles above quench front is not induced by the radial power distribution itself but by the radial temperature distribution because the radial temperature distribution in Test S2-15 is initially flat and then becomes steep with time due to the steep radial power distribution and also the radial temperature distribution in Test S2-21 is initially steep and then becomes flat with time due to the flat radial power distribution.

As shown in Fig. 3.23 (b), the horizontal differential pressure between Bundles 4 and 8 at elevation of 3.235 m exhibits the oscillatory behavior for all of these four tests. These oscillations are corresponding to the ripples observed in the liquid levels in the upper plenum as shown in Fig. 3.8. In spite of these oscillations, it is noted that the pressure in Bundle 8 is slightly higher than the pressure in Bundle 4 before about 250 s and after that time the pressure in Bundle 4 is slightly higher than the pressure in Bundle 8 for all of the four tests.

As shown in Figs. 3.22(a) and 3.23(a), the pressure differences between Bundles 1 and 4 at elevations of 1.905 and 3.235 m are approximately zero and no significant difference is observed among these four tests.

## 3.3 Effects of Radial Power and Temperature Distribution on Two-Dimensional Thermal Behavior in Core

### 3.3.1 Heater Rod Temperature Behavior

Figure 3.24 shows the comparisons of heater rod surface temperatures at 2.33 m in Bundles 4 and 8 among Tests S2-12, S2-14, S2-15 and S2-21.

The initial temperature in Test S2-21 agrees well with that in Test S2-12 in both bundles, while the initial temperature in Test S2-15 in Bundle 8 is slightly lower than that in Test S2-14.

Figures 3.25 (a) through (d) show the comparisons of heater rod surface temperatures among Bundles 2, 4, 6 and 8 in Tests S2-12, S2-14, S2-15 and S2-21, respectively. These temperatures were obtained by averaging all the available temperatures at the same elevation in each bundle. As shown in this figure, the initial temperature distribution in Test S2-21 agrees well with that in Test S2-12 and the temperature difference among bundles in Test S2-21 decreases rapidly with time, becoming the flat radial distribution as in Test S2-14 due to the flat radial power distribution. On the other hand, the temperature difference among bundles in Test S2-15 is much smaller than in Test S2-12 but still larger than in Test S2-14. The radial temperature distribution in Test S2-15 becomes similar to that in Test S2-12 at the later period due to the steep radial power distribution.

The above-mentioned transients of radial temperature distribution in Tests S2-15 and S2-21 are clearly indicated in Figs. 3.26 and 3.27, respectively, by comparing with those in Tests S2-12 and S2-14.

Figure 3.28 compares the quench envelope profiles among Bundles 2, 4, 6 and 8 in each of the present four tests. The quench propagation speed is higher in Bundle 8 and lower in Bundle 4 in Test S2-12 and the quench propagates at almost the same speed in all bundles in Test S2-14 corresponding to the radial power distributions in these two tests, respectively. In Test S2-15, the distribution of quench front is similar to that in Test S2-12, whereas the difference in the quench front elevation between Bundles 4 and 8 is smaller than that in Test S2-12. In Test S2-21, the quench front elevation is higher in Bundle 8 and lower in Bundle 4 during the initial period in accordance with the radial temperature distribution. The difference in the quench front elevation in Test S2-21 becomes smaller with time due to the flat radial power distribution.

### 3.3.2 Heat Transfer Characteristics

The heat transfer coefficients and heat fluxes at 2.33 m in Bundle 4 are compared in Figs. 3.29 and 3.30, respectively, among Tests S2-12, S2-14, S2-15 and S2-21. These heat transfer coefficients and heat fluxes were obtained from the average temperature transients using the heat

transfer calculation code "HEATT"(13).

As shown in these figures, the heat transfer coefficient and the heat flux in Test S2-15 is significantly lower than those in the other three tests during the initial 100 s. This is explained in terms of the different fluid condition due to the different preconditioning procedure used only in this test. The surface temperatures on the non-heated rods and the core side walls remained at higher temperature and for longer time in Test S2-15 than in the other three tests as shown in Figs. 3.31 and 3.32. Resultantly, the superheated steam was generated for longer time in Test S2-15 than in the other three tests due to the longer heating time before the BOCREC in Test S2-15 as mentioned before. Therefore, the additional heat release from the non-heated rods and the side walls and the resultant superheated steam generation resulted in the lower heat flux and the lower heat transfer coefficient in Test S2-15. On the other hand, since the time from the end of initial core heating to the initiation of reflood was reduced to approximately 0 s in Test S2-21, the transients of surface temperatures on the non-heated rods and the side walls in this test were similar to those in Tests S2-12 and S2-14. Therefore, the unfavorable effect of superheated steam on the heat transfer characteristics was not observed in Test S2-21.

As shown in Figs. 3.29 and 3.30, the heat transfer coefficient and the heat flux in Test S2-21 agree well with those in Test S2-12 during the initial 40 s and in the later period those in Test S2-21 approaches those in Test S2-14. This is corresponding to the fact that the radial temperature distribution in Test S2-21 agrees well with that in Test S2-12 at the BOCREC and then approaches that in Test S2-14 with time as discussed in Section 3.3.1 .

In order to clarify the two-dimensional heat transfer characteristics, the average heat transfer coefficients in Bundles 4 and 8 at elevation of 2.33 m are plotted against the time and the distance from the bottom quench front in Figs.3.34 and 3.35, respectively. The difference of heat transfer coefficients between Bundles 4 and 8 is the largest in Test S2-12 and the smallest in Test S2-14 and the band of heat transfer coefficients in Test S2-14 is included in the band in Test S2-12. In Test S2-15, the difference of heat transfer coefficients between Bundles 4 and 8 is initially small but becomes large as the quench front approaches the elevation of 2.33 m according to the development of radial temperature distribution. On the other hand, the difference of heat transfer coefficients between Bundles 4 and 8 in Test S2-21 is relatively large when the distance from the bottom

quench front is larger than 1.8 m and then decreases as the quench front approaches this elevation. These heat transfer behaviors in Tests S2-15 and S2-21 indicate that the effect of radial temperature distribution is more dominant on the difference of heat transfer coefficients between bundles than the effect of radial power distribution itself.

Although the radial distribution of the initial temperature in Test S2-21 is in good agreement with that in Test S2-12 as shown in Fig 3.27, the difference of heat transfer coefficient between Bundles 4 and 8 during the initial period in Test S2-21 is slightly smaller than that in Test S2-12 as shown in Fig. 3.35 . This fact suggests that the effect of radial power distribution itself on the two-dimensional heat transfer characteristics may remain though this effect is much smaller than the effect of radial temperature distribution.

It is shown by comparing Fig. 3.34 with Fig. 3.2 that the difference of heat transfer coefficients between Bundles 4 and 8 is temporarily reduced when the core inlet flow rate is reduced to the LPCI flow rate as well as the magnitude of the heat transfer coefficient. This is corresponding to the fact that the horizontal difference of liquid fraction also diminishes at the time of the reduction of core inlet flow rate as discussed in Section 3.2.2. It is therefore indicated that the liquid fraction has dominant effect on the heat transfer coefficient in the early stage of the transient.

Below the quench front, the heater rod temperature is approximately equal to the saturation temperature and therefore the radial temperature distribution is flat even under the steep radial power distribution. The radial power distribution results in the radial distribution of steam generation rate and the resultant two-dimensional flow below the quench front. However, during the initial period, the difference of steam generation rate below the quench front is relatively small because the quench front is at the lower part of the core where the core heating power is relatively small due to the axial power distribution. Therefore, the radial power distribution below the quench front has little effect on the two-dimensional heat transfer behavior above the quench front.

### 3.3.3 Radial Distribution of Steam Generation Rate

Figures 3.36 (a) through (d) show the comparisons of steam generation rates in Bundles 2, 4, 6 and 8 obtained by the heat balance method with

heated powers divided by the latent heat of evaporation in each bundle for Tests S2-12, S2-14, S2-15 and S2-21, respectively. It is noted by comparing Fig. 3.36 with Fig. 3.25 that the radial distribution of steam generation rate corresponds to the radial distribution of cladding temperature. For example in Test S2-21, as shown in Fig. 3.36 (d), the steam generation rate in Bundle 4 is the highest and that in Bundle 8 is the lowest during the initial 140 s and thereafter the difference among bundles is relatively small. This trend is also observed in the radial distribution of cladding temperatures in Test S2-21 as shown in Fig. 3.25 (d). After the quench of the whole core, the steam generation rate in each bundle agrees well with the corresponding heated power divided by the latent heat of evaporation.

The higher steam generation rate results in the higher steam up-flow rate. However, the steam up-flow rate tends to be flattened over all bundles due to the cross flow from the high power bundles to the low power bundles above the quench front. Therefore, the quantitative estimation of the two-dimensional flow distribution above the quench front is necessary for the evaluation of the two-dimensional heat transfer characteristics.

**Table 3.1** Chronologies of major events for Tests  
S2-12, S2-14, S2-15 and S2-21

## (1) Test S2-12

	Time after BOCREC
Core Power "ON"	-121 s
Ecc Injection Initiation	-2.5
Core Power Decay Initiation	-2.5
BOCREC	0
Maximum Core Temperature (1064 K)	15.5
Maximum Containment-II Pressure (0.224 MPa)	22
Maximum Core Pressure (0.273 MPa)	29
UCSP Extraction Initiation	98
Whole Core Quenched	387.5
UCSP Extraction End	398

## (2) Test S2-14

	Time after BOCREC
Core Power "ON"	-114 s
Ecc Injection Initiation	-3
Core Power Decay Initiation	-3
BOCREC	0
Maximum Core Temperature (965 K)	10
Maximum containment-II Pressure (0.22 MPa)	23
Maximum Core Pressure (0.266 MPa)	28
UCSP Extraction Initiation	77
Whole Core Quenched	368
UCSP Extraction End	377

## (3) Test S2-15

	Time after BOCREC
Core Power "ON"	-17 s
Ecc Injection Initiation	-1
Core Power Decay Initiation	-1
BOCREC	0
Maximum Containment-II Pressure (0.222 MPa)	20
Maximum Core Pressure (0.262 MPa)	26
Maximum Core Temperature (1005 K)	53.5
UCSP Extraction Initiation	79
UCSP Extraction End	379
Whole Core Quenched	385.5

## (4) Test S2-21

	Time after BOCREC
Core Power "ON"	-3 s
ECC Injection Initiation	-1
BOCREC	0
Core Power Decay Initiation	3
Maximum Core Temperature (1058 K)	12
Maximum Containment-II Pressure (0.22 MPa)	21
Maximum Core Pressure (0.27 MPa)	27
UCSP Extraction Initiation	99
Whole Core Quenched	365
UCSP Extraction End	399
Stop Time of ECC injection	409
Starting Time of Dryout of Core	647

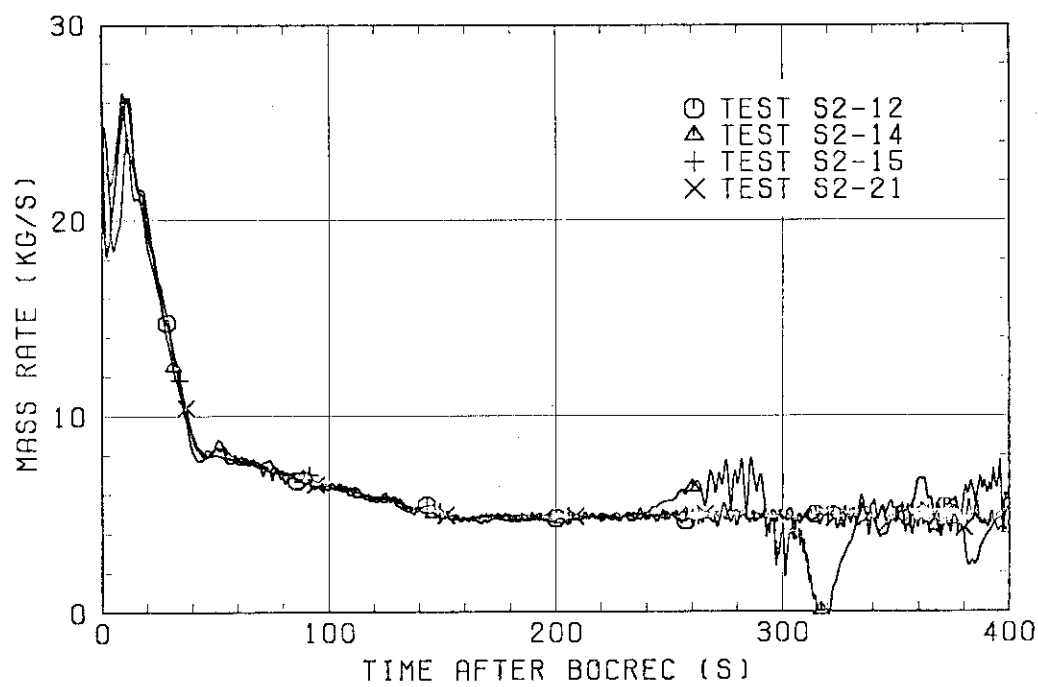


Fig. 3.1 Comparison of ECC injection rates into lower plenum

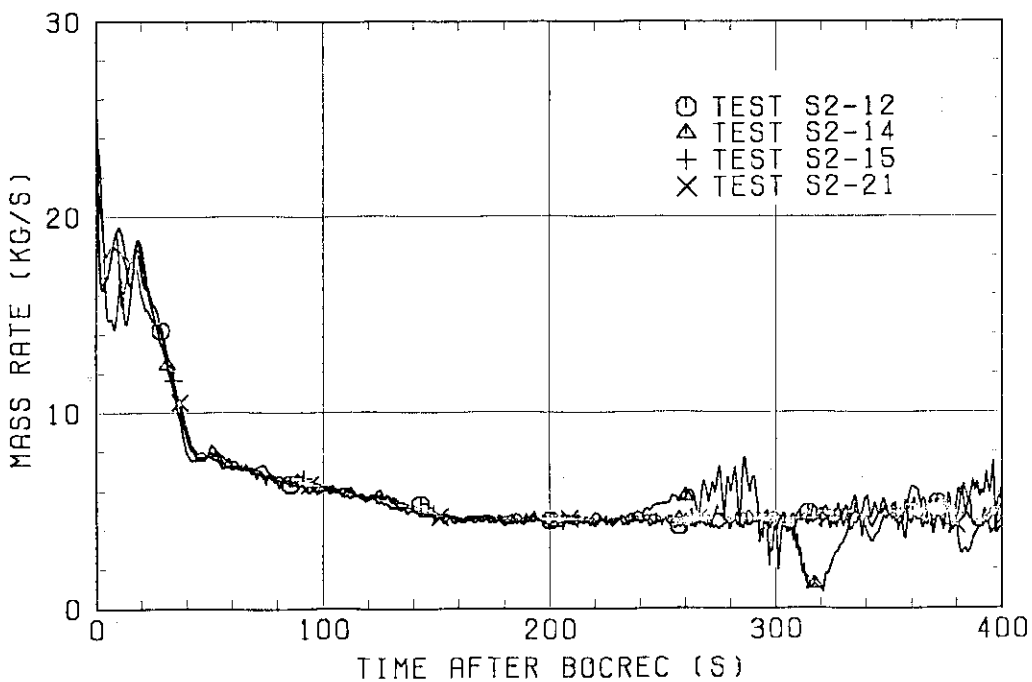


Fig. 3.2 Comparison of core inlet mass flow rates obtained by mass balance

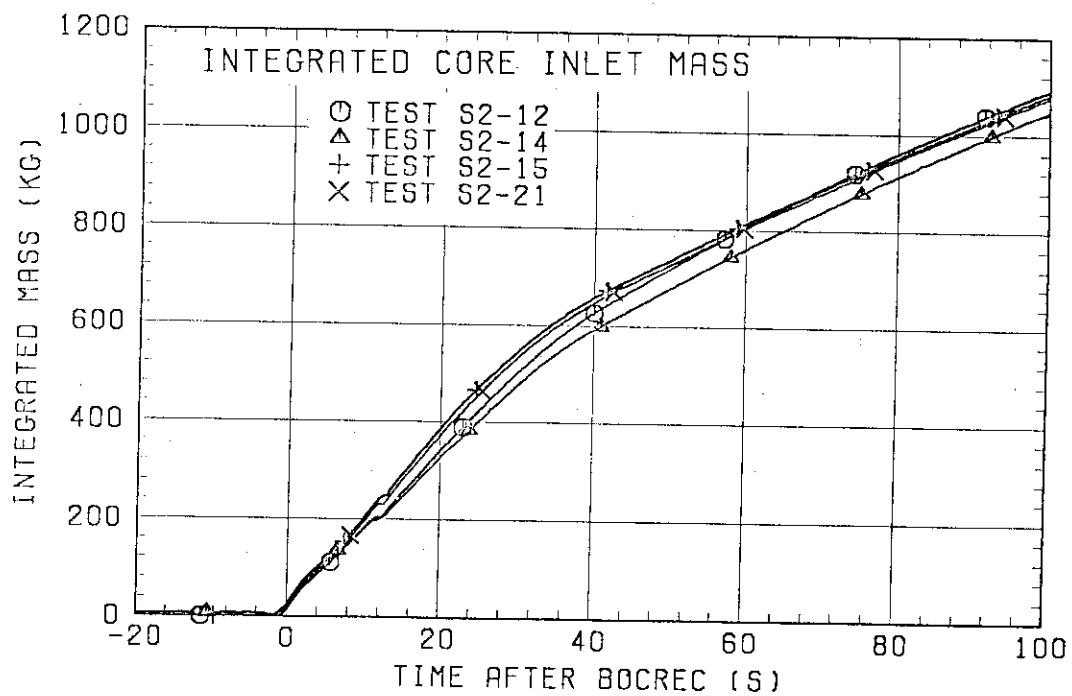


Fig. 3.3 Comparison of integrated core inlet water mass

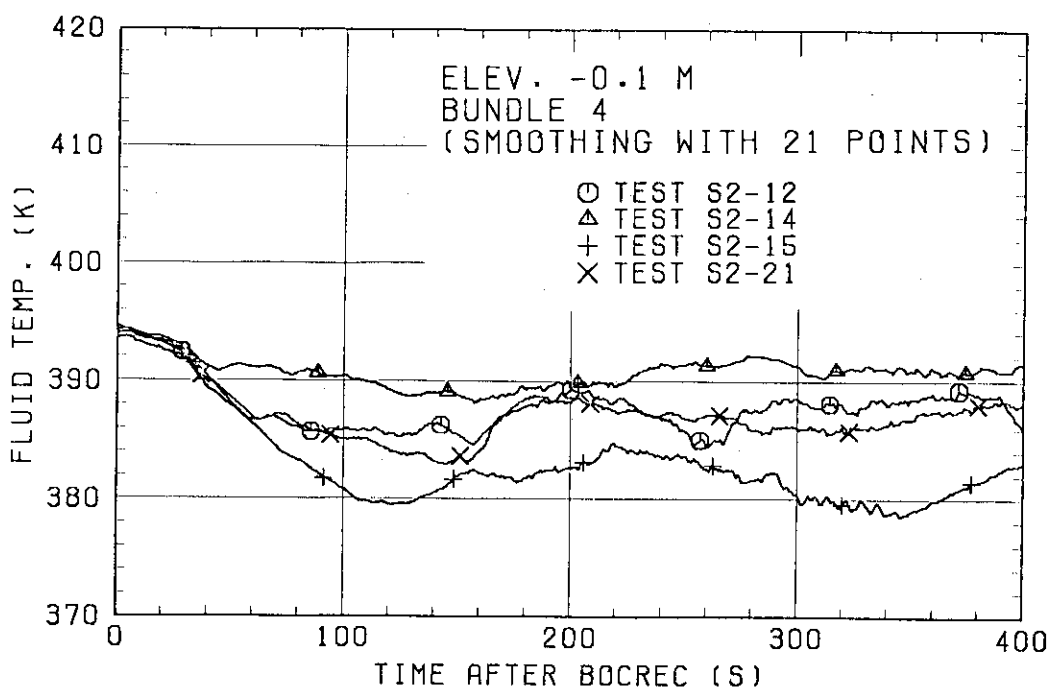


Fig. 3.4 Comparison of core inlet water temperatures

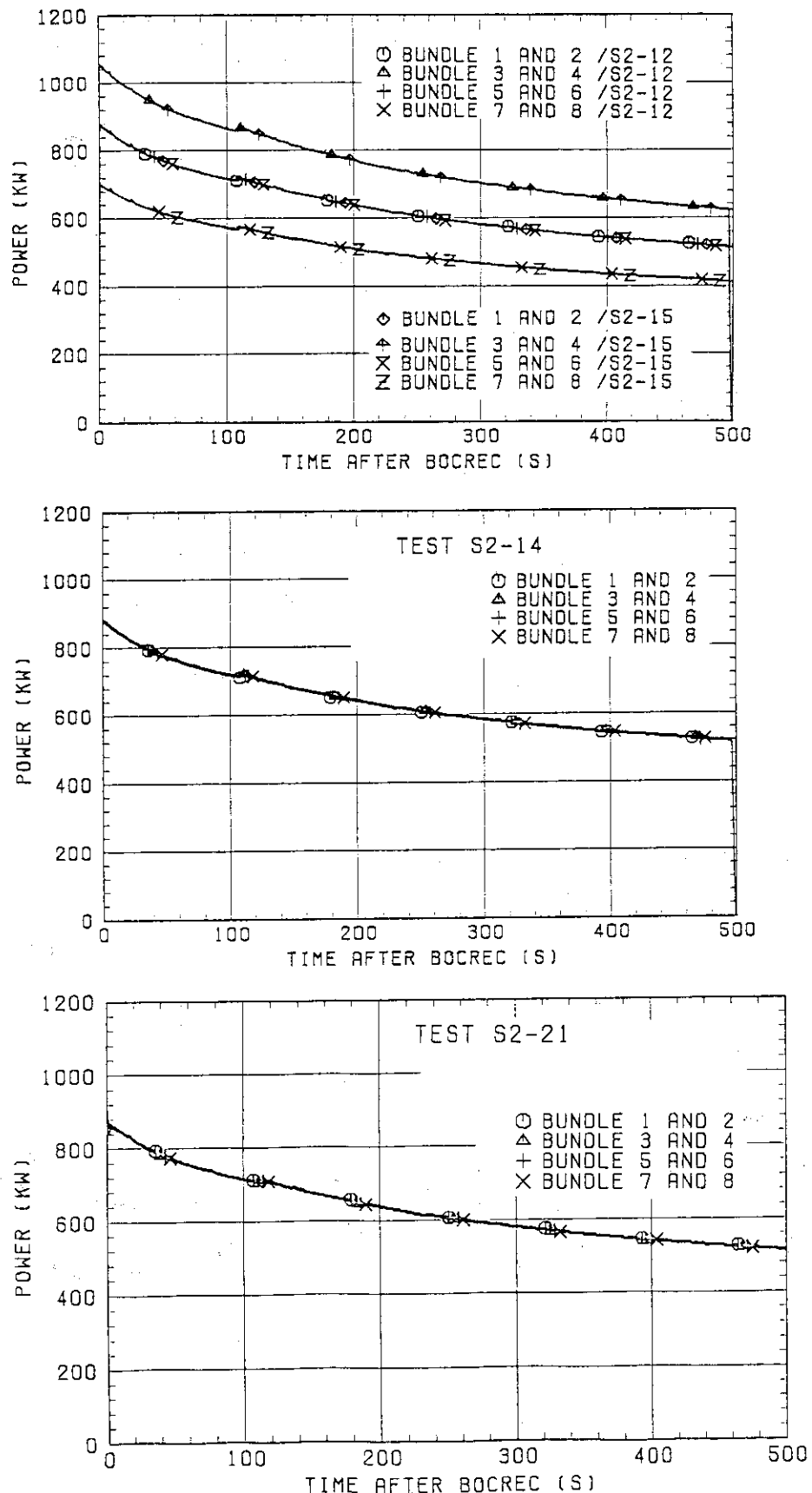


Fig. 3.5 Comparison of core heating powers

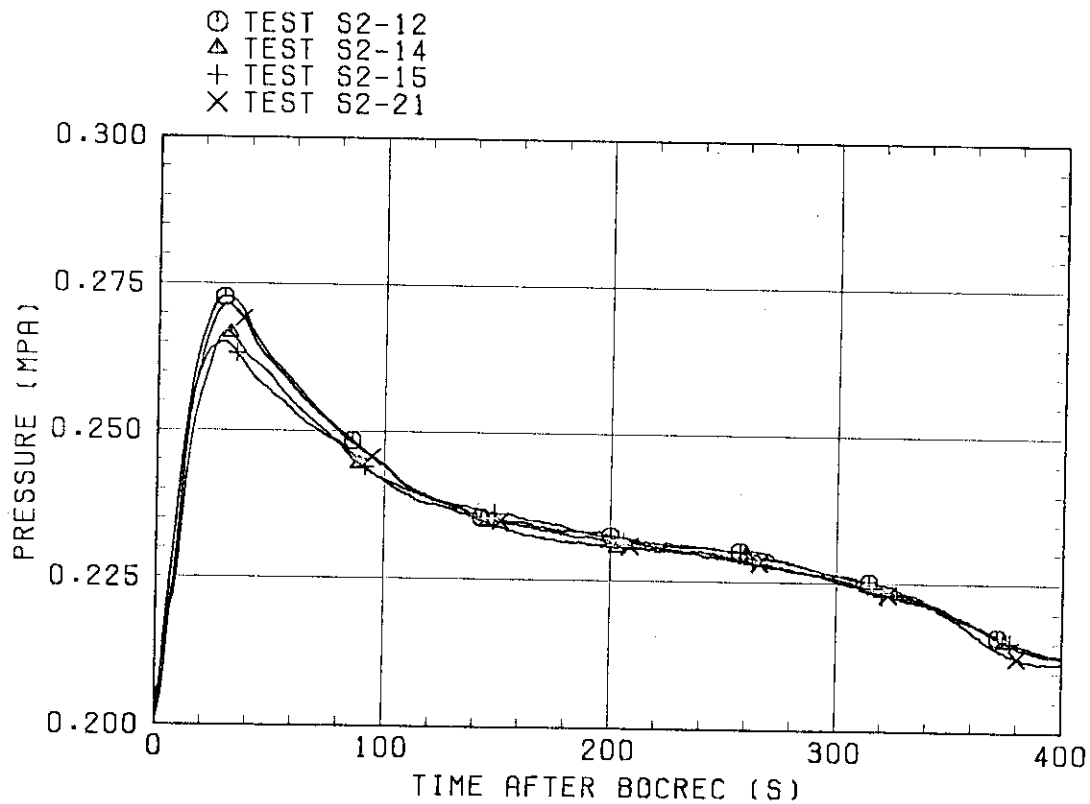


Fig. 3.6 Comparison of pressures at core center

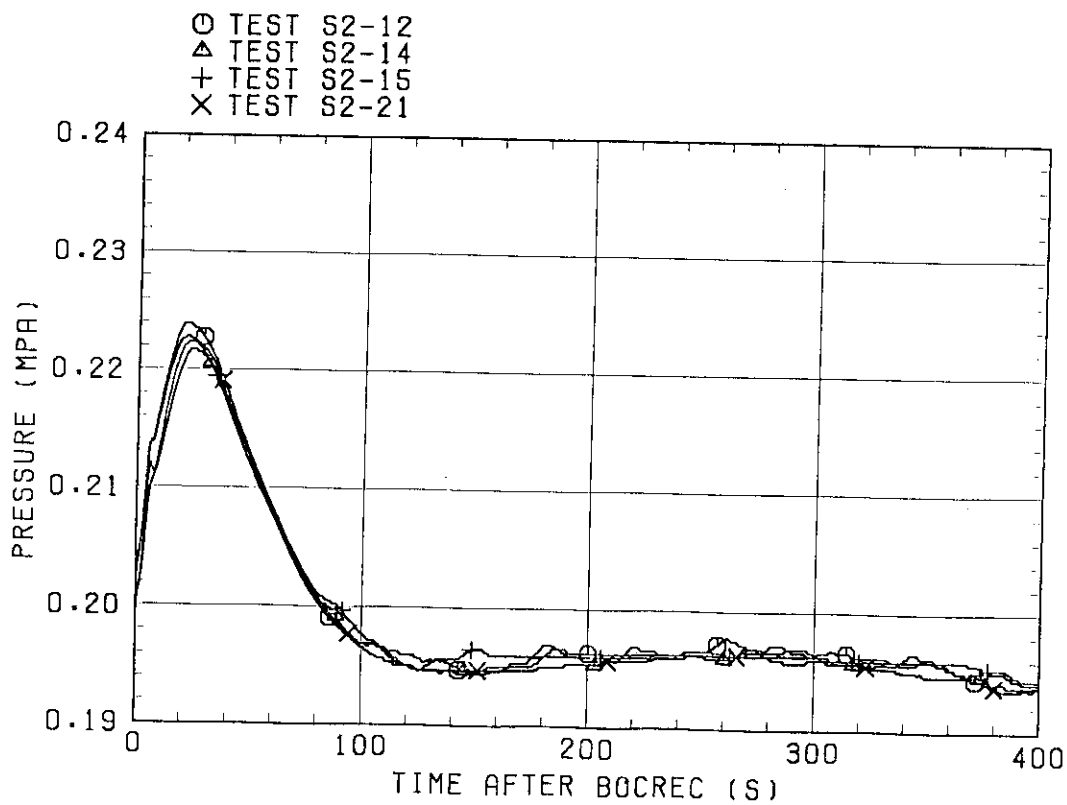


Fig. 3.7 Comparison of pressures at top of containment tank-II

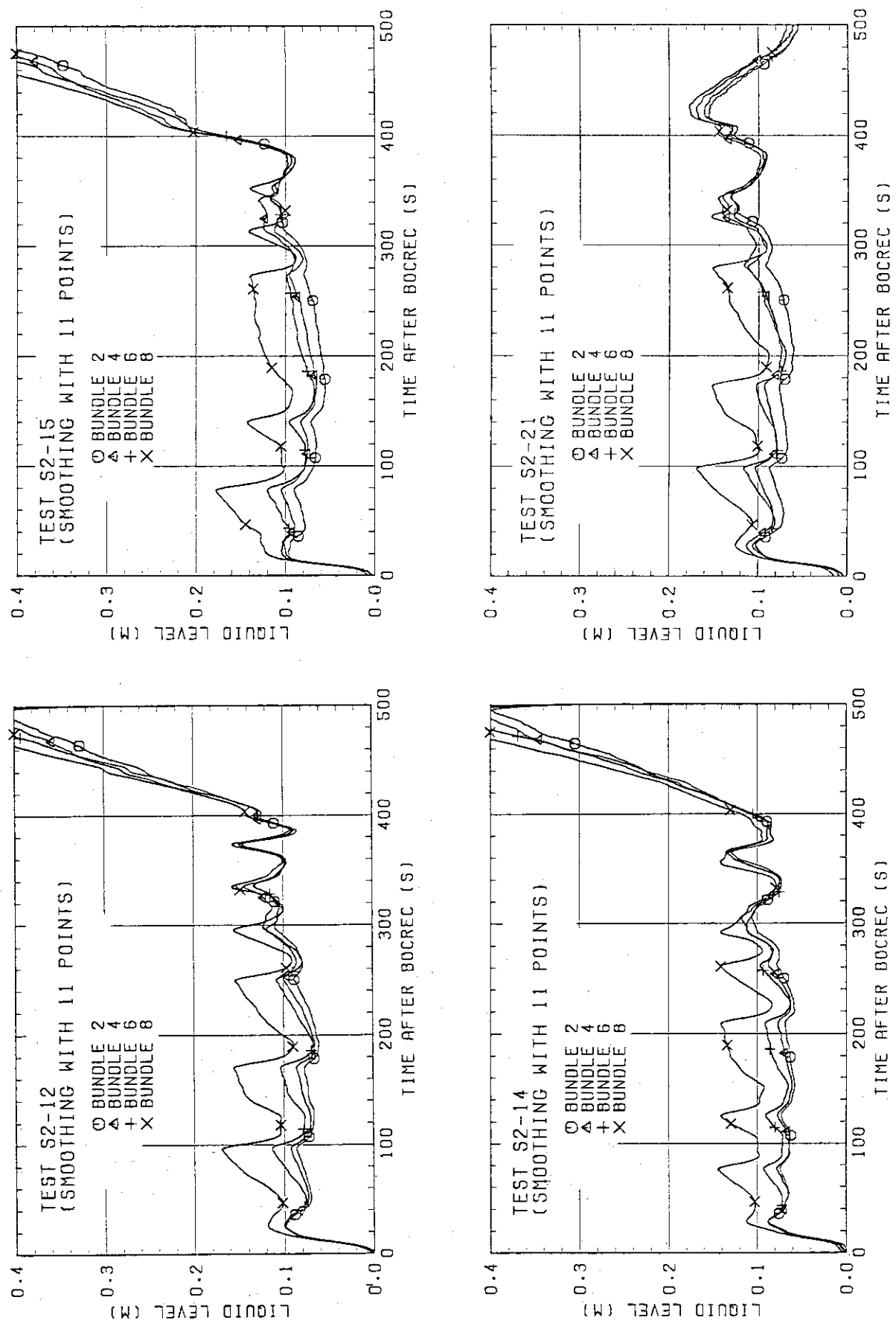


Fig. 3.8 Comparison of liquid levels in upper plenum

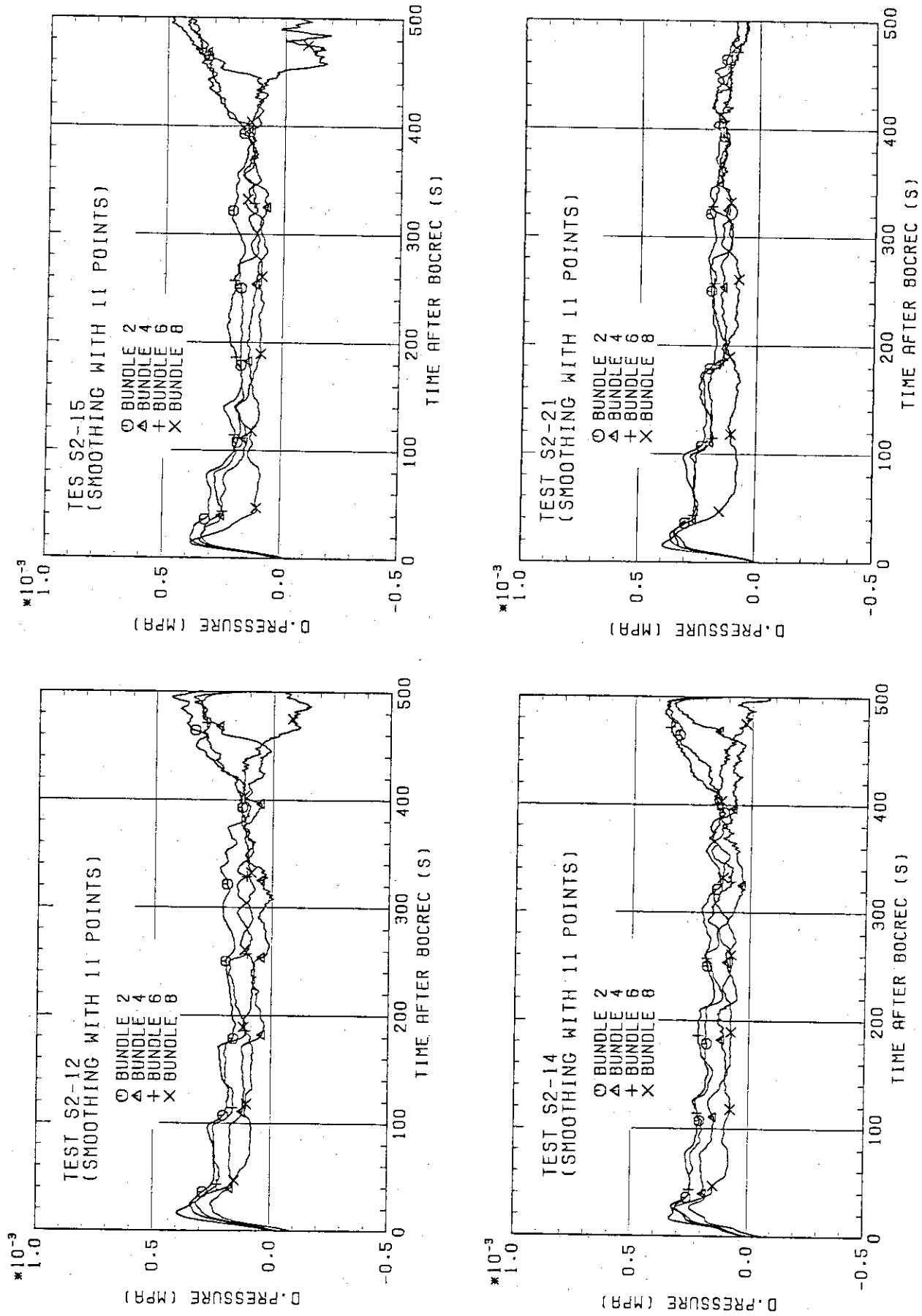


Fig. 3.9 Comparison of differential pressures across end box tie plate

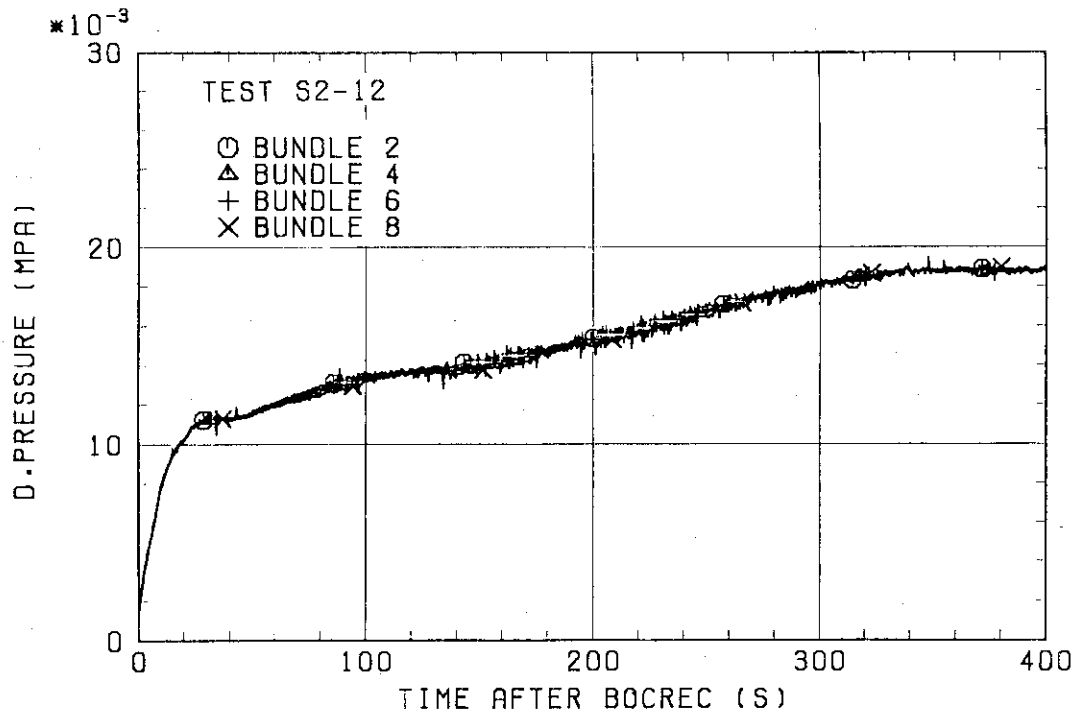


Fig. 3.10 Comparison of differential pressures across core full height among Bundles 2, 4, 6 and 8 in Test S2-12

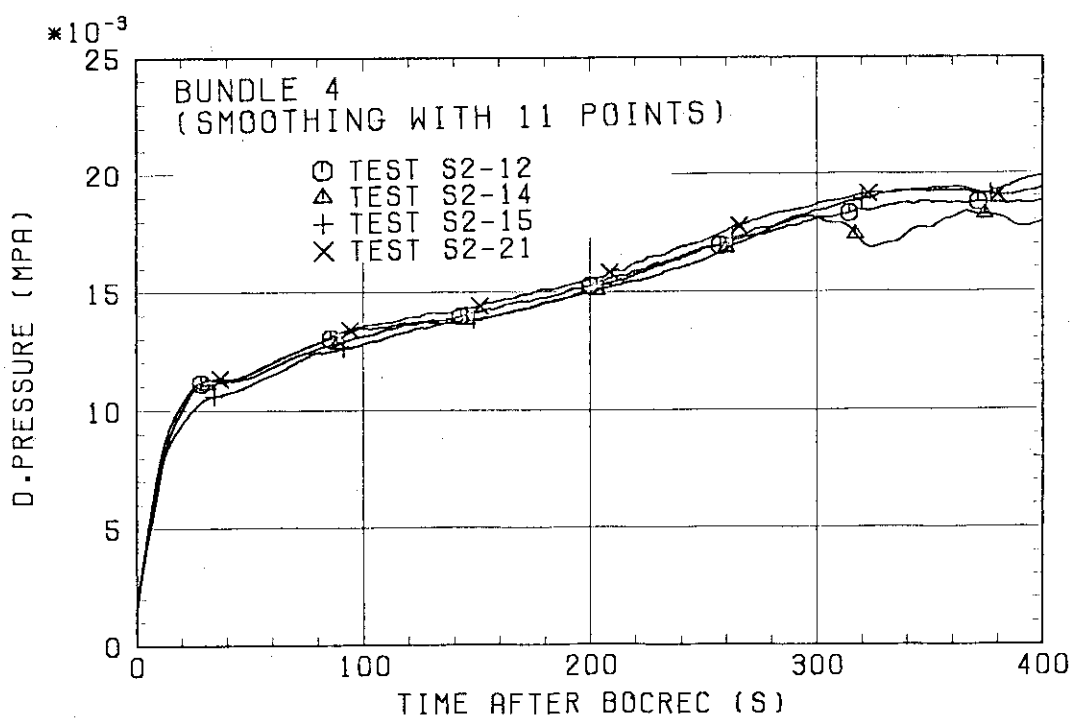
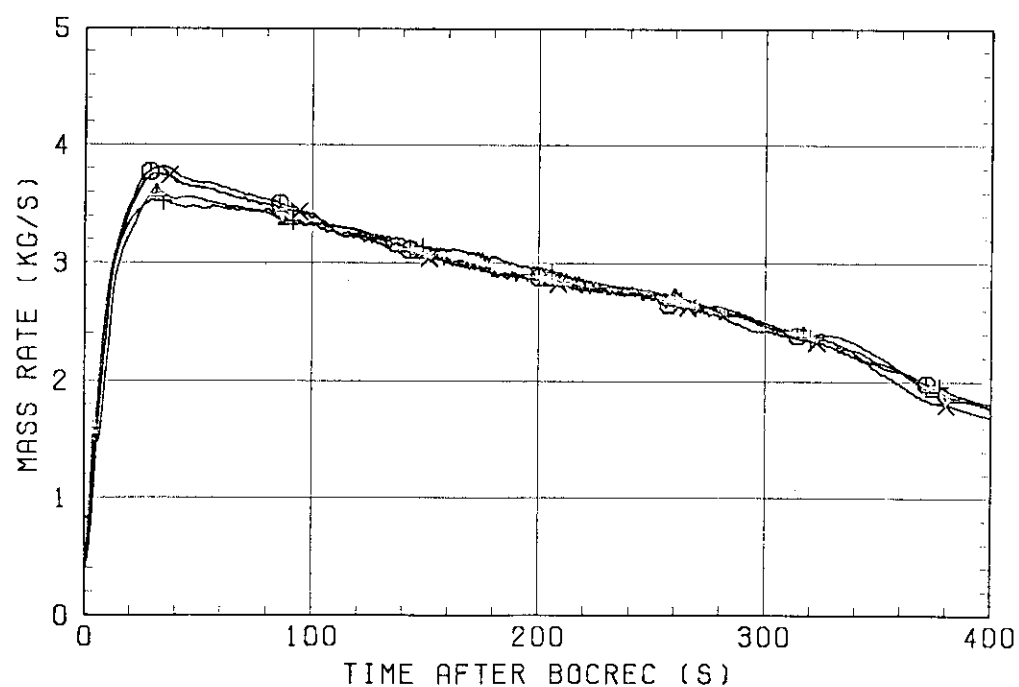
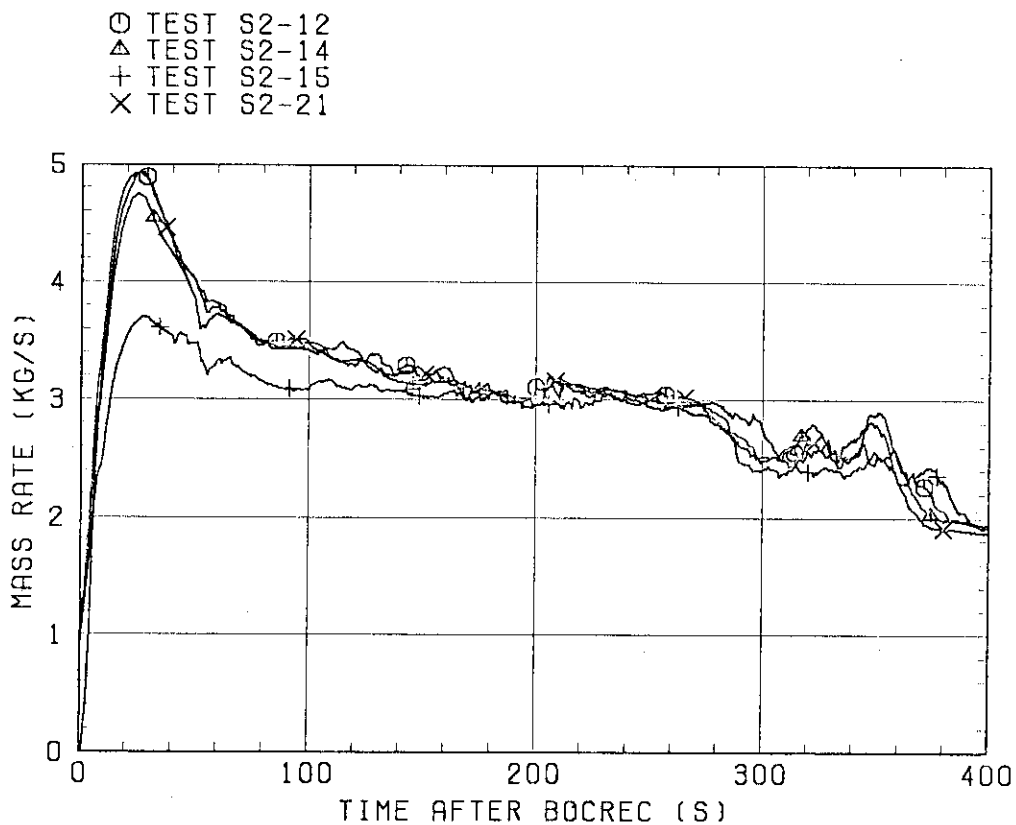


Fig. 3.11 Comparison of differential pressures across core full height in Bundle 4 among Tests S2-12, S2-14, S2-15 and S2-21



## TEST S2-14

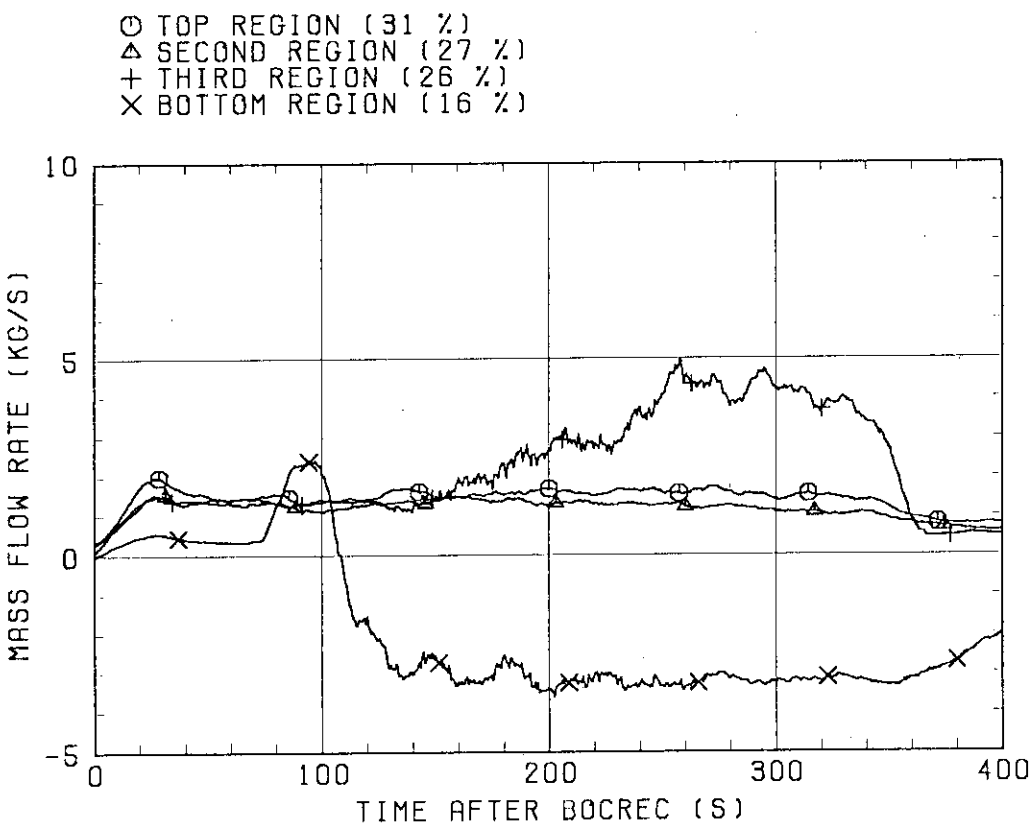


Fig. 3.14 Mass flow rates in 4 regions of hot leg in Test S2-14

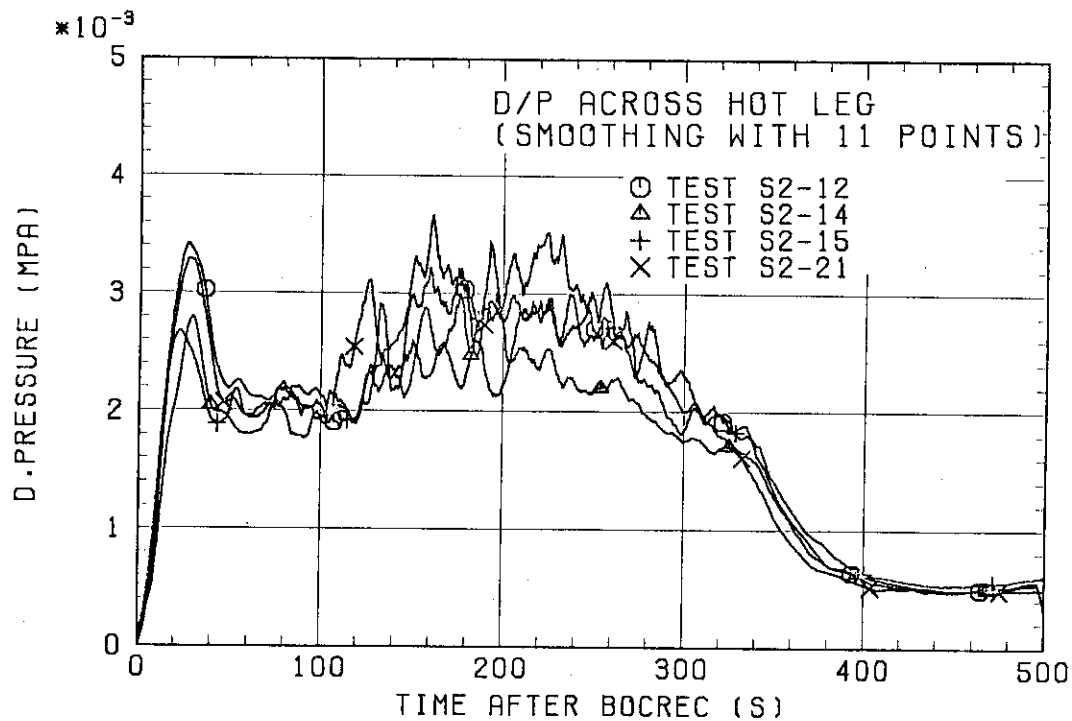


Fig. 3.15 Comparison of differential pressures across hot leg

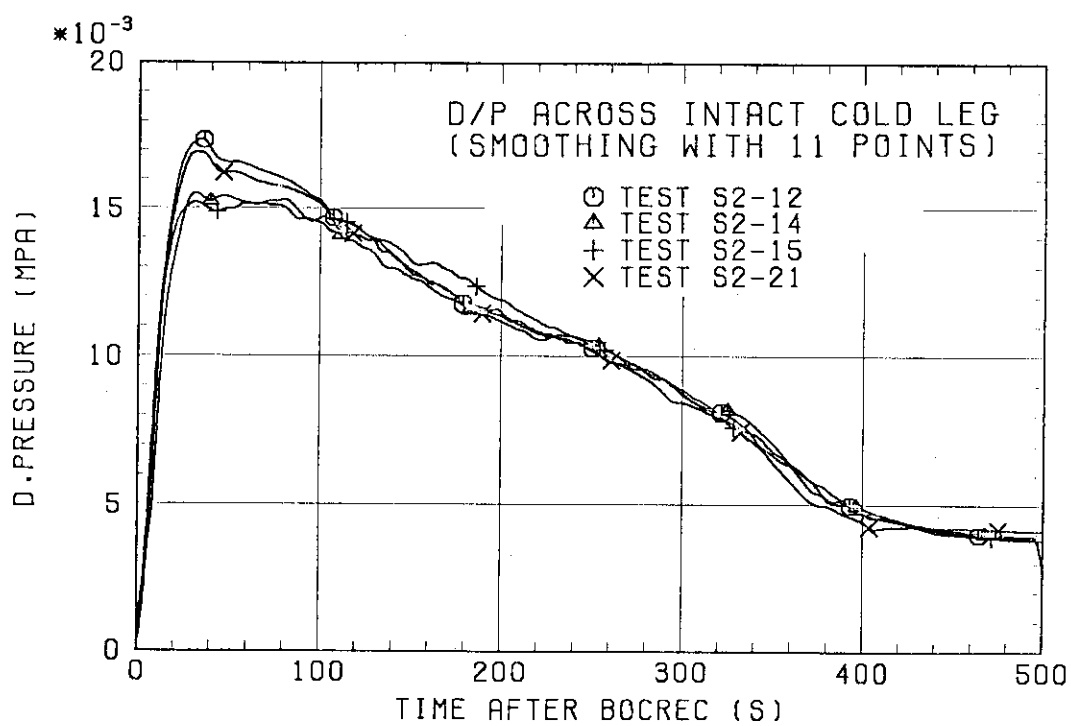


Fig. 3.16 Comparison of differential pressures across intact cold leg

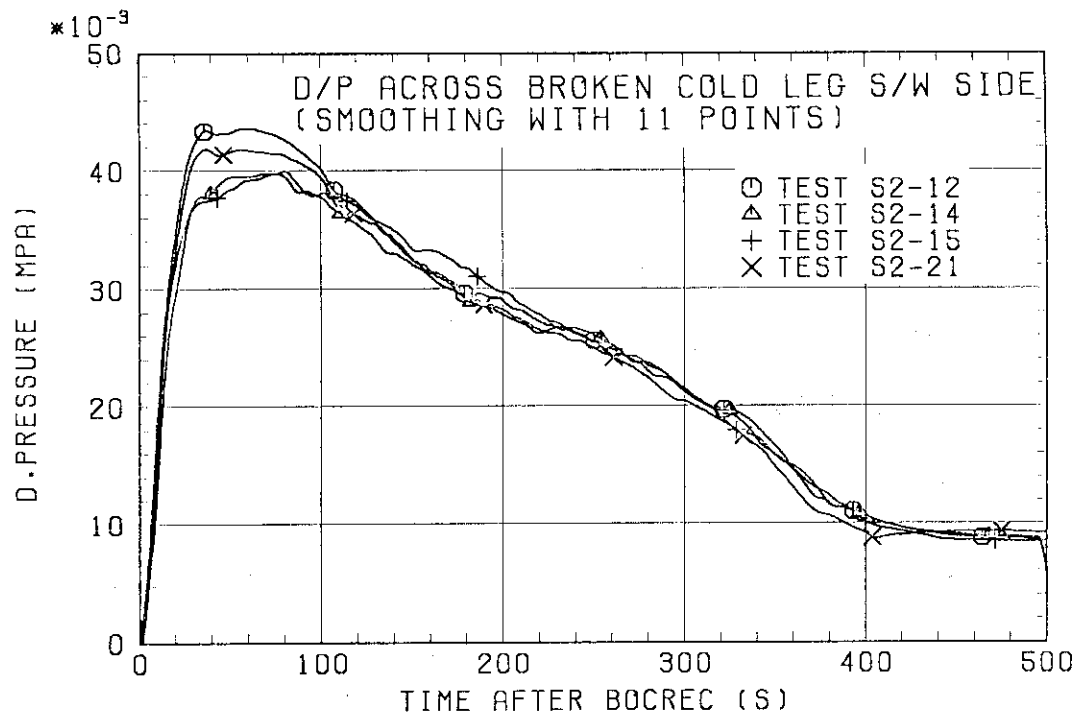


Fig. 3.17 Comparison of differential pressures across broken cold leg steam/water separator side

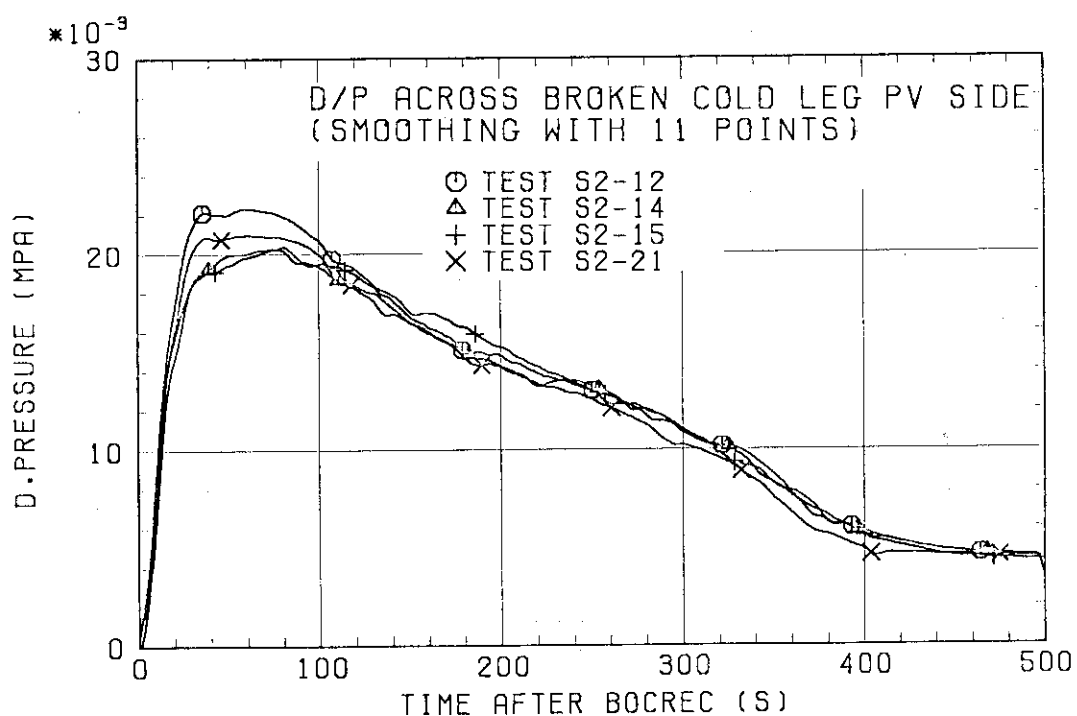


Fig. 3.18 Comparison of differential pressures across broken cold leg pressure vessel side

Line interval = 0.5 kpa

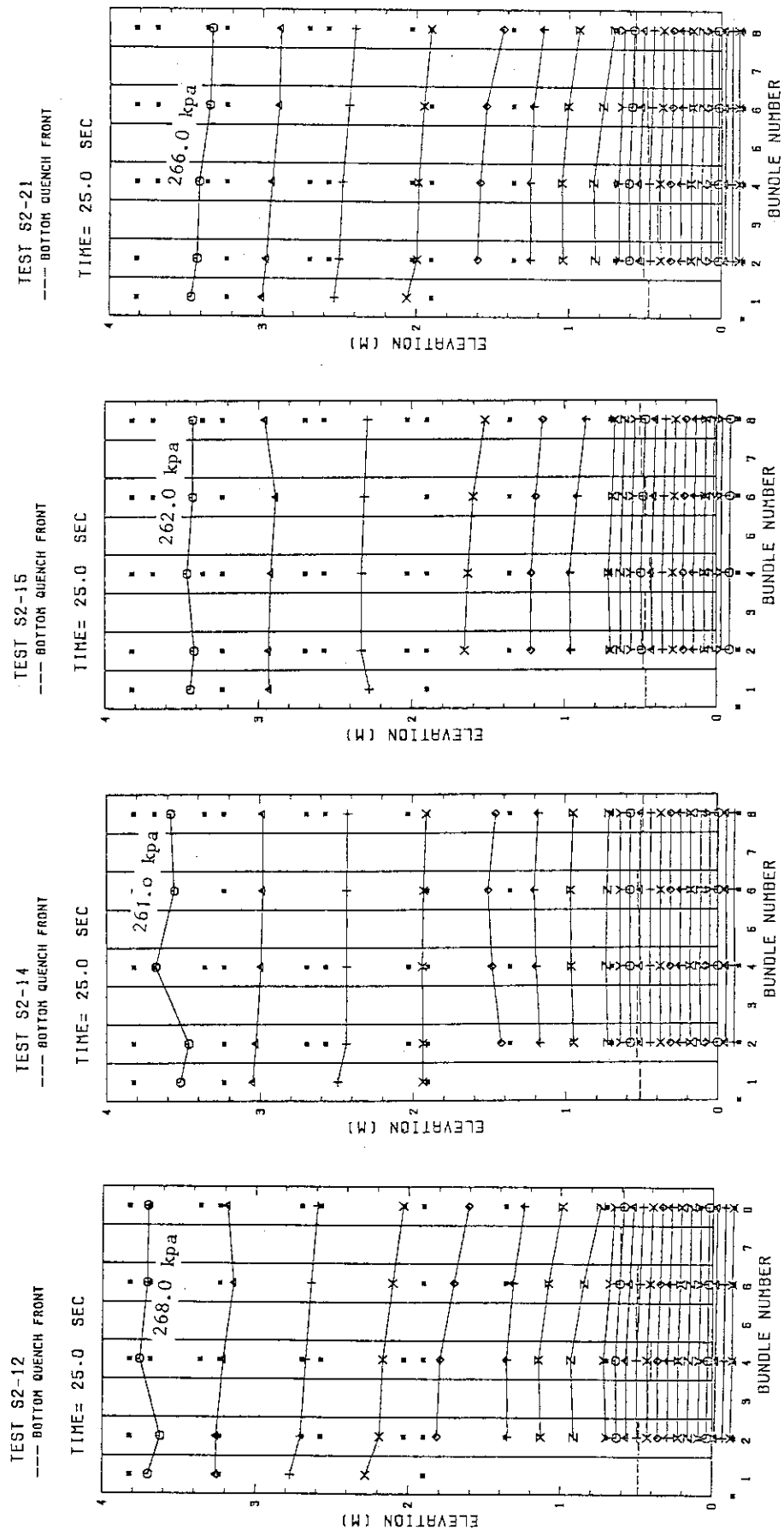


Fig. 3-19 (a) Comparison of equal pressure lines in core and bottom quench front distributions (25 s)

Line interval = 0.5 kpa

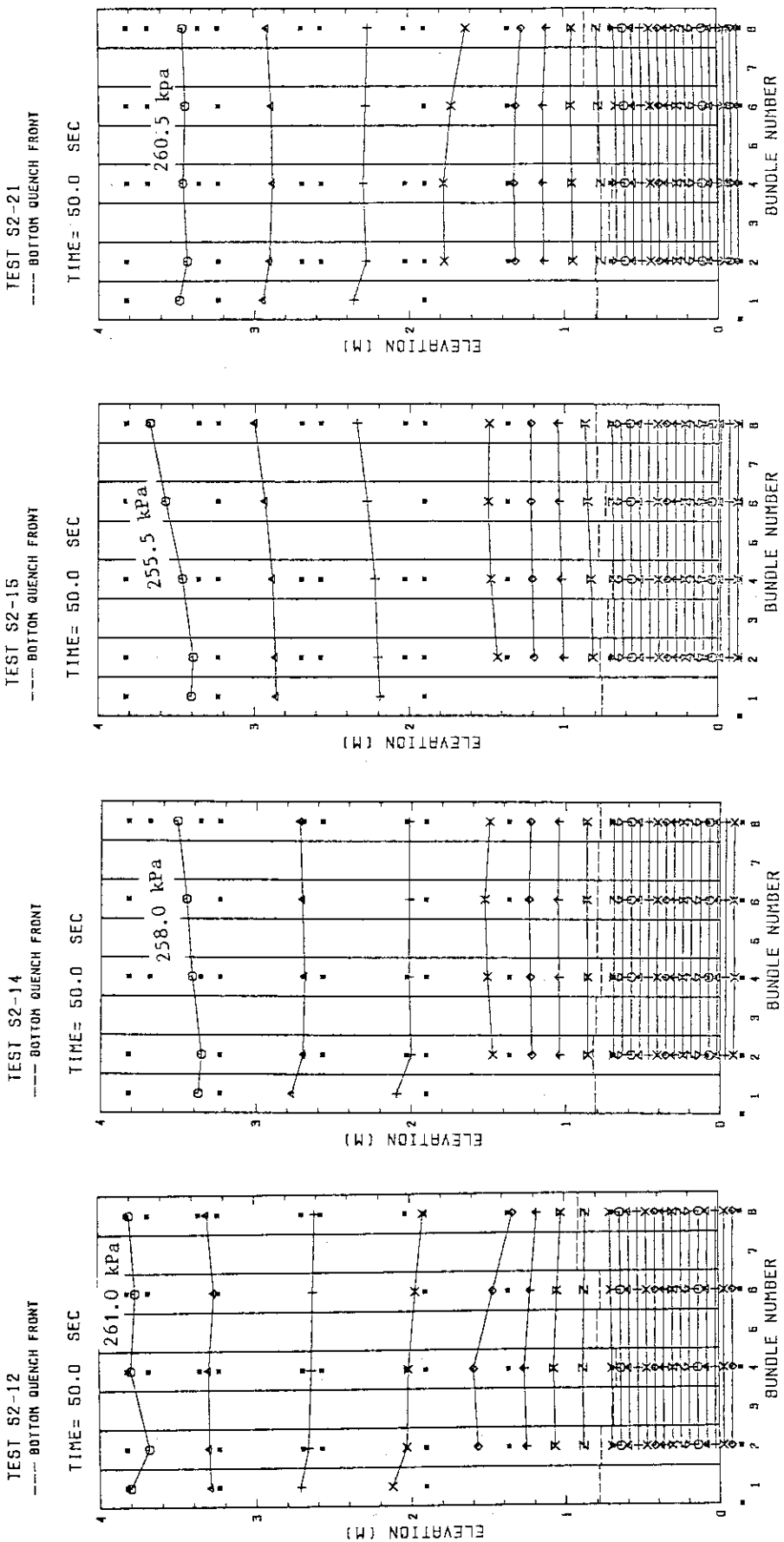


Fig. 3-19 (b) Comparison of equal pressure lines in core and bottom quench front distributions (50 s)

Line interval = 0.5 kpa

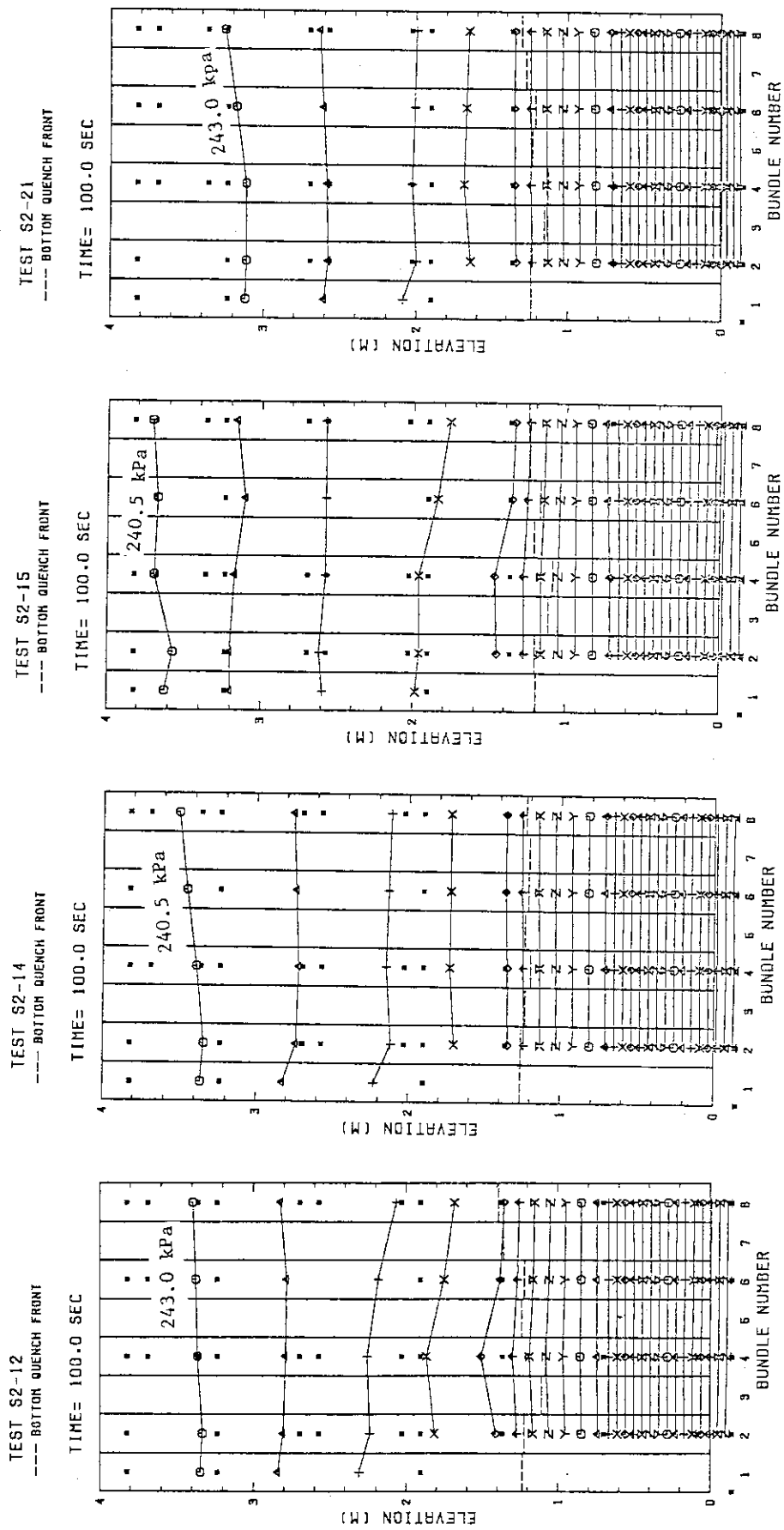


Fig. 3-19 (c) Comparison of equal pressure lines in core and bottom quench front distributions (100 s)

Line interval = 0.5 kpa

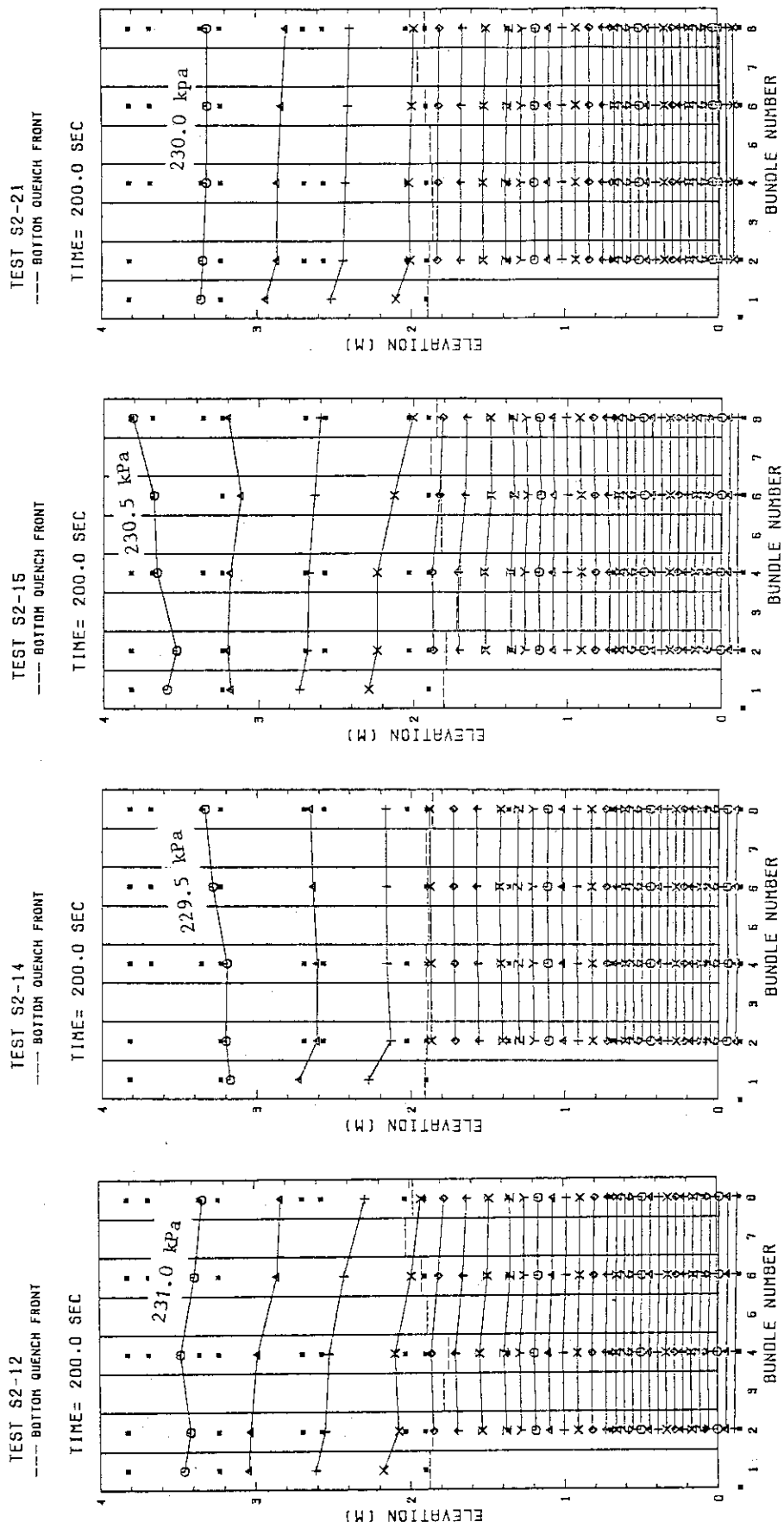


Fig. 3-19 (d) Comparison of equal pressure lines in core and bottom quench front distributions (200 s)

Line interval = 0.5 kpa

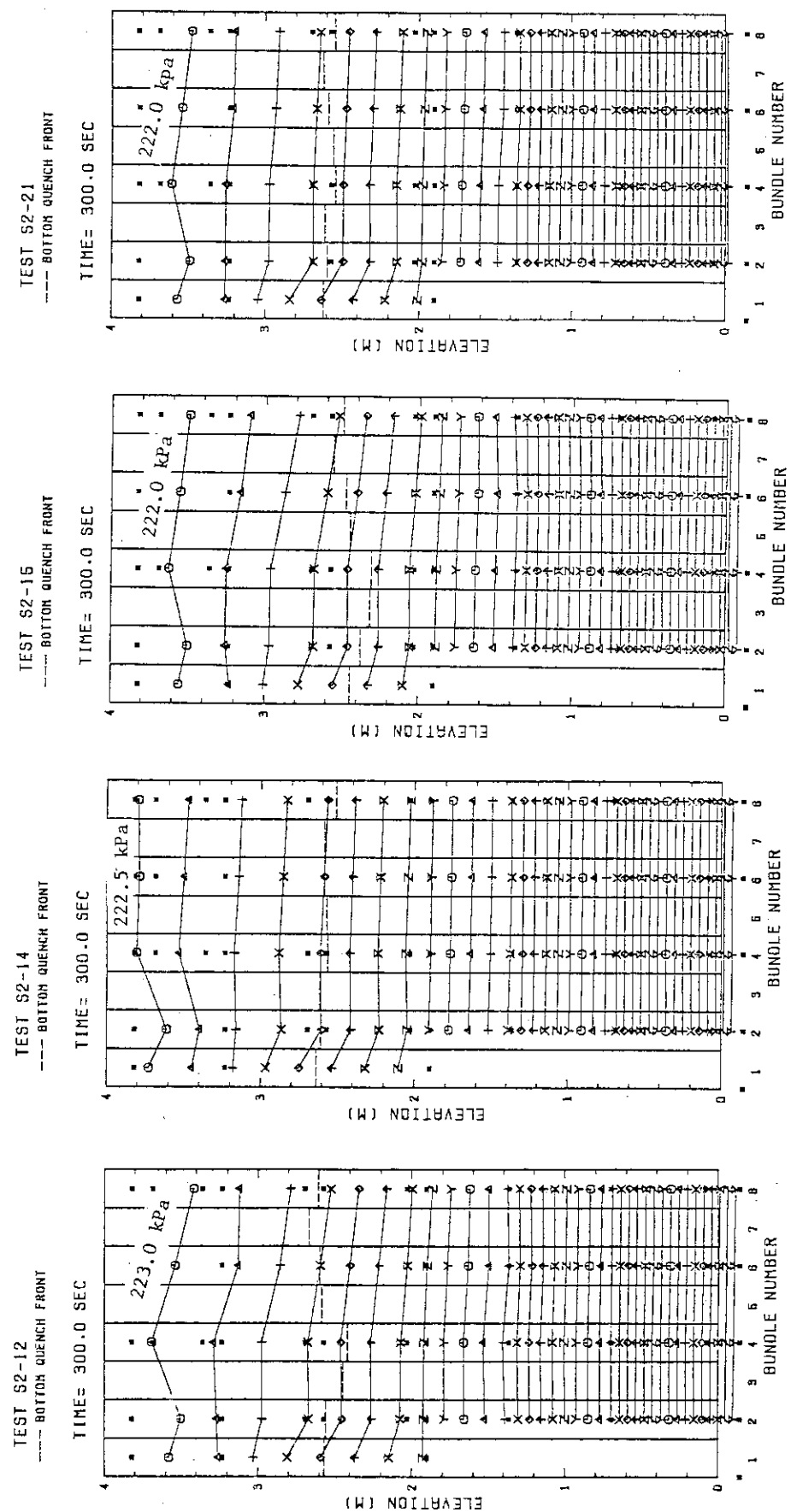


Fig. 3-19 (e) Comparison of equal pressure lines in core and bottom quench front distributions (300 s)

Line interval = 0.5 kPa

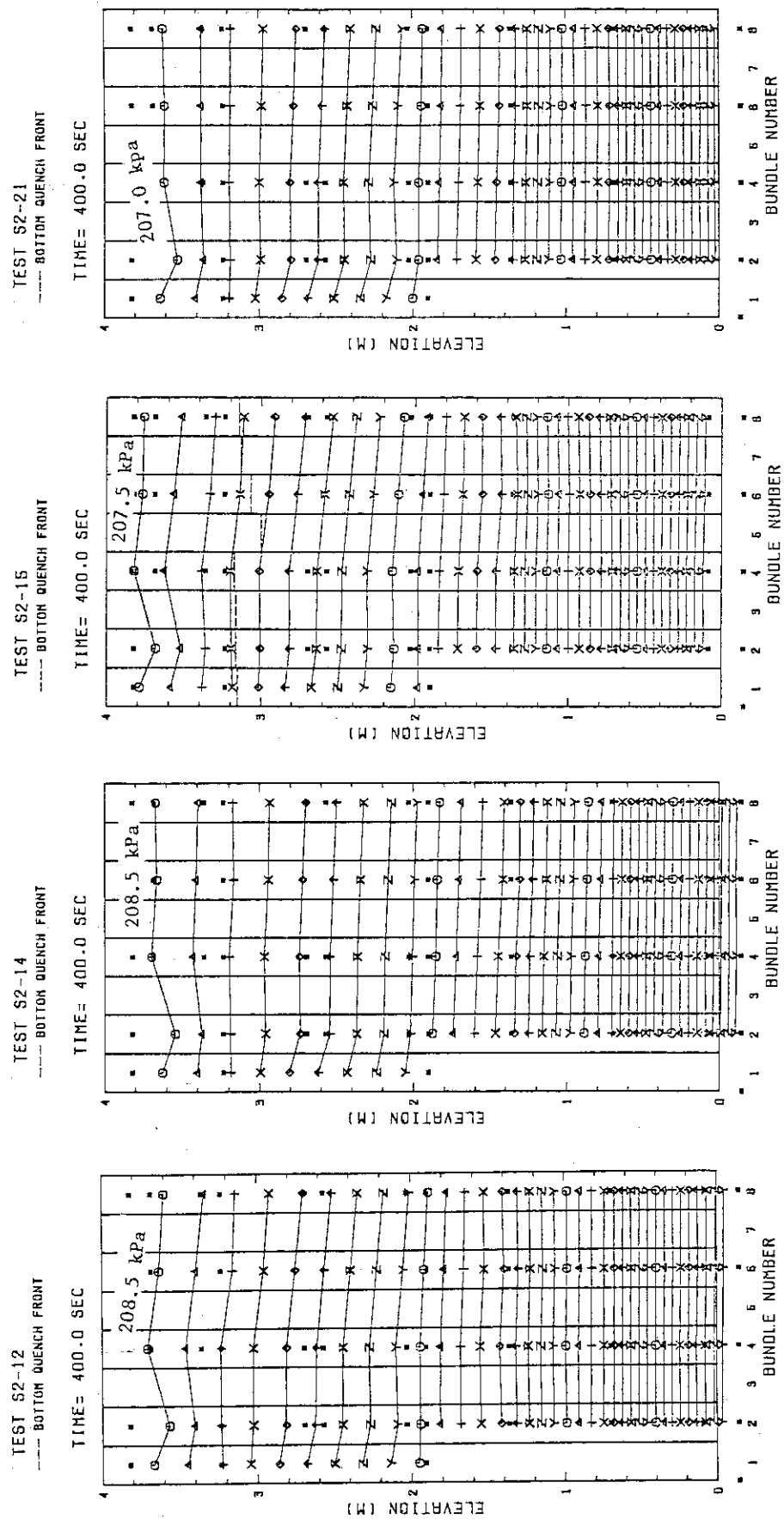


Fig. 3-19 (f) Comparison of equal pressure lines in core and bottom quench front distributions (400 s)

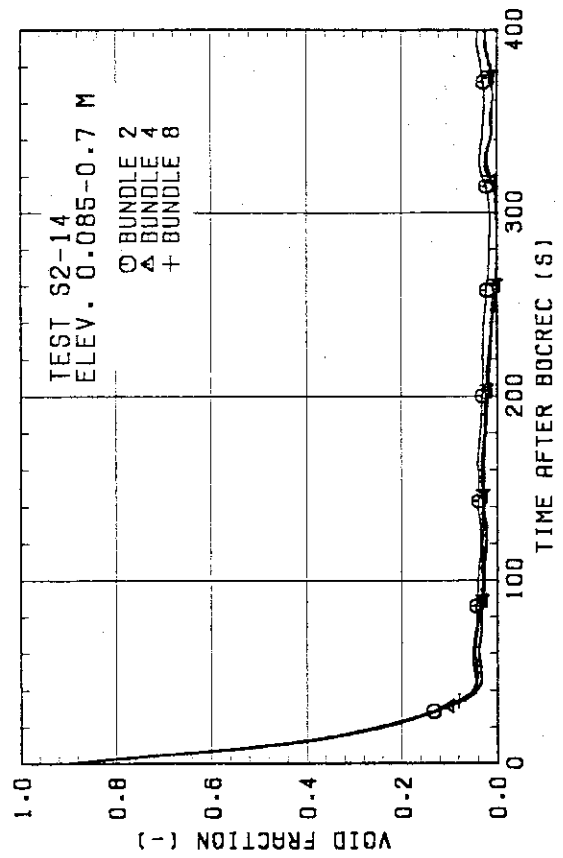
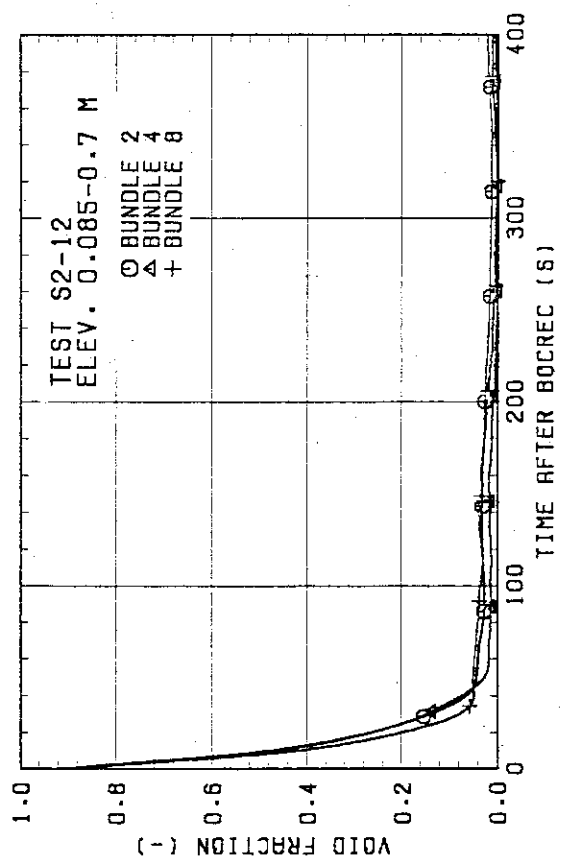
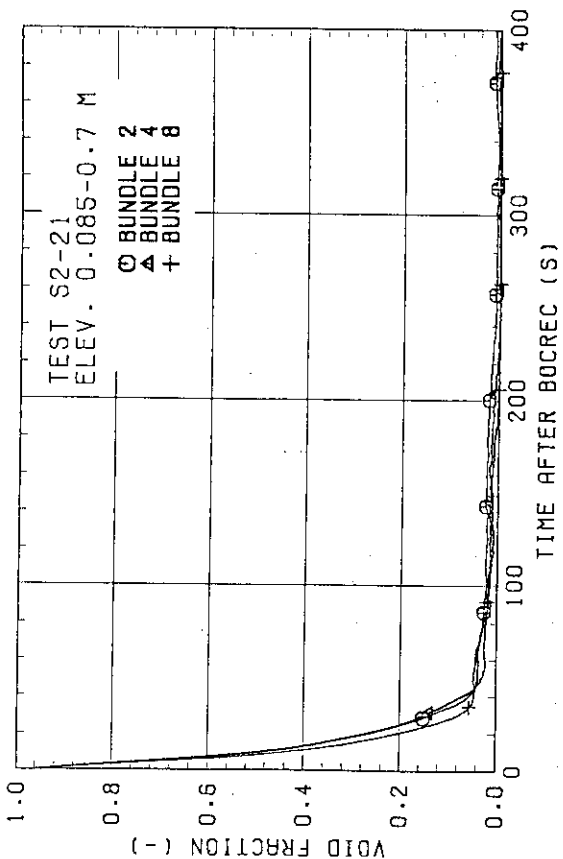
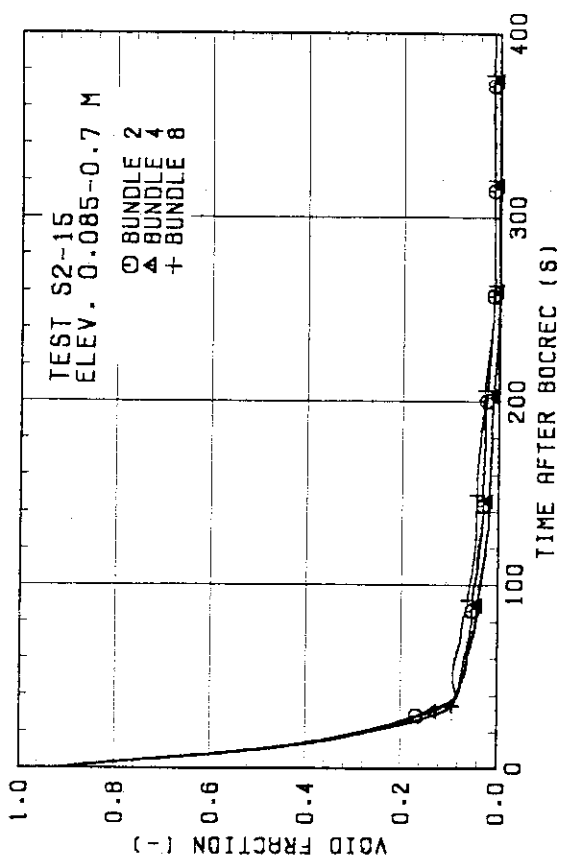


Fig. 3-20 (a) Comparison of void fraction in core (0.085-0.7 m)

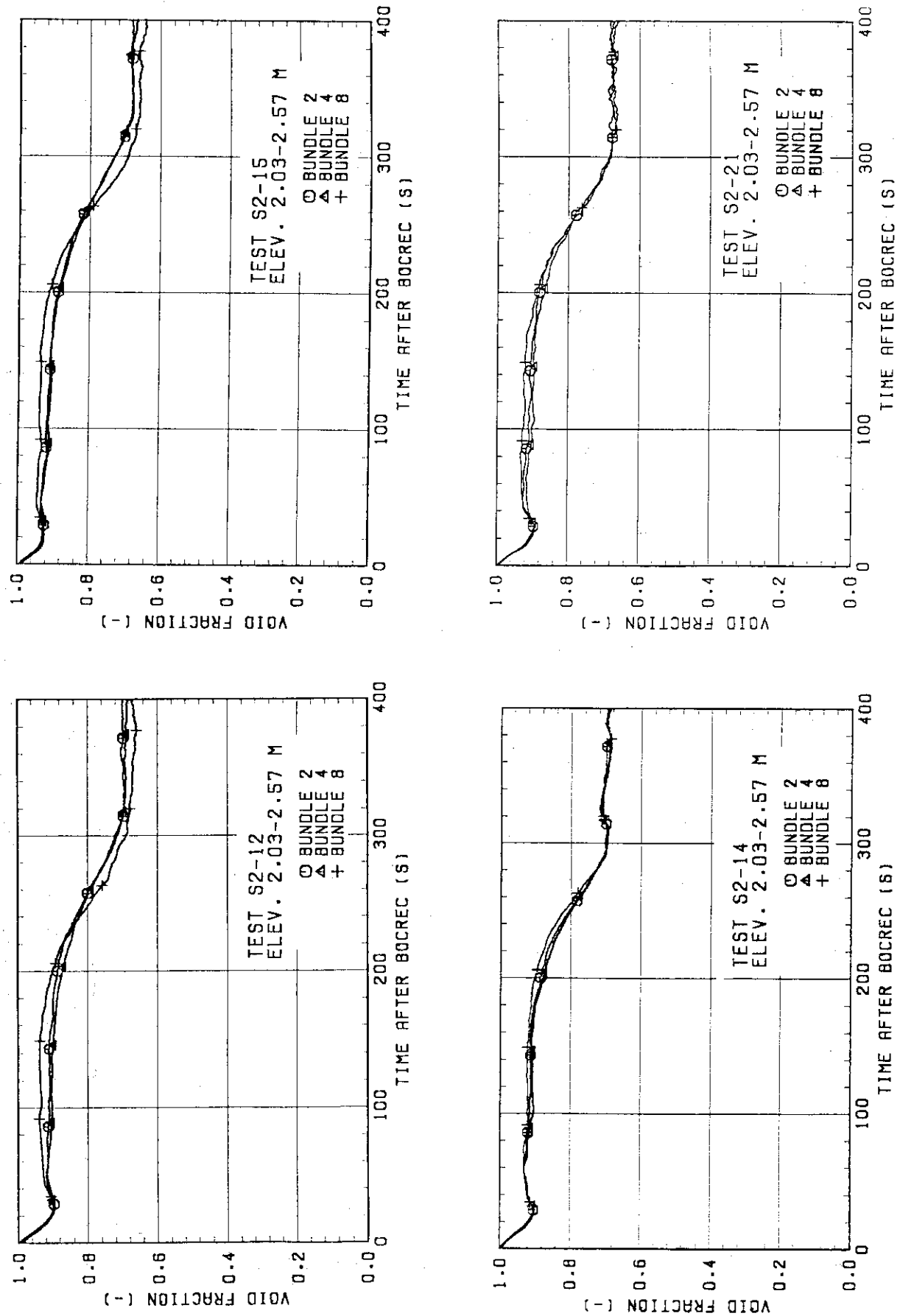


Fig. 3-20 (b) Comparison of void fraction in core (2.03-2.57 m)

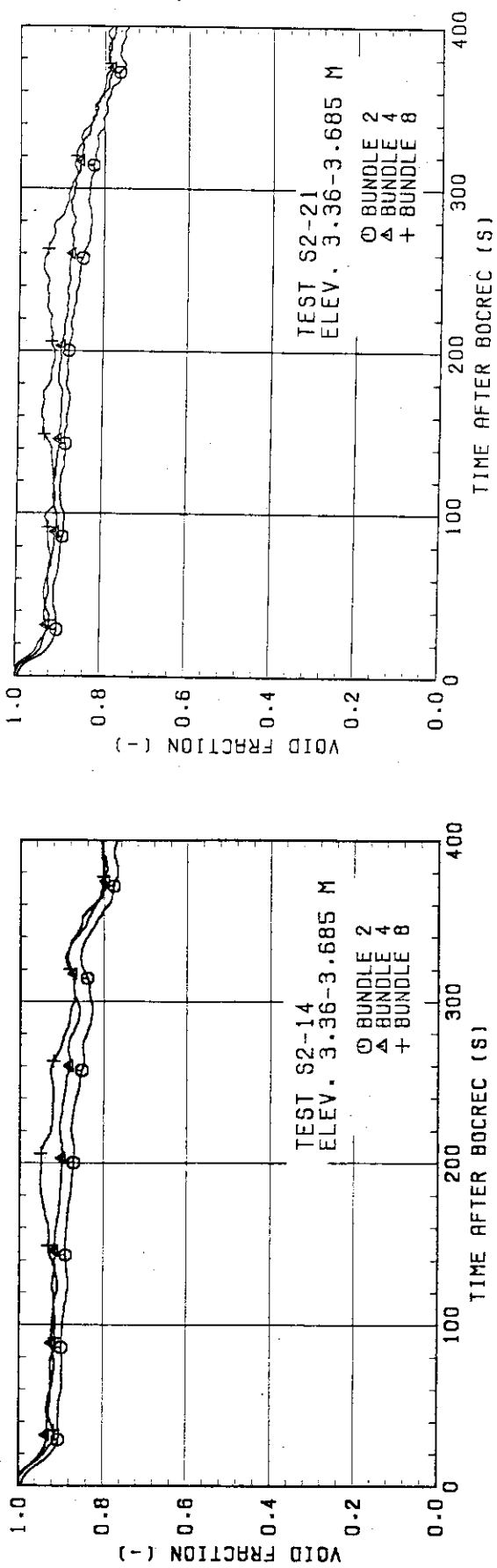
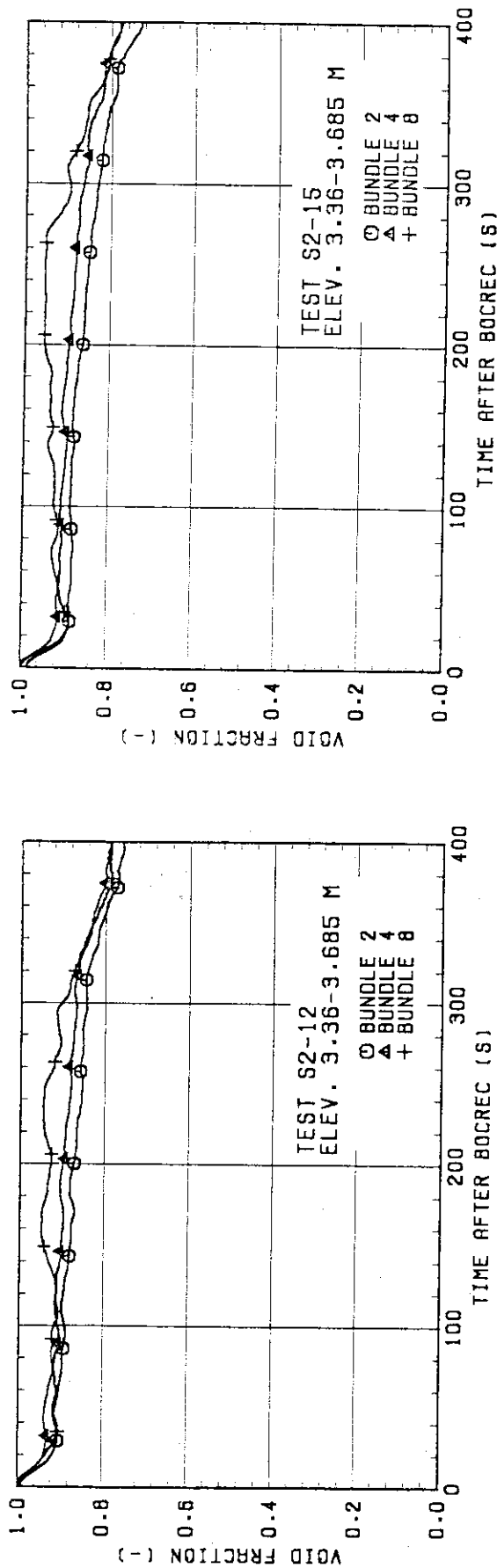


Fig. 3-20 (c) Comparison of void fraction in core (3.36-3.685 m)

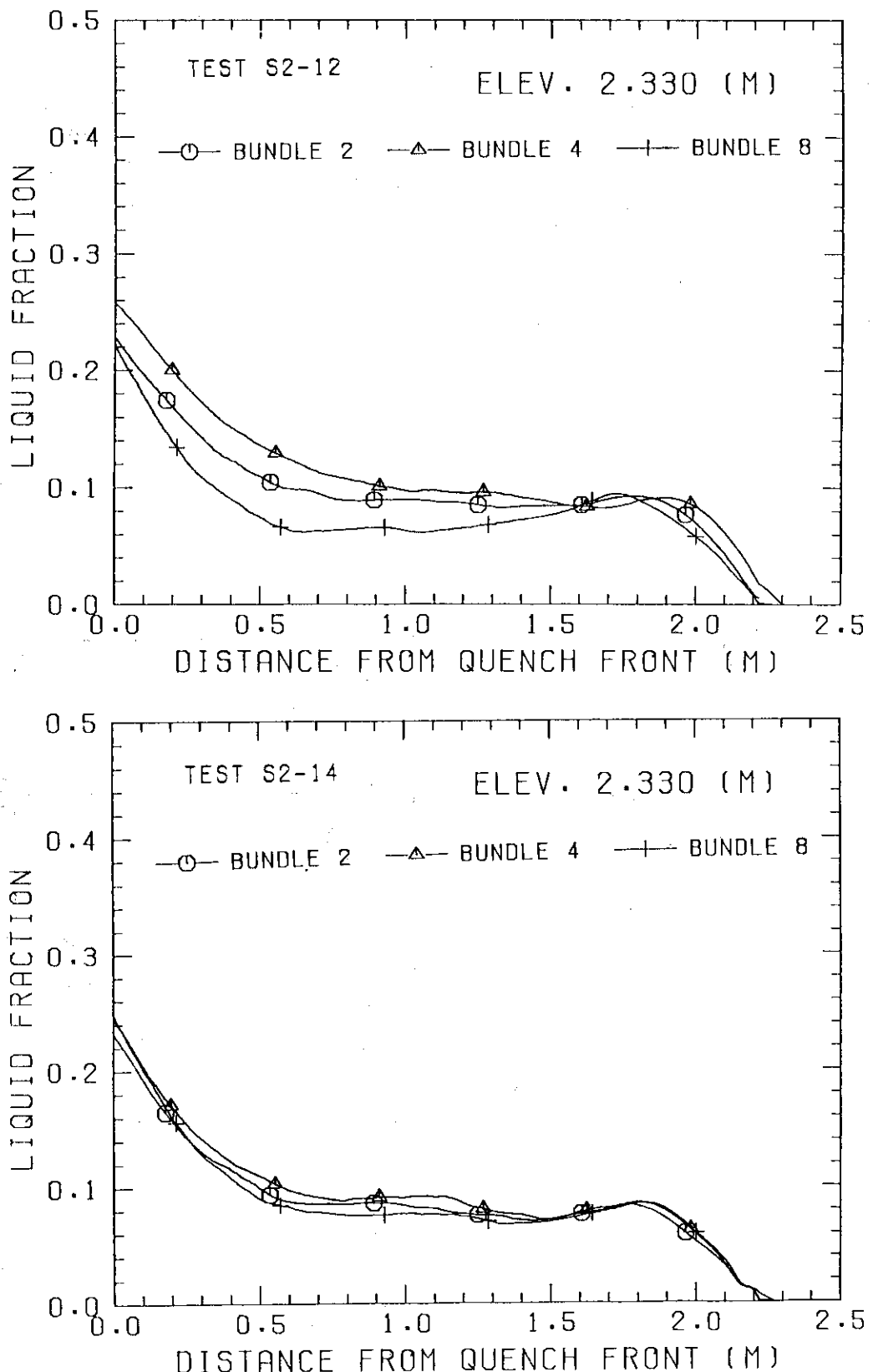


Fig. 3.21 Comparisons of liquid fractions vs. distance from bottom quench front at 2.33 m among Bundles 2, 4 and 8

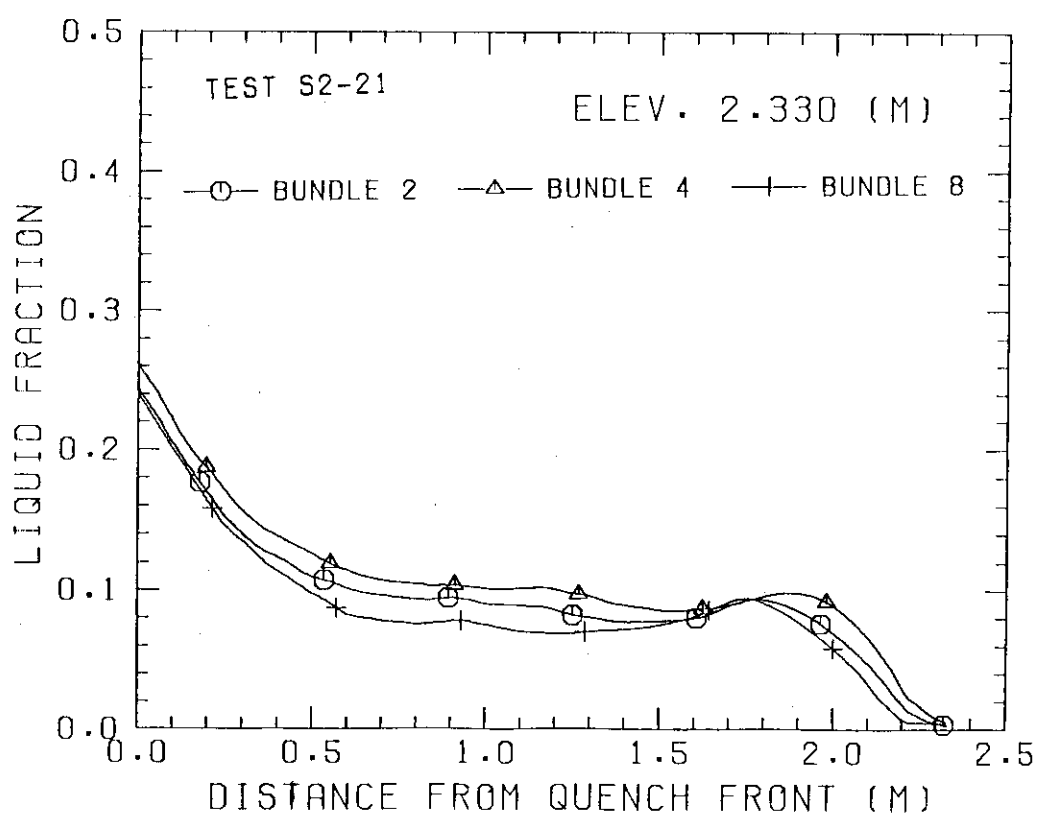
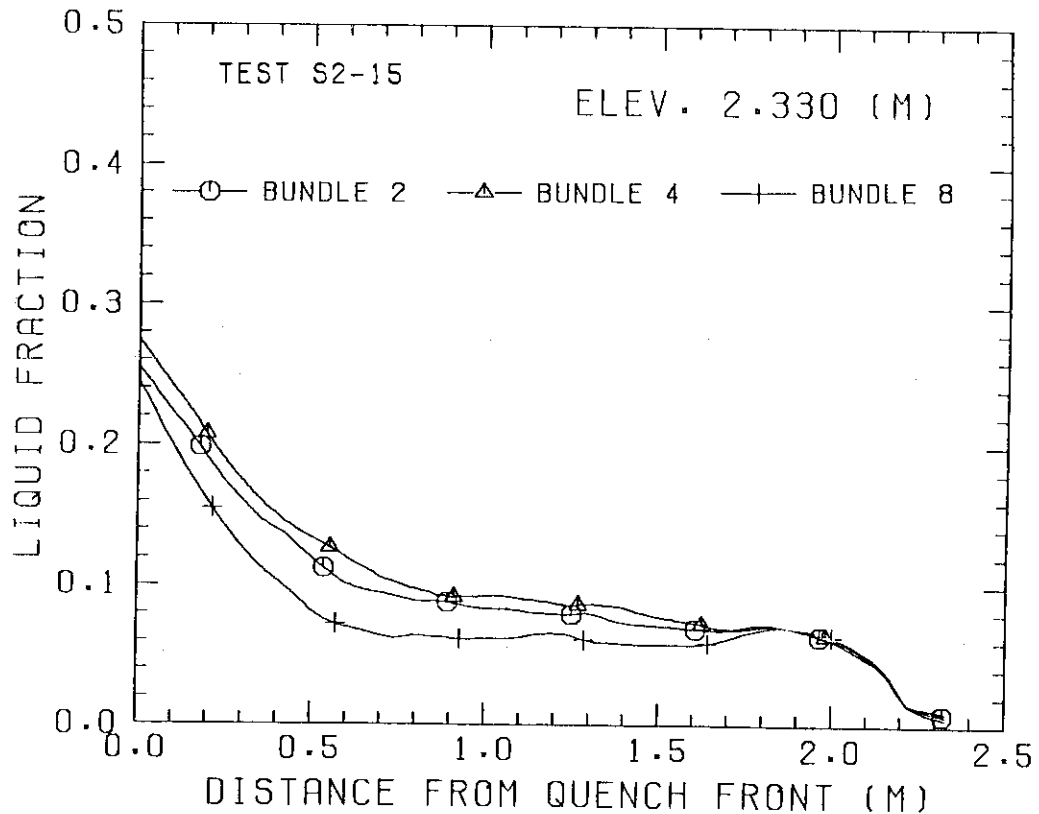
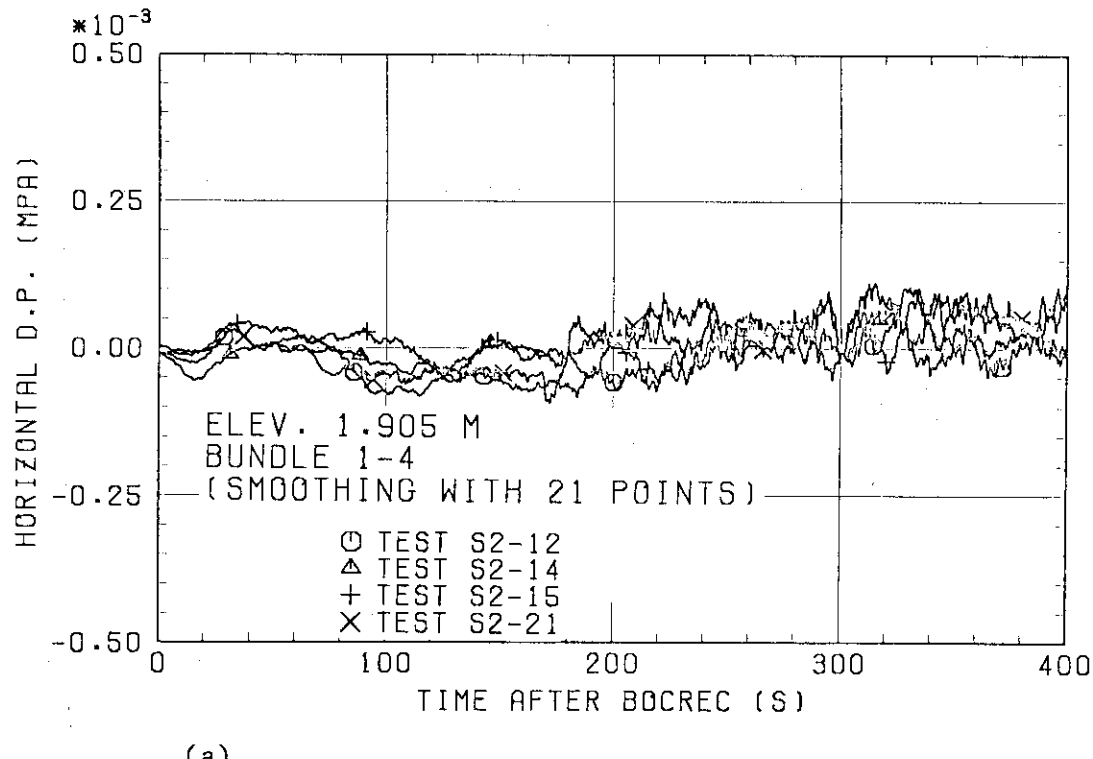
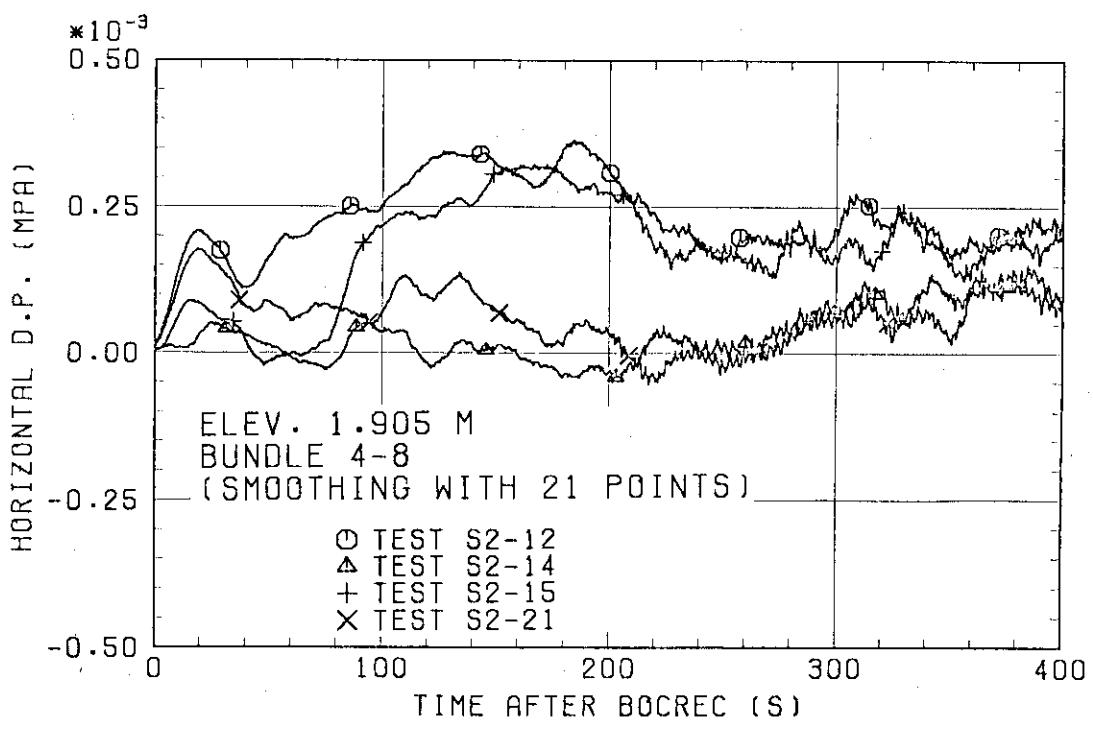


Fig. 3.21 (continue)

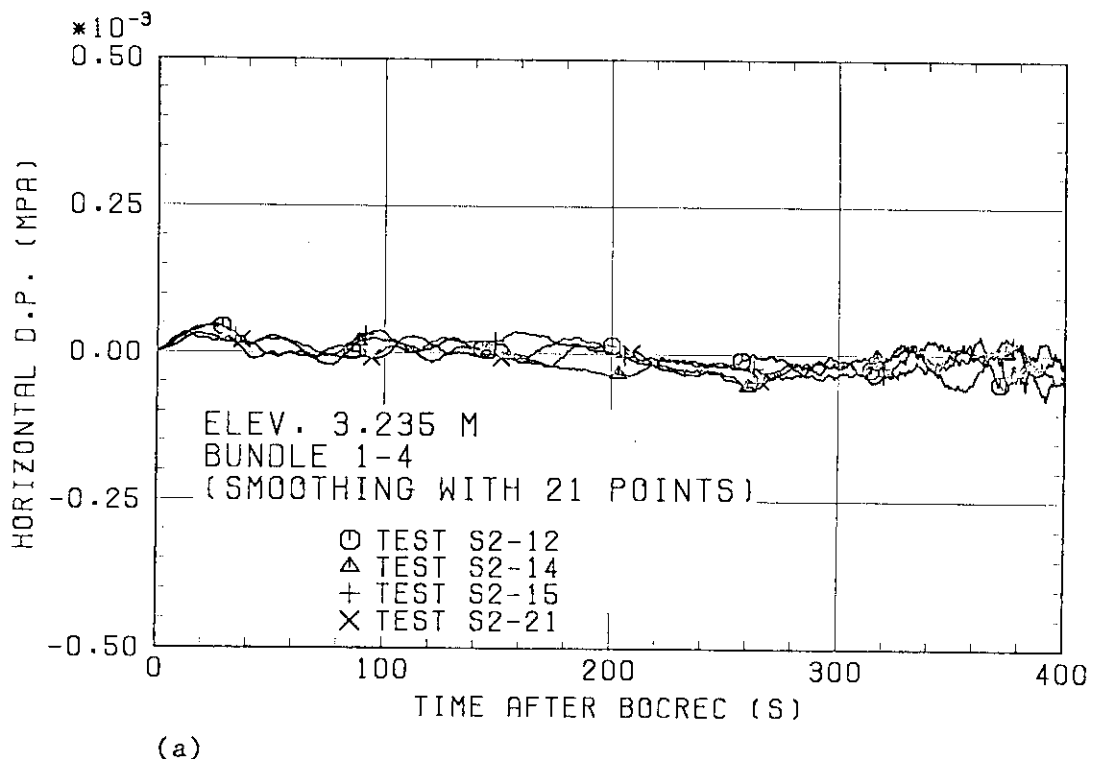


(a)

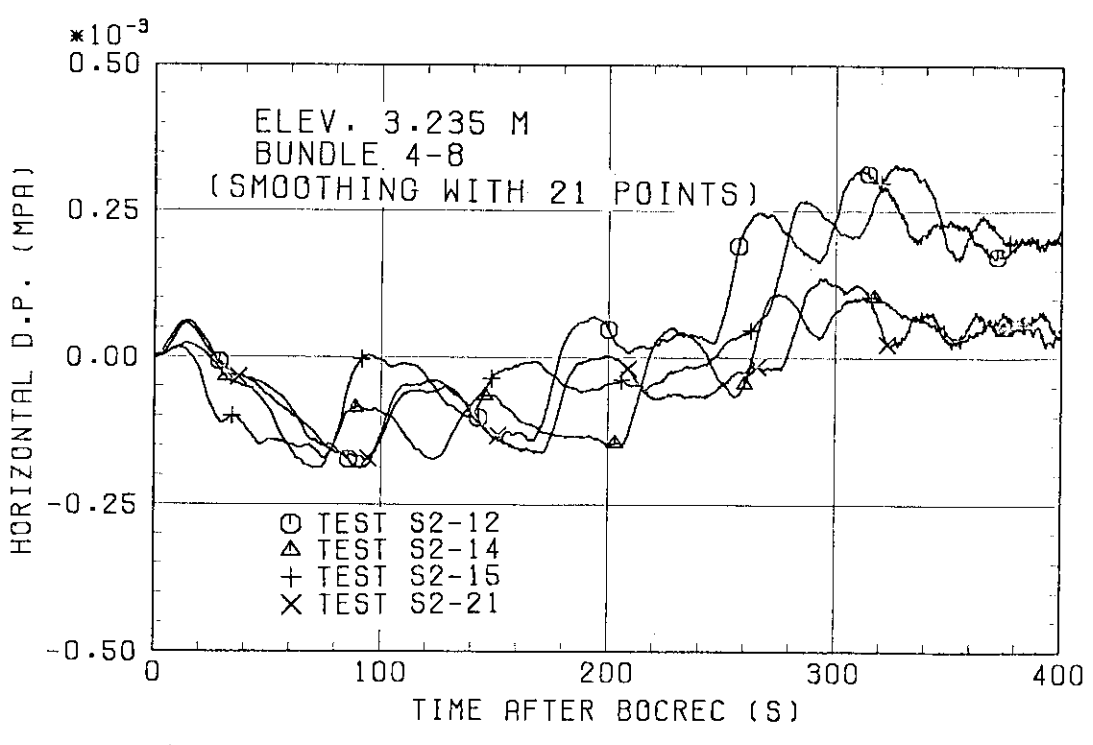


(b)

Fig. 3.22 Comparisons of horizontal differential pressures at 1.905 m

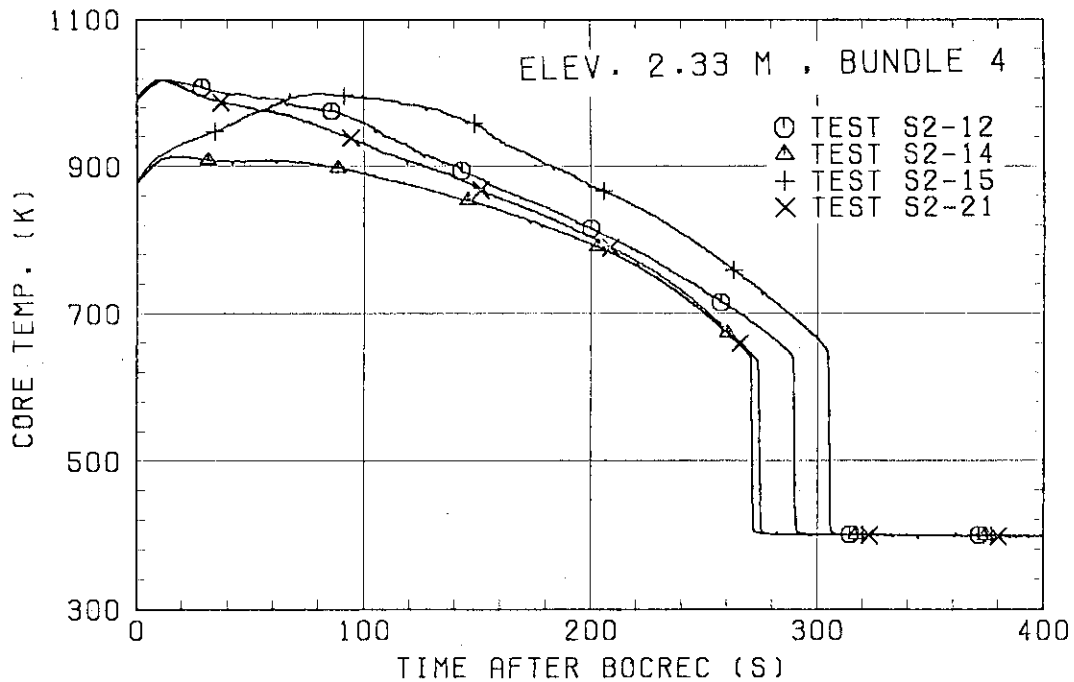


(a)

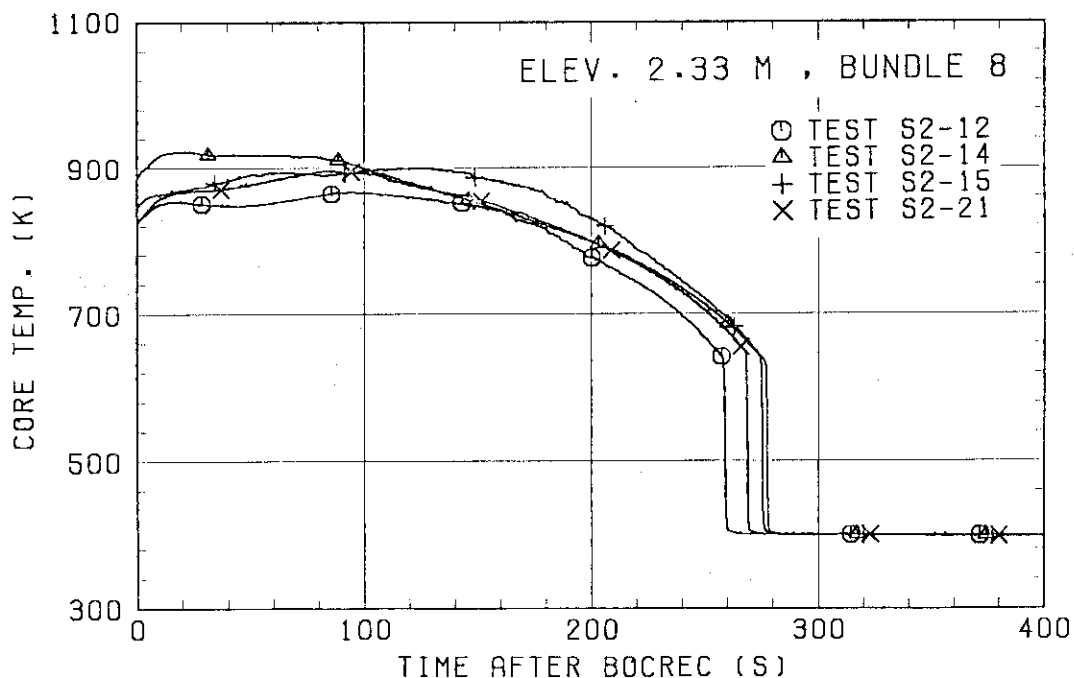


(b)

Fig. 3.23 Comparisons of horizontal differential pressures at 3.235 m



(a)



(b)

Fig. 3.24 Comparisons of heater rod surface temperatures at 2.33 m in Bundles 4 and 8

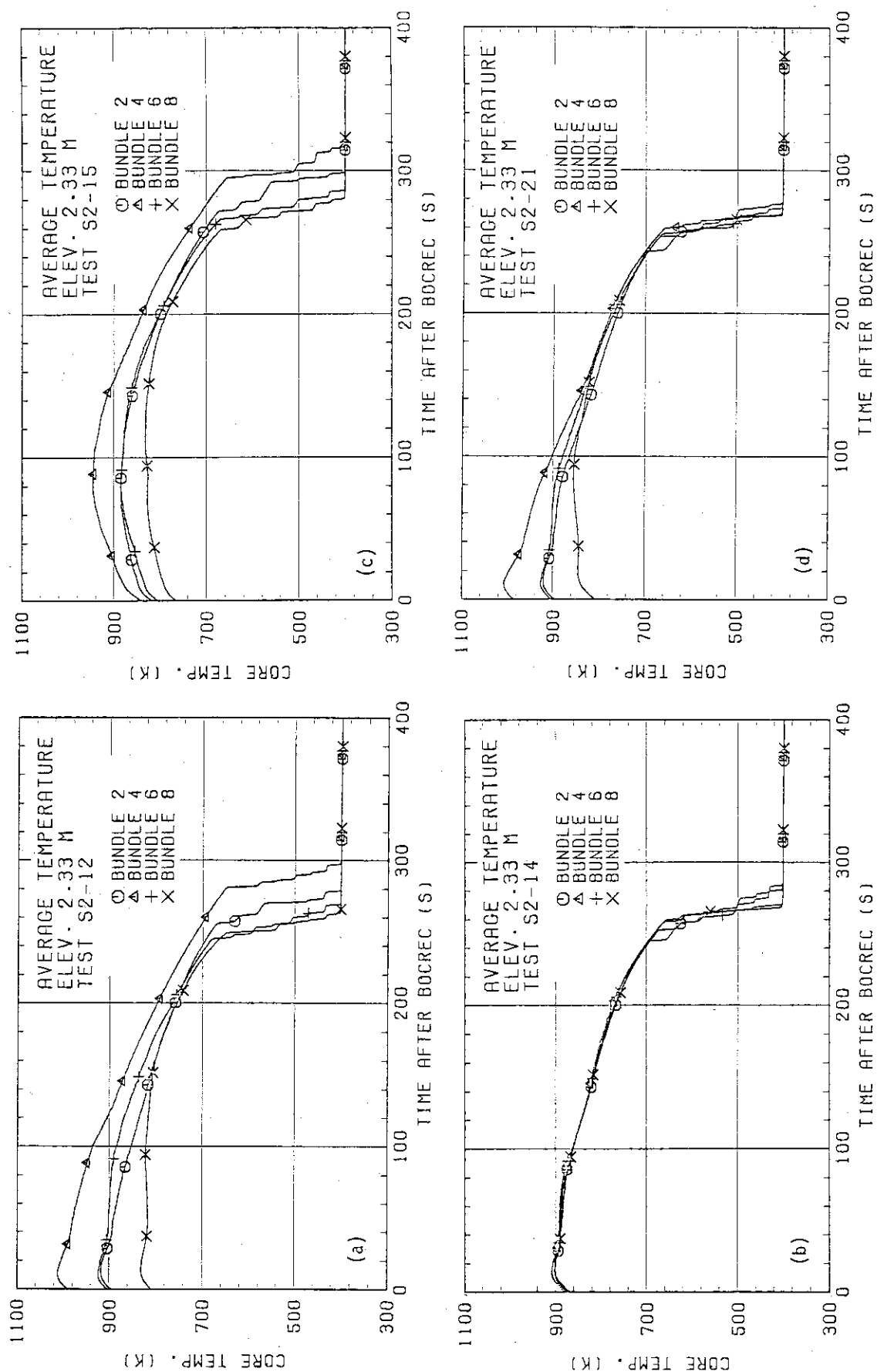


Fig. 3.25 Comparisons of average heater rod surface temperatures among Bundles 2, 4, 6 and 8

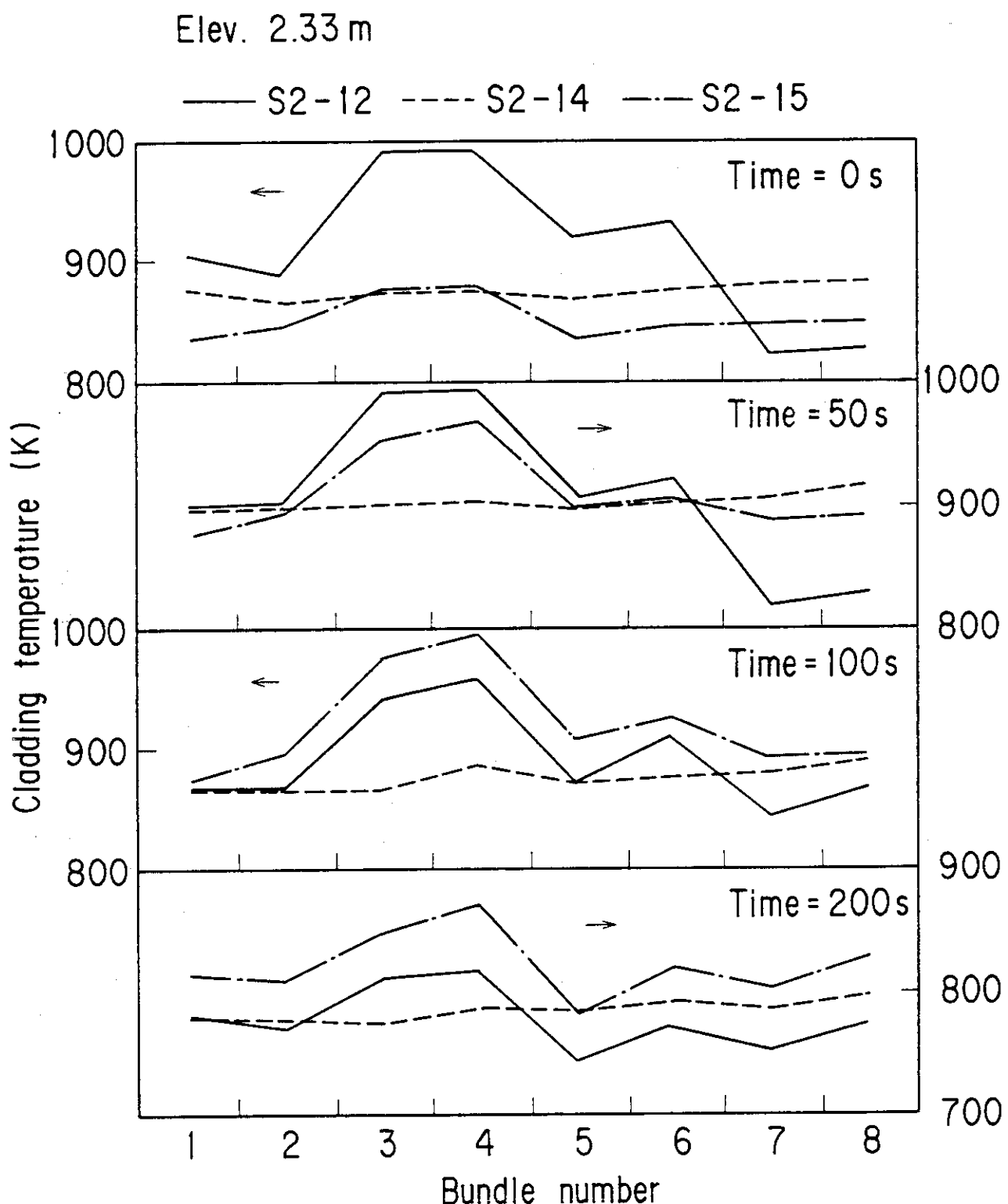


Fig. 3.26 Comparisons of radial temperature distribution at 2.33 m among Tests S2-12, S2-14 and S2-15

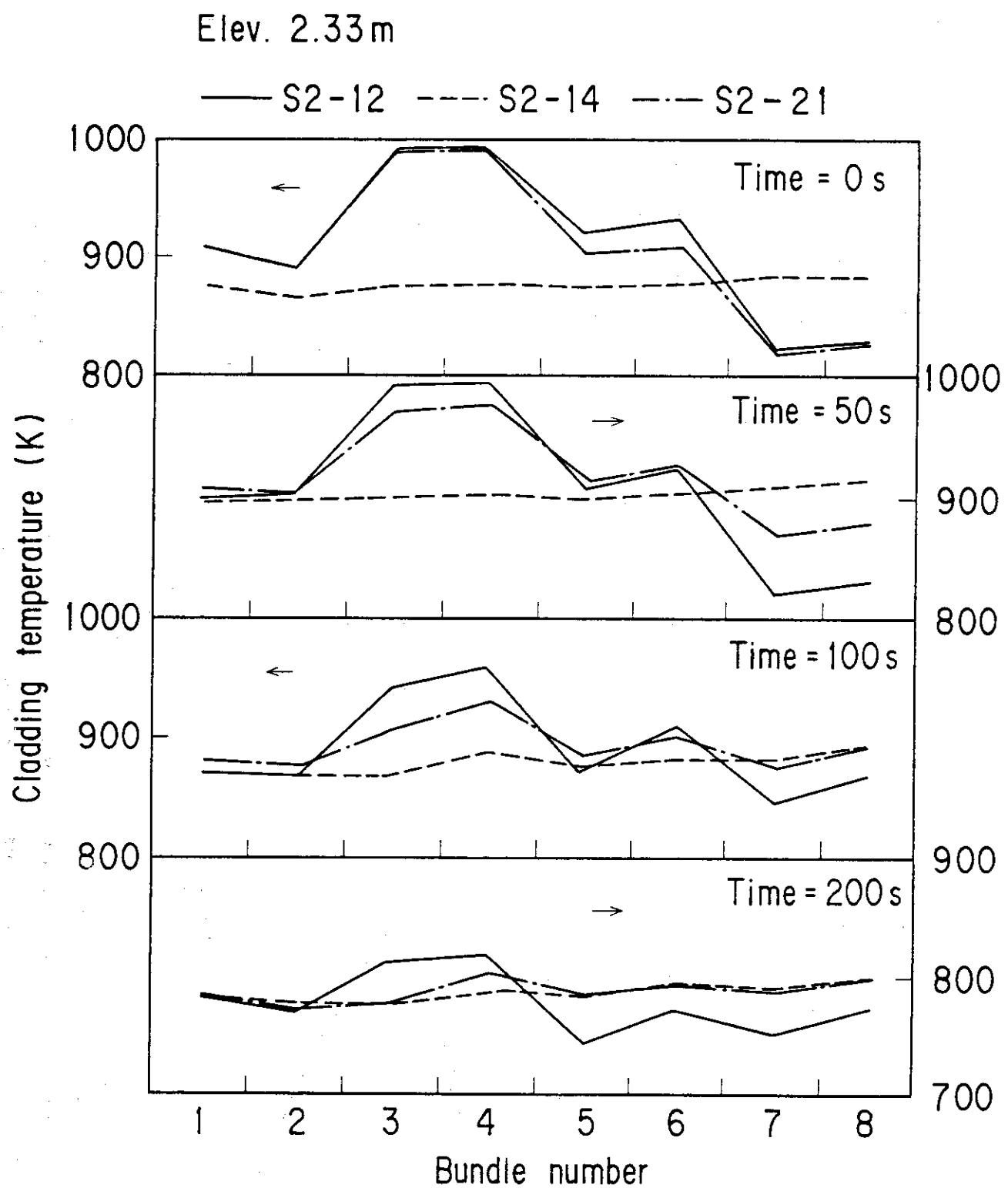


Fig. 3.27 Comparisons of radial temperature distribution at 2.33 m among Tests S2-12, S2-14 and S2-21

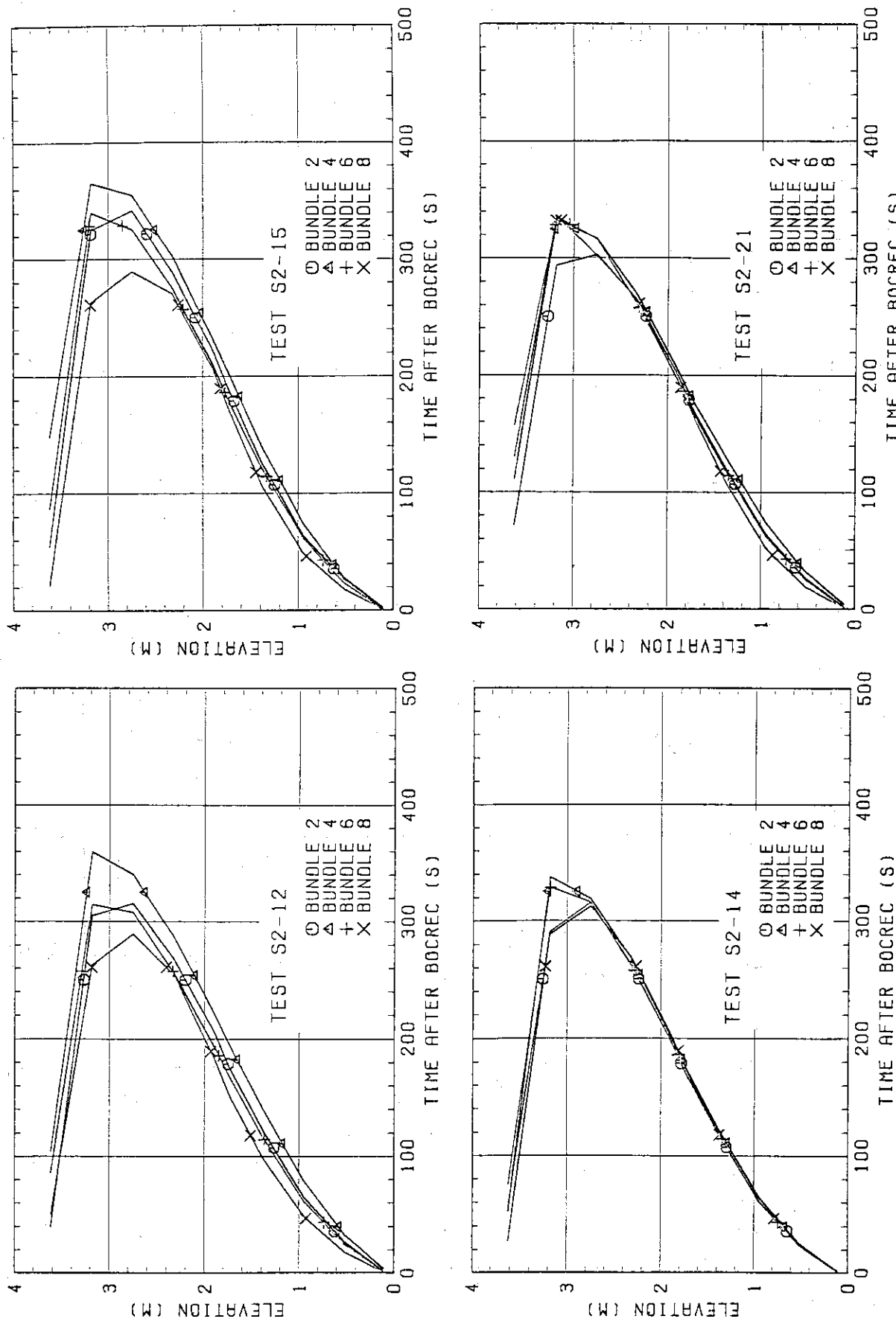


Fig. 3.28 Comparisons of quench front propagation profiles among Bundles  
2, 4, 6 and 8 for each of Test S2-12, S2-14, S2-15 and S2-21

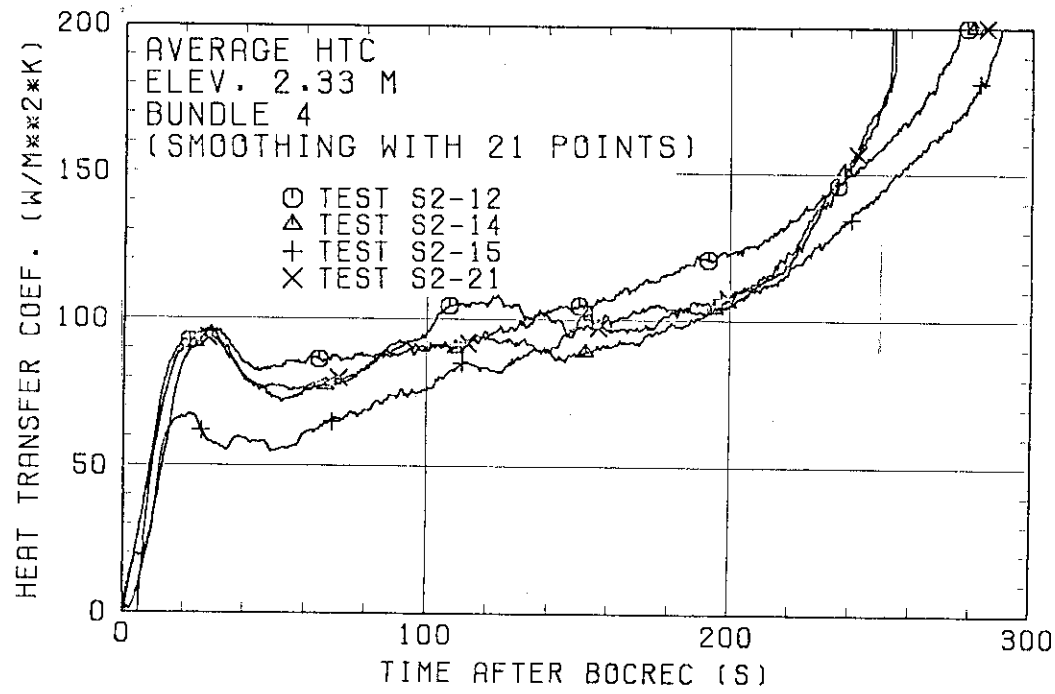


Fig. 3.29 Comparison of average heat transfer coefficients at 2.33 m in Bundle 4

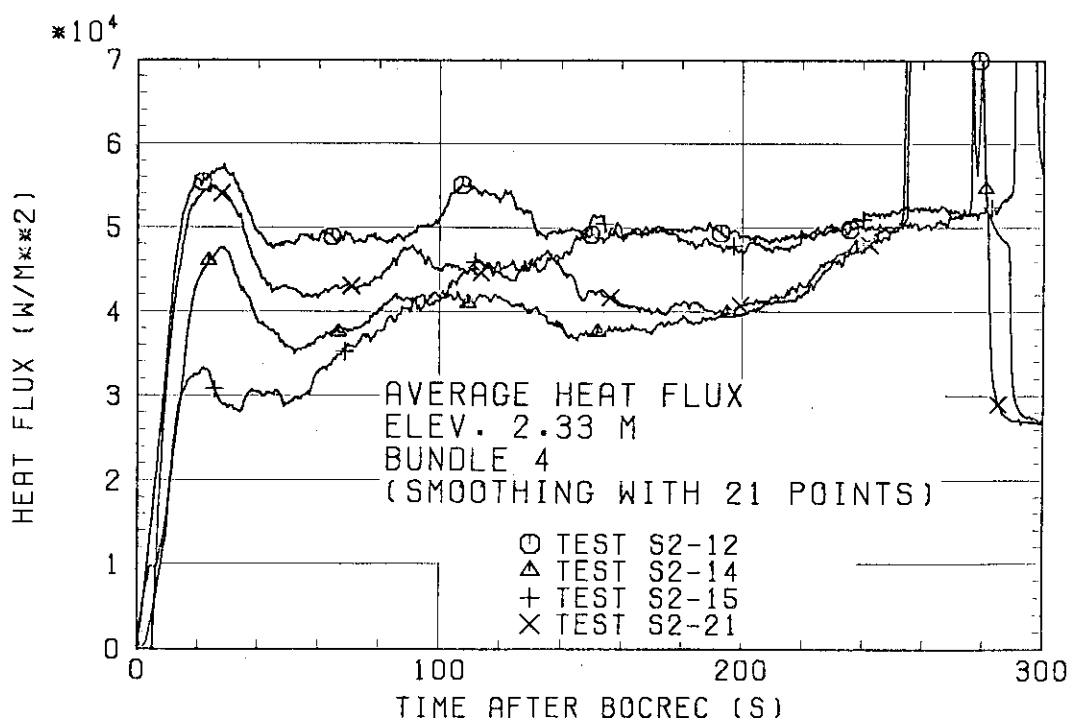


Fig. 3.30 Comparison of average heat fluxes at 2.33 m in Bundle 4

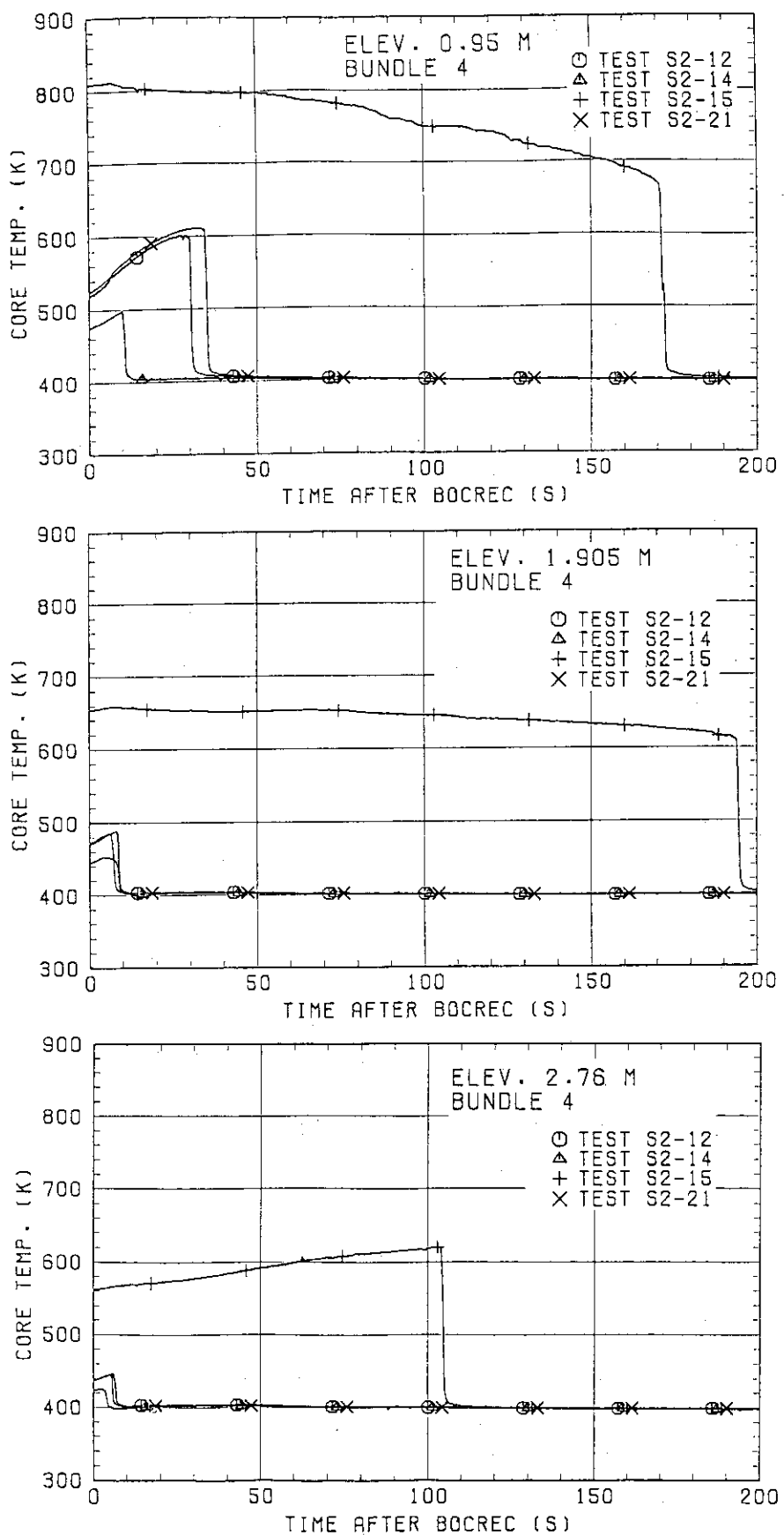


Fig. 3.31 Comparisons of non-heated rod surface temperatures at 0.95, 1.905 and 2.76 m in Bundle 4

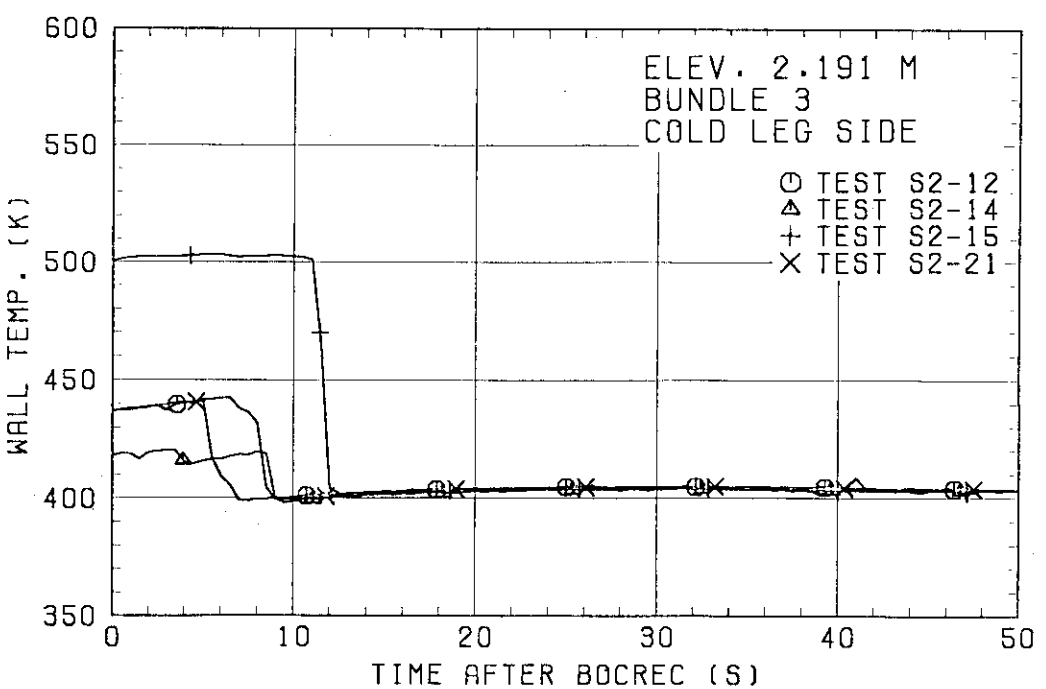
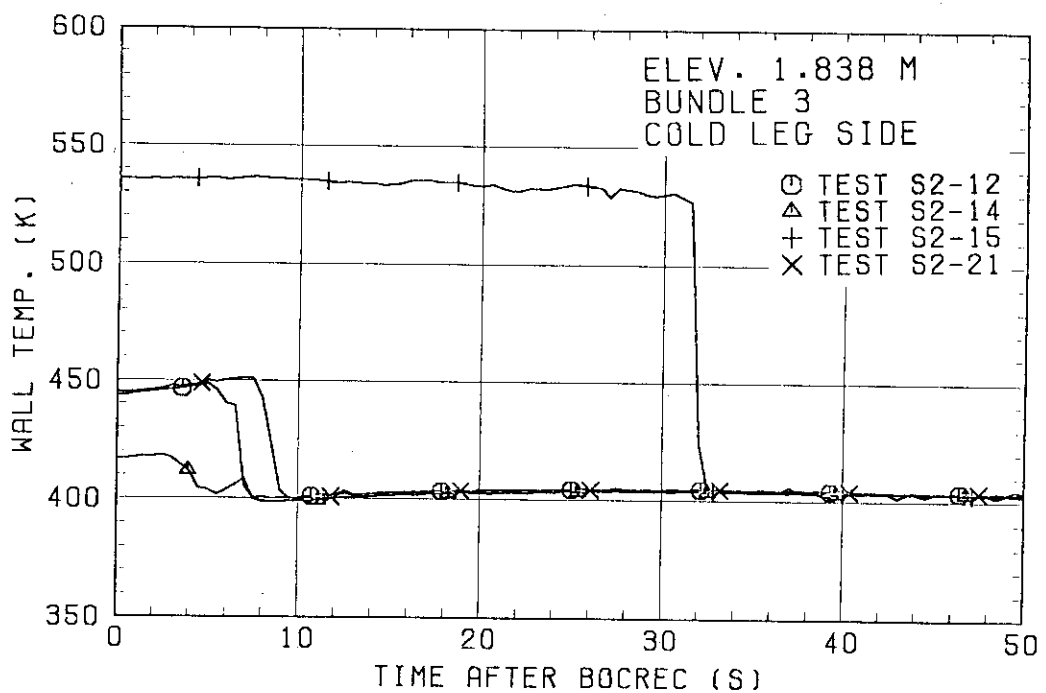


Fig. 3.32 Comparisons of side wall surface temperatures at 1.838 and 2.191 m in Bundle 3

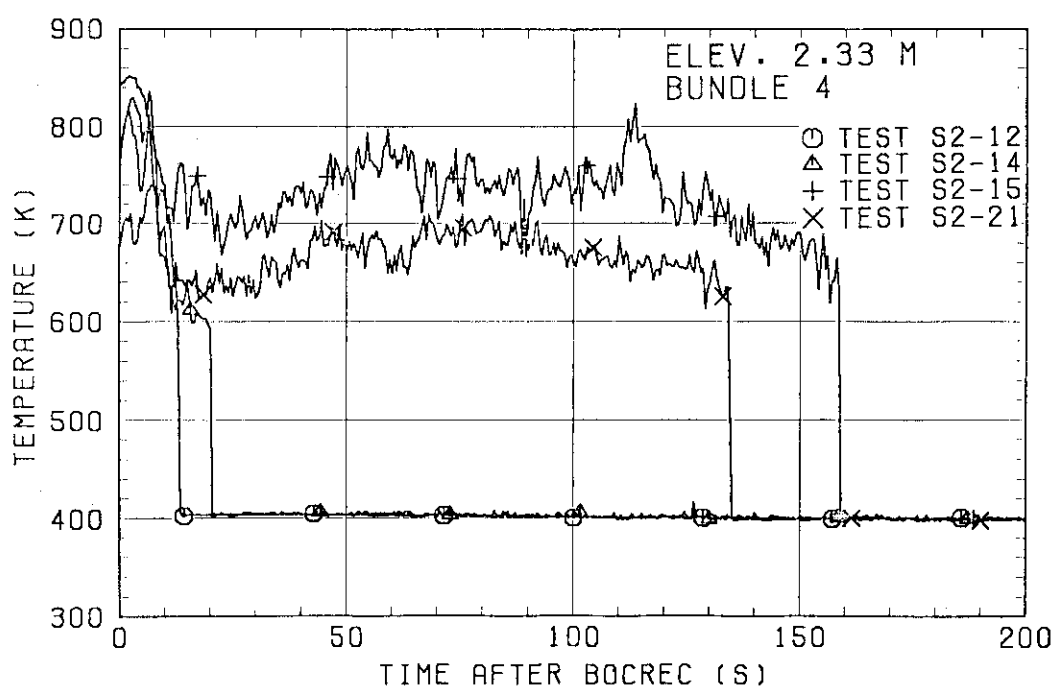
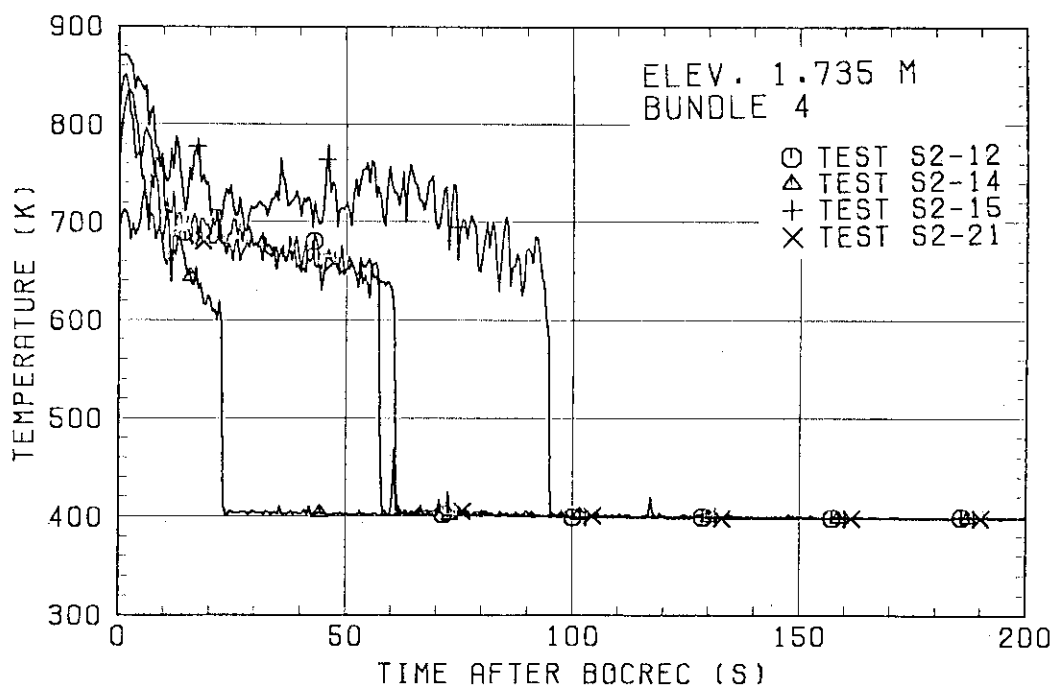
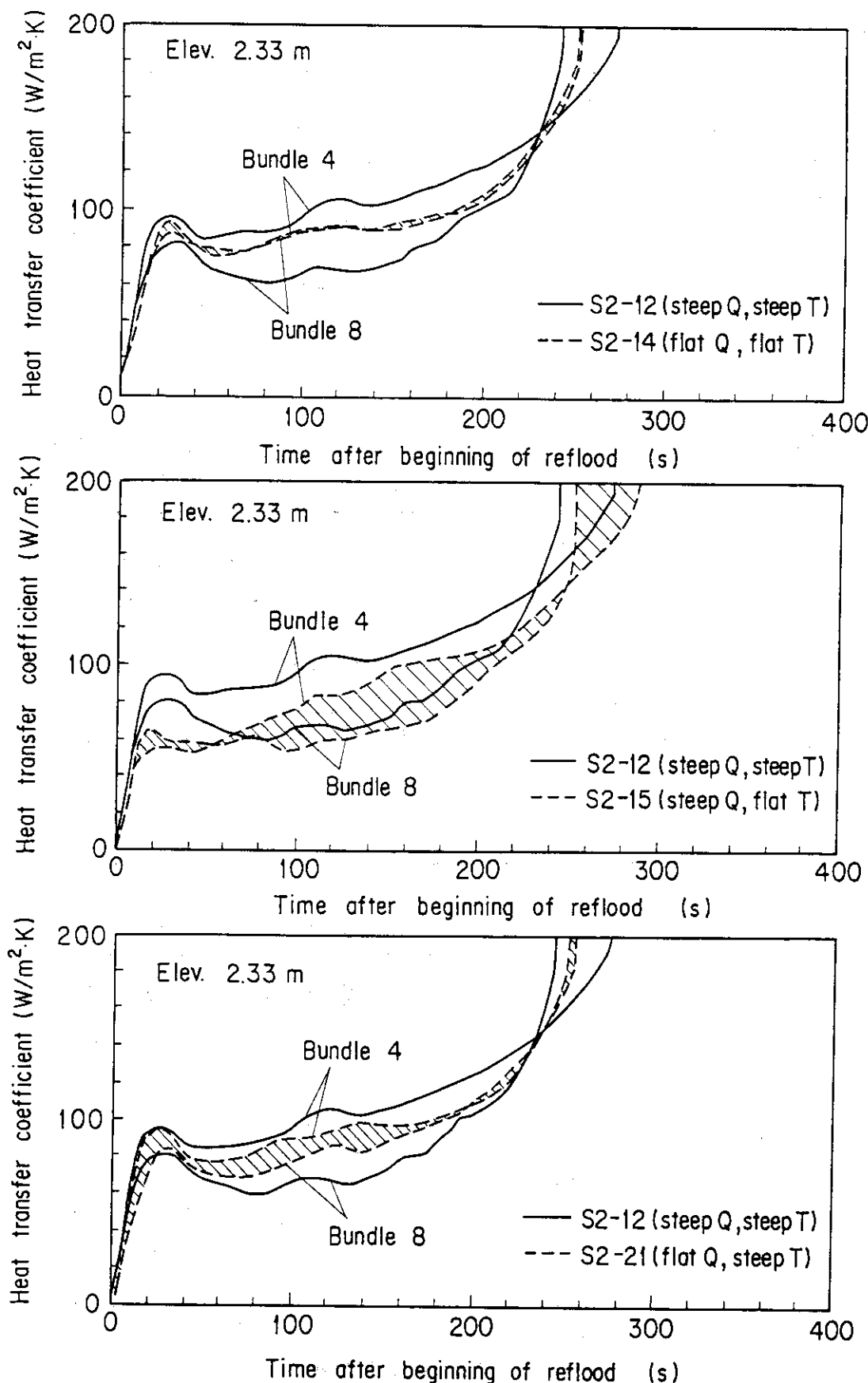


Fig. 3.33 Comparisons of fluid temperatures in core at 1.735 and 2.33 m in Bundle 4



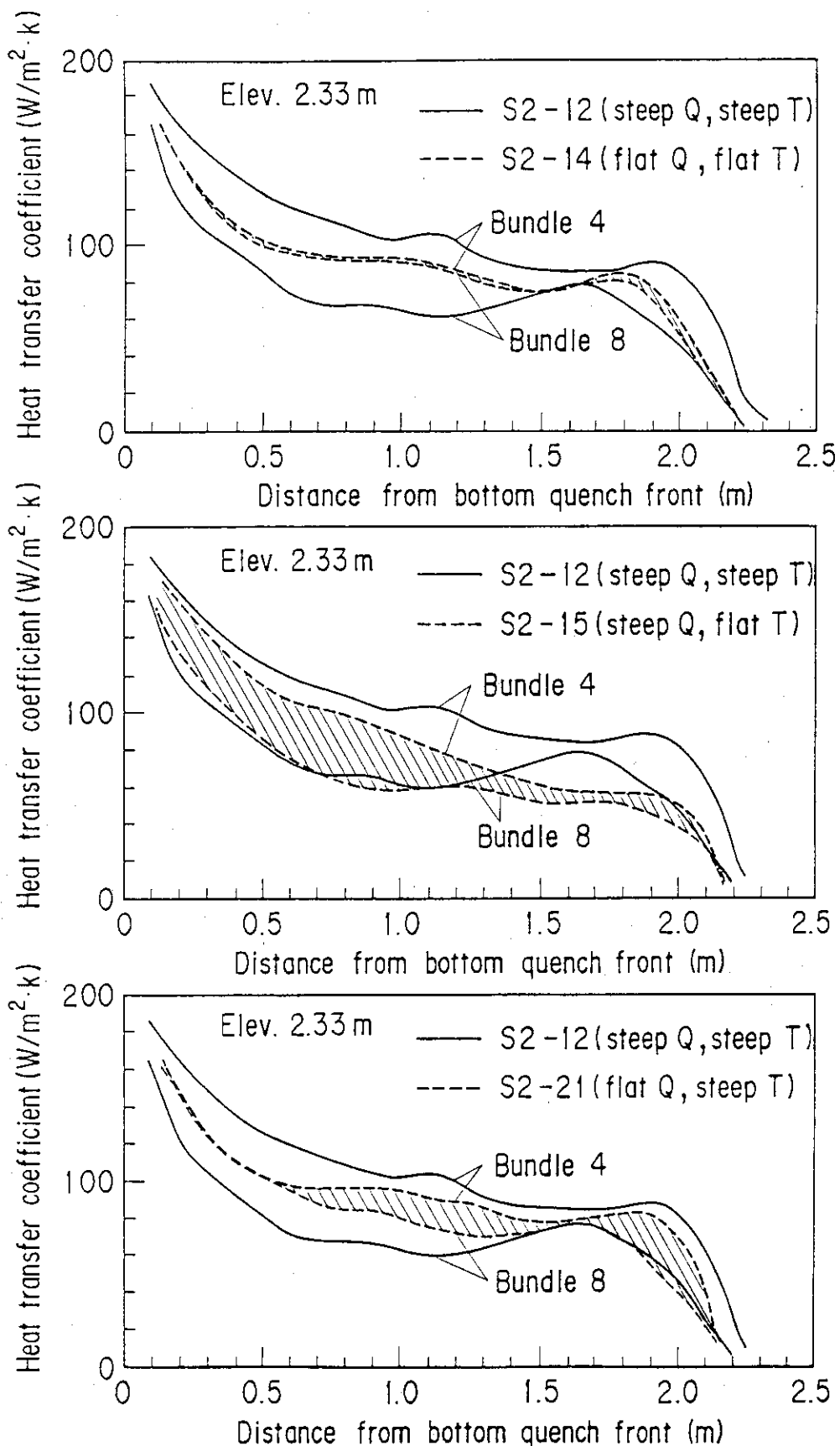


Fig. 3.35 Comparison of average heat transfer coefficient vs. distance from bottom quench front

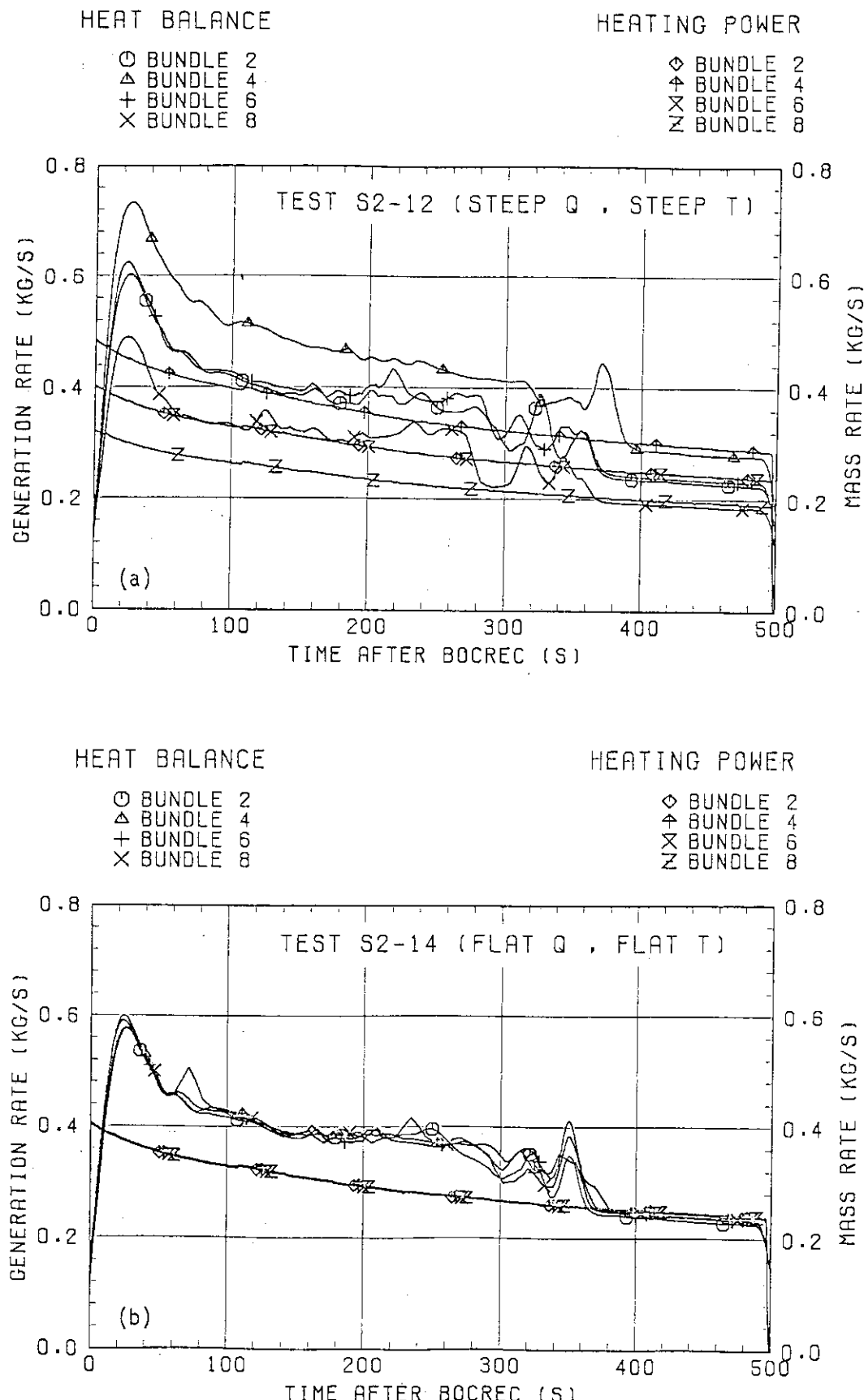


Fig. 3.36 Comparisons between steam generation rates and heating powers divided by latent heat of evaporation in Bundles 2, 4, 6 and 8

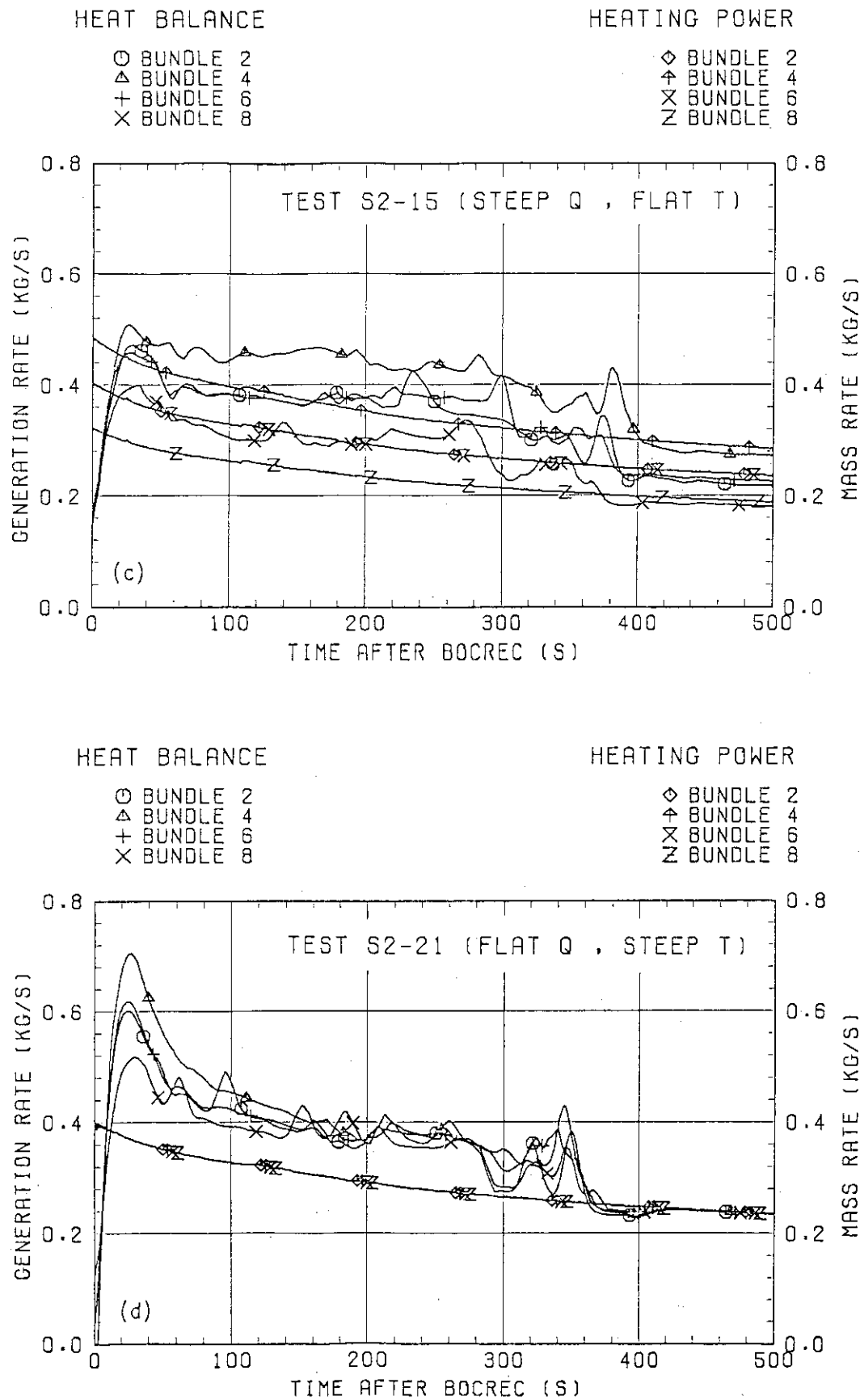


Fig. 3.36 (continue)

#### 4. Conclusions

The SCTF tests indicated that the radial core power distribution has significant effect on the heat transfer enhancement in high power bundles. In order to separately evaluate the effect of the radial power ( $Q$ ) distribution itself and the effect of the radial temperature ( $T$ ) distribution accompanying the radial power distribution, four forced feed tests were performed with four combinations of the radial power distribution (steep  $Q$  or flat  $Q$ ) and the radial temperature distribution at the beginning of reflood (steep  $T$  or flat  $T$ ). The major conclusions are as follows :

- (1) Two-dimensional thermal-hydraulic behavior was clearly observed in the test with steep  $Q$  and steep  $T$ , whereas the thermal-hydraulic behavior in the test with flat  $Q$  and flat  $T$  was almost uniform over all bundles unless the distribution of upper plenum water level would have developed.
- (2) The horizontal flow behavior and two-dimensional heat transfer characteristics in the core in the test with steep  $Q$  and flat  $T$  were similar to those in the test with flat  $Q$  and flat  $T$  during the initial period. As the radial temperature distribution became steep with time due to the steep power distribution, the two-dimensional thermal-hydraulic characteristics in the test with steep  $Q$  and flat  $T$  became similar to those in the test with steep  $Q$  and steep  $T$ .
- (3) The horizontal flow behavior and the two-dimensional heat transfer characteristics in the core in the test with flat  $Q$  and steep  $T$  were initially similar to those in the test with steep  $Q$  and steep  $T$  and then became flat as the radial temperature distribution became flat.
- (4) The radial temperature distribution which accompanied the radial power distribution was the dominant factor of the two-dimensional thermal-hydraulic behavior in the core at least during the initial period.

### Acknowledgment

The authors are much indebted to Dr.Y.Murao for his guidance and encouragement for this program.

They would like to express their appreciation to Mr. T.Iguchi, Dr.H.Akimoto and Mr.T.Hojo for their useful discussions.

### References

- (1) H.Adachi et al., System Pressure Effects on Reflooding Phenomena Observed in the SCTF Core I Forced Flooding Tests, JAERI-M 83-079, (1983).
- (2) Y.Sudo et al., Effect of Upper Plenum Water Accumulation on Reflooding Phenomena under Forced Flooding in SCTF Core I Test, JAERI-M 83-114, (1983).
- (3) T. Iwamura et al., Effects of Core Inlet Water Subcooling on Reflooding Phenomena -SCTF Core I Forced Feed Floding Test-, JAERI-M 83-122, (1983).
- (4) M.Sobajima et al., Examination of Repeatability in Reflood Phenomena under Forced Flooding in SCTF Core I Tests, JAERI-M 83-237, (1984)
- (5) T.Iwamura et al., Effects of Upper Plenum Injection on Thermo-Hydrodynamic Behavior under Refill and Reflood Phases, JAERI-M 84-221, (1984).
- (6) M.Sobajima et al., Charcteristics of Lower Plenum Injection Reflood Tests in SCTF Core I, JAERI-M 84-223, (1984).
- (7) T.Iwamura et al., Two-dimensional Thermal-hydraulic Behavior in Core in SCTF Core -II Cold Leg Injection Tests (Radial Power Profile Test Results), JAERI-M 85-106, (1985).
- (8) T.Iwamura et al., Effects of Radial Core Power Profile on Core Thermo-Hydraulic Behavior during Reflood Phase in PWR-LOCA, J. Nucl. Sci.Tech., vol. 20, No.9, pp. 743-751, (1983).
- (9) M.Sobajima et al., Design of Slab Core Test Facility (SCTF) in Large Scale Reflood Test Program, Part II: JAERI-M to be published.
- (10) H. Adachi et al., Development of SCTF Cold Leg Injection Test Method for Eliminating U-Tube Oscillation during the Initial Period, JAERI-M to be published.

### Acknowledgment

The authors are much indebted to Dr.Y.Murao for his guidance and encouragement for this program.

They would like to express their appreciation to Mr. T.Iguchi, Dr.H.Akimoto and Mr.T.Hojo for their useful discussions.

### References

- (1) H.Adachi et al., System Pressure Effects on Reflooding Phenomena Observed in the SCTF Core I Forced Flooding Tests, JAERI-M 83-079, (1983).
- (2) Y.Sudo et al., Effect of Upper Plenum Water Accumulation on Reflooding Phenomena under Forced Flooding in SCTF Core I Test, JAERI-M 83-114, (1983).
- (3) T. Iwamura et al., Effects of Core InJet Water Subcooling on Reflooding Phenomena -SCTF Core I Forced Feed Floding Test-, JAERI-M 83-122, (1983).
- (4) M.Sobajima et al., Examination of Repeatability in Reflood Phenomena under Forced Flooding in SCTF Core I Tests, JAERI-M 83-237, (1984)
- (5) T.Iwamura et al., Effects of Upper Plenum Injection on Thermo-Hydrodynamic Behavior under Refill and Reflood Phases, JAERI-M 84-221, (1984).
- (6) M.Sobajima et al., Charcteristics of Lower Plenum Injection Reflood Tests in SCTF Core I, JAERI-M 84-223, (1984).
- (7) T.Iwamura et al., Two-dimensional Thermal-hydraulic Behavior in Core in SCTF Core -II Cold Leg Injection Tests (Radial Power Profile Test Results), JAERI-M 85-106, (1985).
- (8) T.Iwamura et al., Effects of Radial Core Power Profile on Core Thermo-Hydraulic Behavior during Reflood Phase in PWR-LOCA, J. Nucl. Sci.Tech., vol. 20, No.9, pp. 743-751, (1983).
- (9) M.Sobajima et al., Design of Slab Core Test Facility (SCTF) in Large Scale Reflood Test Program, Part II: JAERI-M to be published.
- (10) H. Adachi et al., Development of SCTF Cold Leg Injection Test Method for Eliminating U-Tube Oscillation during the Initial Period, JAERI-M to be published.

- (11) A. Ohnuki et al., Study on ECC Injection Modes in Reflood Tests with SCTF Core II - Comparison between Gravity and Forced Feeds - JAERI-M, to be published.
- (12) H.Akimoto et al., Evaluation Report on CCTF Core -II Reflood Test C2-6 (Run 64)-Effect of radial power profile - , JAERI-M 85-027, (1985).
- (13) M.Osakabe and Y.Sudo., Heat Transfer Calculation of Simulated Heater Rods throughout Reflood Phase in Postulated PWR-LOCA Experiments, J. Nucl. Sci. Tech., Vol.20, No.7, 559 - 570, (1983).
- (14) D.Liles et al., TRAC-PF1/Mode 1 An Advanced Best-Estimate Computer Program for Pressurized Water Reactor Thermal-Hydraulic Analysis, NUREG/CR-3567, (1984).

## Appendix A Slab Core Test Facility (SCTF) Core-II

### A.1 Test Facility

The Slab Core Test Facility is designed under the following design philosophy and design criteria:

#### a. Design Philosophy

- (1) The facility should provide the capability to study the two-dimensional thermohydraulic behavior in a reactor pressure vessel especially due to the radial power distribution during the end of blowdown, refill and reflood phases of a postulated LOCA in a PWR.
- (2) To properly simulate the core heat transfer and hydrodynamics, a special emphasis is put on the proper simulation of the components in the pressure vessel. Provided as the components in the pressure vessel are the simulated core, downcomer, core baffle region, lower plenum, upper plenum and upper head. On the other hand, simplified primary coolant loops are also provided. Provided as the primary coolant loop components are a hot leg, an intact cold leg, broken cold legs and a steam/water separator which is to simulate single steam phase flow downstream of a steam generator and to measure the flow rate of carryover water coming from the upper plenum.

#### b. Design Criteria

- (1) The reference reactor to be simulated in SCTF is the Trojan reactor in the United States which is a four-loop 3300 MWe PWR. The Ooi reactor etc. in Japan are also referred which are of the similar type to the Trojan reactor except the provision of UHI system.
- (2) A full scale radial and axial section of core with single bundle width of the pressurized water reactor is provided as the simulated core of SCTF.
- (3) The simulated core consists of 8 bundles arranged in a row. Each bundle has electrically heated rods simulating fuel rods and non-heated rods with 16×16 array, with the diameter and the pitch for Trojan which has 15×15 rod array.
- (4) The flow area and fluid volume of components are scaled down based on the nominal core flow area scaling, 1/21.
- (5) To properly simulate the flow behavior of carryover water or entrainment, the elevations of hot leg and cold legs are designed

- to be the same as the PWR as much as possible.
- (6) A honeycomb structure is used for side walls with surface plates which accommodates the slab core, the upper plenum and the upper part of lower plenum, so as to minimize the effect of walls on the core heat transfer and hydrodynamics.
  - (7) To investigate the effect of flow resistance in the primary loop are provided the orifices of which dimension is changeable.
  - (8) The maximum allowable temperature of the simulated fuel rods is 900°C (1173 K) and the maximum allowable pressure of the facility is 0.6 MPa.
  - (9) The facility is equipped with the hot leg equivalent to four hot legs connecting the upper plenum and the steam/water separator, the intact cold leg equivalent to three intact cold legs connecting the steam/water separator and the downcomer and the two broken cold legs, one is for the steam/water separator side and another for the pressure vessel side.
  - (10) The ECCS consists of an accumulator (Acc), a low pressure coolant injection (LPCI) system and a combined injection system.
  - (11) ECC water injection ports are at the cold leg, the hot leg, the upper plenum, the downcomer, the lower plenum and above the upper core support plate. These ports are to be chosen according to the objective of the test.
  - (12) For better simulation of lower plenum flow resistance, simulated fuel rods do not penetrate through the bottom plate of the lower plenum but terminate at below the bottom of the core.
  - (13) For measurements in the pressure vessel including core, the feature of the slab geometry of the pressure vessel is utilized as much as possible. Design and arrangement of the instruments are done so as to be able to carry out installation, calibration and removal of the instruments.
  - (14) View windows are provided where flow pattern recognition is important. Their locations are the interface between the core and the upper plenum, the hot leg, the pressure vessel side broken cold leg and the downcomer.
  - (15) Blocked bundle test is carried out in Core-I in order to investigate the effect of ballooned fuel rods and unblocked normal bundle test follows in the Core-II and -III.
  - (16) Types of break simulated are cold leg break and hot leg break.

- (17) The components and systems such as the containment tanks and ECC water supply system in CCTF are shared with SCTF to the maximum extent.

The overall schematic diagram of SCTF is shown in Fig. A-1. The principal dimensions of the facility is shown in Table A-1, and the comparison of dimensions between SCTF and the reference PWR is shown in Fig. A-2.

#### A.1.1 Pressure Vessel and Internals

The pressure vessel is of slab geometry as shown in Fig. A-3. The height of the components in the pressure vessel is almost the same as the reference reactor's, and the flow area and the fluid volume of each component are scaled down based on the nominal core flow area scaling, 1/21.

The core consists of 8 bundles arranged in a row and each bundle includes heater rods and non-heated rods with 16×16 array. The core is enveloped by the honeycomb thermal insulator which is attached on the back surface of core wall plate.

The downcomer is located at one end of the pressure vessel which corresponds to the periphery of the actual reactor pressure vessel. The core baffle region located between the core and the downcomer is basically isolated for Core-II to minimize uncertainty in actual core flow. However, some leak holes are still existing. For better understanding, the cross section of the pressure vessel at the elevation of midplane of the core is shown in Fig. A-4.

The design of upper plenum internals is based on that for the new Westinghouse 17×17 array fuel assemblies. The internals consist of control rod guide tubes, support columns and orifice plates which are attached to the upper core support plate (UCSP). The UCSP has some open holes without internals. Those arrangement is shown in Fig. A-5. The radius of each internal is scaled down based on the factor of 8/15 of an actual reactor. Baffle plates are inserted in the guide tubes. The elevation and the configuration of baffle plates are shown in Figs. A-6 and A-7.

The heights of the hot leg and cold legs are designed as close to the reference PWR as possible. However, in order to avoid the interference of the nozzles in the downcomer, the heights of nozzles for the

broken cold leg and the intact cold leg are shifted down compared to that of the hot leg as shown in Fig. A-3.

#### A.1.2 Simulated Core

The simulated core for the SCTF Core-II consists of 8 heater rod bundles arranged in a row. Each bundle has 234 electrically heated rods and 22 non-heated rods. The dimensions of the heater rods are based on 15×15 fuel rods bundle for a PWR and the heated length and the outer diameter of each heater rod are 3.66 m and 10.7 mm, respectively. A heater rod consists of a nichrome heater element, boron nitride (BN) or magnesium oxide (MgO) depending on elevation in the heated zone and Nichrofer 7216 (equivalent to Inconel 600) sheath. The sheath thickness is about 1.0 mm and is thicker than the actual fuel cladding because of the requirements for thermocouple installation. The heater element is a helical coil and has a 17 step chopped cosine axial power profile as shown in Fig. A-8. The peaking factor is 1.4.

Non-heated rods are either pipes or solid rods of stainless steel with 13.8 mm O.D. The heater rods and non-heated rods are fixed at the top of the core allowing downward expansion. In Fig. A-9, relative elevation of rods and spacers is shown.

For better simulation of flow resistance in the lower plenum the simulated fuel rods end in the lower plenum and do not penetrate through the bottom plate of the lower plenum as shown in Fig. A-9.

#### A.1.3 Primary Loops and ECCS

Primary loops consist of a hot leg equivalent to four hot legs in area, a steam/water separator for simulating single steam phase flow downstream of the steam generator and for measuring flow rate of carry over water, an intact cold leg equivalent to three intact loops, a broken cold leg on the pressure vessel side and a broken cold leg on the steam/water separator side. These two broken cold legs are connected to two containment tanks through break valves, respectively. The arrangement of the primary loops is shown in Fig. A-10. The flow area of each loop is scaled down based on the core flow area scaling, 1/21. It should be emphasized that the cross section of the hot leg is an elongated circle with an actual height to realize proper flow pattern in the hot leg. The steam/water separator has a steam generator inlet

plenum simulator to correctly simulate the flow characteristics of carryover water into the U-tubes. The cross section of the hot leg and the configuration of the steam generator inlet plenum simulator are shown in Fig. A-11.

A pump simulator and a loop seal part are provided for the intact cold leg. The arrangement of the intact cold leg is shown in Fig. A-12. The pump simulator consists of the casing and duct simulators and an orifice plate as shown in Fig. A-13. The loop resistance is adjusted with the orifice plates attached to the intact cold leg, the steam/water separator side and pressure vessel side broken cold legs and the pump simulator.

ECCS consists of the Acc and an LPCI systems. Injection ports are located as already described in the design criteria section. Besides, the UCSP water extraction system and the UCSP water injection system are provided for combined injection tests.

#### A.1.4 Containment Tanks and Auxiliary System

Two containment tanks are provided to SCTF. The containment tank-I is connected with the downcomer through the pressure vessel side broken cold leg and the containment tank-II is connected with the steam/water separator through the steam/water separator side broken cold leg. Especially in the containment tank-I, carryover water from the downcomer is measured by the differentiation of the liquid level. These containment tanks and auxiliary system such as a pressurizer for injecting water from the Acc tanks, etc. are shared with CCTF.

#### A.2 Instrumentation

The instrumentation in SCTF has been provided both by JAERI and USNRC. The JAERI-provided instrumentation includes the measurement of temperatures, pressures, differential pressures, liquid levels, flow velocities, and heating powers. USNRC has provided film probes, impedance probes, string probes, liquid level detectors (LLDs), fluid distribution grids (FDGs), turbine meters, drag disks, densitometers, spool pieces and video optical probes. Location of each instrument is shown in Figs. A-14 through A-32.

Table A-1 Principal Dimensions of Test Facility

## 1. Core Dimension

(1) Quantity of Bundle	8 Bundles
(2) Bundle Array	1×8
(3) Bundle Pitch	230 mm
(4) Rod Array in a Bundle	16×16
(5) Rod Pitch in a Bundle	14.3 mm
(6) Quantity of Heater Rod in a Bundle	234 rods
(7) Quantity of Non-Heated Rod in a Bundle	22 rods
(8) Total Quantity of Heater Rods	234×8=1872 rods
(9) Total Quantity of Non-Heated Rods	22×8=176 rods
(10) Effective Heated Length of Heater Rod	3660 mm
(11) Diameter of Heater Rod	10.7 mm
(12) Diameter of Non-Heated Rod	13.8 mm

## 2. Flow Area &amp; Fluid Volume

(1) Core Flow Area (Nominal)	0.227 m <sup>2</sup>
(2) Core Fluid Volume	0.92 m <sup>3</sup>
(3) Baffle Region Flow Area	0.10 m <sup>2</sup>
(4) Baffle Region Fluid Volume (Nominal)	0.36 m <sup>3</sup>
(5) Effective Core Flow Area Based on the Measured Level-Volume Relationship Shown in Fig. 4-7 Including Gap between Core Barrel and Pressure Vessel Wall and Various Penetration Holes	0.35 m <sup>2</sup>
(6) Downcomer Flow Area	0.121 m <sup>2</sup>
(7) Upper Annulus Flow Area	0.158 m <sup>2</sup>
(8) Upper Plenum Horizontal Flow Area	0.525 m <sup>2</sup>
(9) Upper Plenum Fluid Volume	1.16 m <sup>3</sup>
(10) Upper Head Fluid Volume	0.86 m <sup>3</sup>
(11) Lower Plenum Fluid Volume	1.38 m <sup>3</sup>
(12) Steam Generator Inlet Plenum Simulator Flow Area	0.626 m <sup>2</sup>
(13) Steam Generator Inlet Plenum Simulator Fluid Volume	0.931 m <sup>3</sup>
(14) Steam Water Separator Fluid Volume	5.3 m <sup>3</sup>
(15) Flow Area at the Top Plate of Steam Generator Inlet Plenum Simulator	0.195 m <sup>2</sup>
(16) Hot Leg Flow Area	0.0826m <sup>2</sup>
(17) Intact Cold Leg Flow Area (Diameter = 297.9 mm)	0.9697m <sup>2</sup>
(18) Broken Cold Leg Flow Area (Diameter = 151.0 mm)	0.0179m <sup>2</sup>

Table A-1 (Continued)

(19) Containment Tank-I Fluid Volume	30	m <sup>3</sup>
(20) Containment Tank-II Fluid Volume	50	m <sup>3</sup>
(21) Flow Area of Exhausted Steam Line from Containment Tank-II to the Atmosphere	see Ref. (1)	

## 3. Elevation &amp; Height

(1) Top Surface of Upper Core Support Plate (UCSP)	0	mm
(2) Bottom Surface of UCSP	- 76	mm
(3) Top of the Effective Heated Length of Heater Rod	- 393	mm
(4) Bottom of the Skirt in the Lower Plenum	-5270	mm
(5) Bottom of Intact Cold Leg	+ 724	mm
(6) Bottom of Hot Leg	+1050	mm
(7) Top of Upper Plenum	+2200	mm
(8) Bottom of Steam Generator Inlet Plenum Simulator	+1933	mm
(9) Centerline of Loop Seal Bottom	-2281	mm
(10) Bottom Surface of End Box	- 185.1	mm
(11) Top of the Upper Annulus of Downcomer	+2234	mm
(12) Height of Steam Generator Inlet Plenum Simulator	1595	mm
(13) Height of Loop Seal	3140	mm
(14) Inner Height of Hot Leg Pipe	737	mm
(15) Bottom of Lower Plenum	-5770	mm
(16) Top of Upper Head	+2887	mm

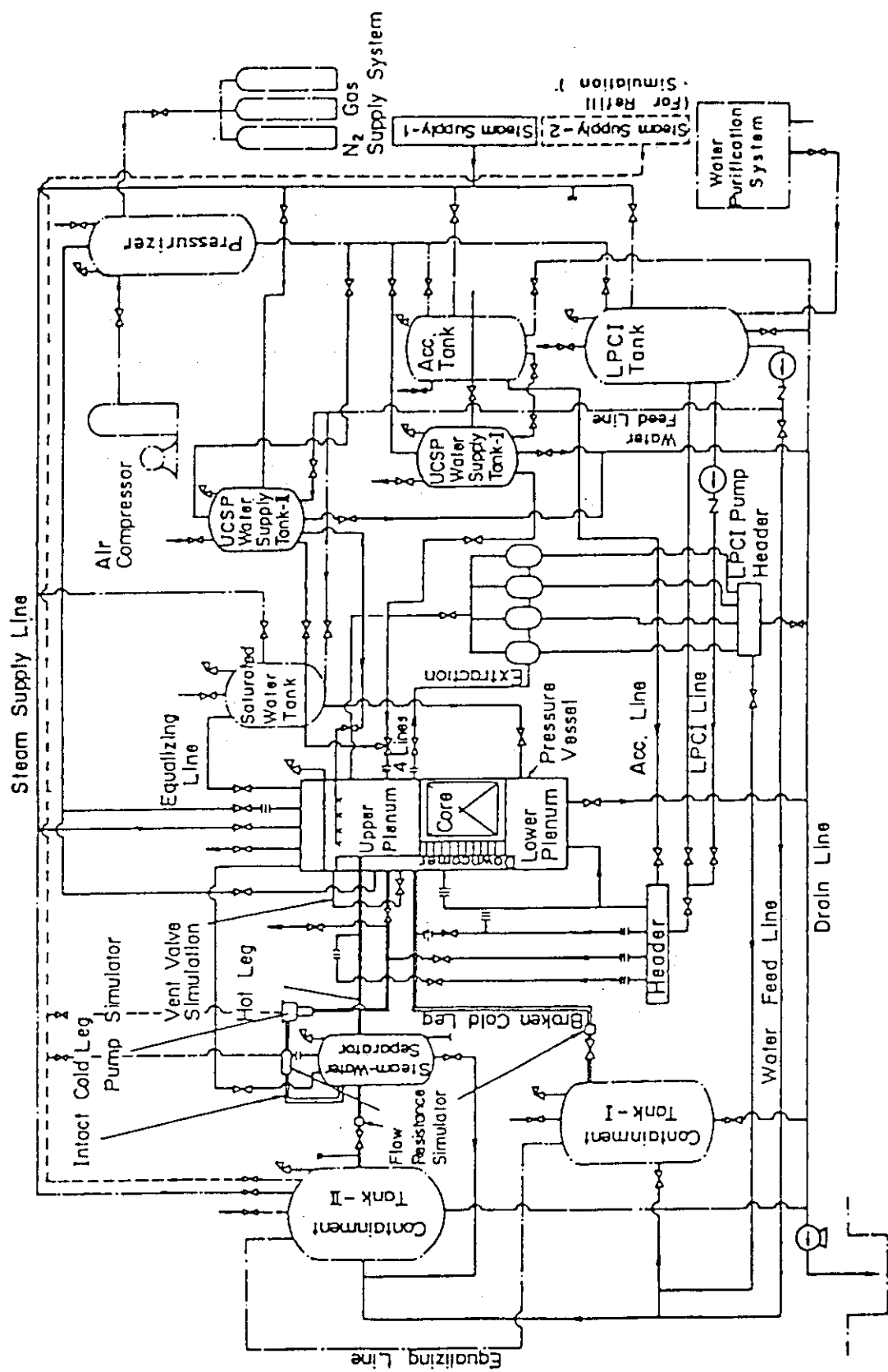


Fig. A-1 Schematic Diagram of Slab Core Test Facility

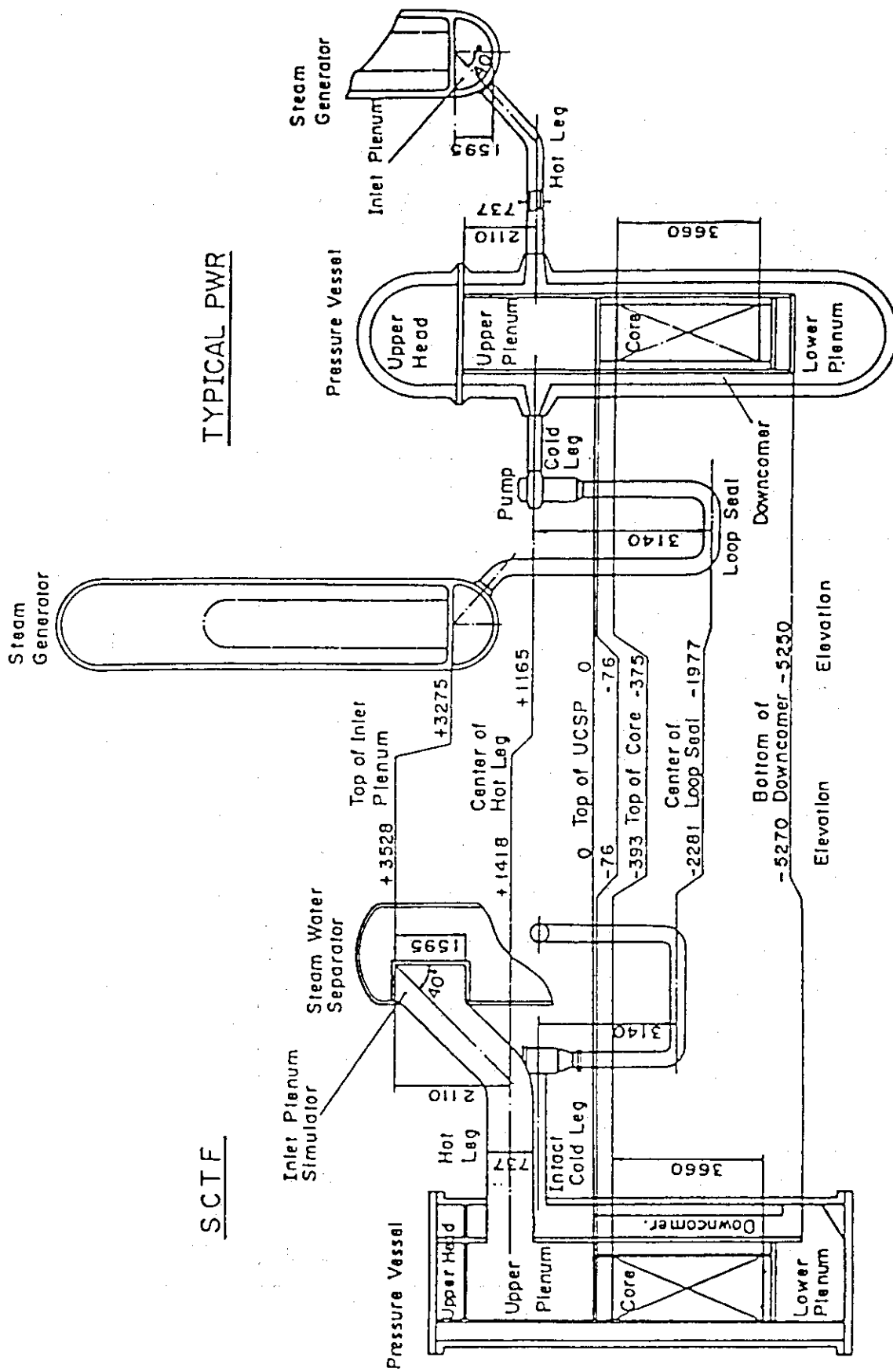


Fig. A-2 Comparison of Dimensions between SCTF and a Reference PWR

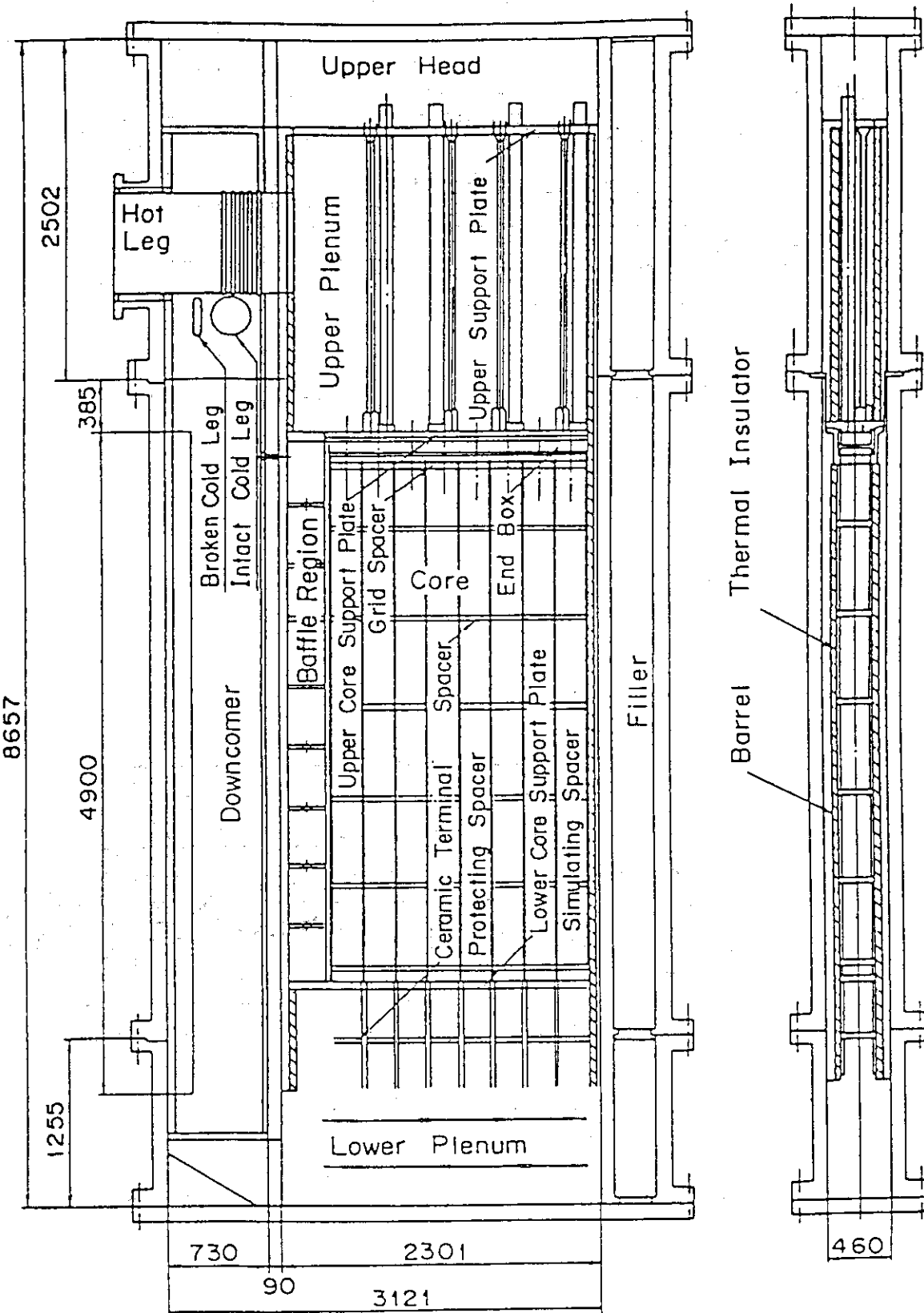


Fig. A-3 Vertical Cross Section of the Pressure Vessel

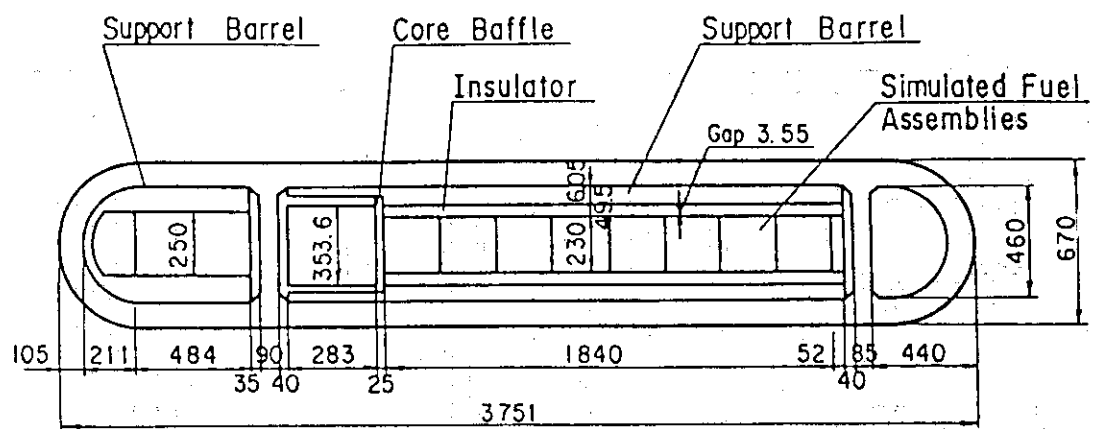
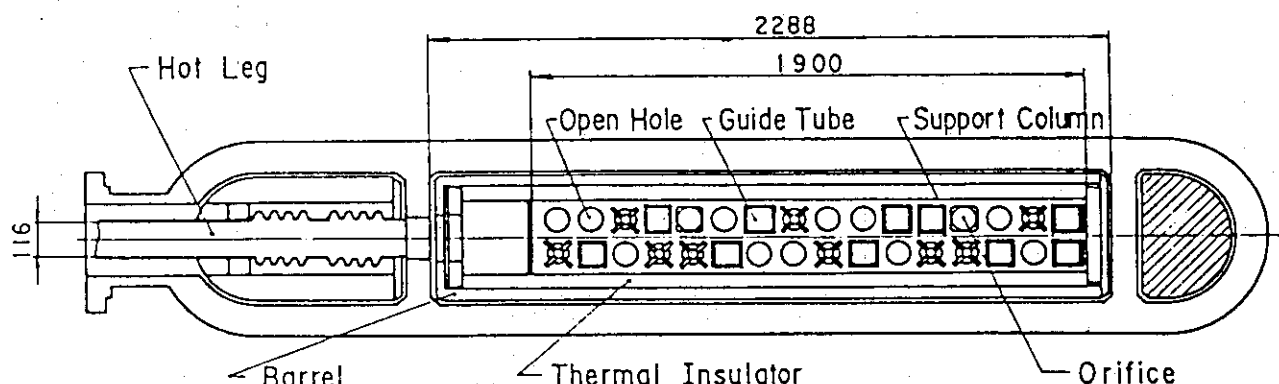


Fig. A-4 Horizontal Cross Section of the Pressure Vessel (1)



Upper Plenum Cross Section

Fig. A-5 Horizontal Cross Section of the Pressure Vessel (2)

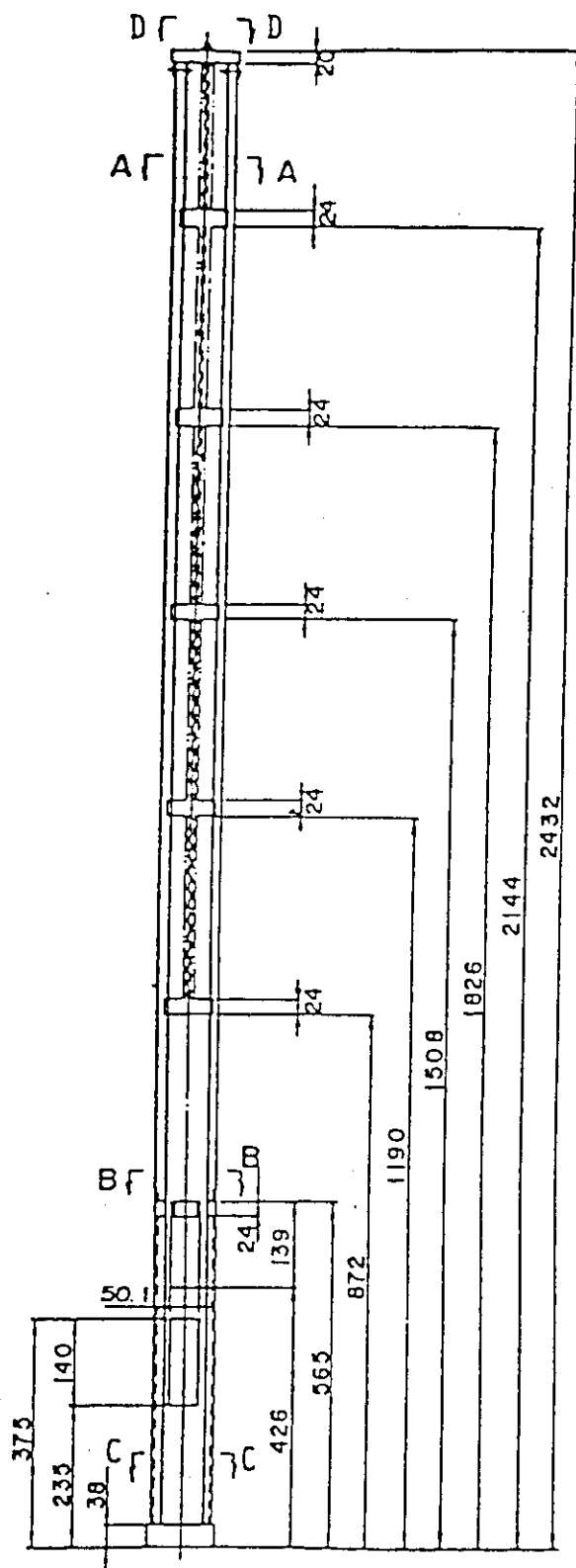


Fig. A-6 Dimension of Guide Tube (1)

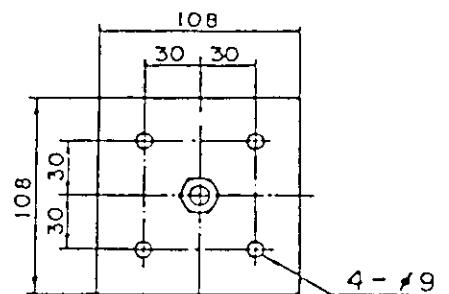
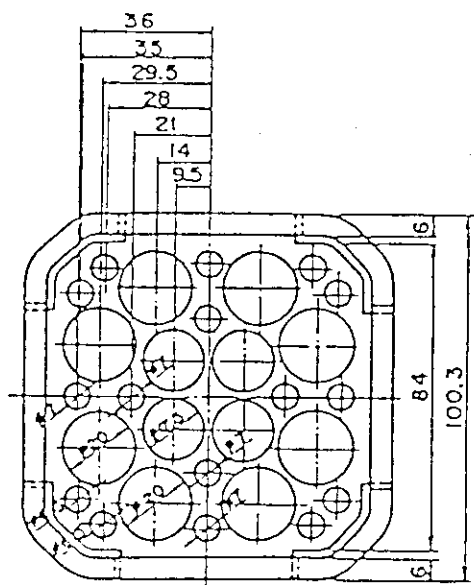
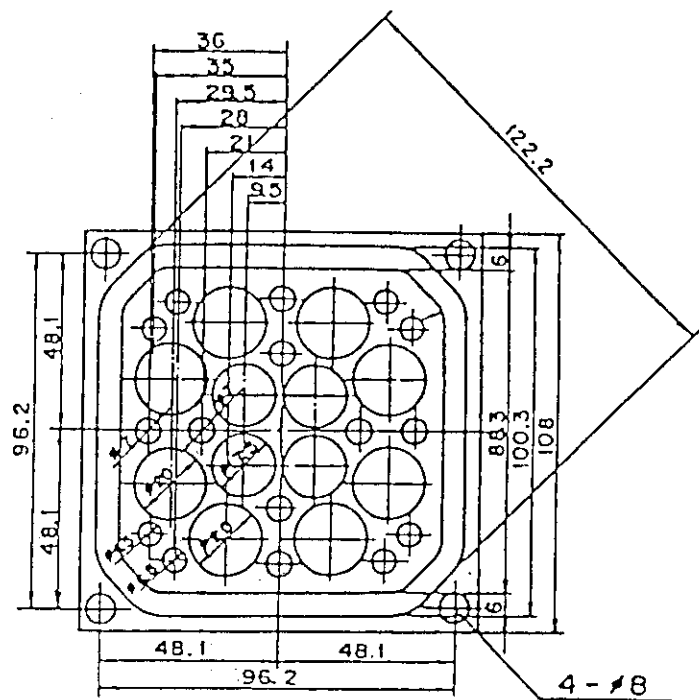
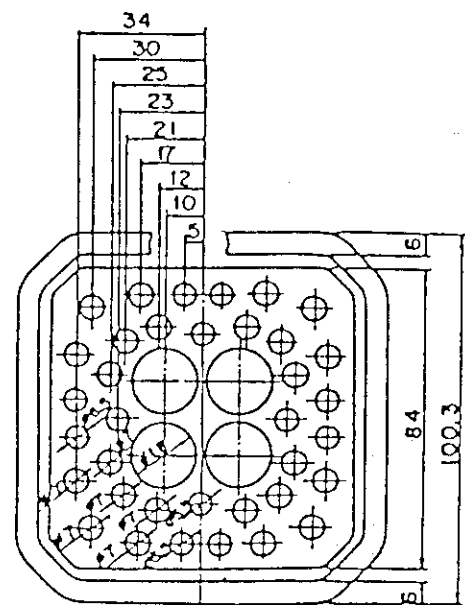


Fig. A-7 Dimension of Guide Tube (2)

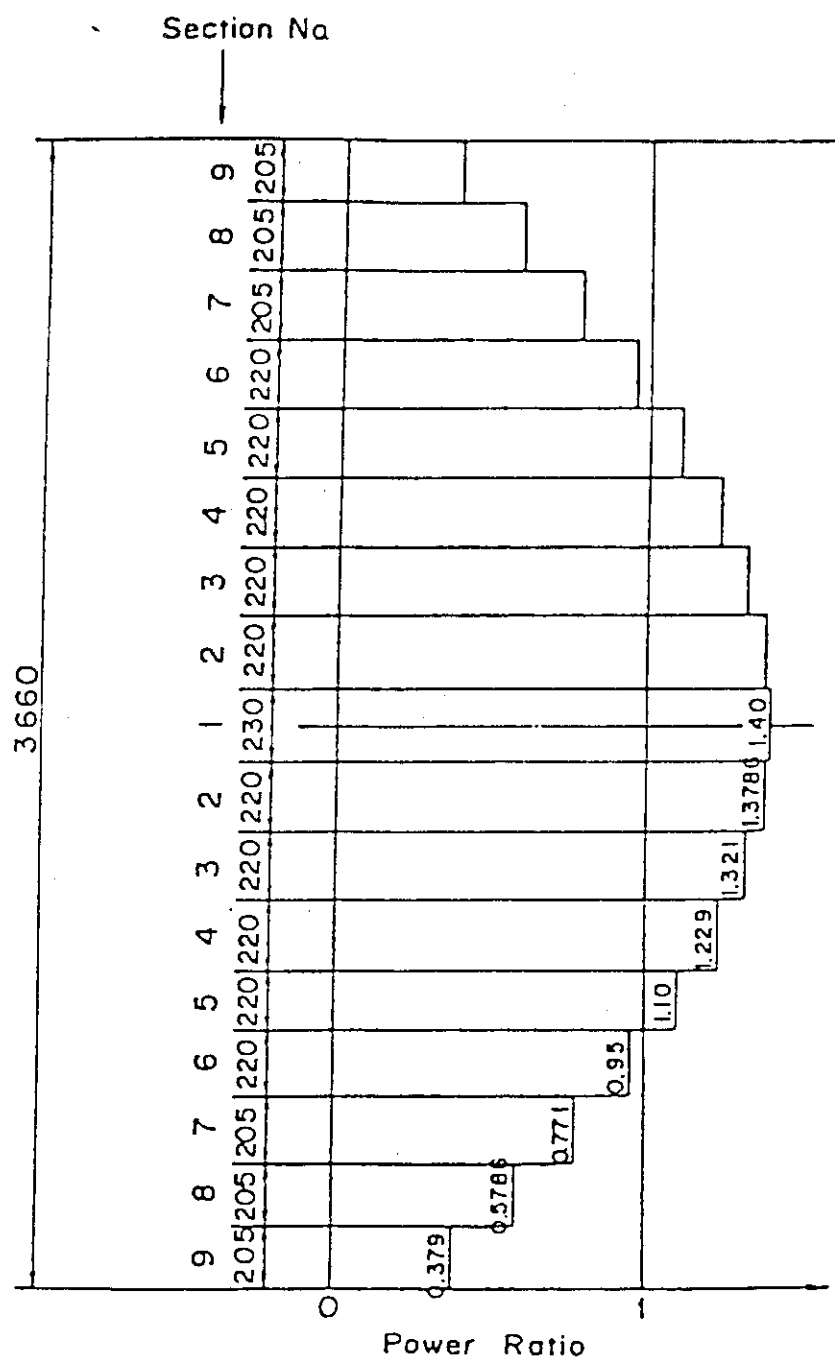


Fig. A-8 Axial Power Distribution of Heater Rod

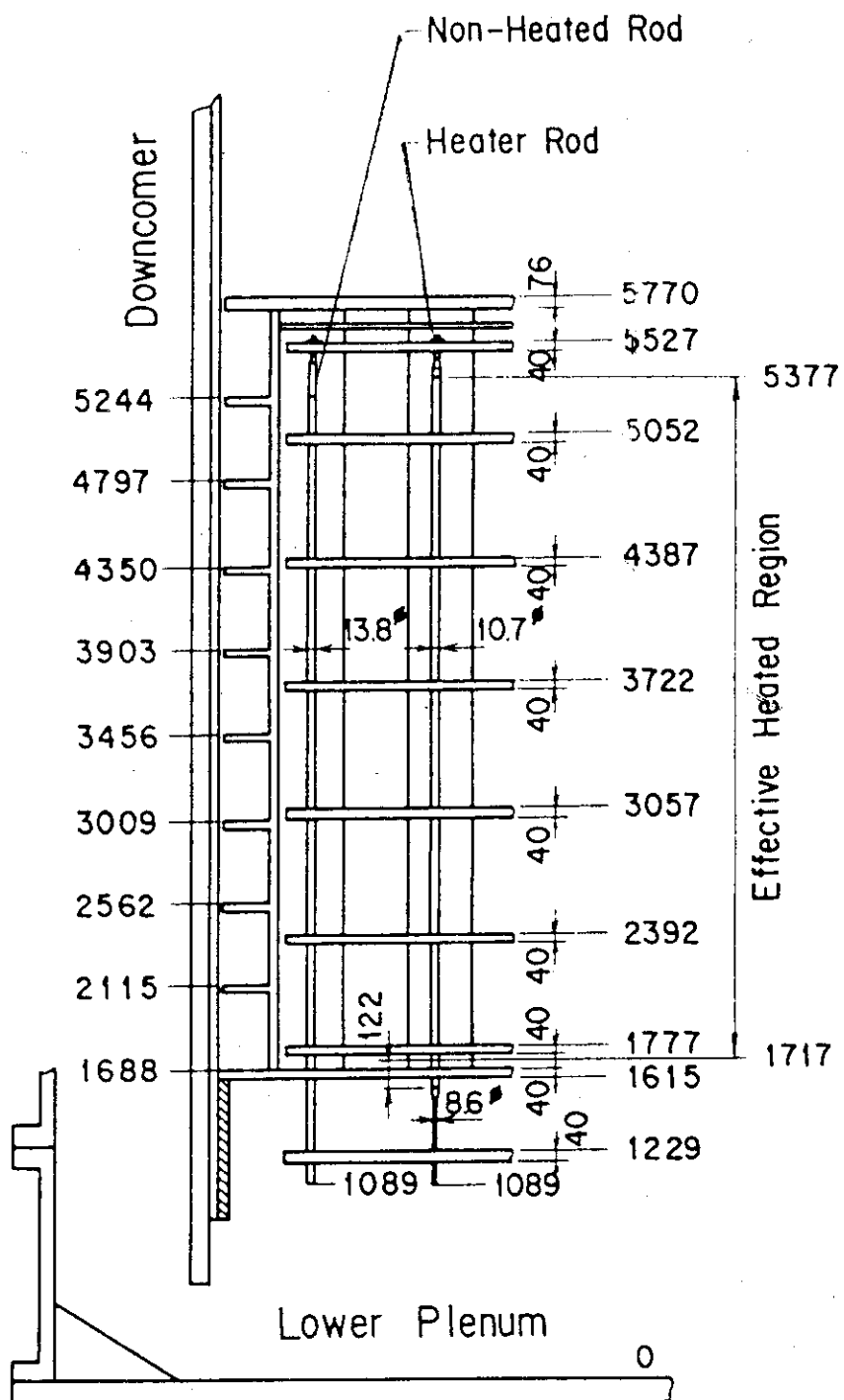


Fig. A-9 Relative Elevation and Dimension of the Core in SCTF

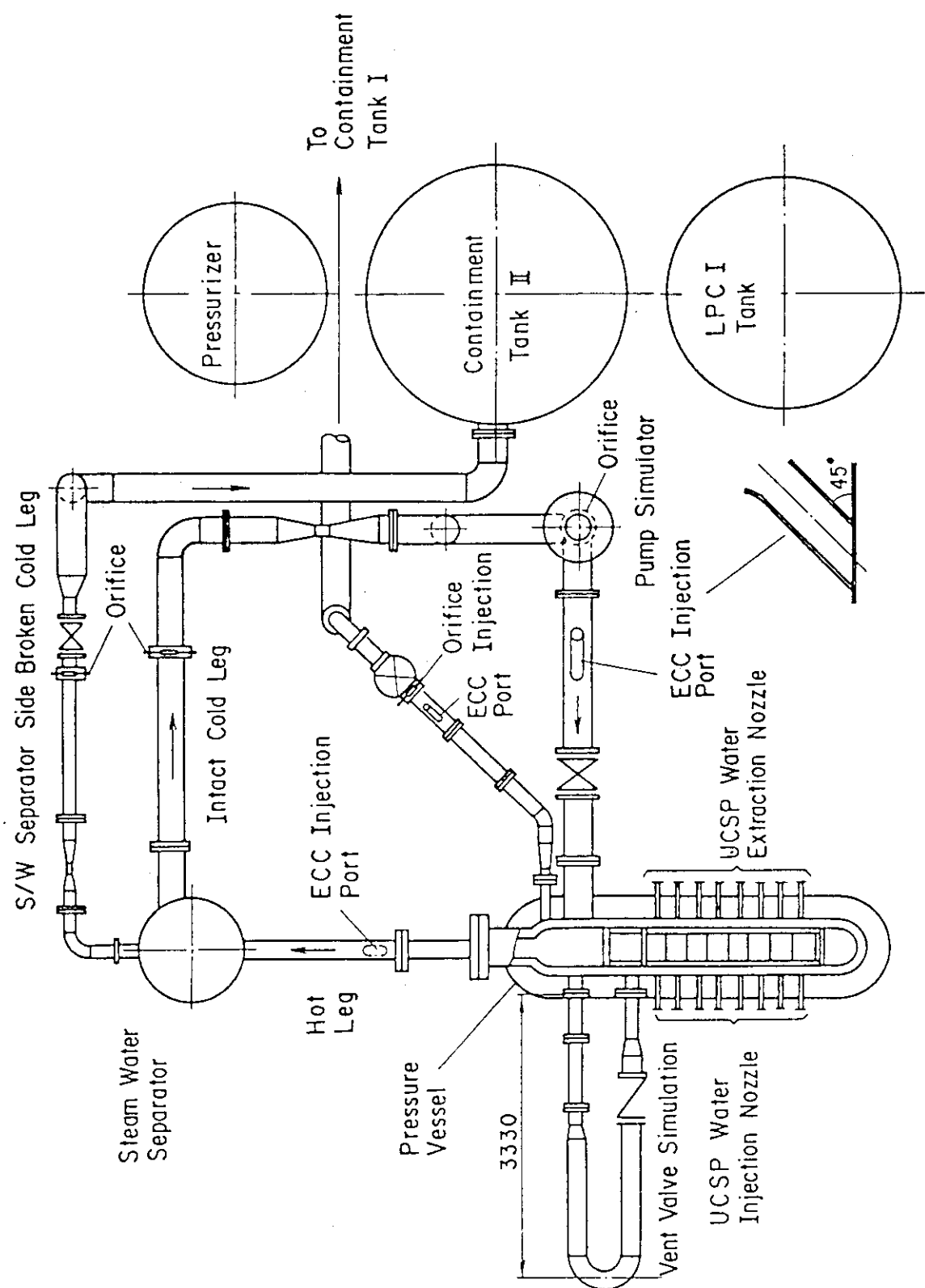


Fig. A-10 Overview of the Arrangements of the SCTR

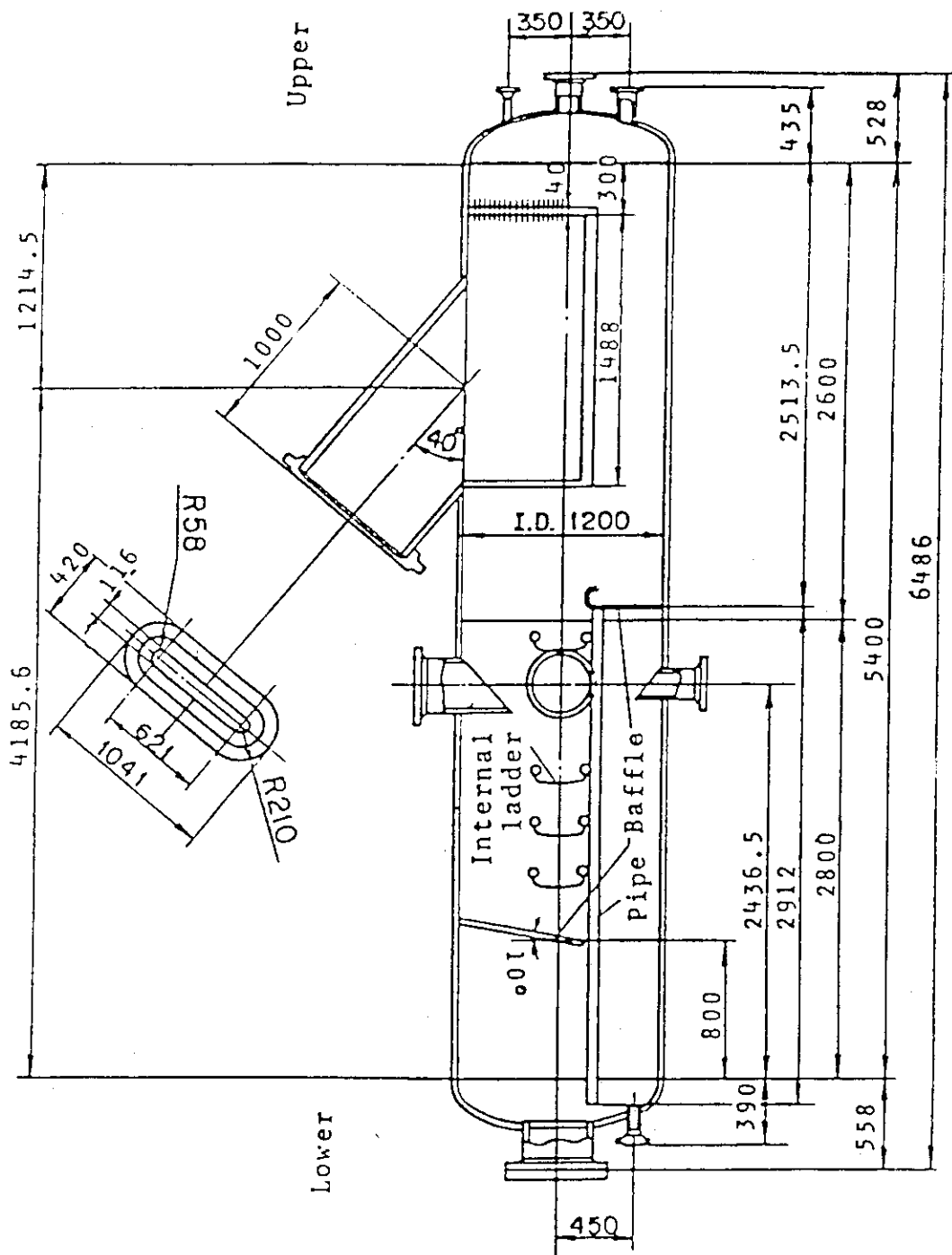


Fig. A-11 Steam/Water Separator

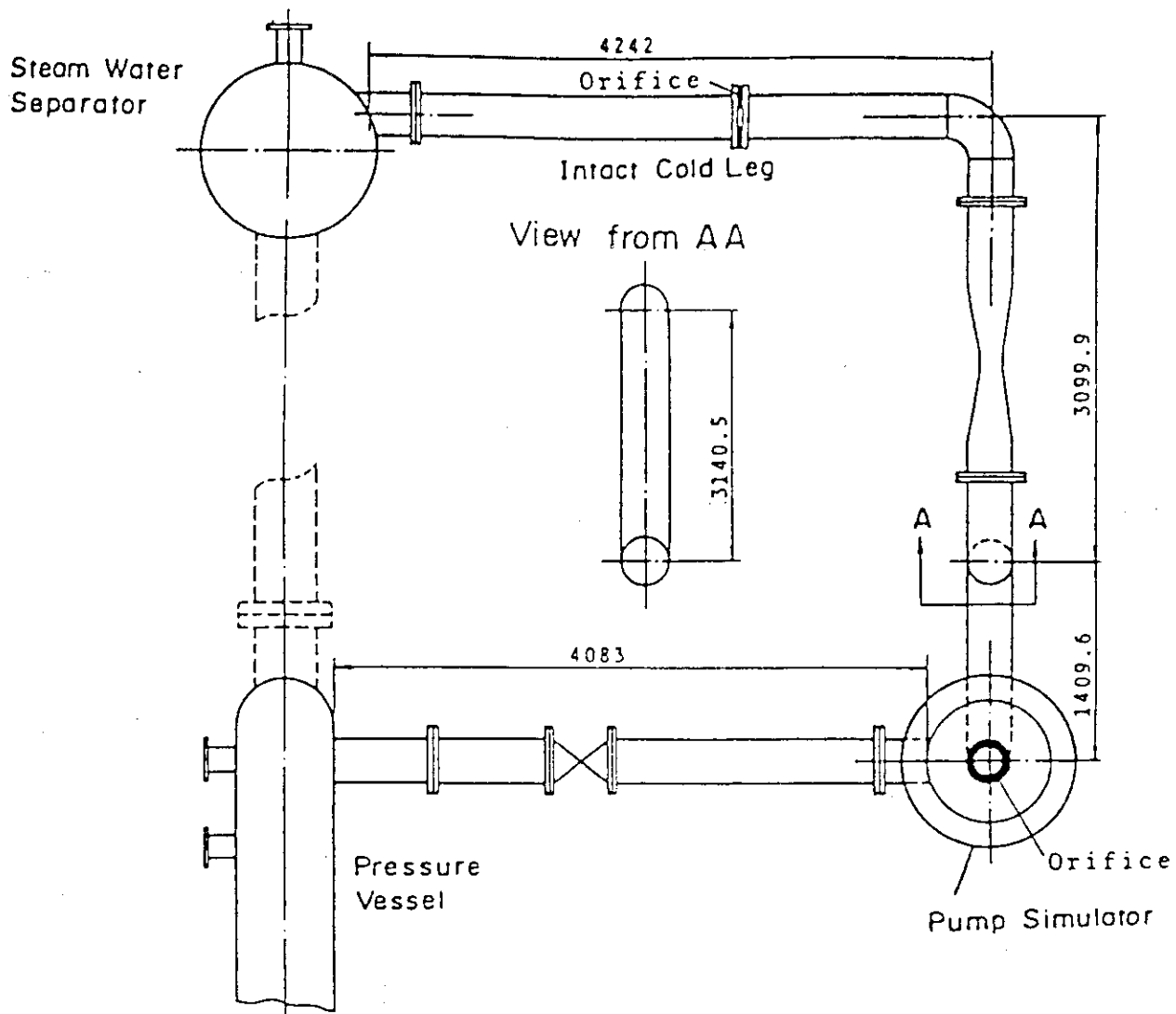


Fig. A-12 Arrangement of Intact Cold Leg

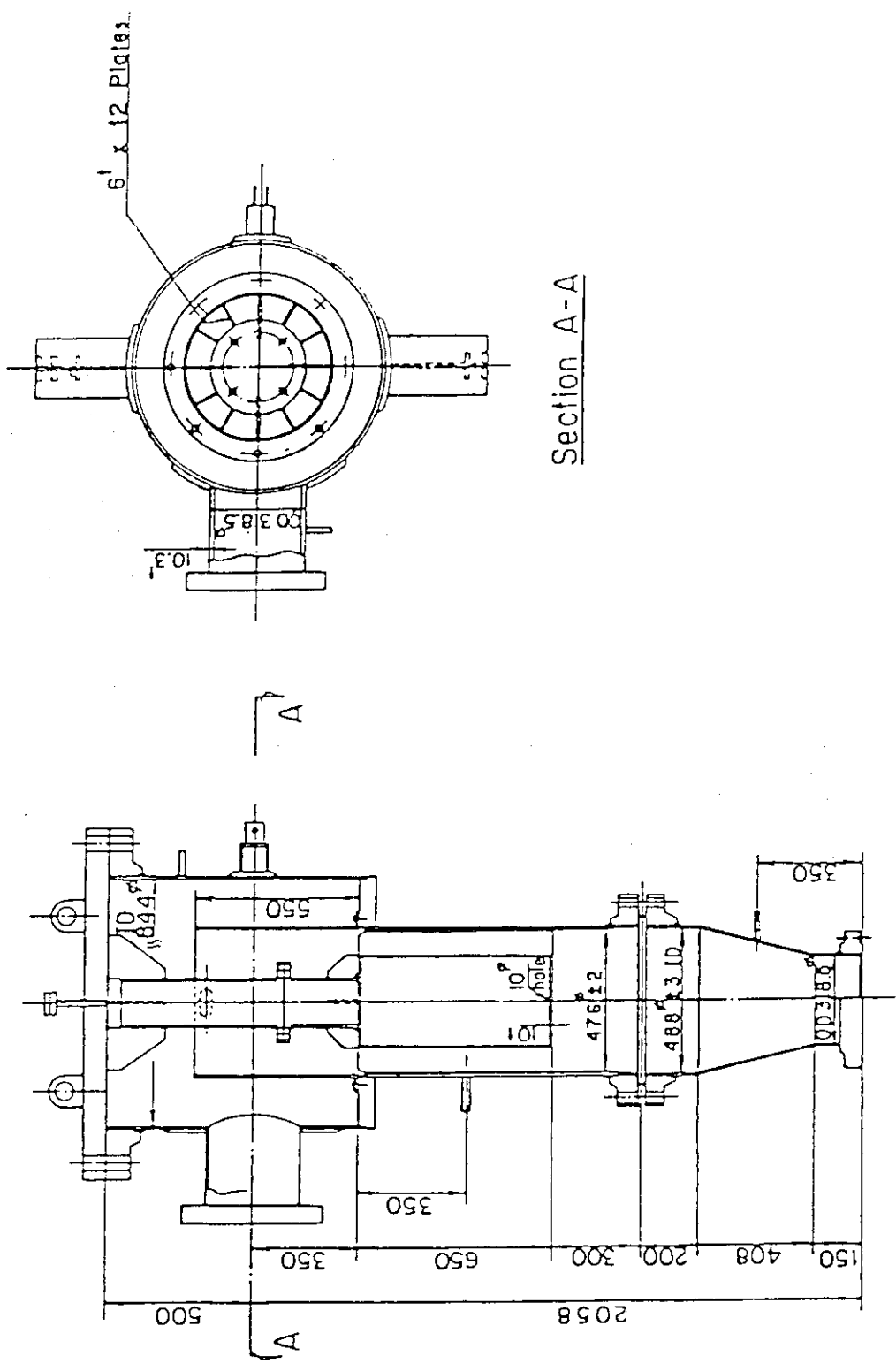
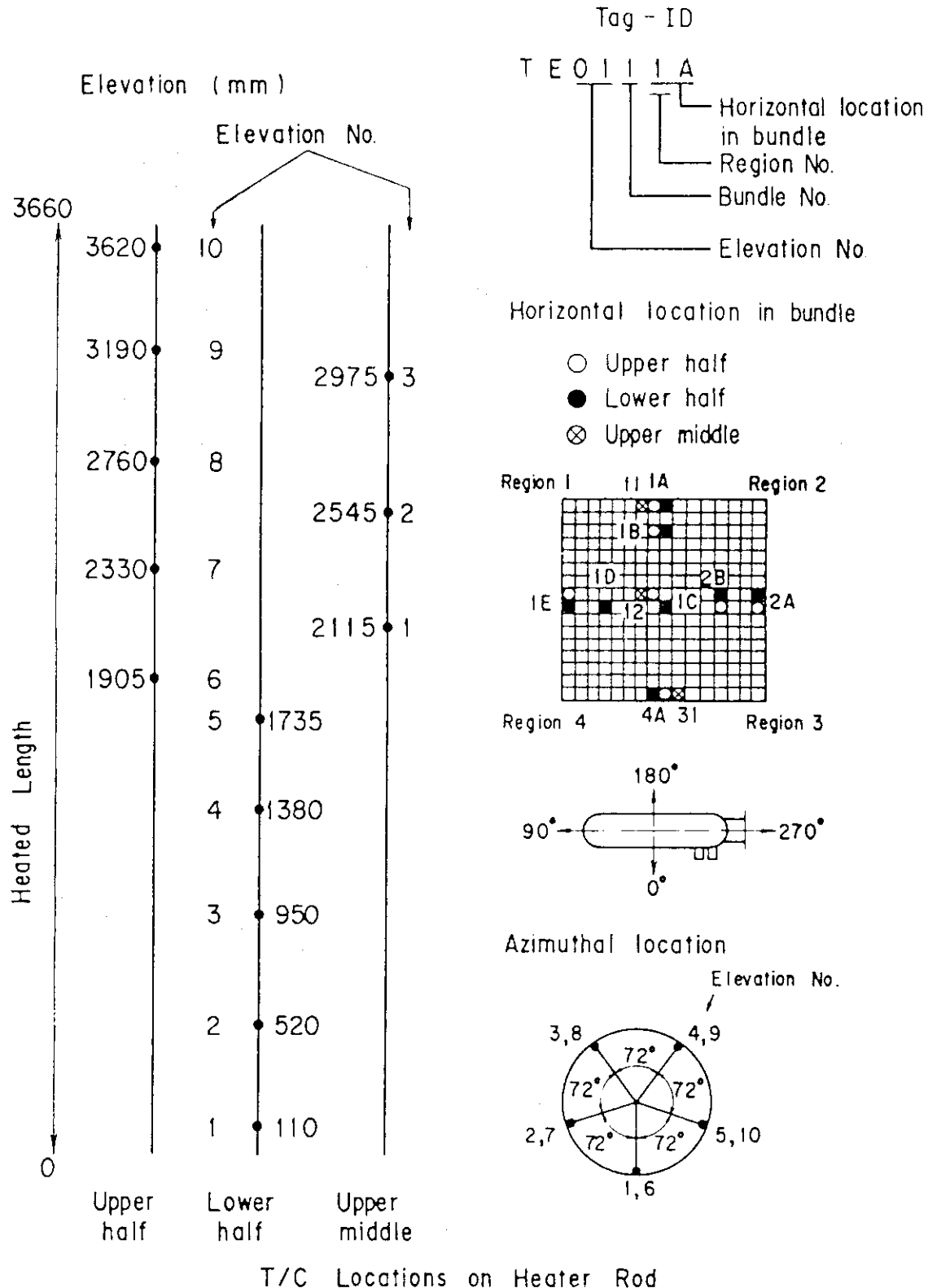


Fig. A-13 Configuration and Dimension of Pump Simulator



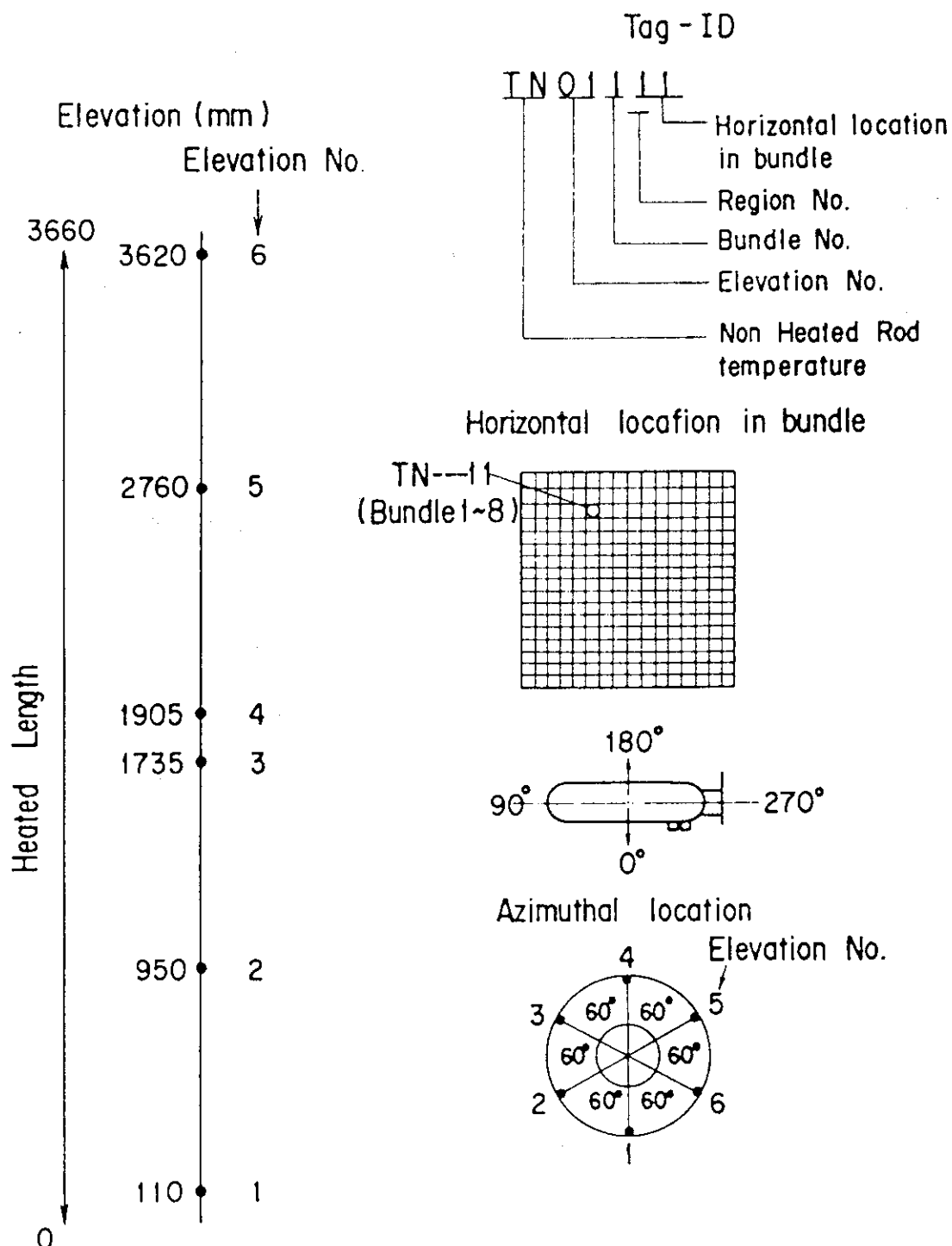
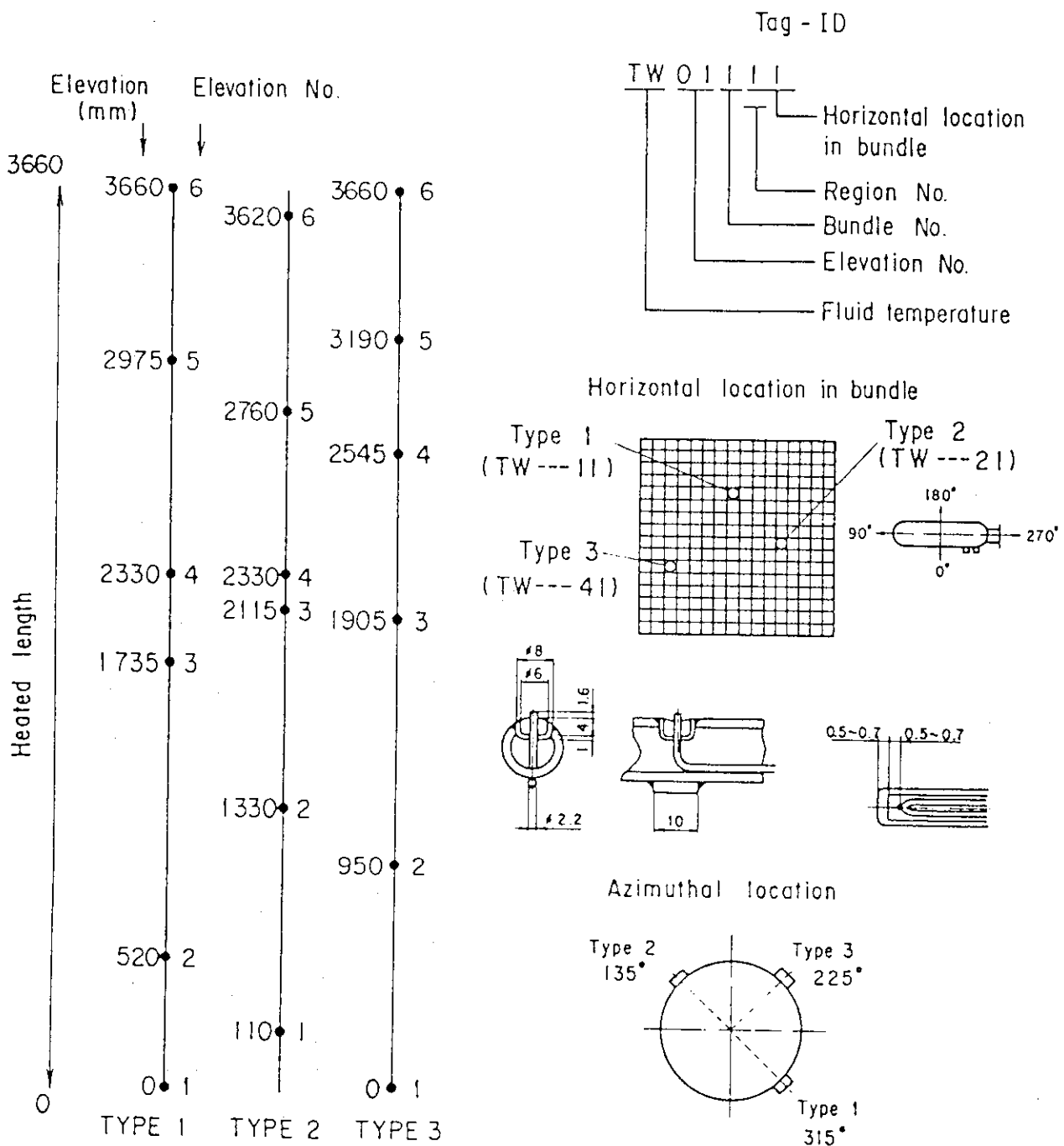


Fig. A-15 Thermocouple Locations of Non-Heated Rod Surface Temperature Measurements



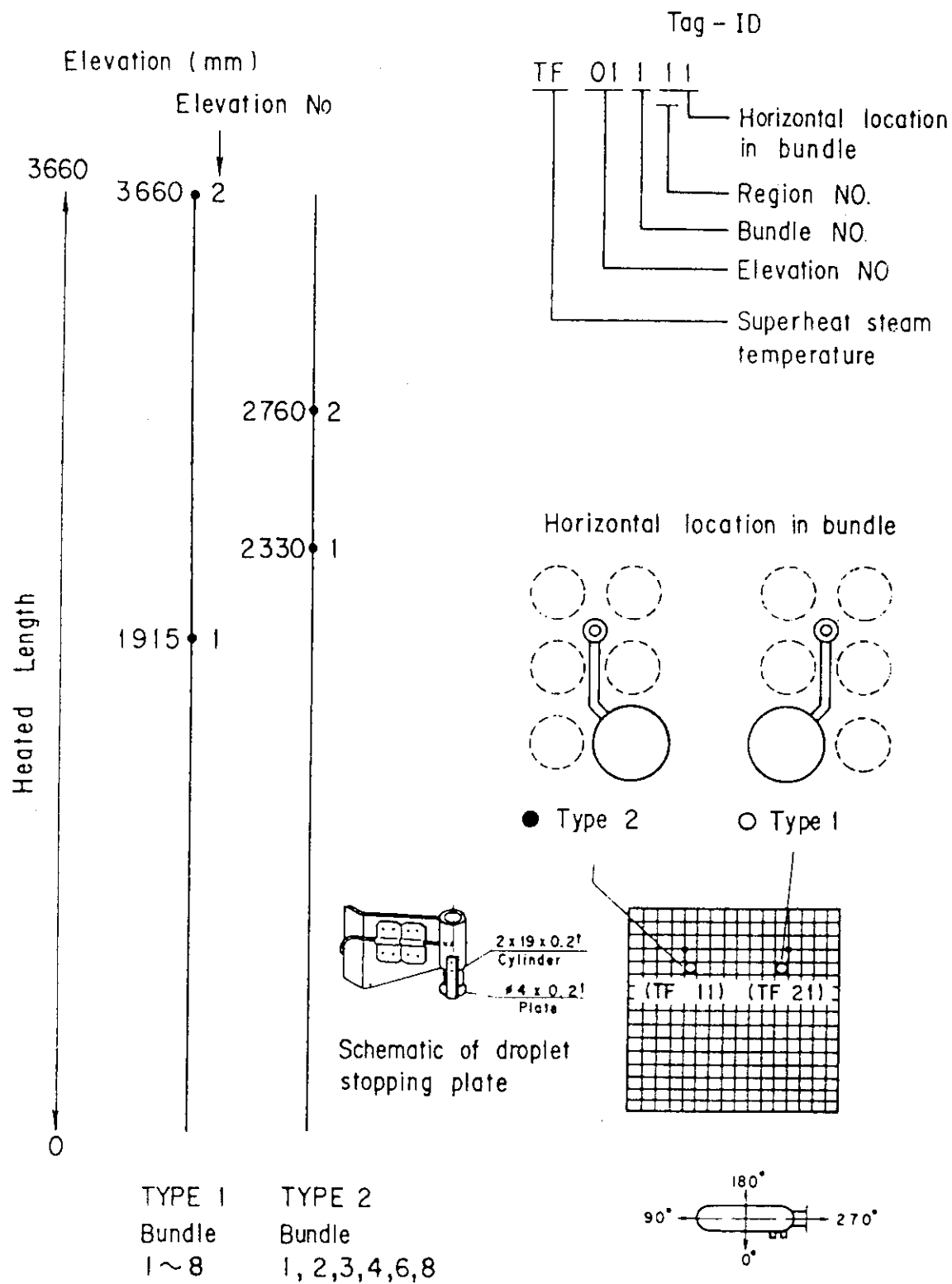


Fig. A-17 Thermocouple Locations of Steam Temperature Measurements in Core

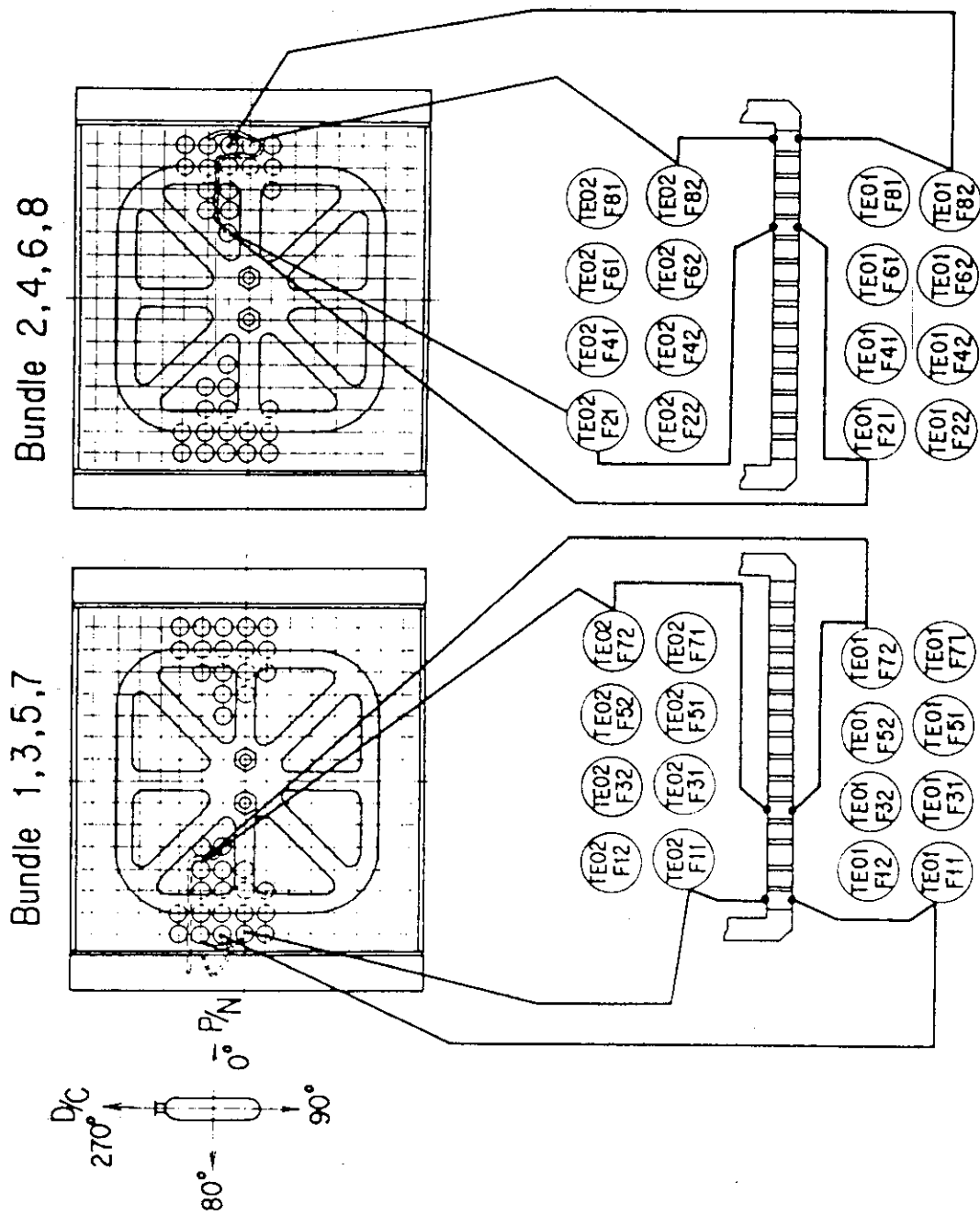


Fig. A-18 Thermocouple Locations of Fluid Temperature Measurement just above and below End Box Tie Plate

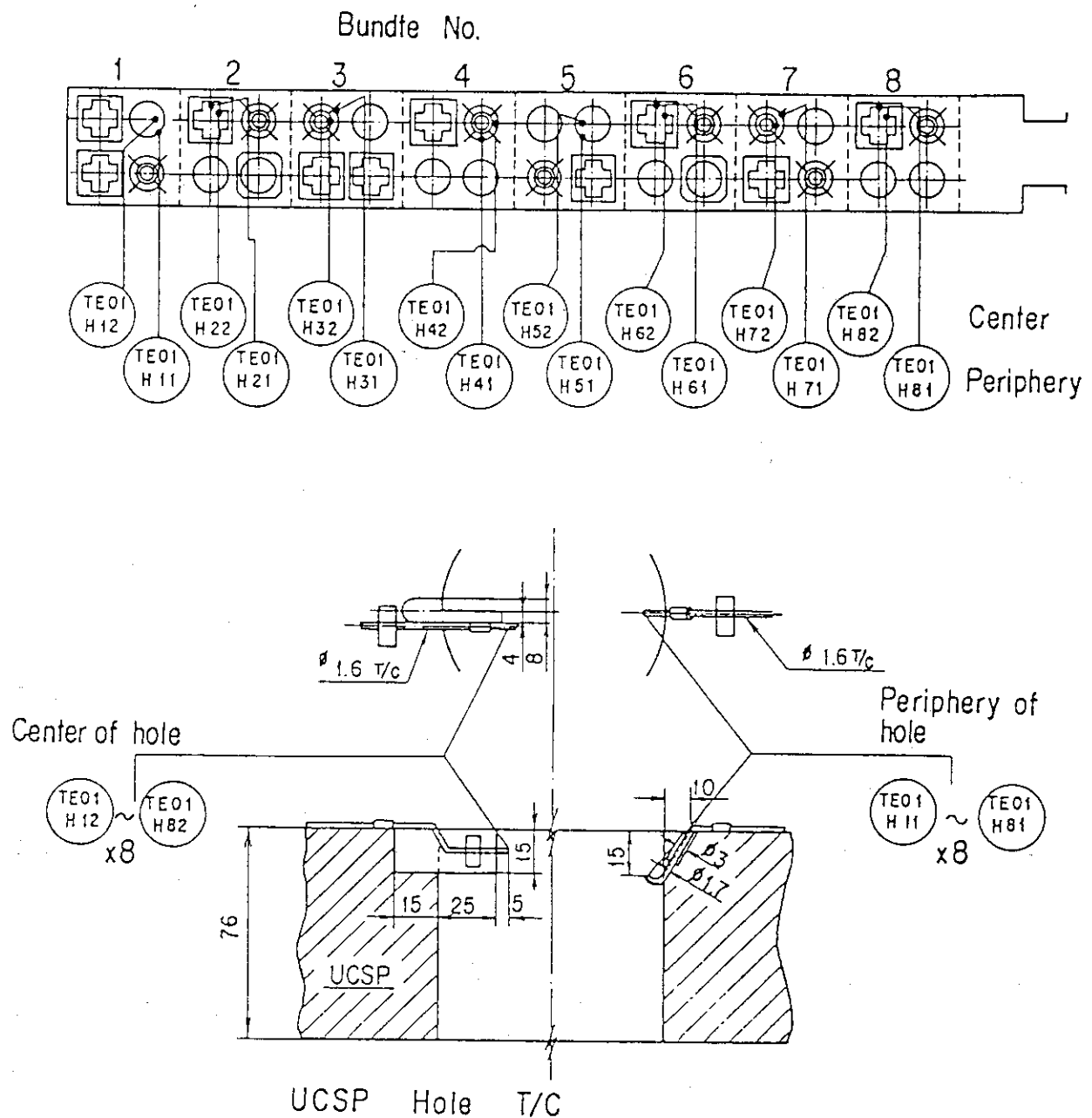


Fig. A-19 Thermocouple Locations of Fluid Temperature Measurements at Center and Periphery of UCSP Holes

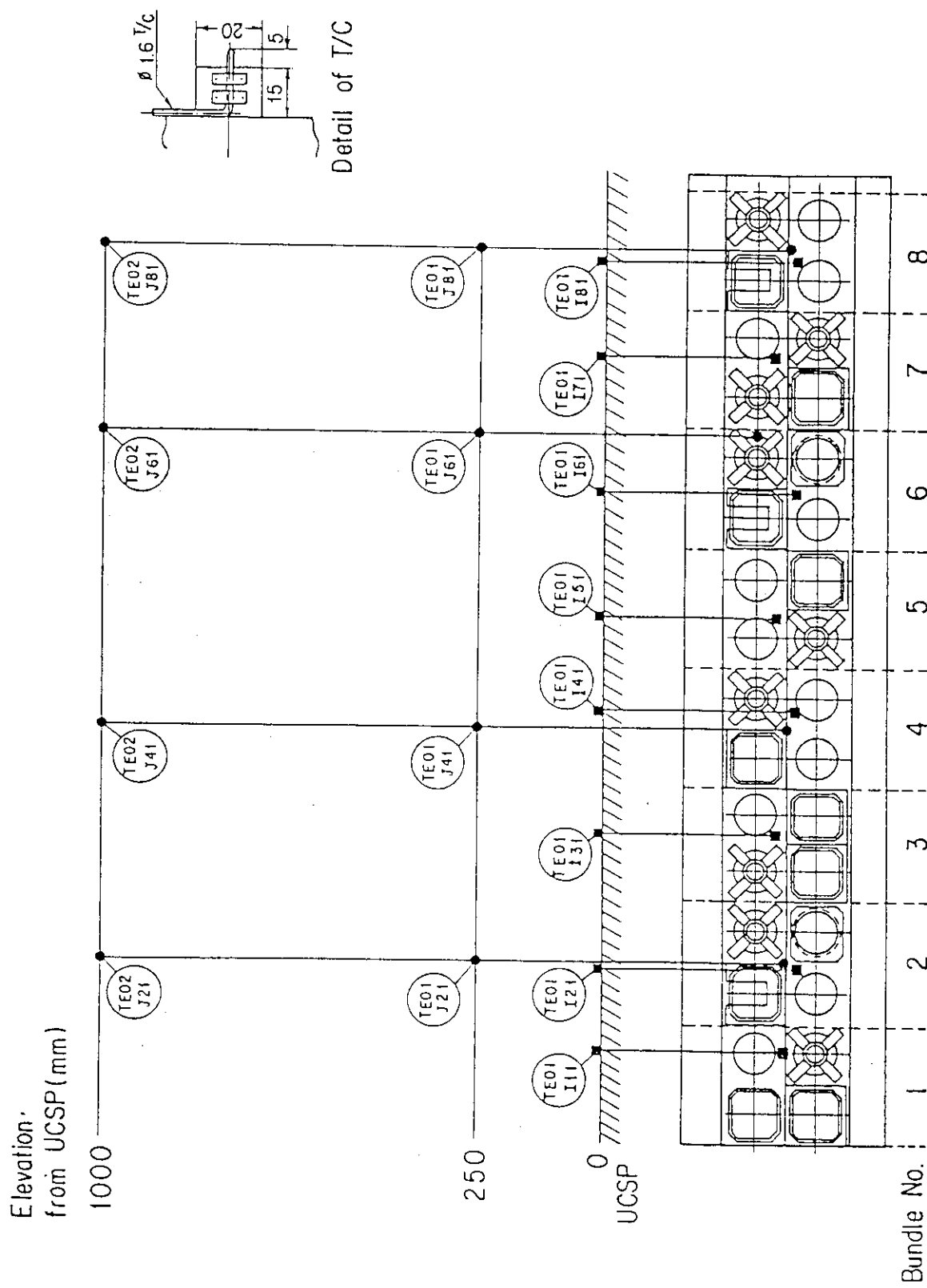


Fig. A-20 Thermocouple Locations of Fluid Temperature Measurements  
on and above UCSP

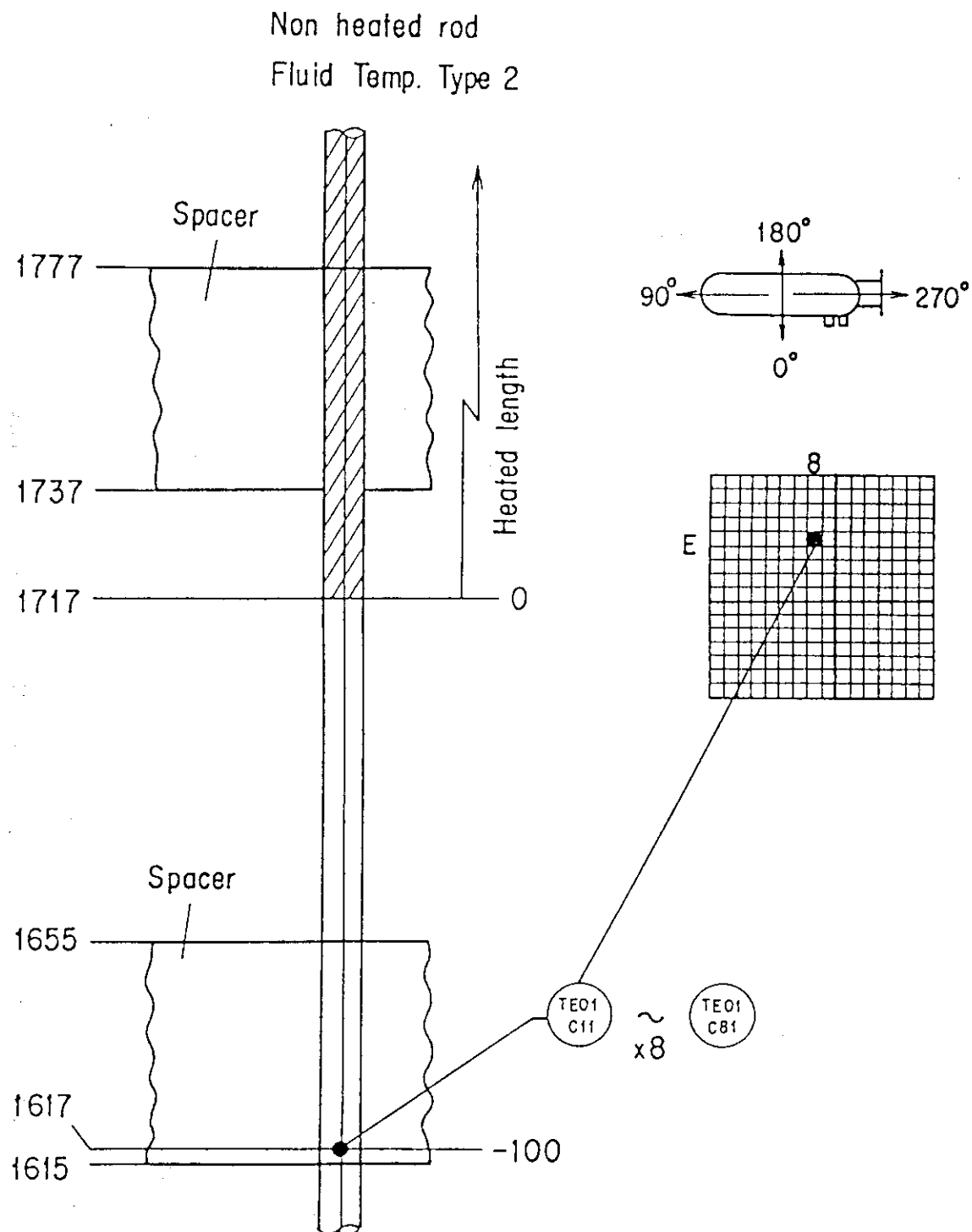


Fig. A-21 Thermocouple Locations of Fluid Temperature Measurements at Core Inlet

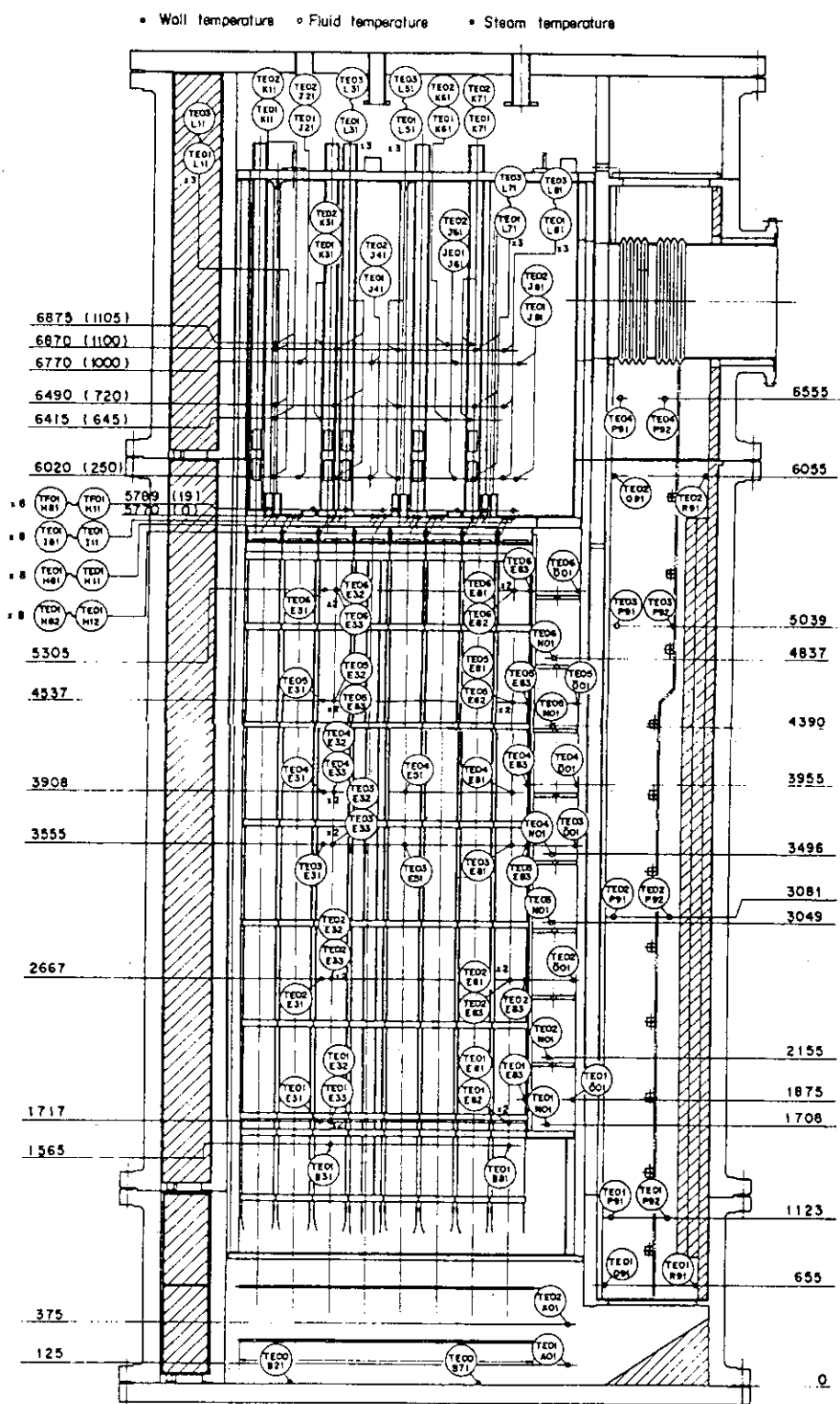


Fig. A-22 Thermocouple Locations of Temperature Measurements in Pressure Vessel except Core Region

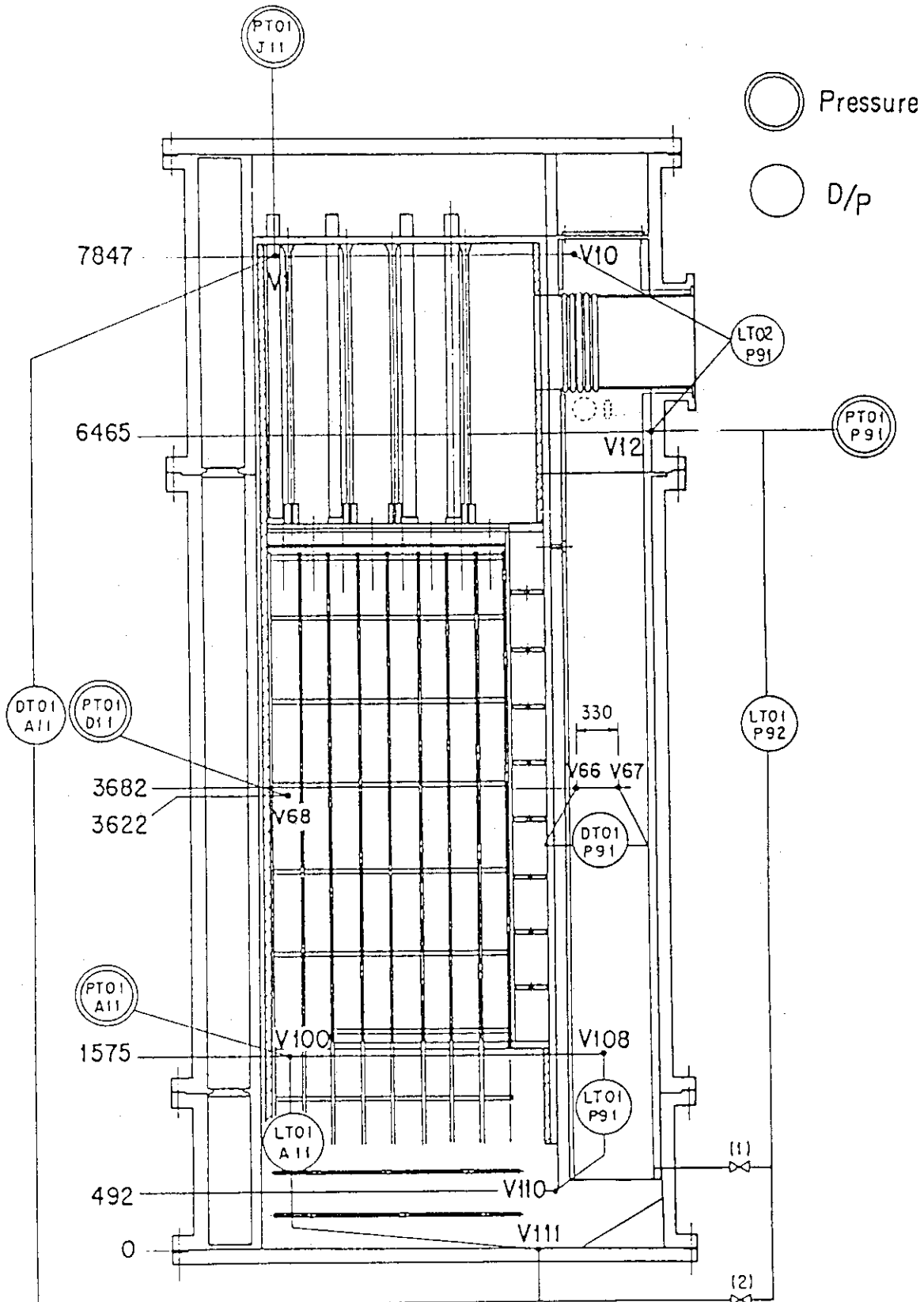


Fig. A-23 Location of Pressure Measurements in Pressure Vessel, Differential Pressure Measurements between Upper and Lower Plenums and Liquid Level Measurements in Downcomer and Lower Plenum

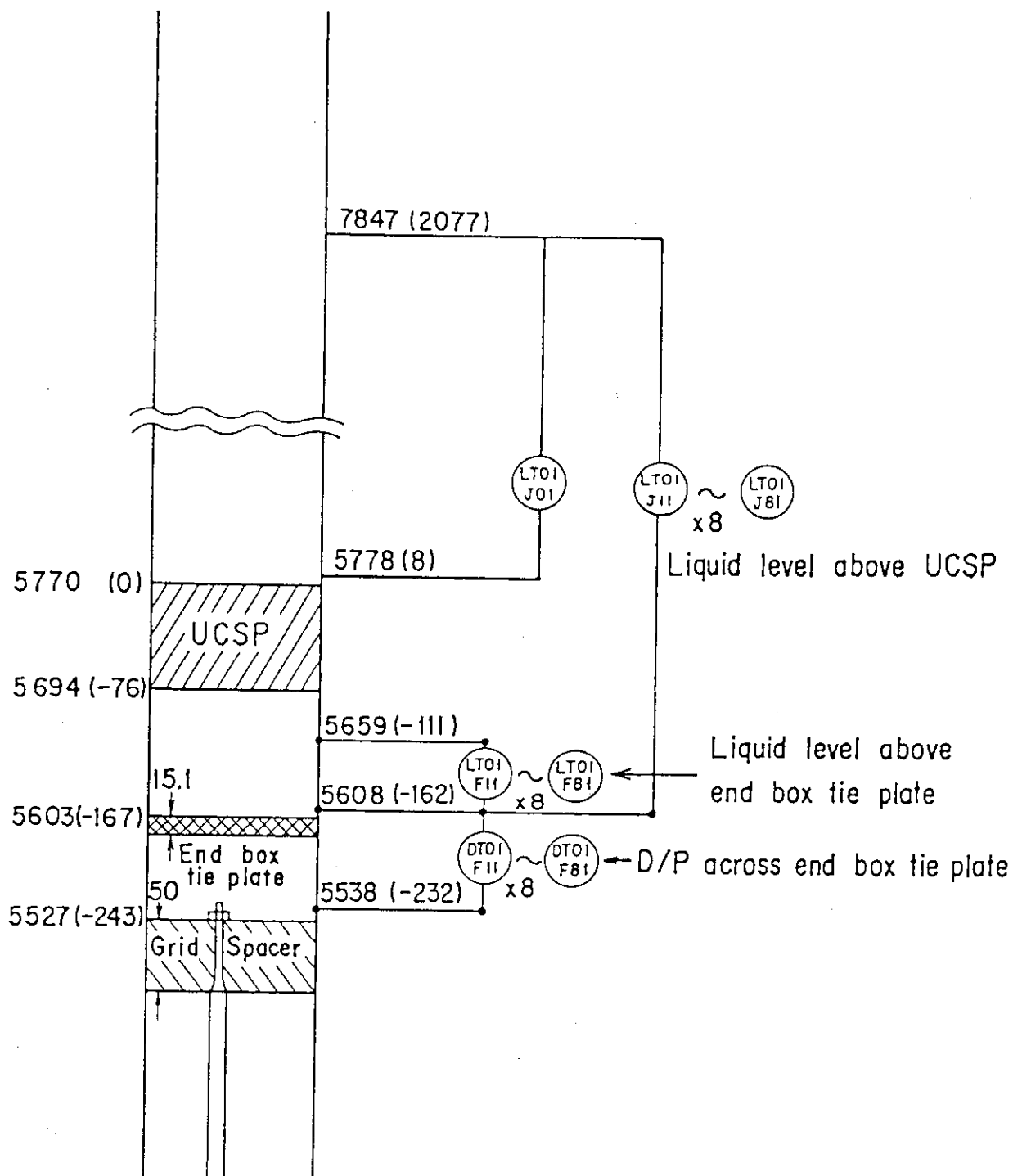


Fig. A-24 Locations of Differential Pressure Measurements across End Box Tie Plate and Liquid Level Measurements above UCSP and End Box Tie Plate

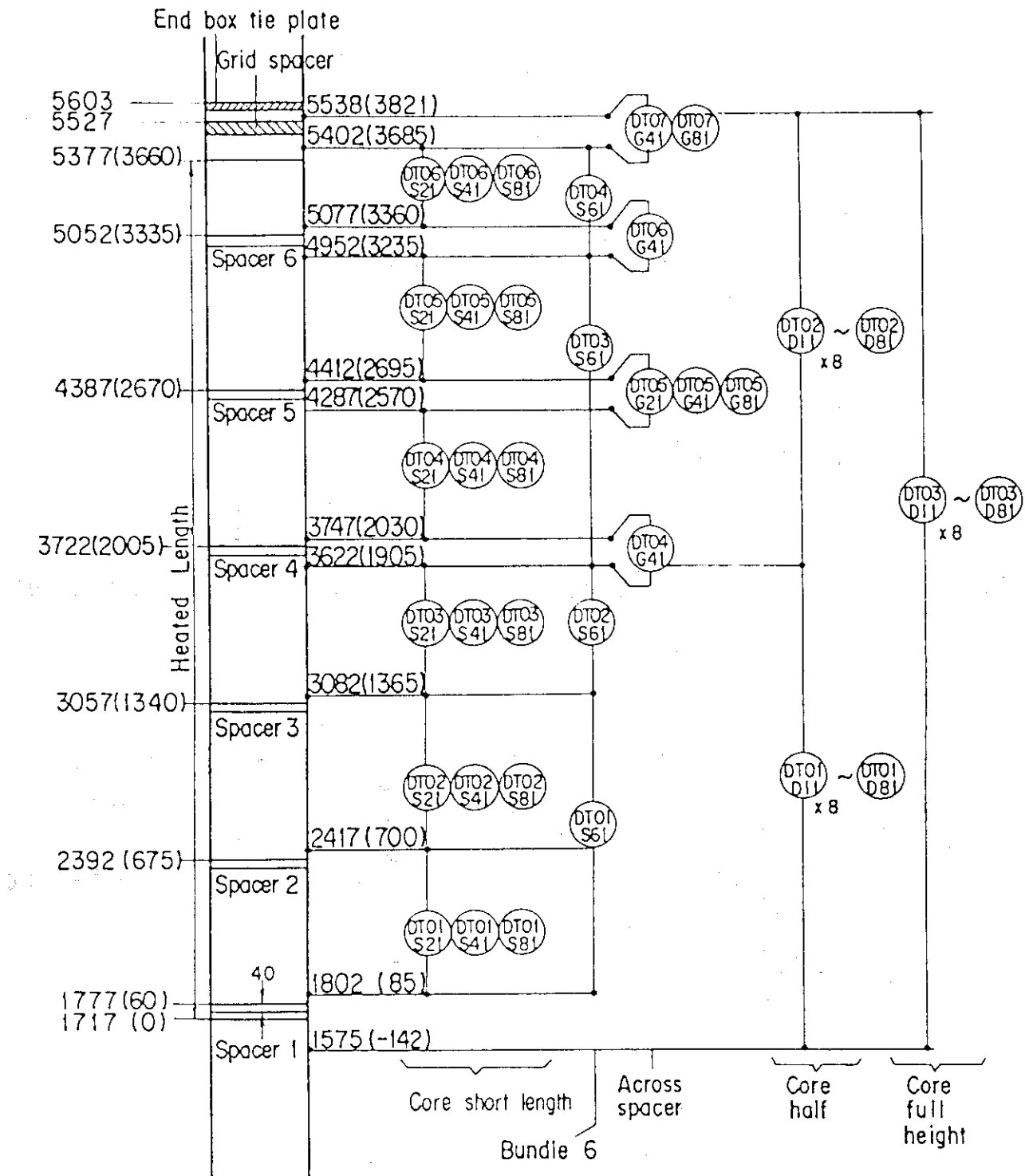


Fig. A-25 Locations of Vertical Differential Pressure Measurements in Core

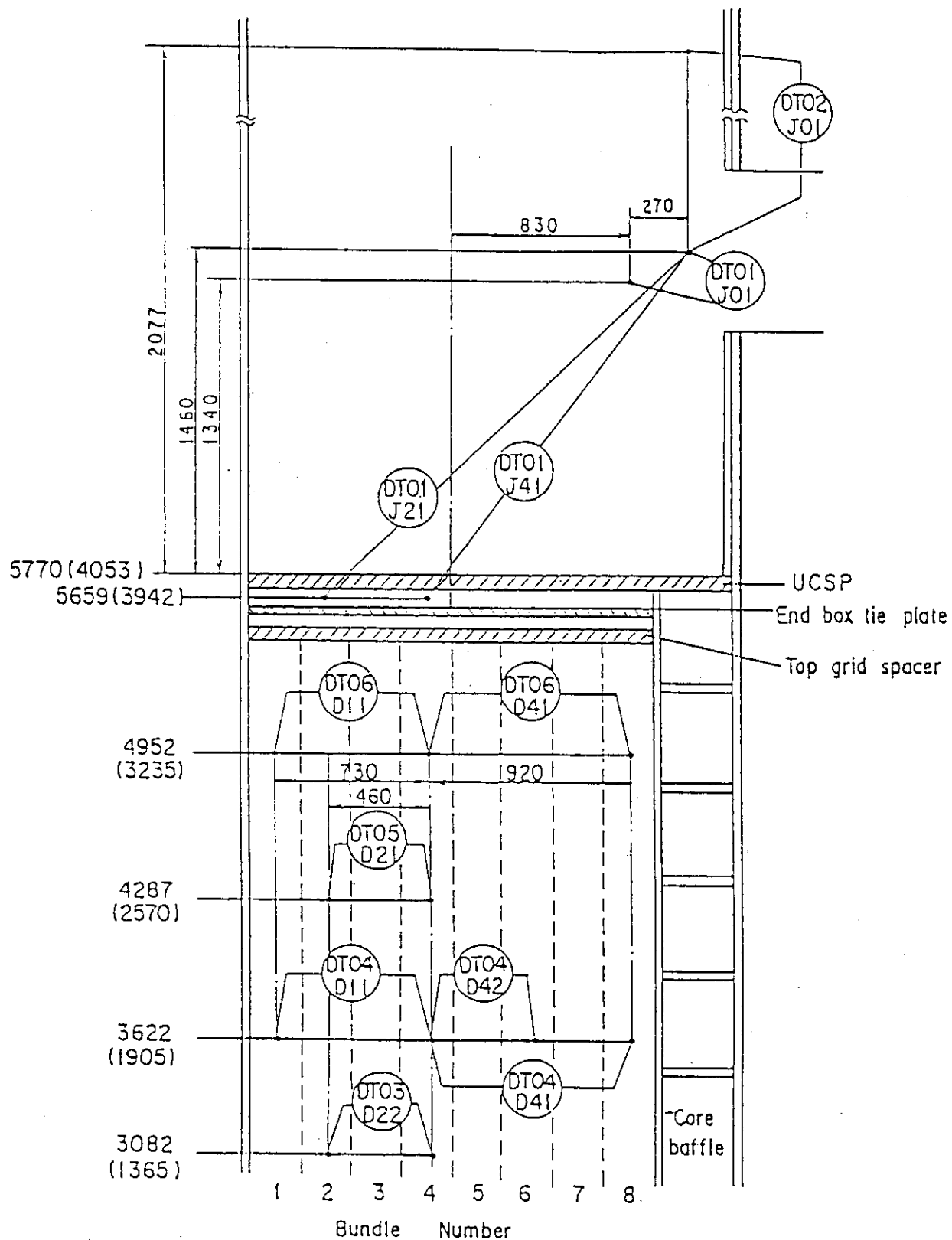


Fig. A-26 Measurement Locations of Horizontal Differential Pressures in Core and Differential Pressures in Upper Plenum

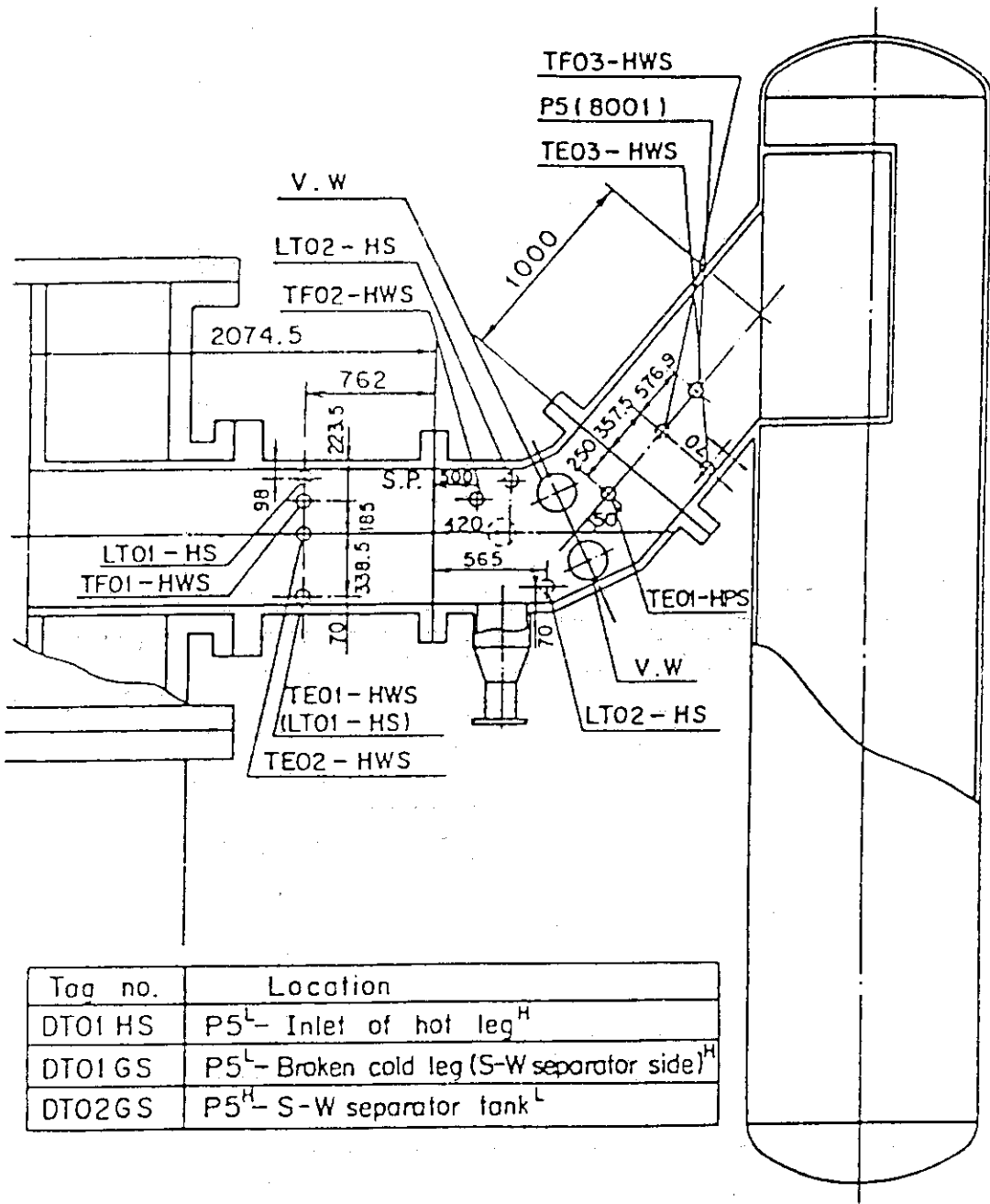


Fig. A-27 Locations of Hot Leg Instrumentation

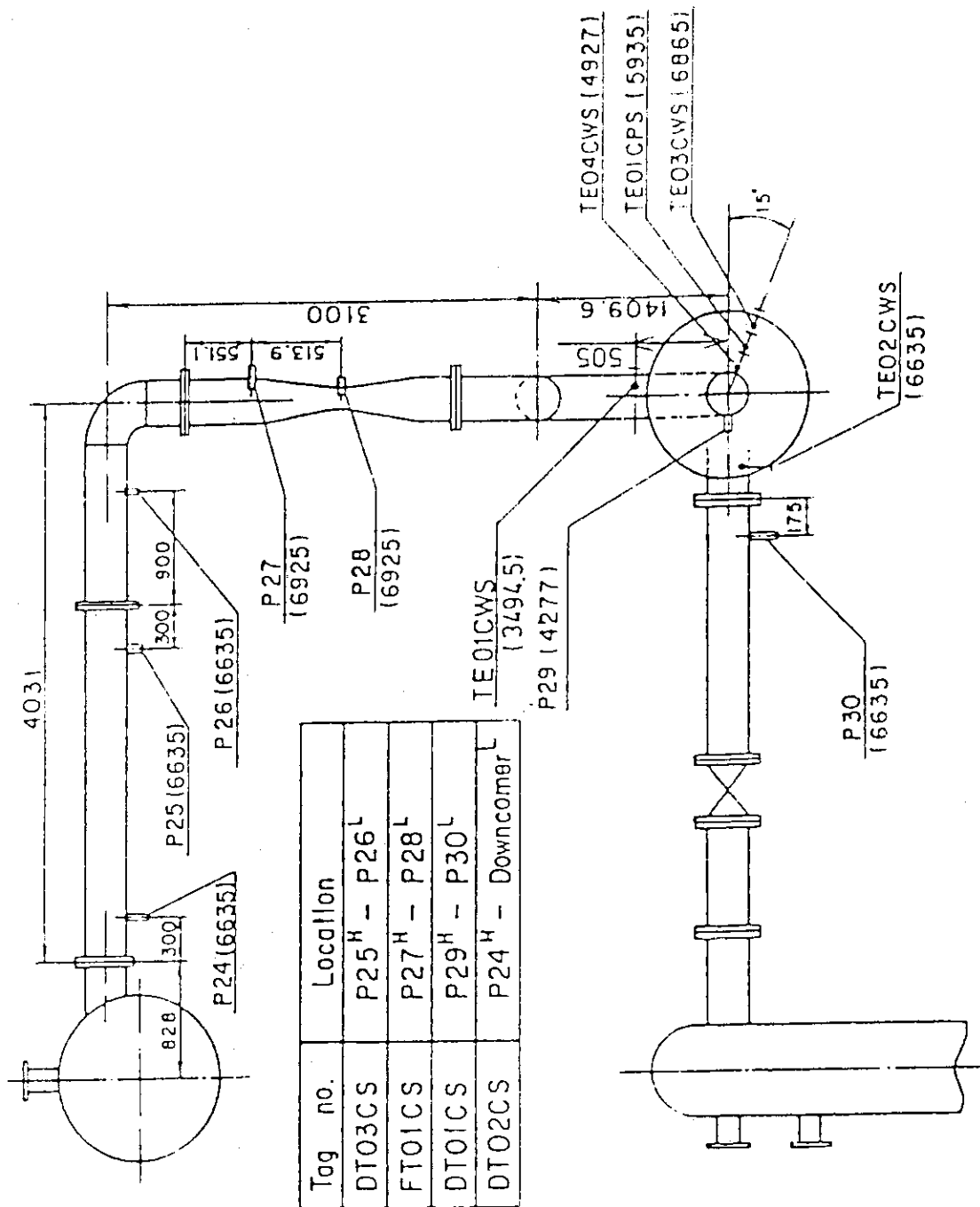


Fig. A-28 Locations of Intact Cold Leg Instrumentation

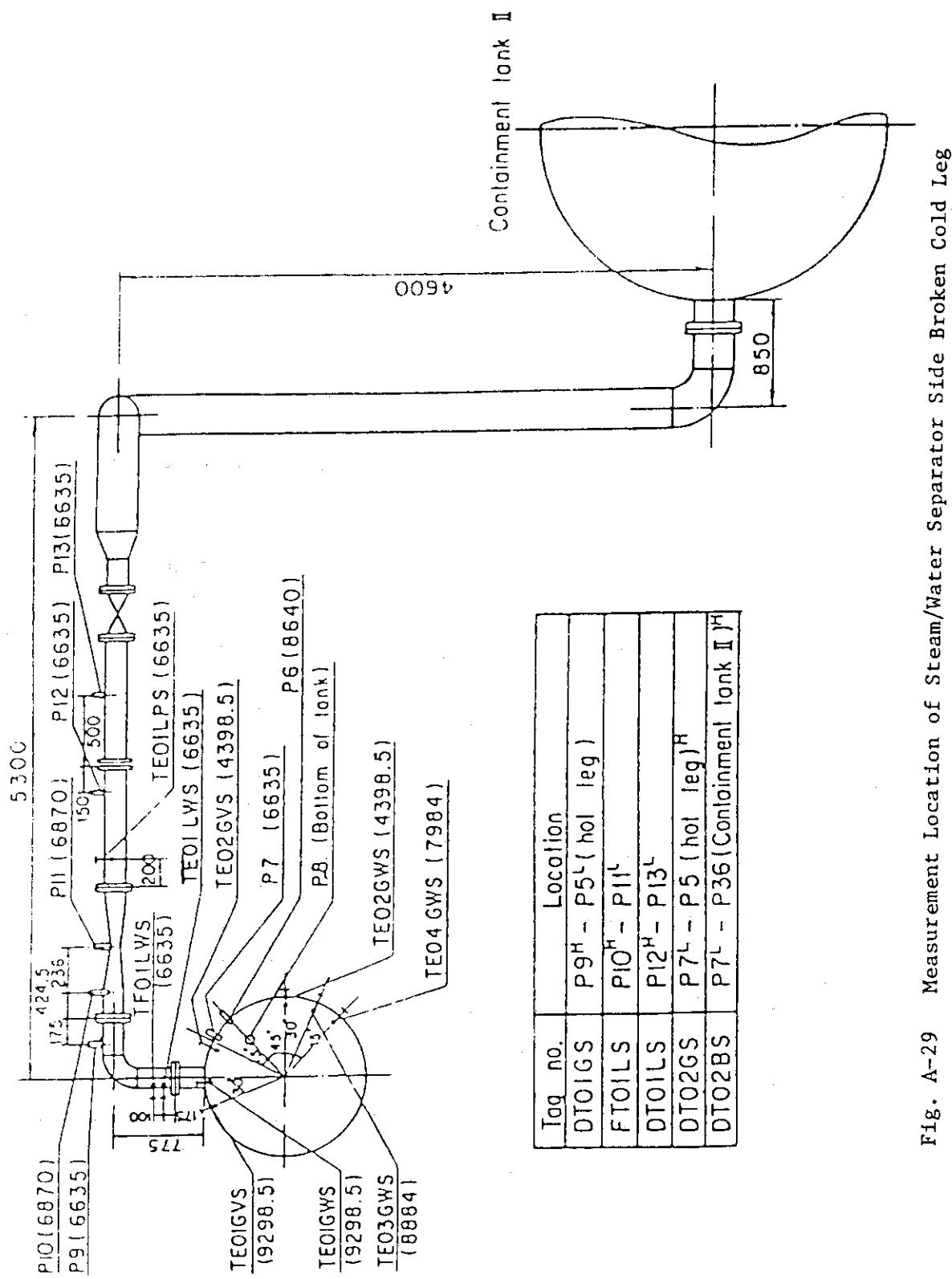


Fig. A-29 Measurement Location of Steam/Water Separator Side Broken Cold Leg

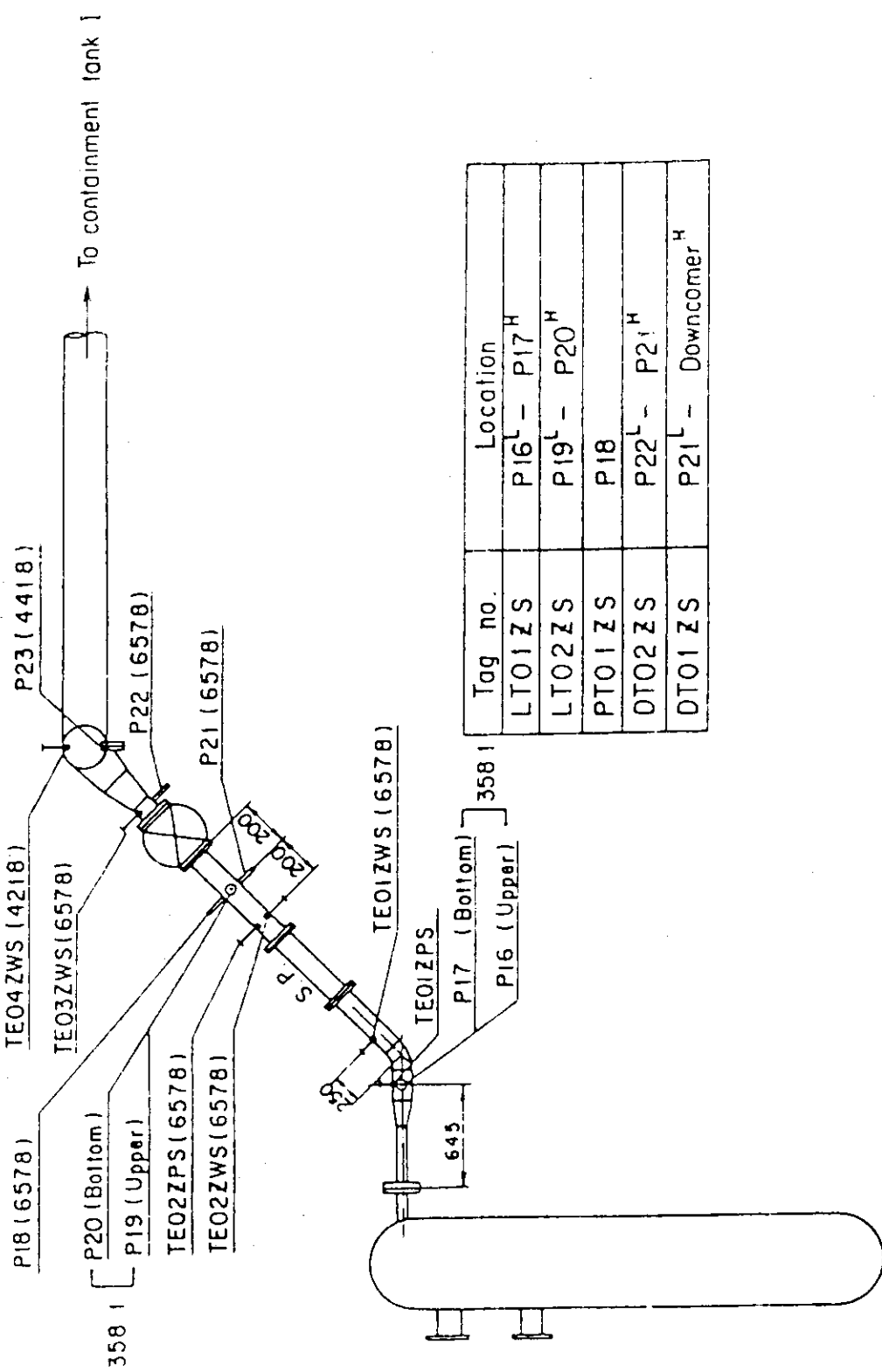


Fig. A-30 Measurement Location of Pressure Vessel Side Broken Cold Leg

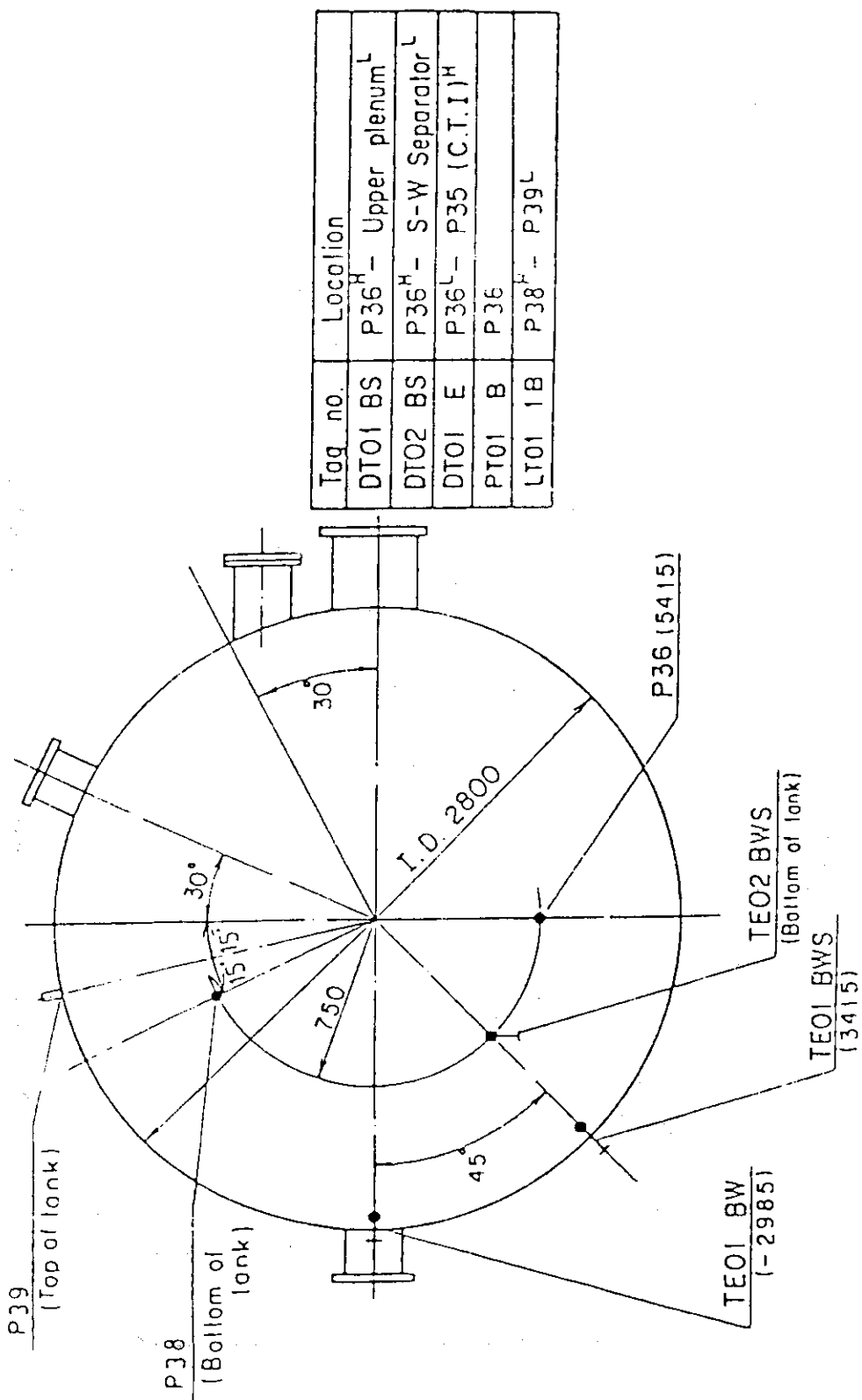


Fig. A-31 Locations of Containment Tank-II Instrumentation

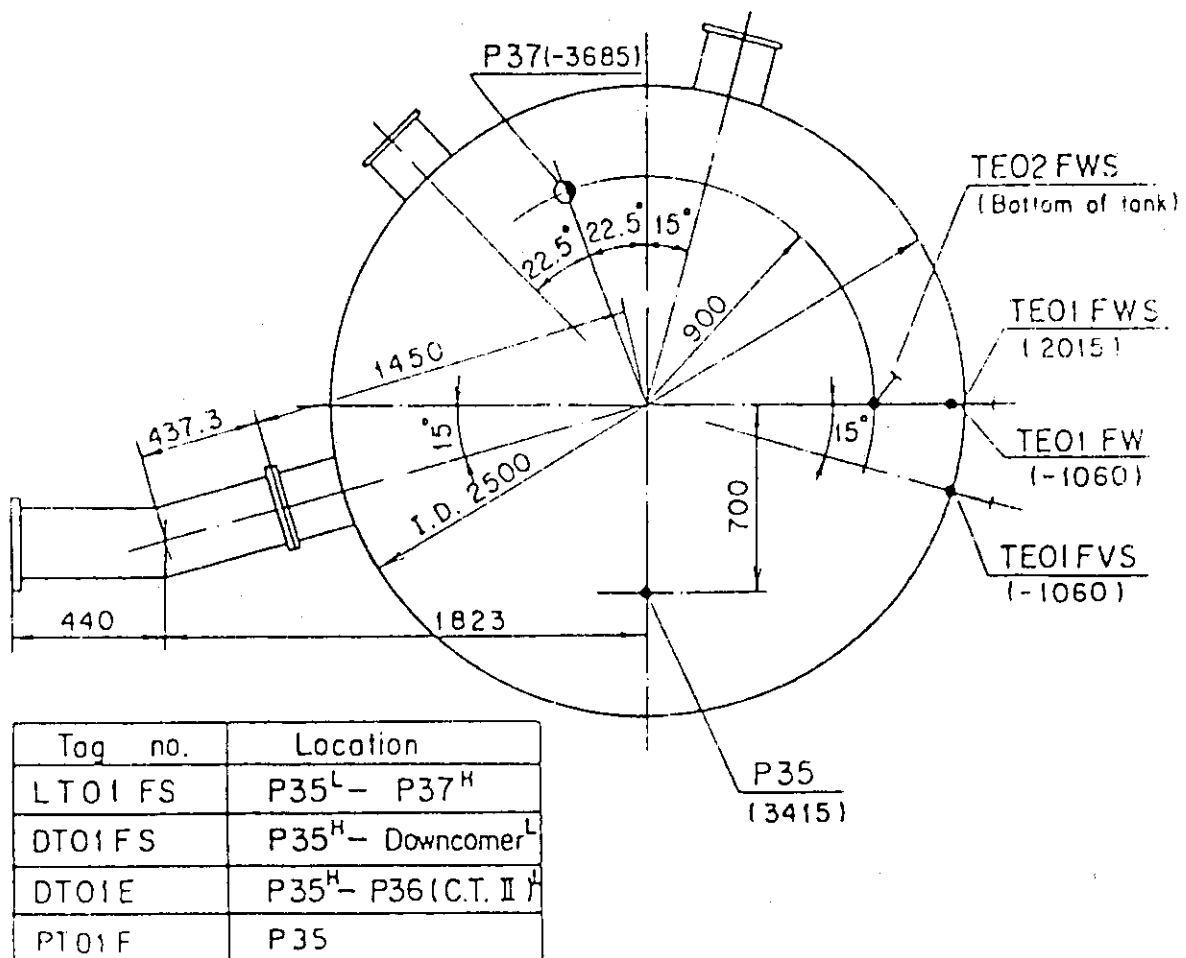
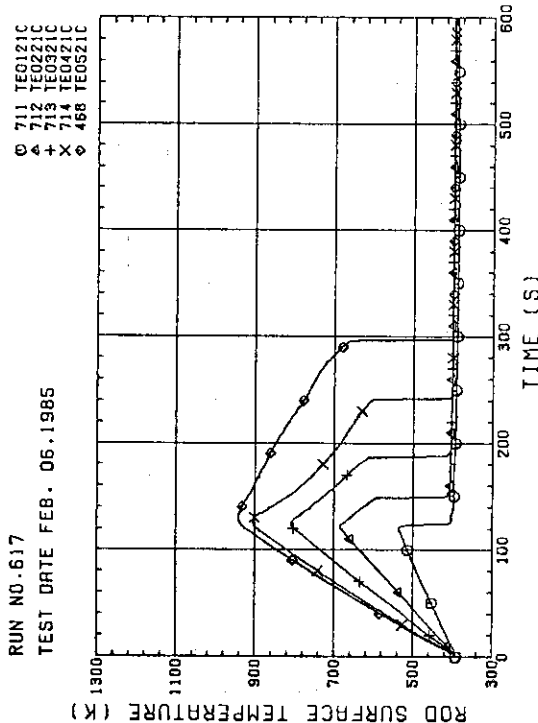
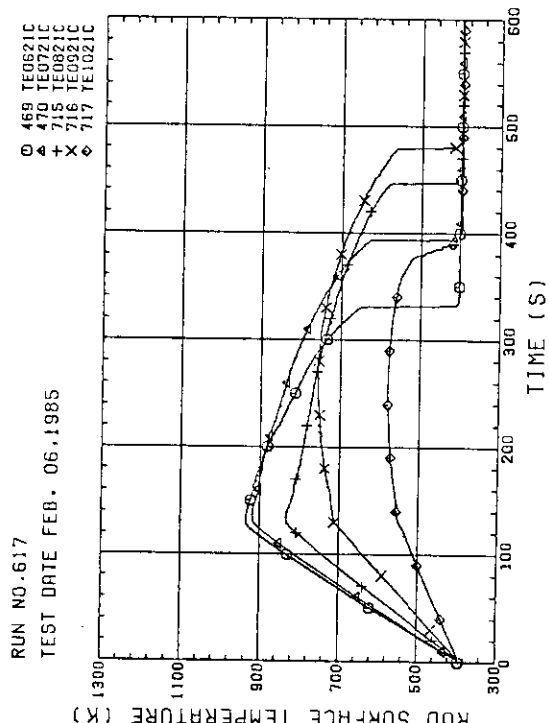
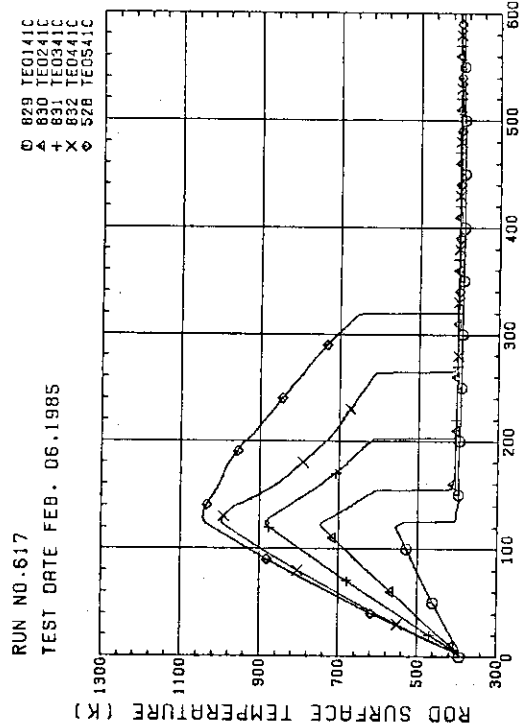
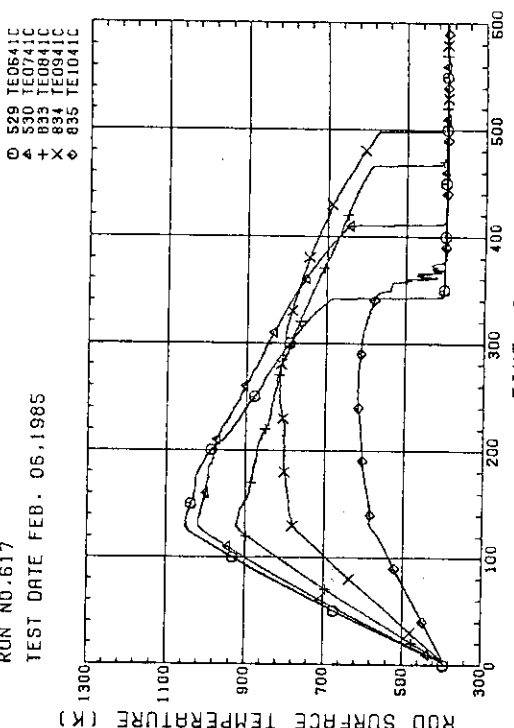
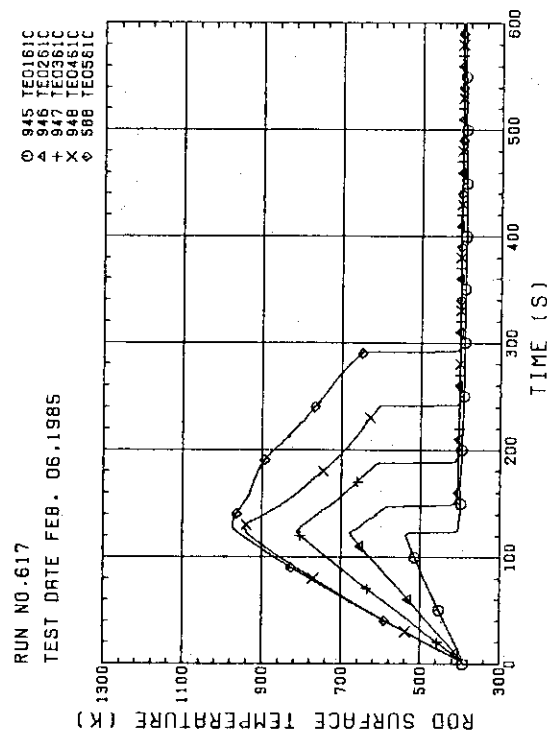
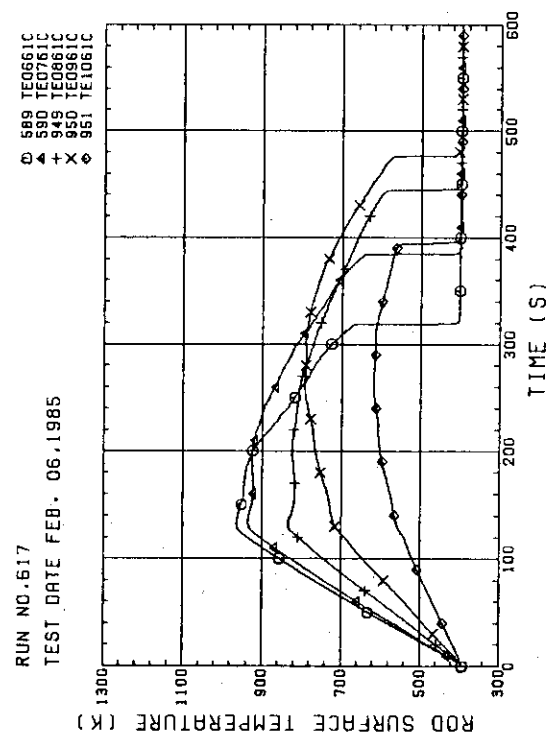
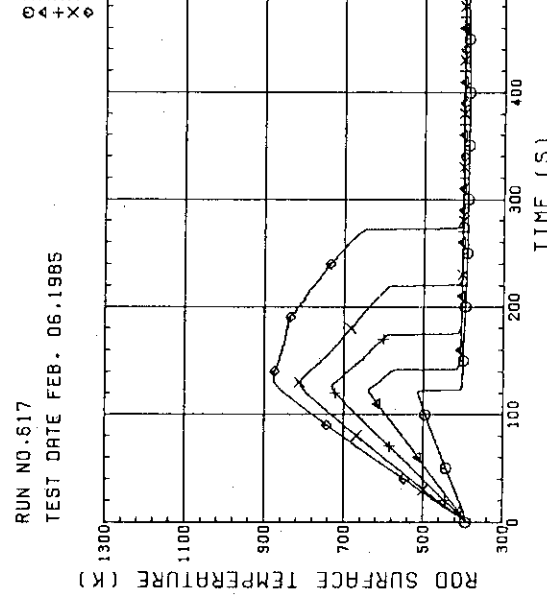
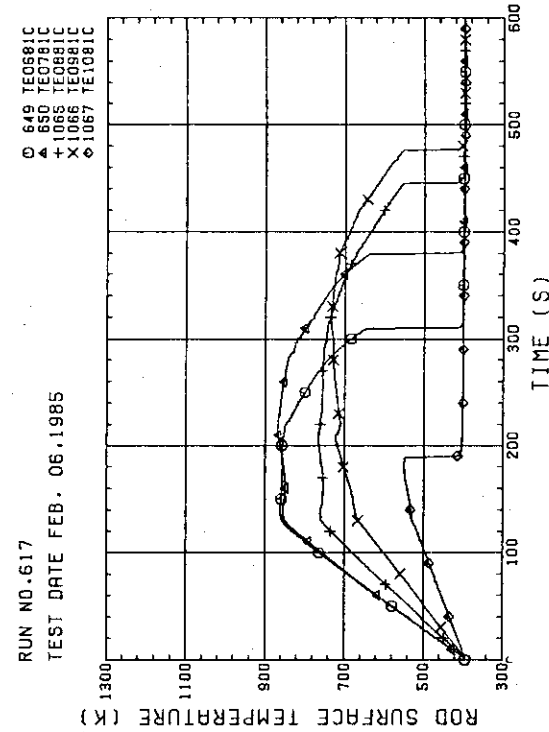


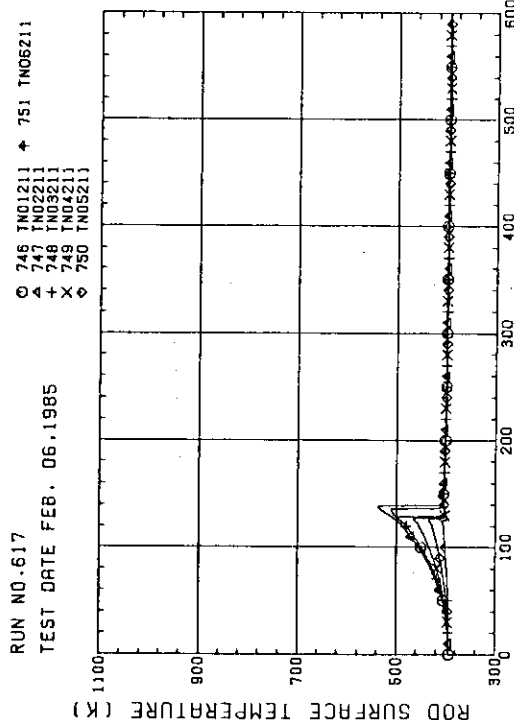
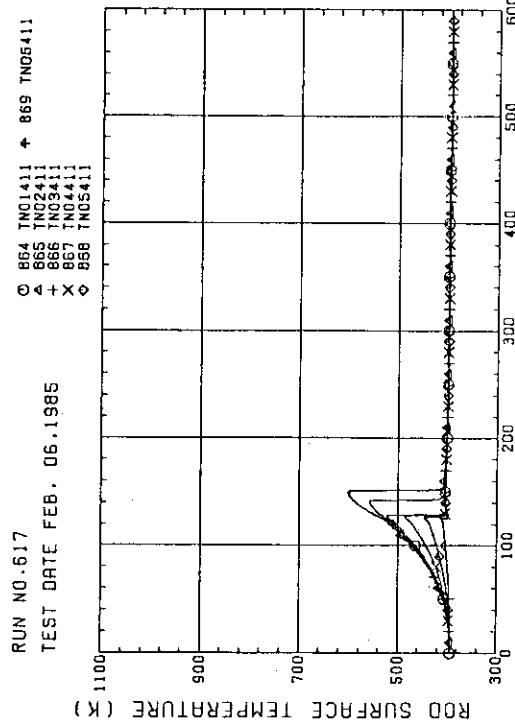
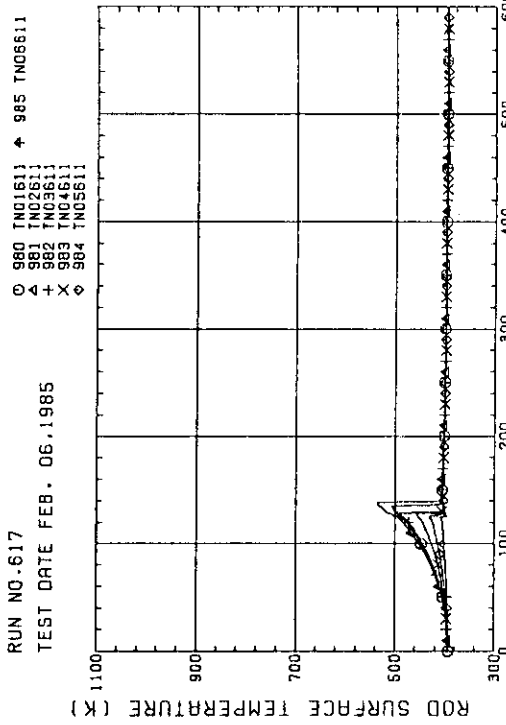
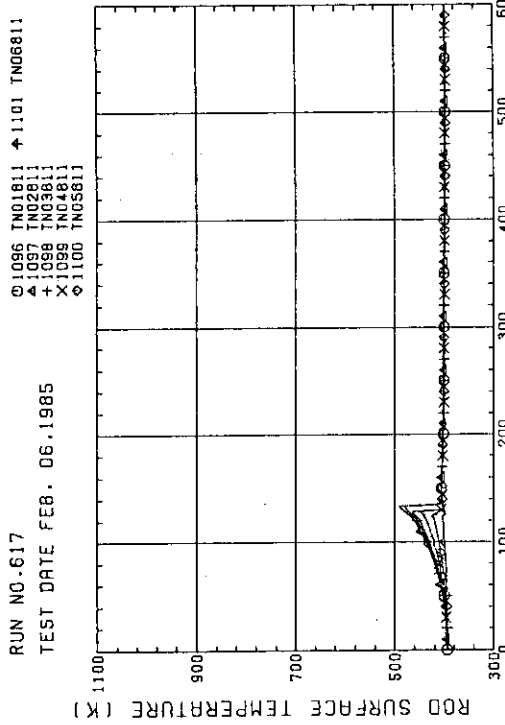
Fig. A-32 Locations of Containment Tank-I Instrumentation

## Appendix B Selected Data of Test S2-12

Fig. B-1 ~ B-8	Heater rod temperature
Fig. B-9 ~ B-12	Non-heated rod temperatures
Fig. B-13 ~ B-16	Steam Temperatures
Fig. B-17 ~ B-18	Fluid temperatures just above end box tie plate
Fig. B-19 ~ B-20	Fluid temperatures at core inlet
Fig. B-21 ~ B-24	Fluid temperatures in core
Fig. B-25 ~ B-26	Liquid levels above end box tie plate
Fig. B-27 ~ B-28	Liquid levels above UCSP
Fig. B-29	Liquid levels in hot leg
Fig. B-30 ~ B-31	Differential pressures across core full height
Fig. B-32 ~ B-33	Differential pressures across end box tie plate
Fig. B-34 ~ B-37	Horizontal differential pressures in core
Fig. B-38 ~ B-42	Differential pressures in primary loops
Fig. B-43 ~ B-44	Pressures in pressure vessel and containment tanks
Fig. B-45 ~ B-46	Bundle powers
Fig. B-47	ECC flow rates

Fig. B-1 HEATER ROD TEMPERATURE  
(BUNDLE 2-1C, LOWER HALF)Fig. B-2 HEATER ROD TEMPERATURE  
(BUNDLE 2-1C, UPPER HALF)Fig. B-3 HEATER ROD TEMPERATURE  
(BUNDLE 4-1C, LOWER HALF)Fig. B-4 HEATER ROD TEMPERATURE  
(BUNDLE 4-1C, UPPER HALF)

Fig. B-5 HEATER ROD TEMPERATURE  
(BUNDLE 6-1C, LOWER HALF)Fig. B-6 HEATER ROD TEMPERATURE  
(BUNDLE 6-1C, UPPER HALF)Fig. B-7 HEATER ROD TEMPERATURE  
(BUNDLE 6-1C, LOWER HALF)Fig. B-8 HEATER ROD TEMPERATURE  
(BUNDLE 6-1C, UPPER HALF)

Fig. B-9 NON-HEATED ROD TEMPERATURE  
(BUNDLE 2+1)Fig. B-10 NON-HEATED ROD TEMPERATURE  
(BUNDLE 4-1)Fig. B-11 NON-HEATED ROD TEMPERATURE  
(BUNDLE 6-1)Fig. B-12 NON-HEATED ROD TEMPERATURE  
(BUNDLE 8-1)

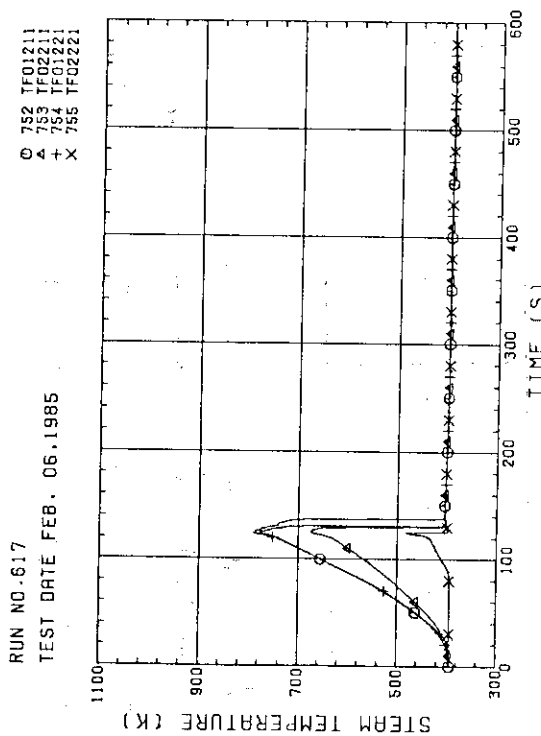


Fig. B-13 STEAM TEMPERATURE IN CORE, BUNDLE 2  
(01211-1.735M. 02211-1.875M. 02221-1.915M)

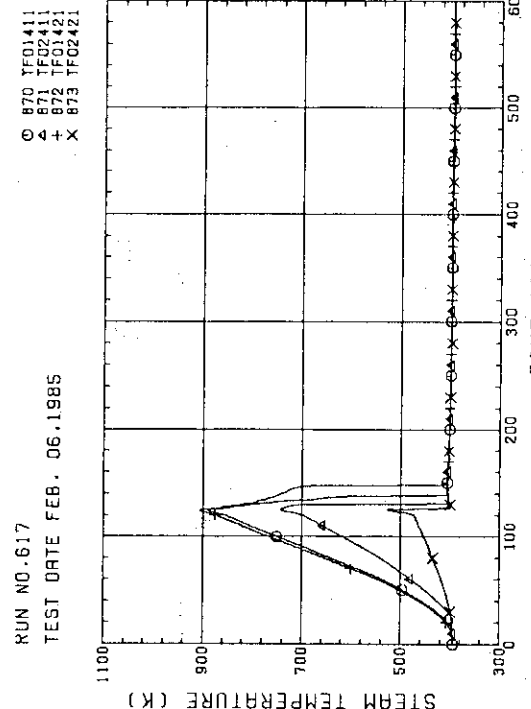


Fig. B-14 STEAM TEMPERATURE IN CORE, BUNDLE 4  
(01411-1.735M. 02411-1.875M. 01421-1.38M. 02421-1.915M)

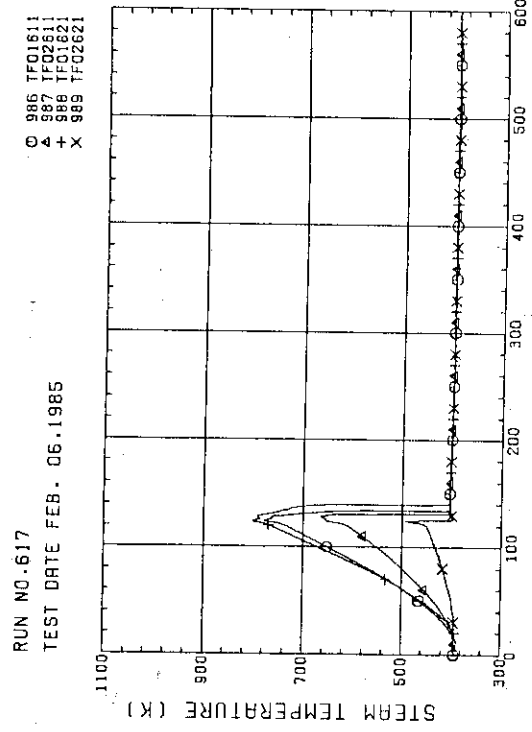


Fig. B-15 STEAM TEMPERATURE IN CORE, BUNDLE 6

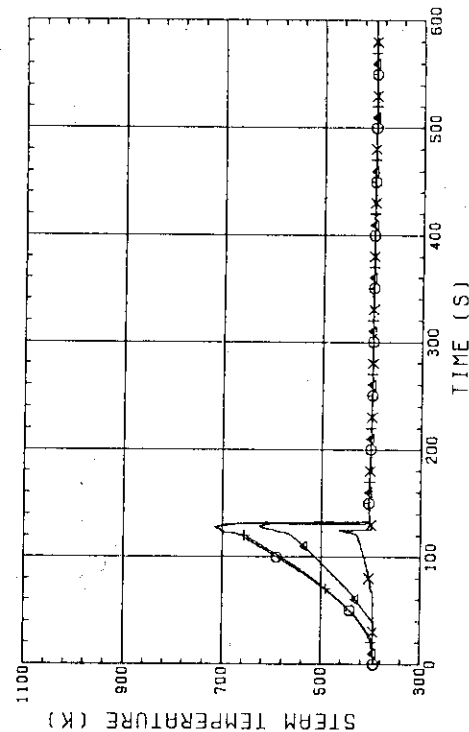


Fig. B-16 STEAM TEMPERATURE IN CORE, BUNDLE 6

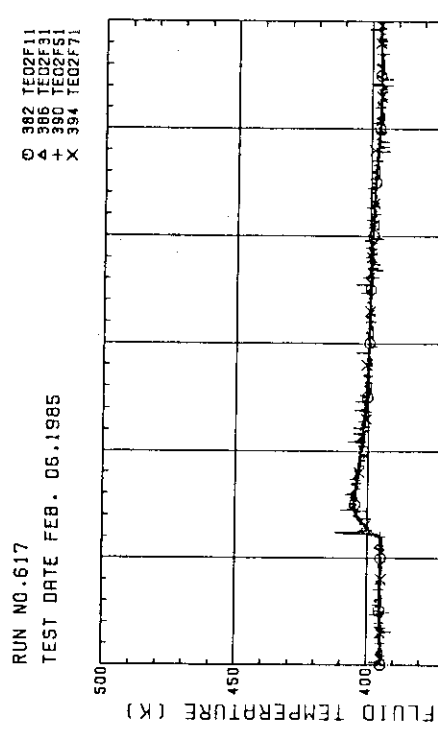


Fig. B-17 FLUID TEMPERATURE JUST ABOVE END BOX TIE PLATE  
(BUNDLE 1,3,5,7, OPPOSITE SIDE OF COLD LEG, OUTER)

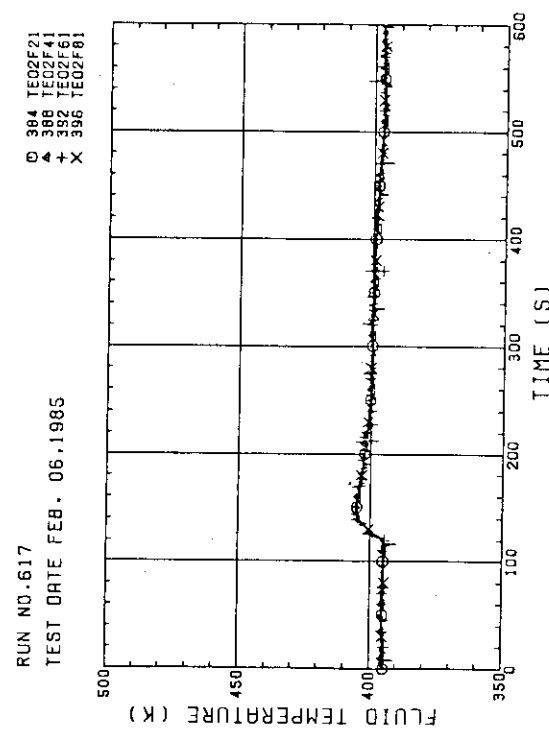


Fig. B-18 FLUID TEMPERATURE JUST ABOVE END BOX TIE PLATE  
(BUNDLE 2,4,6,8, COLD LEG SIDE, INNER)

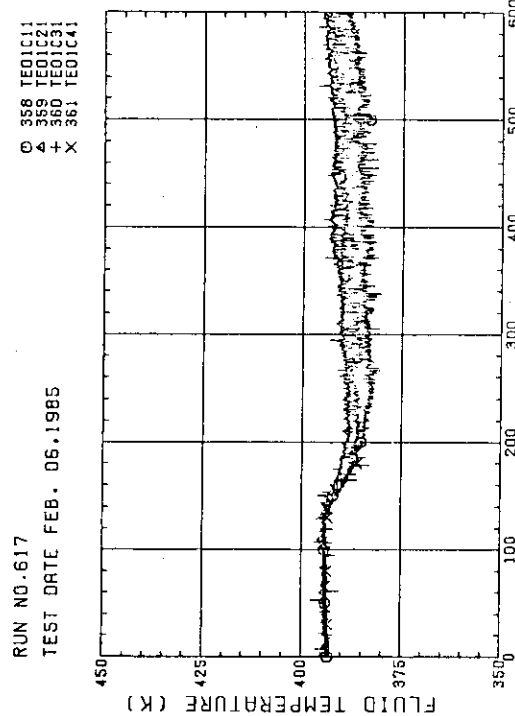


Fig. B-19 FLUID TEMPERATURE AT CORE INLET  
(BUNDLE 1,2,3,4, 100MM BELOW HEATED PART)

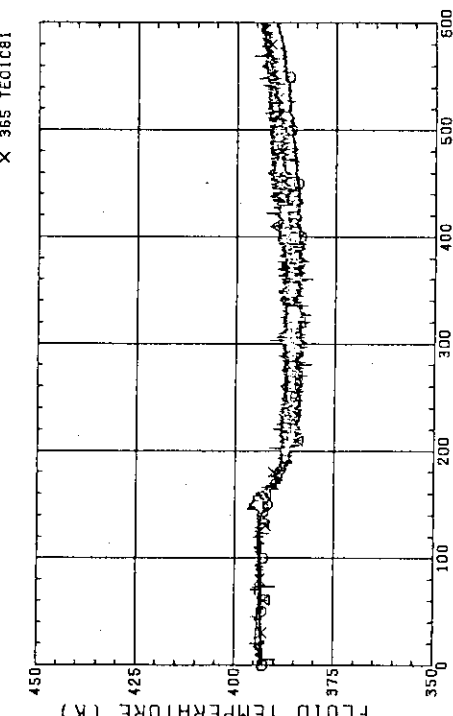
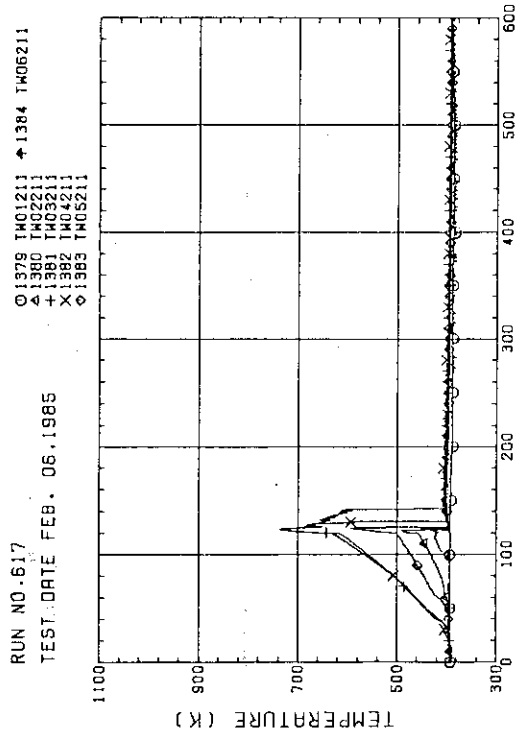
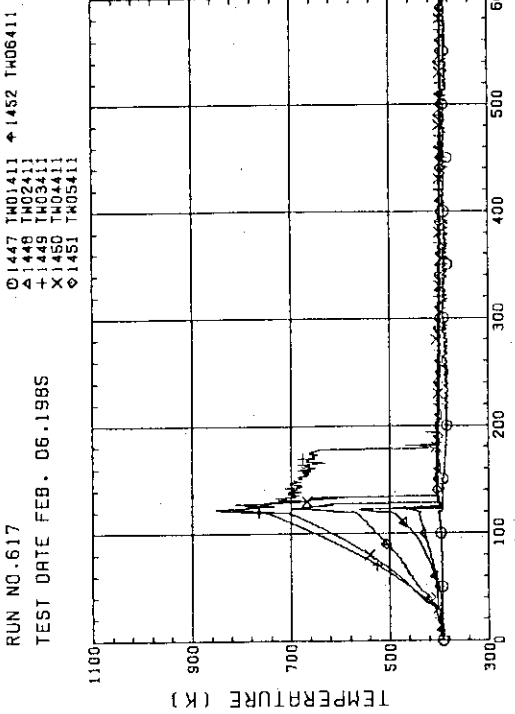
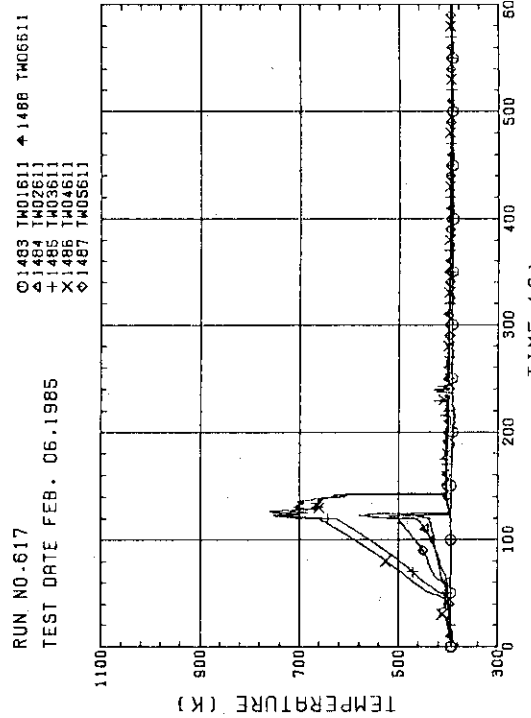
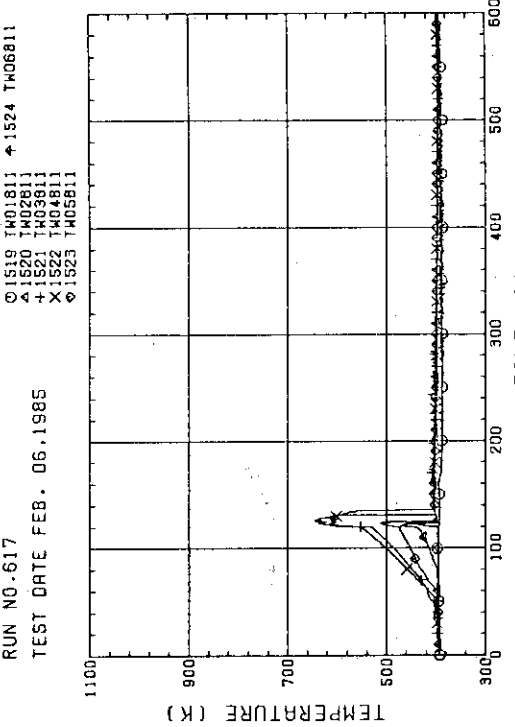
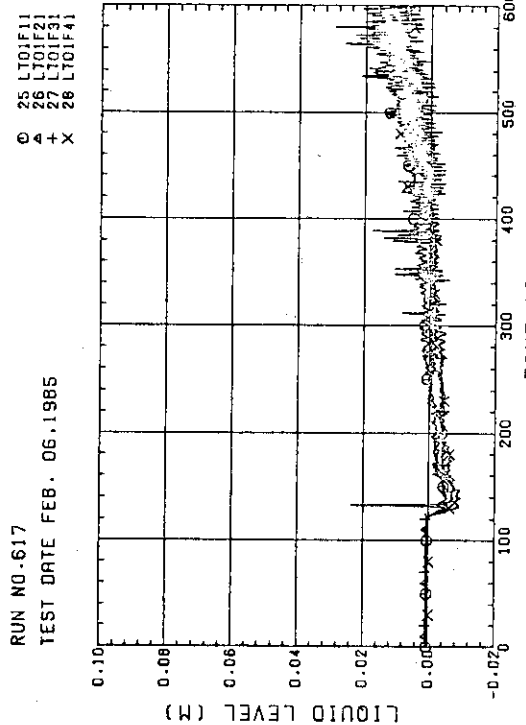
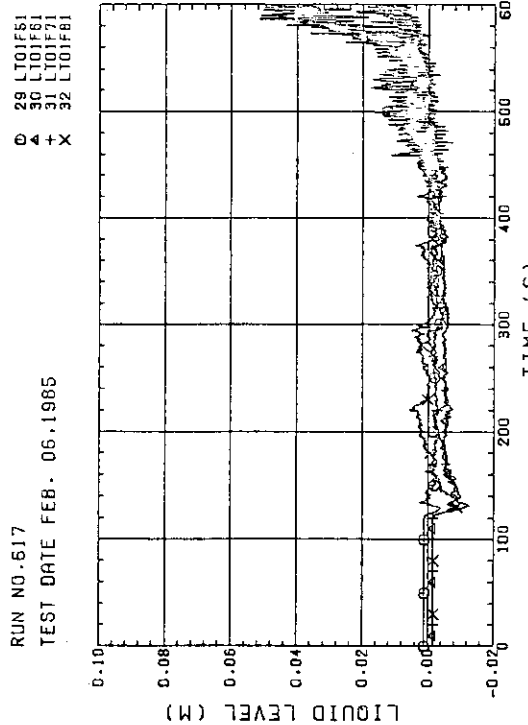
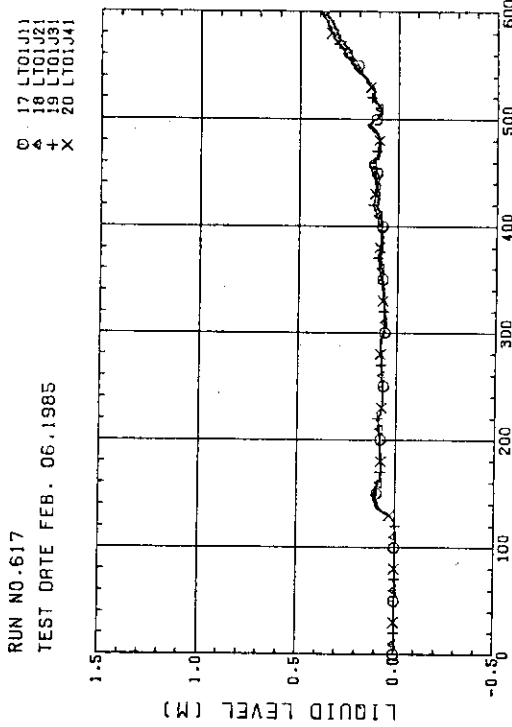
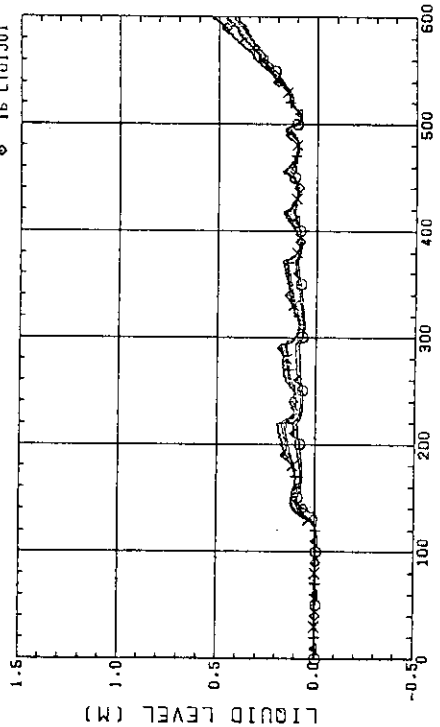


Fig. B-20 FLUID TEMPERATURE AT CORE INLET  
(BUNDLE 5,6,7,8, 100MM BELOW HEATED PART)

Fig. B-21 TEMPERATURE FOR SPUTTERING DETECTION  
BUNDLE 2 . REGION 1 , TYPE 1Fig. B-22 TEMPERATURE FOR SPUTTERING DETECTION  
BUNDLE 4 . REGION 1 , TYPE 1Fig. B-23 TEMPERATURE FOR SPUTTERING DETECTION  
BUNDLE 6 . REGION 1 , TYPE 1Fig. B-24 TEMPERATURE FOR SPUTTERING DETECTION  
BUNDLE 8 . REGION 1 , TYPE 1

Fig. B-25 LIQUID LEVEL ABOVE END BOX TIE PLATE  
(BUNDLE 1.2.3.4)Fig. B-26 LIQUID LEVEL ABOVE END BOX TIE PLATE  
(BUNDLE 5.6.7.8)Fig. B-27 LIQUID LEVEL ABOVE UCSP  
(BUNDLE 1.2.3.4)Fig. B-28 LIQUID LEVEL ABOVE UCSP  
(BUNDLE 5.6.7.8 AND CORE BAFFLE)

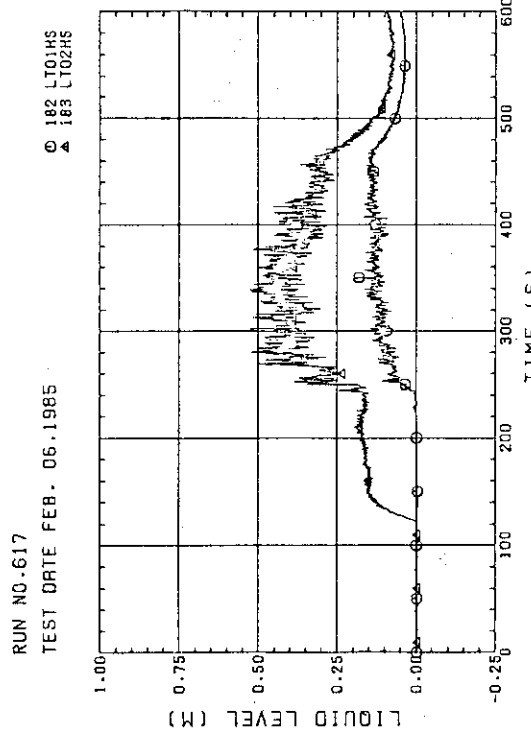


Fig. B-29 LIQUID LEVEL IN HOT LEG (01HS - PV SIDE. 02HS - STEAM/WATER SEPARATOR SIDE)

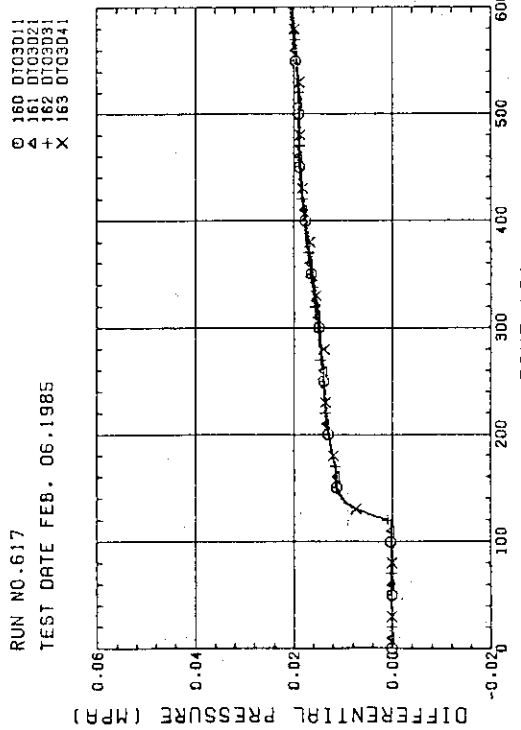


Fig. B-31 DIFFERENTIAL PRESSURE OF CORE FULL HEIGHT (BUNDLE 5,6,7,8)

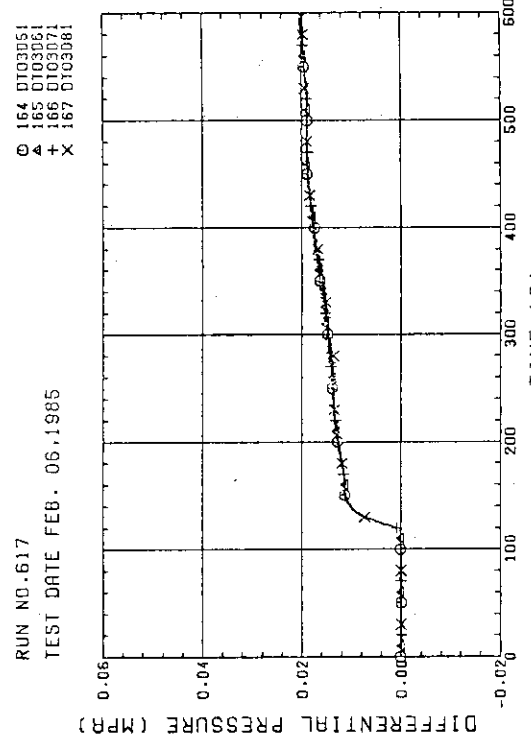


Fig. B-32 DIFFERENTIAL PRESSURE ACROSS END BOX TIE PLATE (BUNDLE 1,2,3,4)

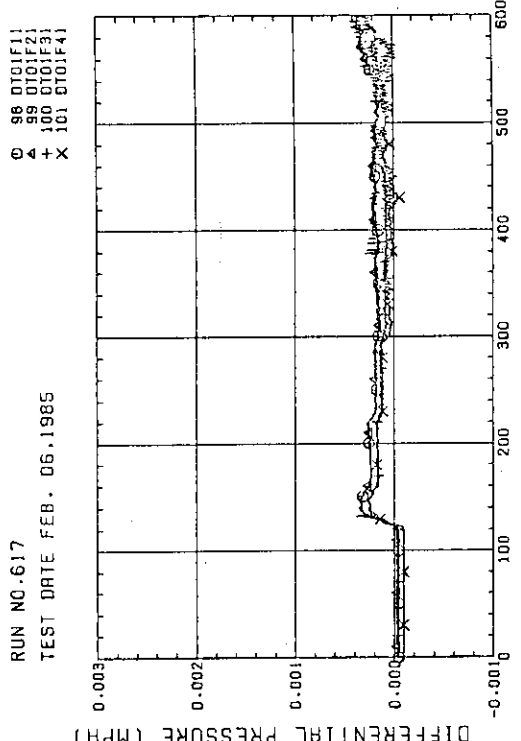


Fig. B-33 DIFFERENTIAL PRESSURE OF CORE FULL HEIGHT (BUNDLE 1,2,3,4)

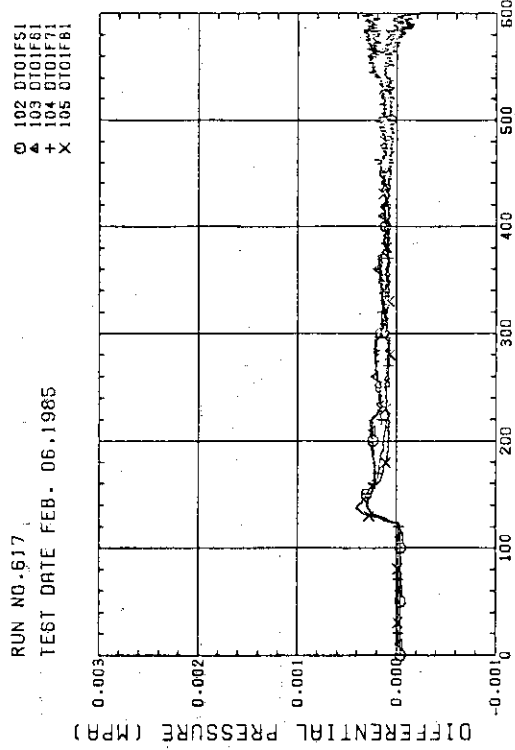


Fig. B-33 DIFFERENTIAL PRESSURE ACROSS END BOX TIE PLATE (BUNDLE 5, 6, 7, 8)

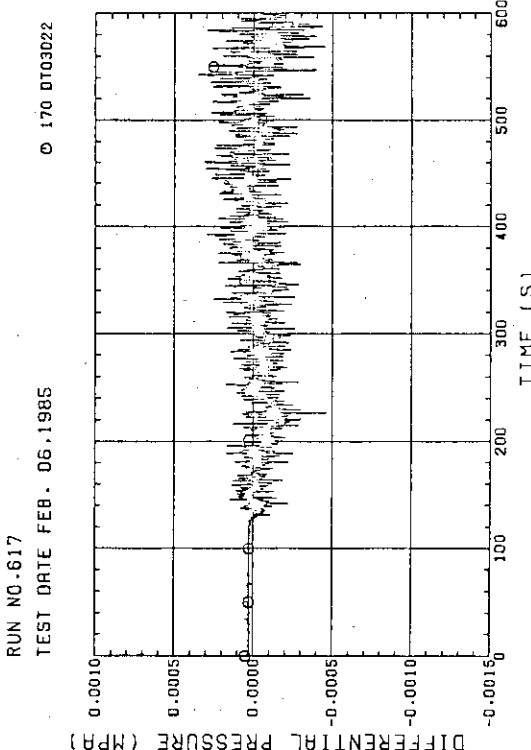


Fig. B-34 DIFFERENTIAL PRESSURE, HORIZONTAL AT 1365 MM (BUNDLE 2-4)

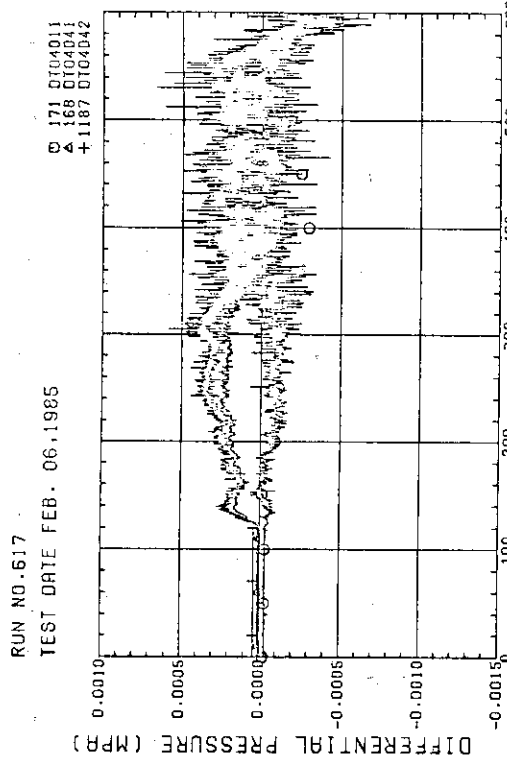


Fig. B-35 DIFFERENTIAL PRESSURE, HORIZONTAL AT 1905 MM (11-BUNDLE 1-4, 41-BUNDLE 4-8, 42-BUNDLE 4-6)

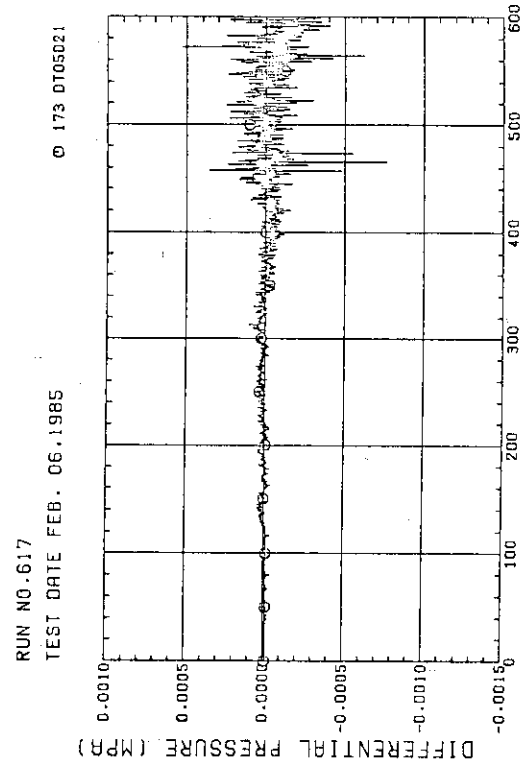


Fig. B-36 DIFFERENTIAL PRESSURE, HORIZONTAL AT 2570 MM (BUNDLE 2-4)

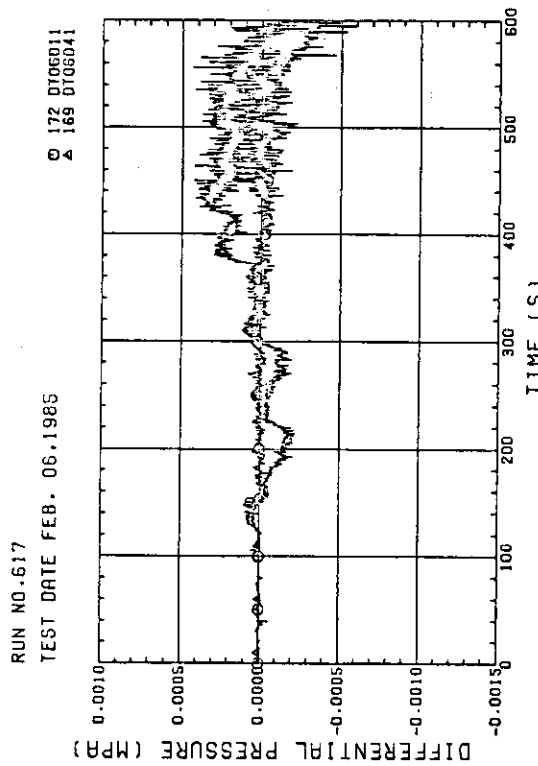
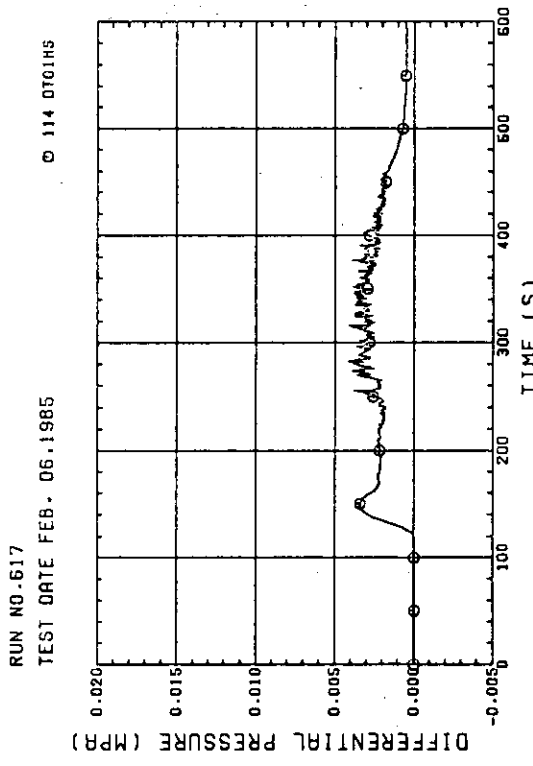
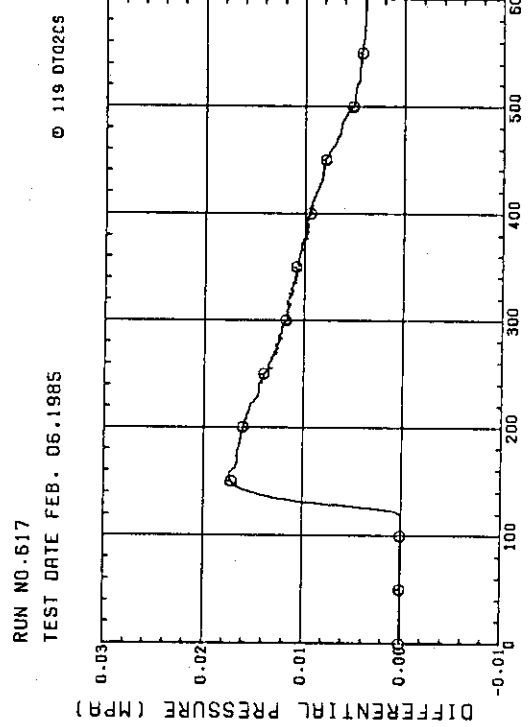
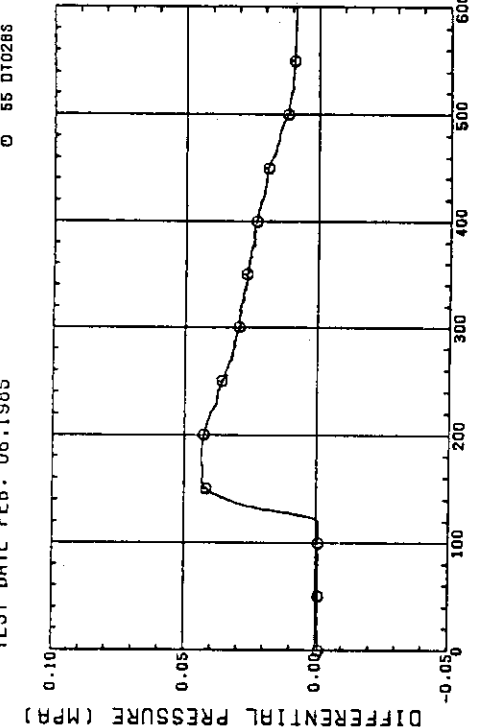
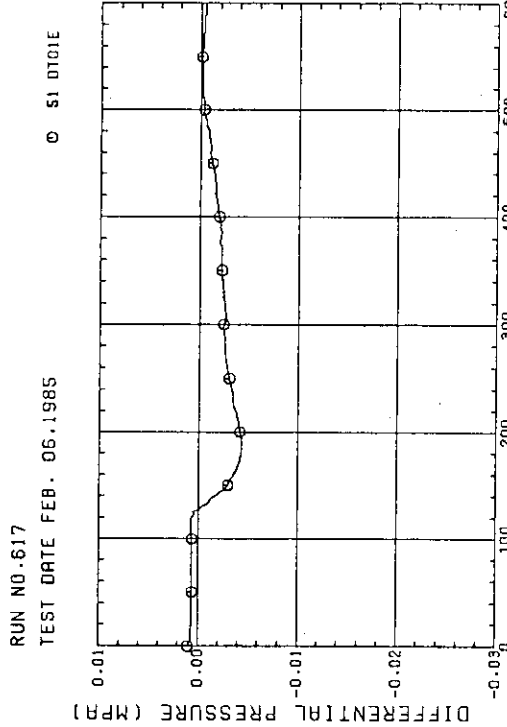
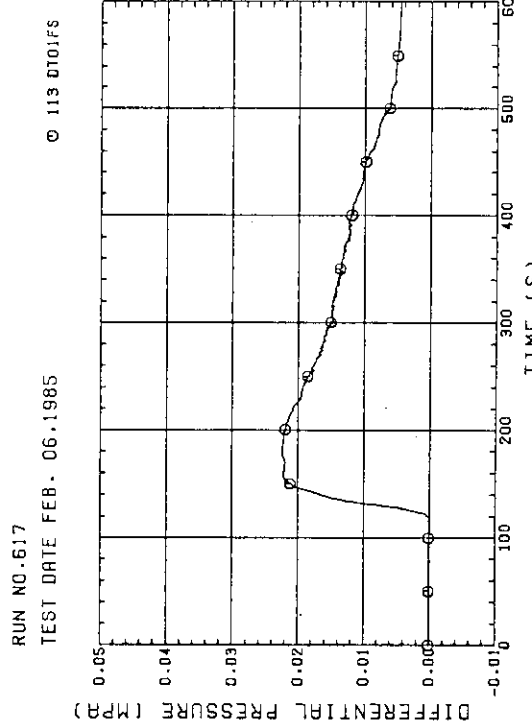
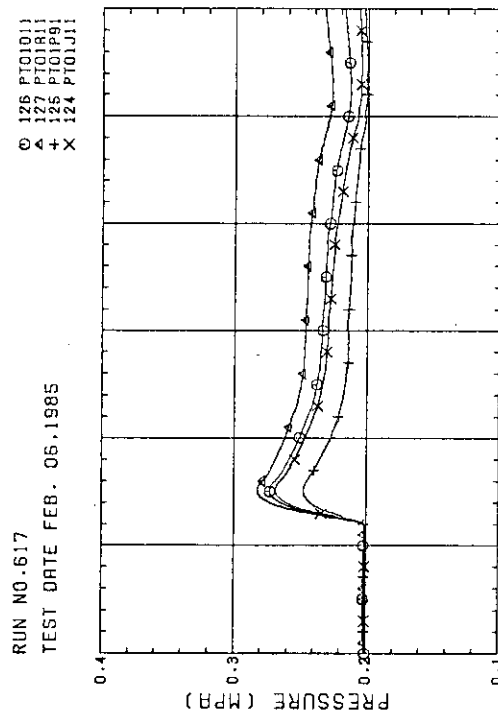
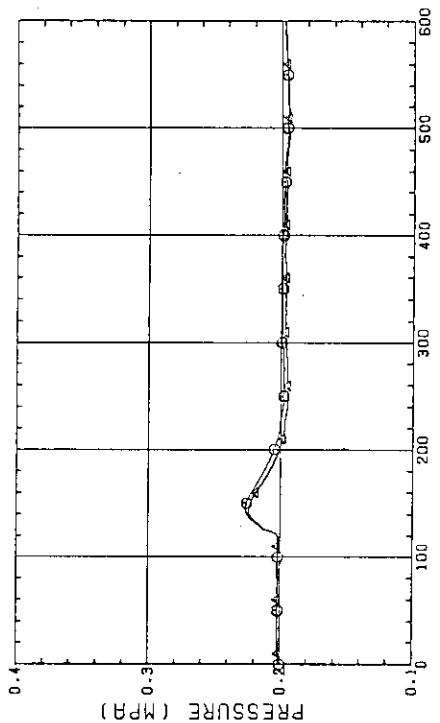
Fig. B-37 DIFFERENTIAL PRESSURE, HORIZONTAL AT 3235 MH  
(11-BUNDLE 1-4, 41-BUNDLE 4-8)Fig. B-38 DIFFERENTIAL PRESSURE OF HOT LEG,  
HOT LEG INLET - STEAM/WATER SEPARATOR INLET

Fig. B-39 DIFFERENTIAL PRESSURE OF INTACT COLD LEG

Fig. B-40 DIFFERENTIAL PRESSURE, STEAM/WATER SEPARATOR -  
CONTAINMENT TANK-11

Fig. B-41 DIFFERENTIAL PRESSURE, CONTAINMENT TANK-II -  
CONTAINMENT TANK-IFig. B-42 DIFFERENTIAL PRESSURE OF BROKEN COLD LEG - PV SIDE.  
CONTAINMENT TANK-II - CONTAINMENT TANK-IFig. B-43 PRESSURE IN PV (J - TOP OF PV, B - CORE CENTER, A -  
CORE INLET, P - BELOW COLD LEG NOZZLE IN DOWNCOMER)Fig. B-44 PRESSURE AT TOP OF CONTAINMENT TANK-I AND CONTAINMENT  
TANK-II (F-CONTAINMENT TANK-I, B-CONTAINMENT TANK-II)

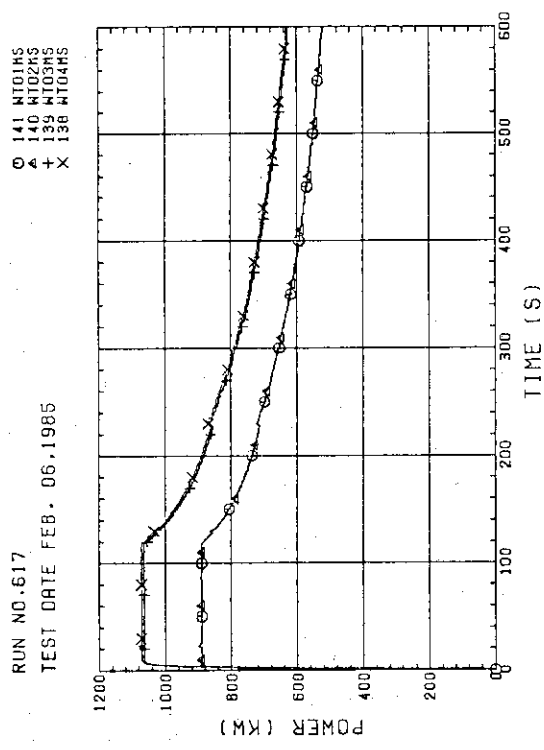


Fig. B-45 BUNDLE POWER (BUNDLE 1,2,3,4)

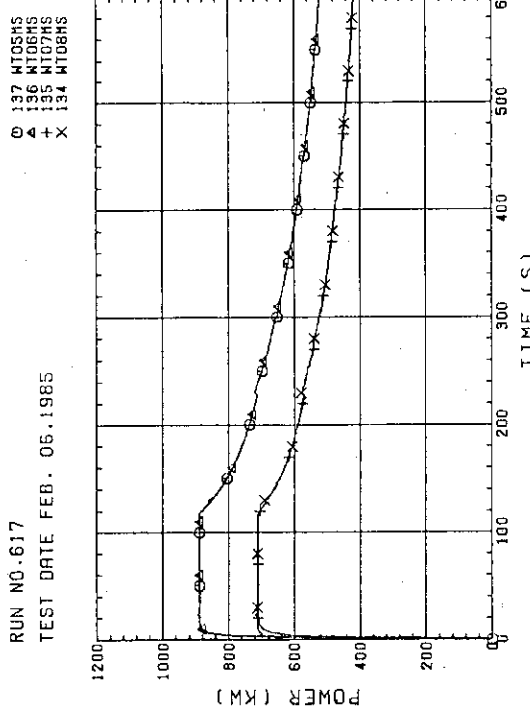
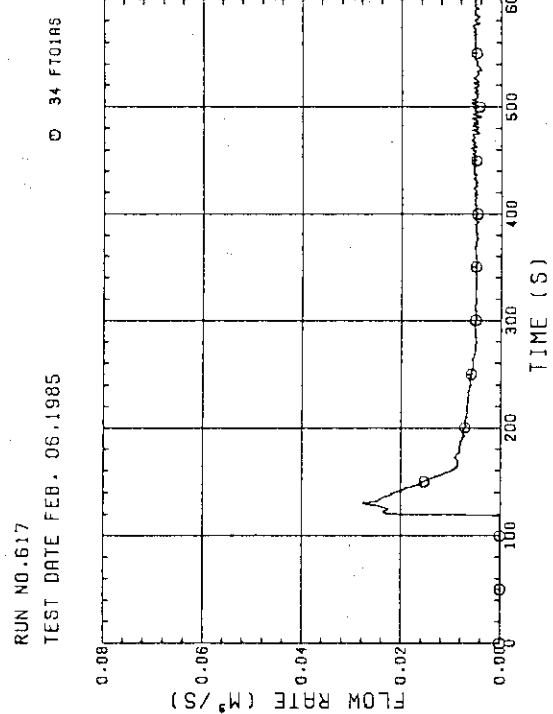


Fig. B-46 BUNDLE POWER (BUNDLE 5,6,7,8)

Fig. B-47 FLOW RATE OF ECC WATER (01-LOWER PLENUM,  
02-INTRACT COLD LEG, 03-BROKEN COLD LEG)

## Appendix C Selected Data of Test S2-14

Fig. C-1 ~ C-8	Heater rod temperatures
Fig. C-9 ~ C-12	Hon-heated rod temperatures
Fig. C-13 ~ C-16	Steam temperatures
Fig. C-17 ~ C-18	Fluid temperatures just above end box tie plate
Fig. C-19 ~ C-20	Fluid temperatures at core inlet
Fig. C-21 ~ C-24	Fluid temperatures in core
Fig. C-25 ~ C-26	Liquid levels above end box tie plate
Fig. C-27 ~ C-28	Liquid levels above UCSP
Fig. C-29	Liquid levels in hot leg
Fig. C-30 ~ C-31	Differential pressures across core full height
Fig. C-32 ~ C-33	Differential pressures across end box tie plate
Fig. C-34 ~ C-37	Horizontal differential pressures in core
Fig. C-38 ~ C-42	Differential pressures in primary loops
Fig. C-43 ~ C-44	Pressures in pressure vessel and containment tanks
Fig. C-45 ~ C-46	Bundle powers
Fig. C-47	ECC flow rates

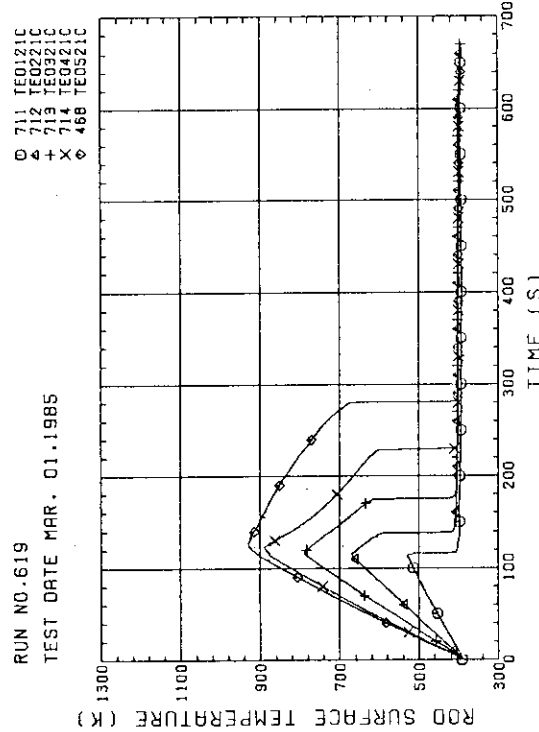


Fig. C-1 HEATER ROD TEMPERATURE (BUNDLE 2-1C, LOWER HALF)

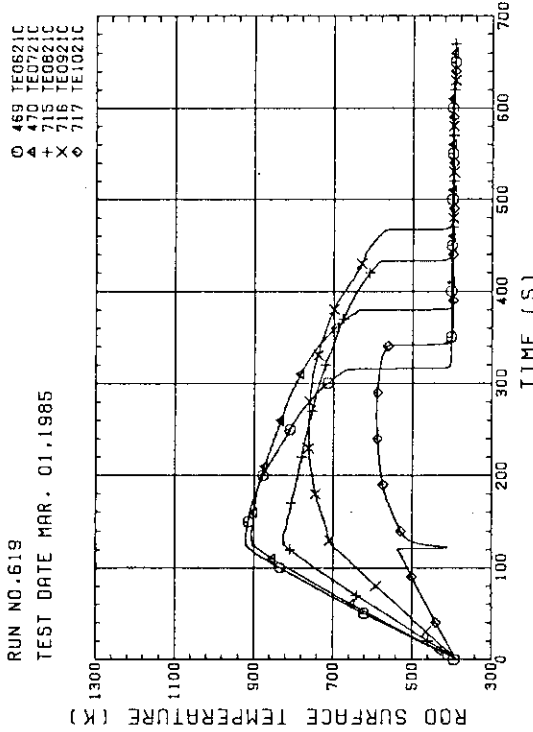


Fig. C-2 HEATER ROD TEMPERATURE (BUNDLE 2-1C, UPPER HALF)

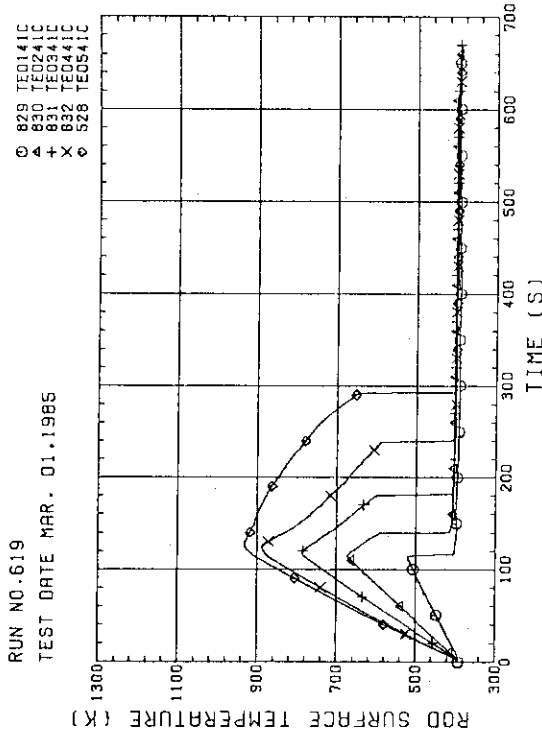


Fig. C-3 HEATER ROD TEMPERATURE (BUNDLE 4-1C, LOWER HALF)

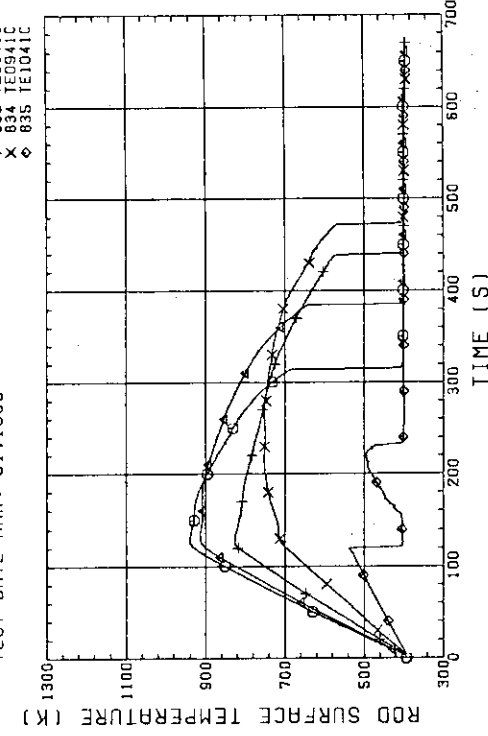
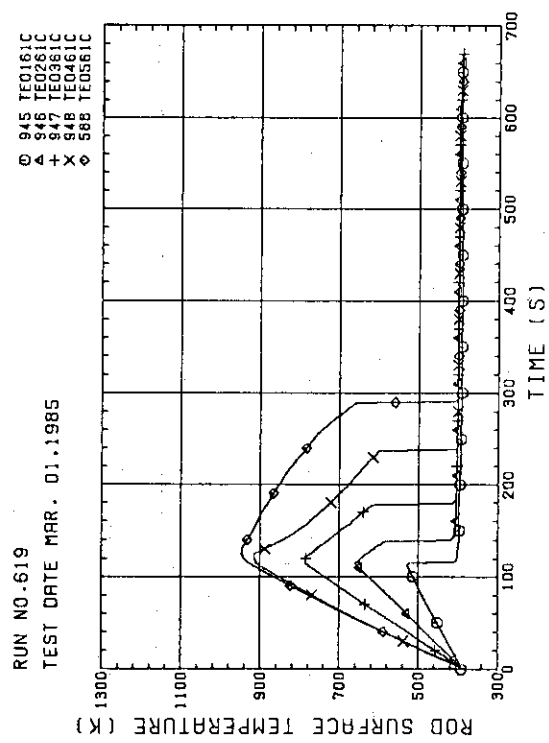
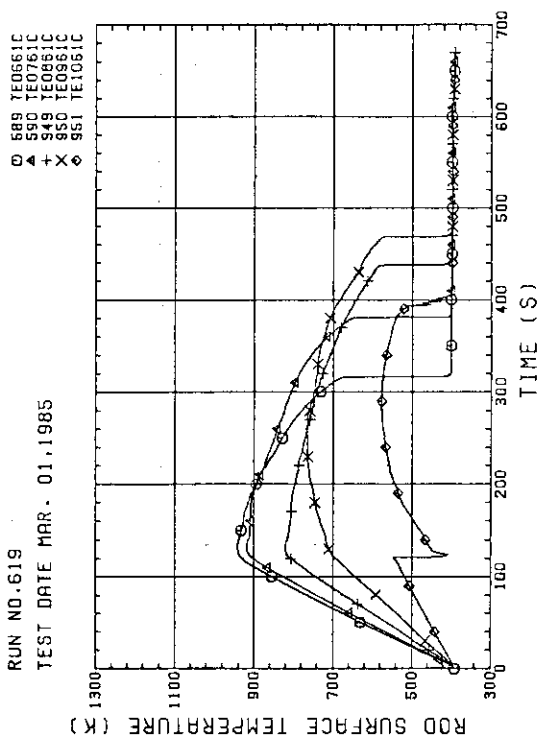
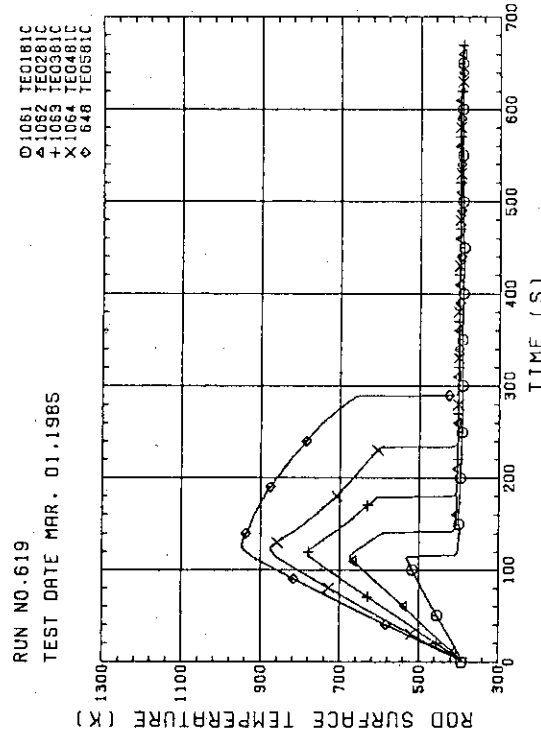
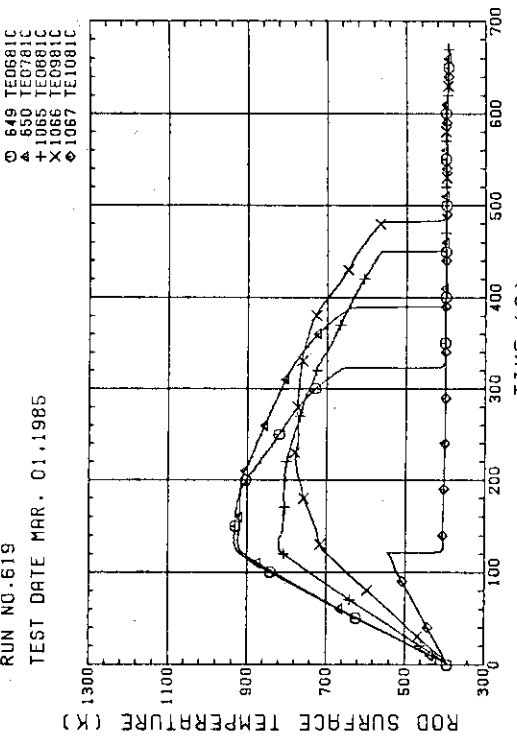
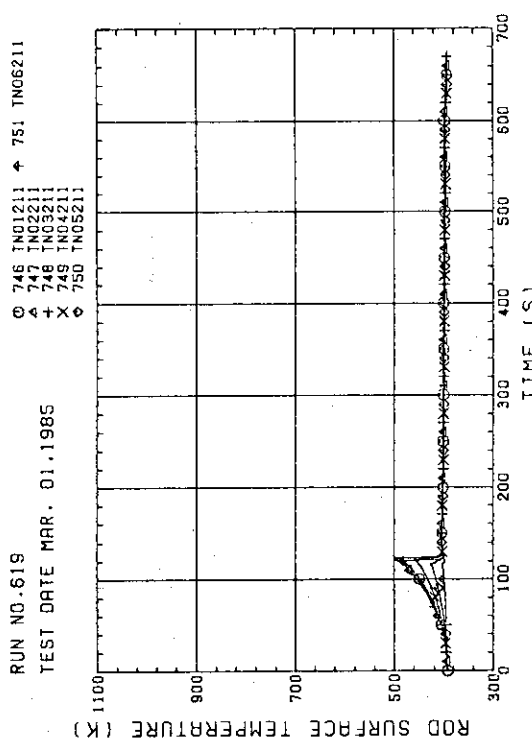
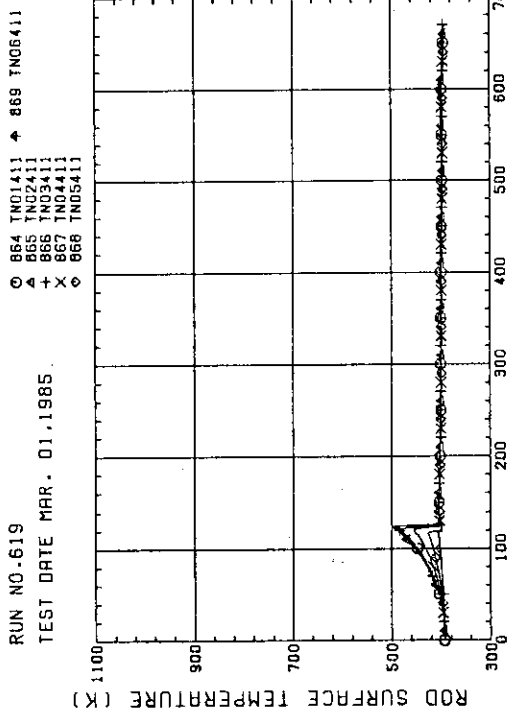
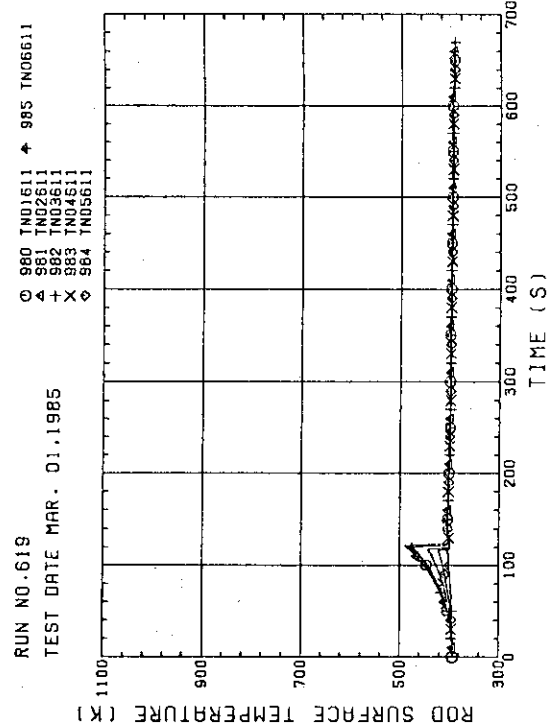
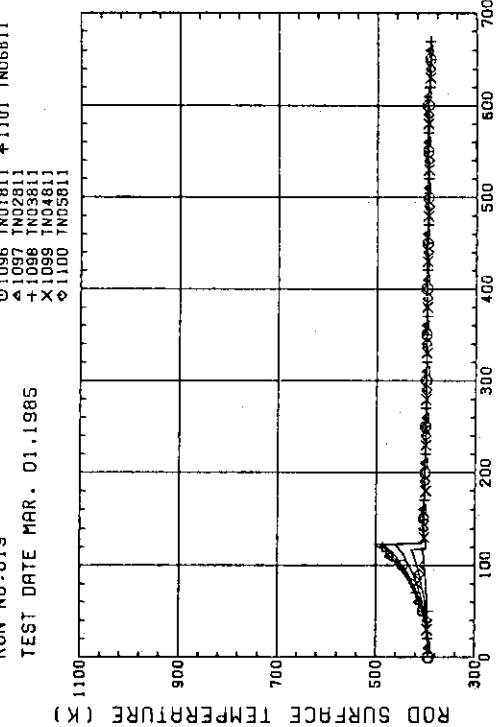


Fig. C-4 HEATER ROD TEMPERATURE (BUNDLE 4-1C, UPPER HALF)

Fig. C-5 HEATER ROD TEMPERATURE  
(BUNDLE 6-1C, LOWER HALF)Fig. C-6 HEATER ROD TEMPERATURE  
(BUNDLE 6-1C, UPPER HALF)Fig. C-7 HEATER ROD TEMPERATURE  
(BUNDLE 8-1C, LOWER HALF)Fig. C-8 HEATER ROD TEMPERATURE  
(BUNDLE 8-1C, UPPER HALF)

Fig. C-9 NON-HEATED ROD TEMPERATURE  
(BUNDLE 2-1)Fig. C-10 NON-HEATED ROD TEMPERATURE  
(BUNDLE 4-1)Fig. C-11 NON-HEATED ROD TEMPERATURE  
(BUNDLE 6-1)Fig. C-12 NON-HEATED ROD TEMPERATURE  
(BUNDLE 6-1)

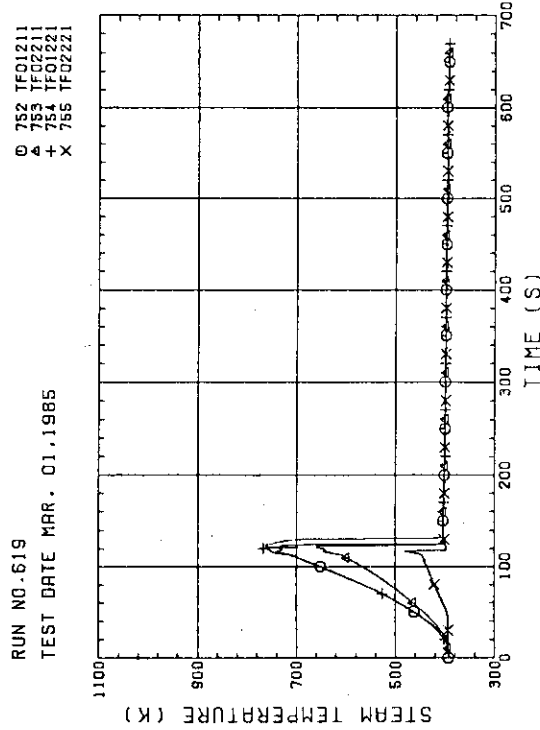


Fig. C-13 STEAM TEMPERATURE IN CORE, BUNDLE 2 (01211-1.735M, 02221-1.38H, 02421-1.915H)

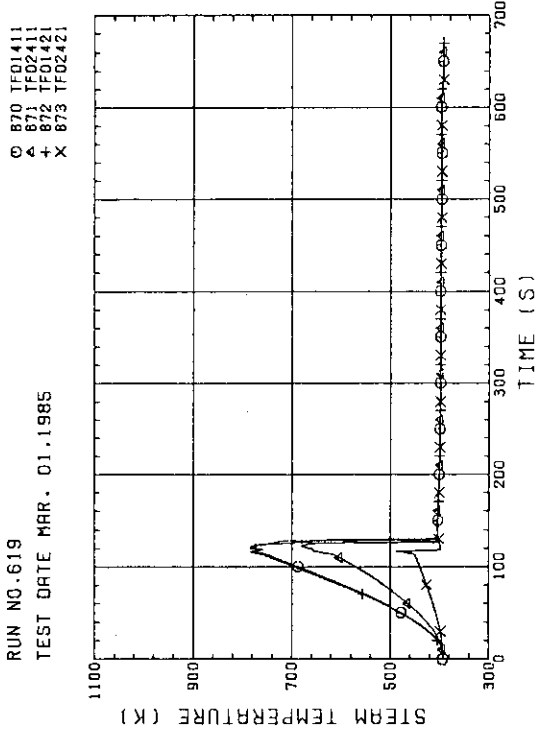


Fig. C-14 STEAM TEMPERATURE IN CORE, BUNDLE 4 (01411-1.735M, 02411-1.875M, 01421-1.38H, 02421-1.915H)

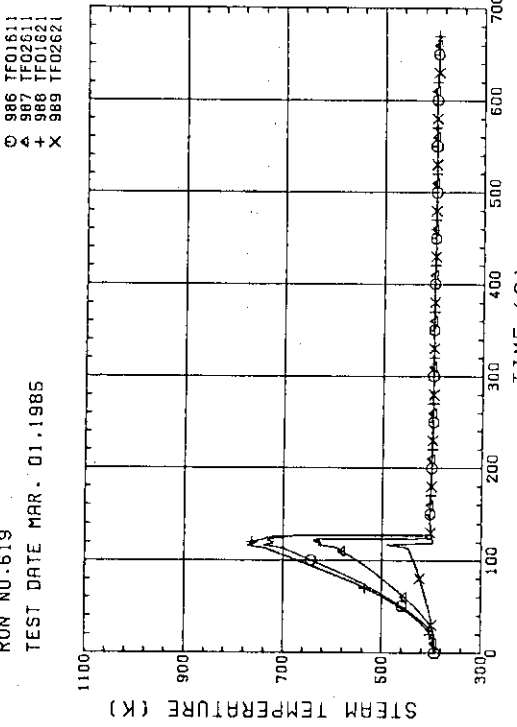


Fig. C-15 STEAM TEMPERATURE IN CORE, BUNDLE 6

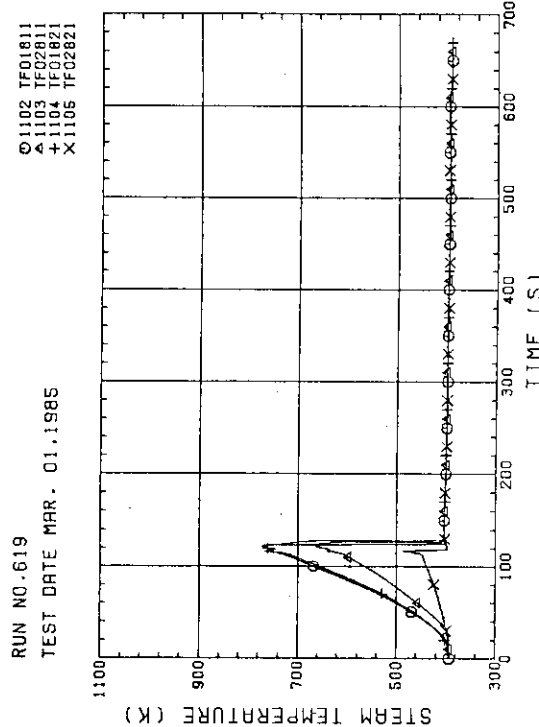


Fig. C-16 STEAM TEMPERATURE IN CORE, BUNDLE 8

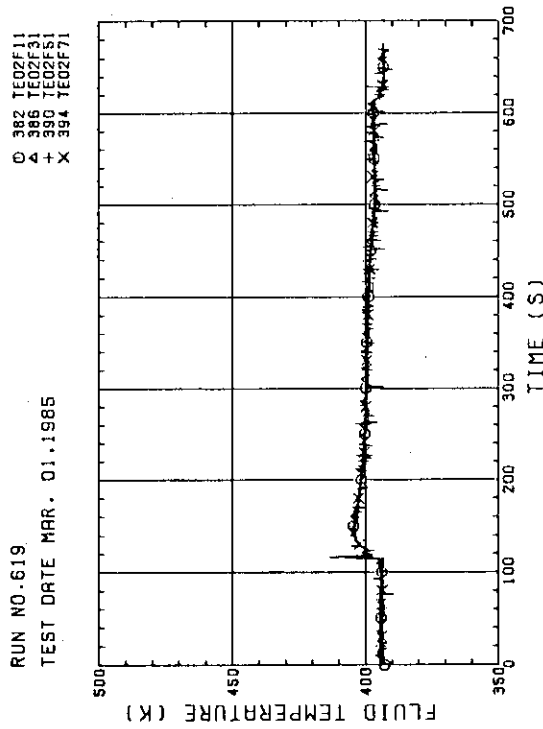


Fig. C-17 FLUID TEMPERATURE JUST ABOVE END BOX TIE PLATE (BUNDLE 1.3.5.7. OPPOSITE SIDE OF COLD LEG. OUTER)

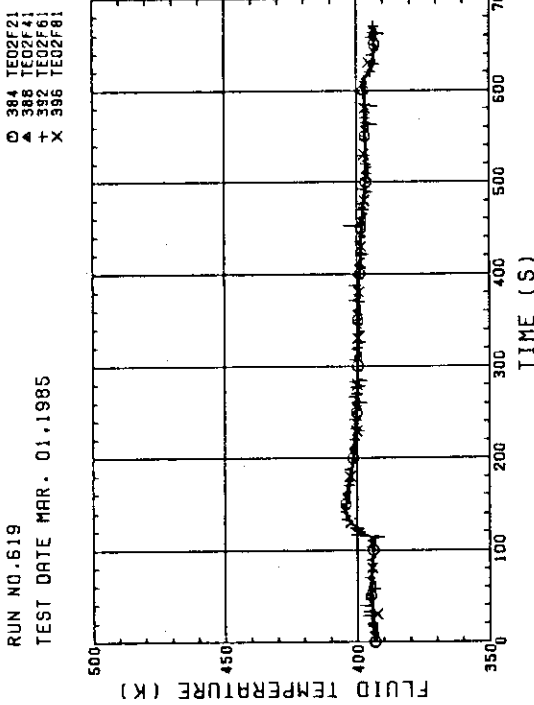


Fig. C-18 FLUID TEMPERATURE JUST ABOVE END BOX TIE PLATE (BUNDLE 2.4.6.8. COLD LEG SIDE, INNER)

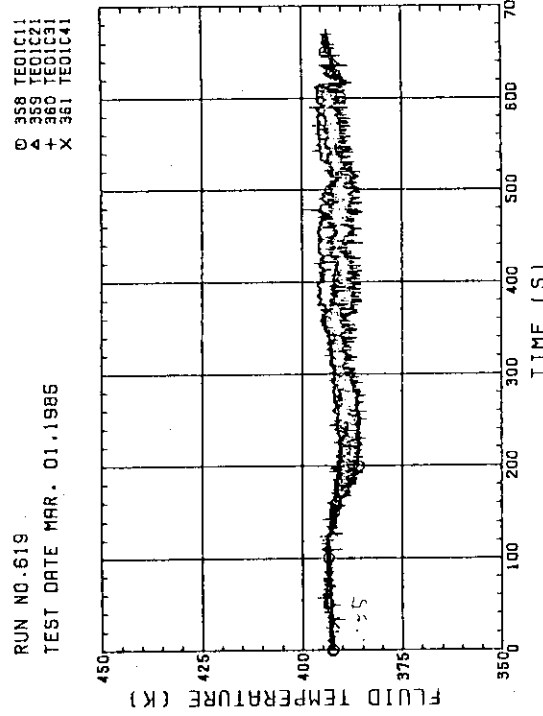


Fig. C-19 FLUID TEMPERATURE AT CORE INLET (BUNDLE 1.2.3.4. 100MM BELOW HEATED PART)

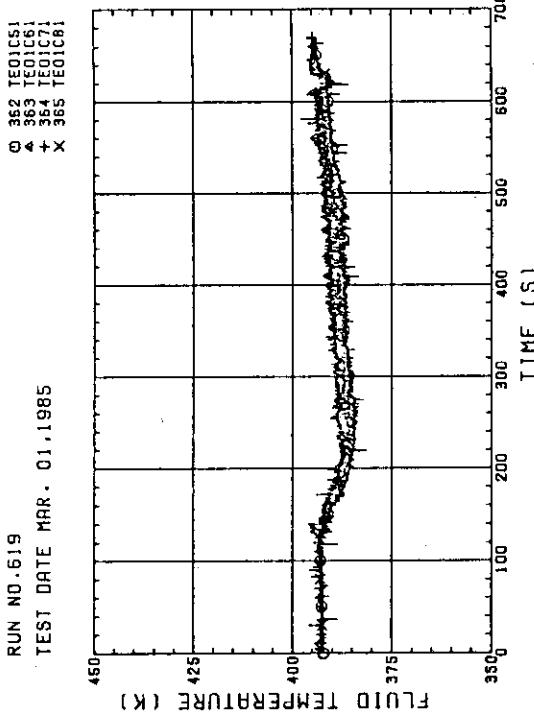
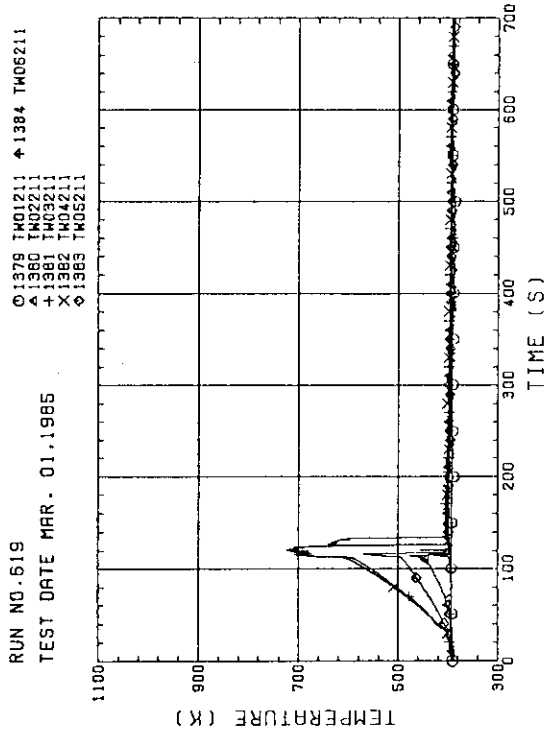
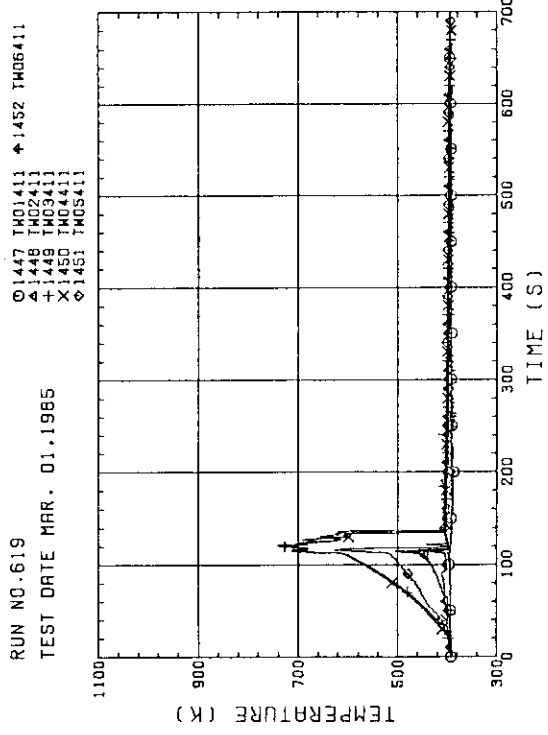
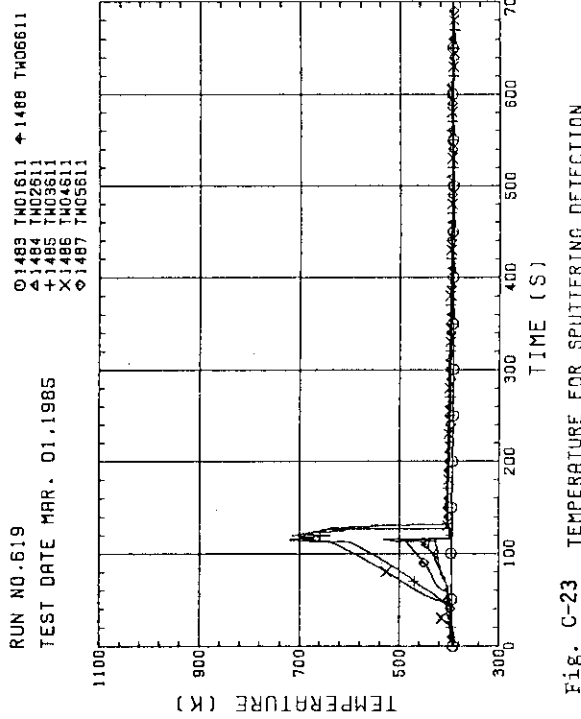
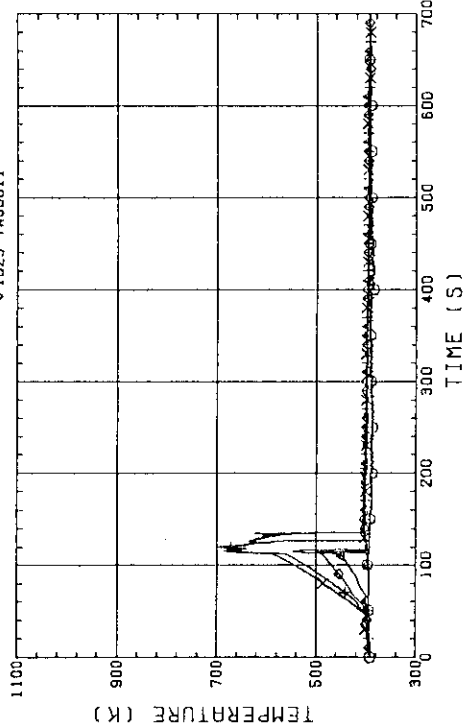
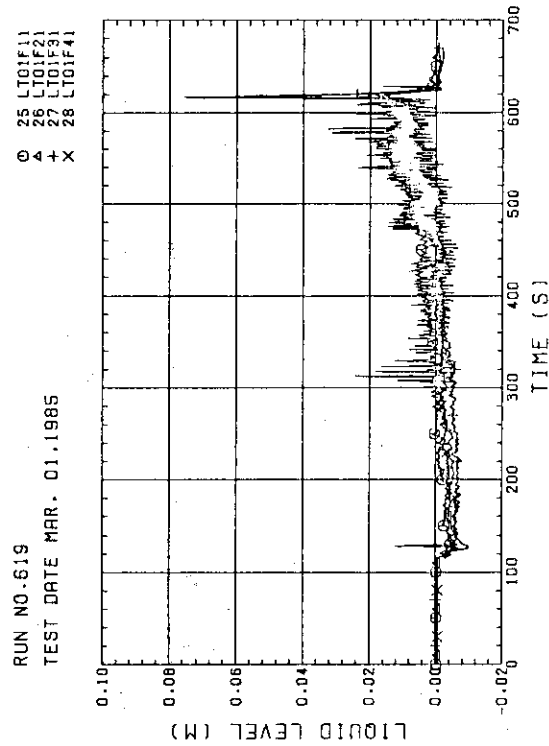
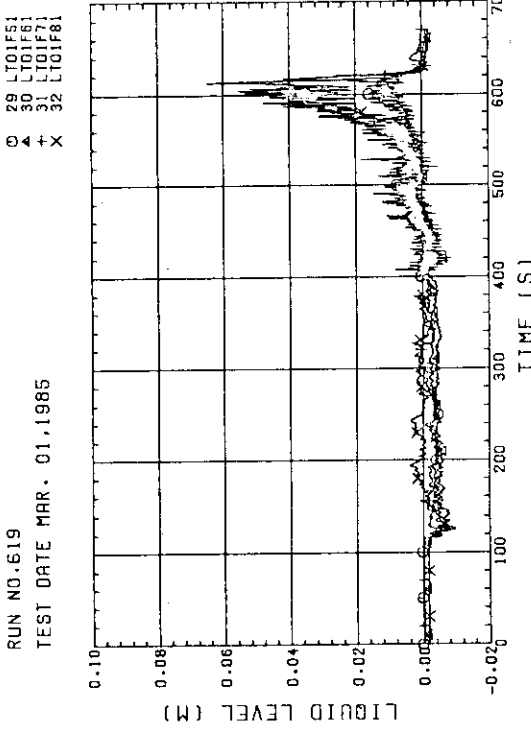
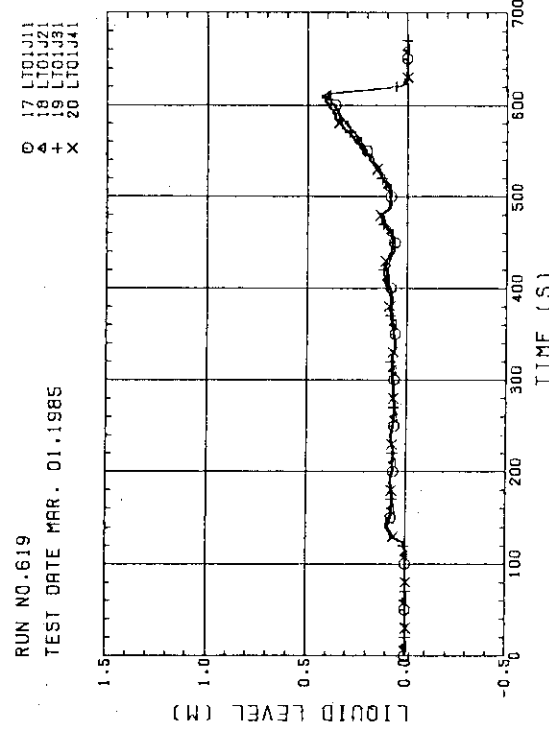
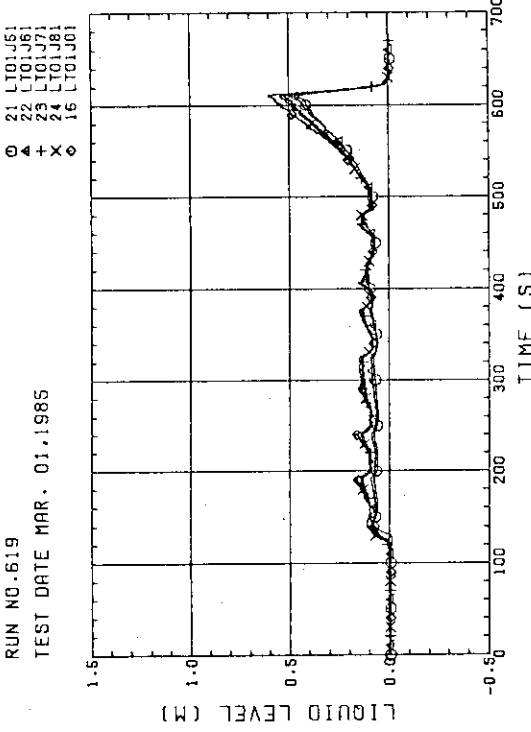


Fig. C-20 FLUID TEMPERATURE AT CORE INLET (BUNDLE 5.6.7.8. 100MM BELOW HEATED PART)

Fig. C-21 TEMPERATURE FOR SPUTTERING DETECTION  
BUNDLE 2 , REGION 1 , TYPE 1Fig. C-22 TEMPERATURE FOR SPUTTERING DETECTION  
BUNDLE 4 . REGION 1 , TYPE 1Fig. C-23 TEMPERATURE FOR SPUTTERING DETECTION  
BUNDLE 6 . REGION 1 , TYPE 1Fig. C-24 TEMPERATURE FOR SPUTTERING DETECTION  
BUNDLE 8 . REGION 1 , TYPE 1

Fig. C-25 LIQUID LEVEL ABOVE END BOX TIE PLATE  
(BUNDLE 1,2,3,4)Fig. C-26 LIQUID LEVEL ABOVE END BOX TIE PLATE  
(BUNDLE 5,6,7,8)Fig. C-27 LIQUID LEVEL ABOVE UCSP  
(BUNDLE 1.2.3.4)Fig. C-28 LIQUID LEVEL ABOVE UCSP  
(BUNDLE 5,6,7,8 AND CORE BAFFLE)

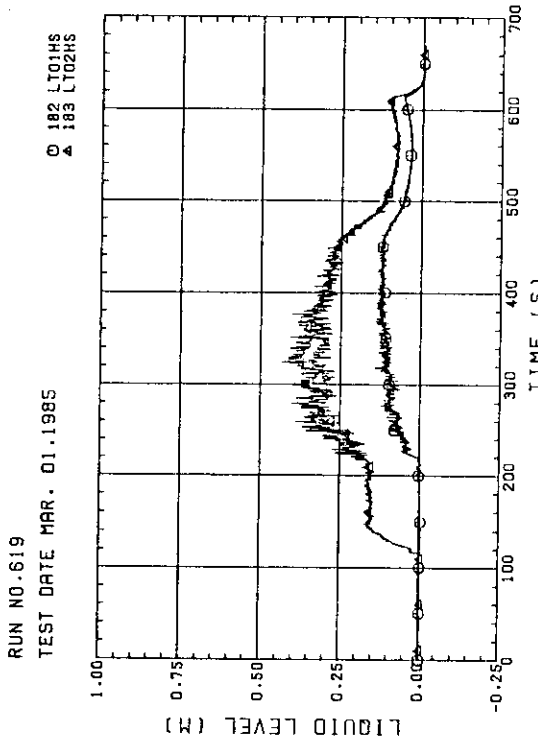


Fig. C-29 LIQUID LEVEL IN HOT LEG  
(01HS - PV SIDE, 02HS - STEAM/WATER SEPARATOR SIDE)

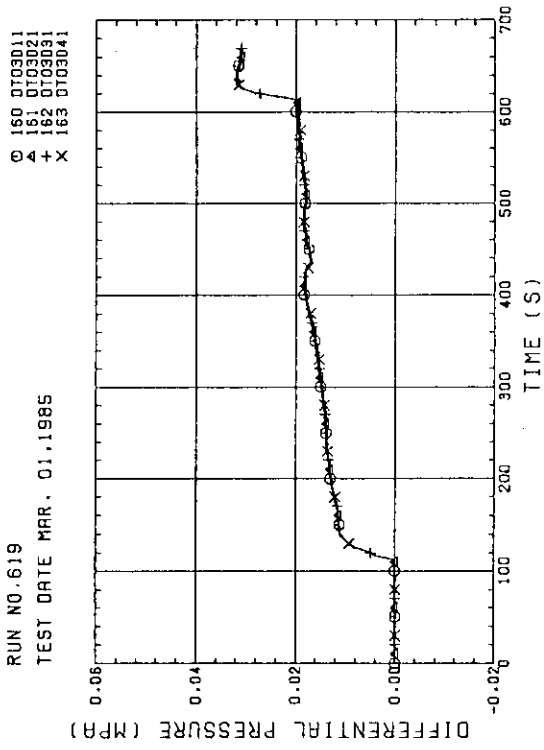


Fig. C-30 DIFFERENTIAL PRESSURE OF CORE FULL HEIGHT  
(BUNDLE 1,2,3,4)

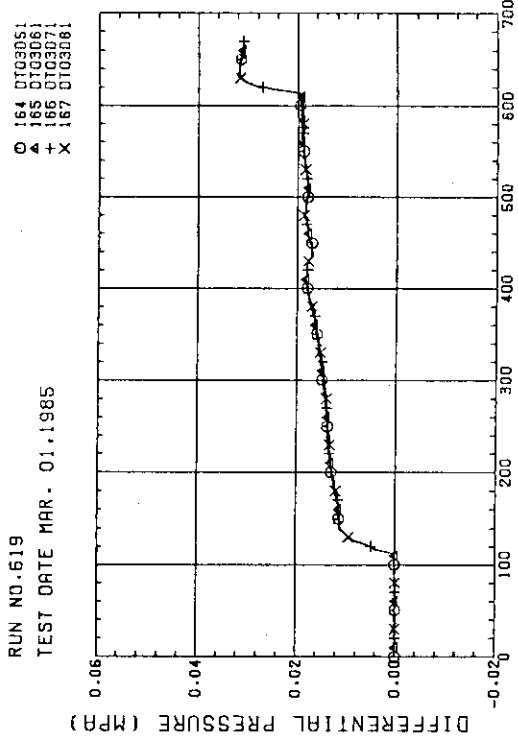


Fig. C-31 DIFFERENTIAL PRESSURE OF CORE FULL HEIGHT  
(BUNDLE 5,6,7,8)

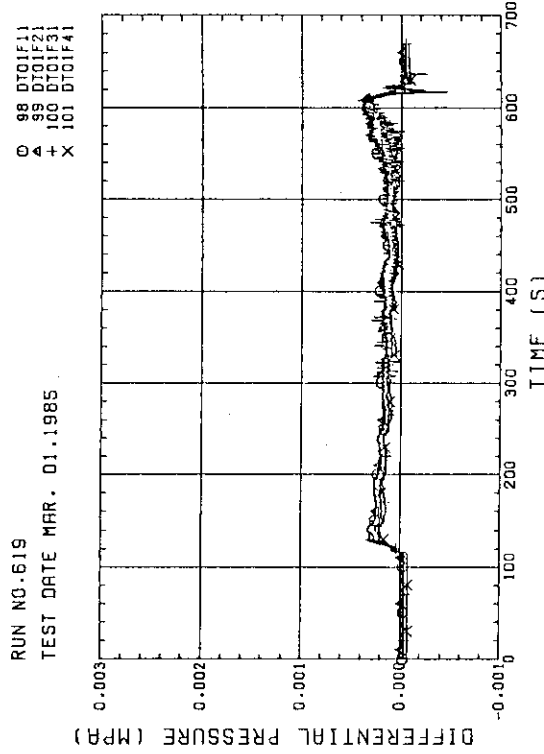


Fig. C-32 DIFFERENTIAL PRESSURE ACROSS END BOX TIE PLATE  
(BUNDLE 1,2,3,4)

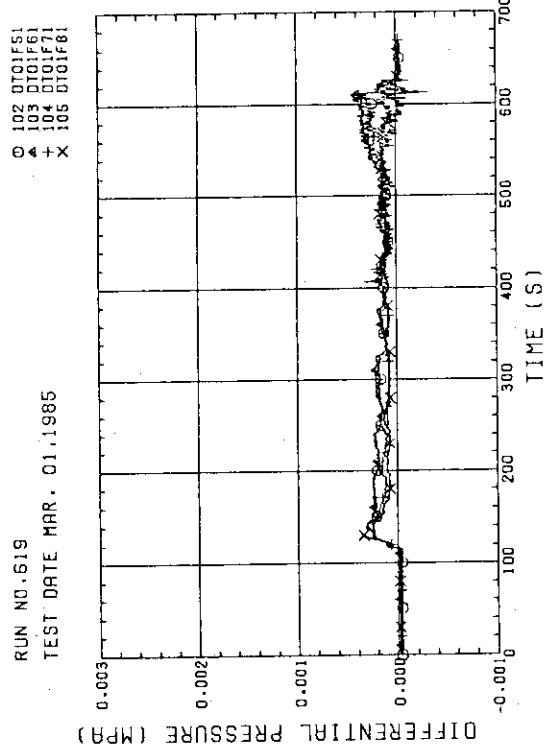


Fig. C-33 DIFFERENTIAL PRESSURE ACROSS END BOX TIE PLATE (BUNDLE 5,6,7,8)

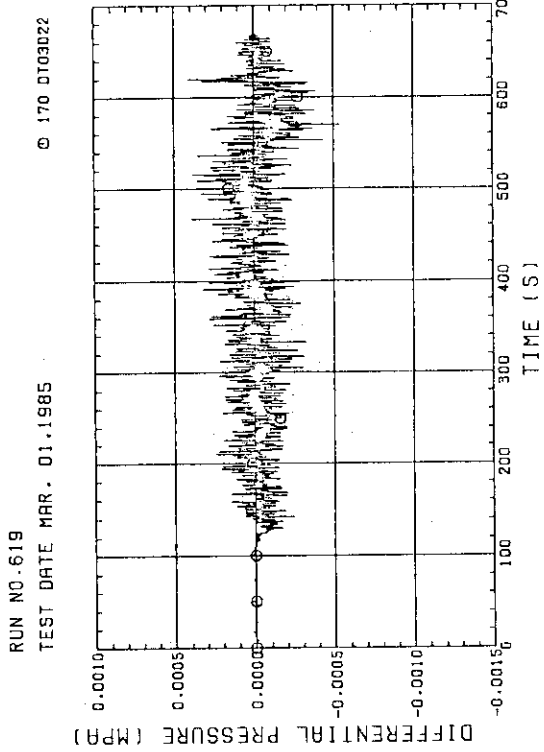


Fig. C-34 - DIFFERENTIAL PRESSURE, HORIZONTAL AT 1365 MM (BUNDLE 2-4)

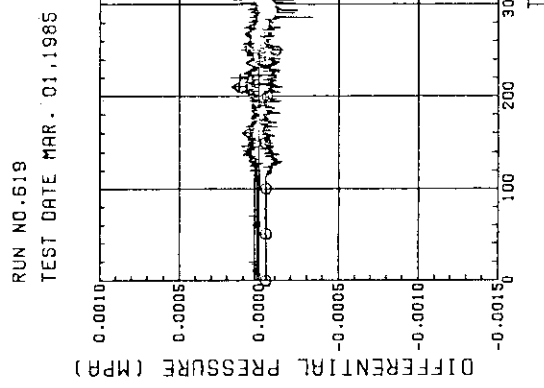


Fig. C-35 DIFFERENTIAL PRESSURE, HORIZONTAL AT 1905 MM (11-BUNDLE 1-4, 41-BUNDLE 4-8, 42-BUNDLE 4-6)

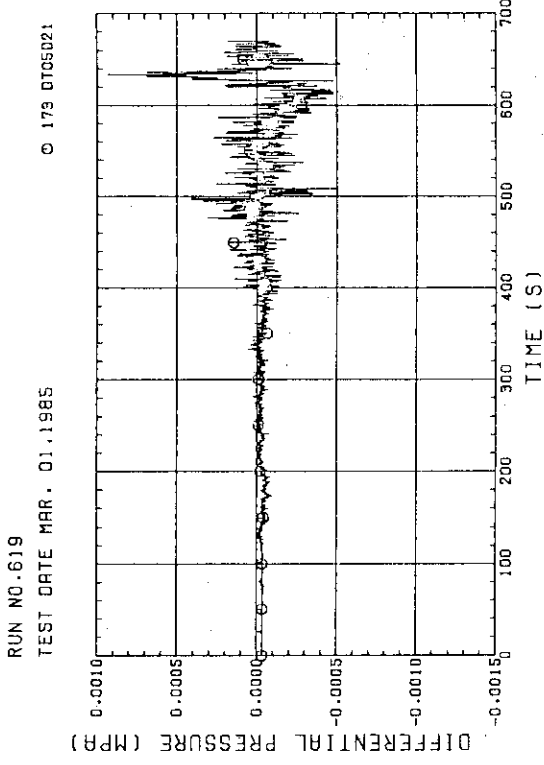


Fig. C-36 DIFFERENTIAL PRESSURE, HORIZONTAL AT 2570 MM (BUNDLE 2-4)

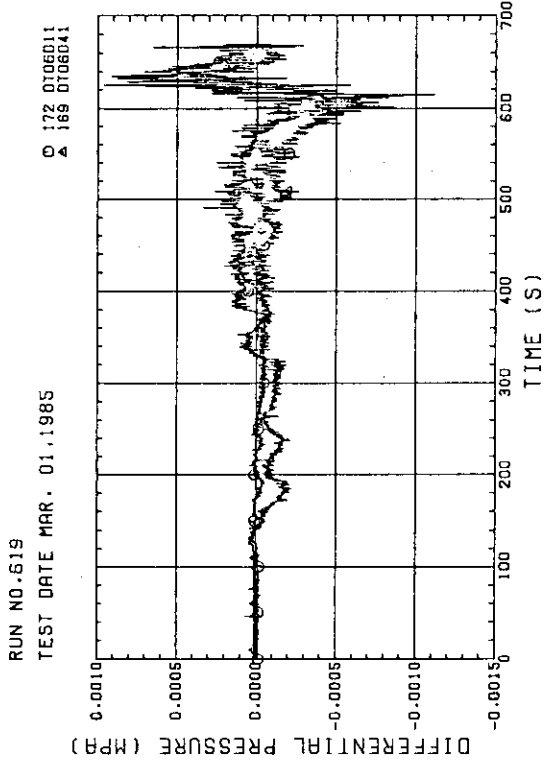


Fig. C-37 DIFFERENTIAL PRESSURE, HORIZONTAL AT 3235 MM  
(11-BUNDLE 1-4, 41-BUNDLE 4-8)

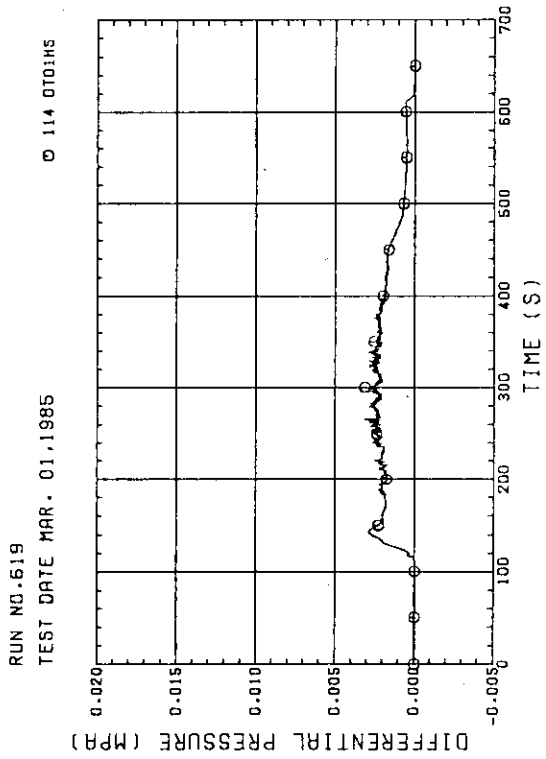


Fig. C-38 DIFFERENTIAL PRESSURE OF HOT LEG,  
HOT LEG INLET - STEAM/WATER SEPARATOR INLET

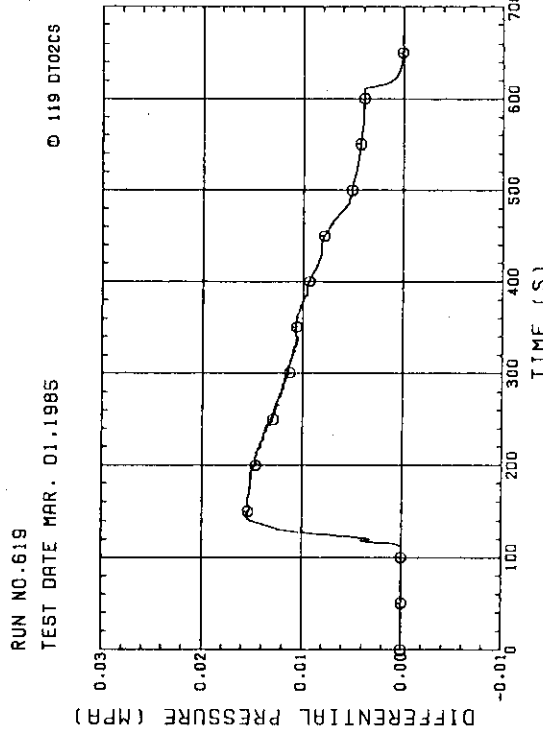


Fig. C-39 DIFFERENTIAL PRESSURE OF INTACT COLD LEG

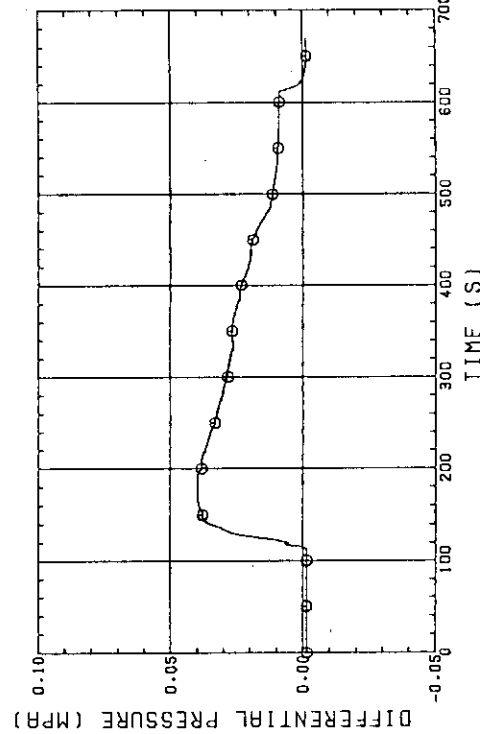
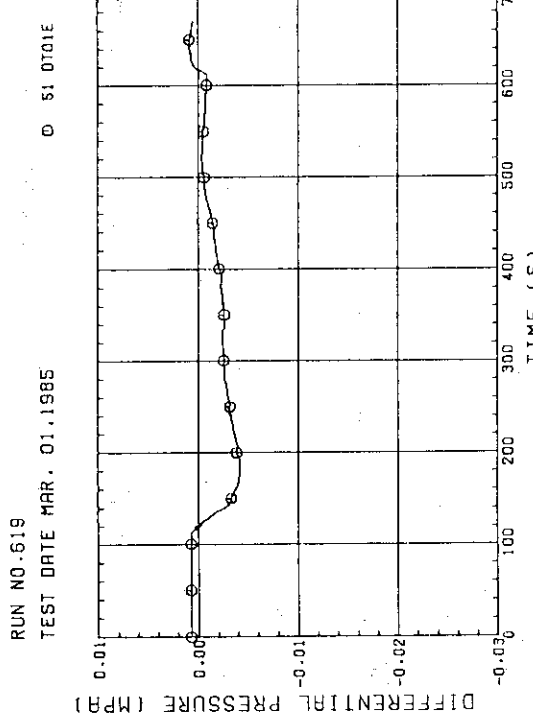
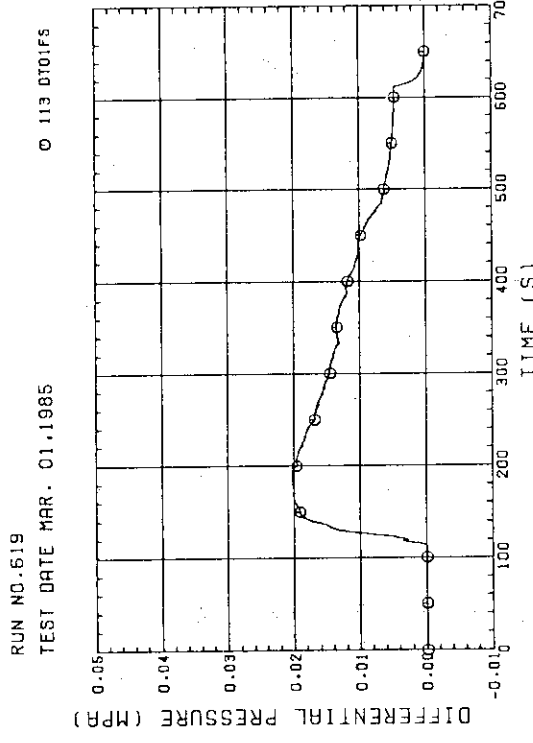
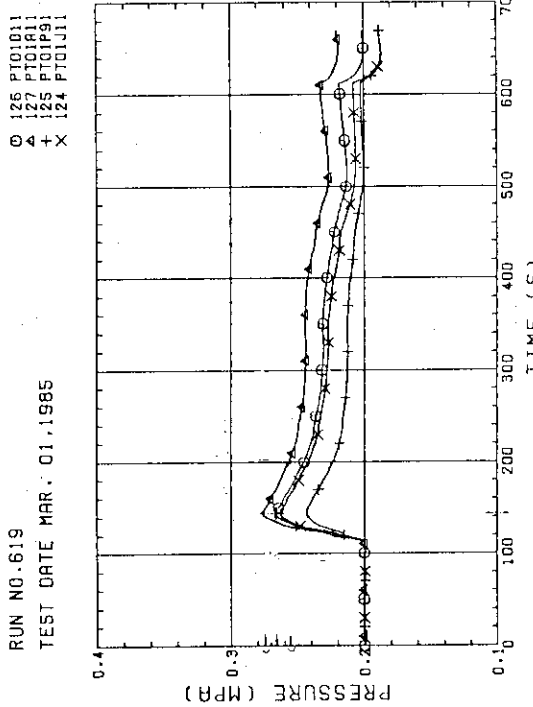
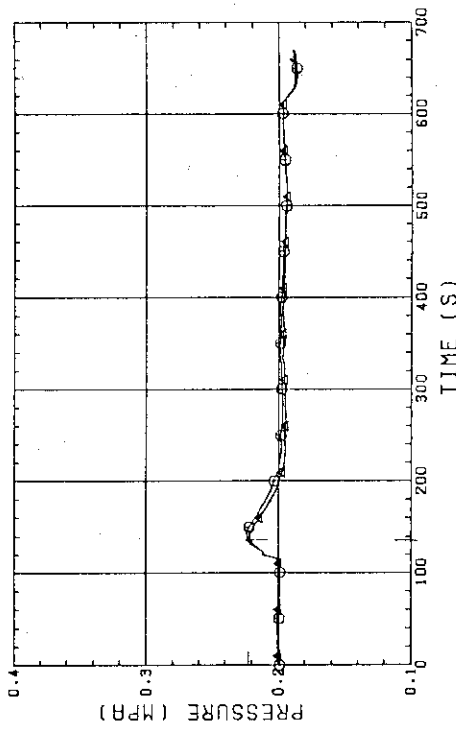
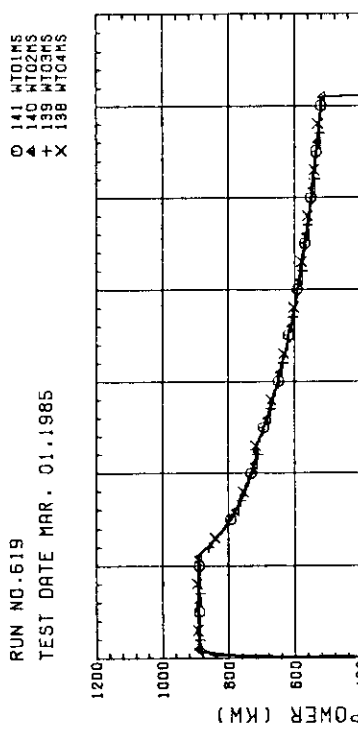
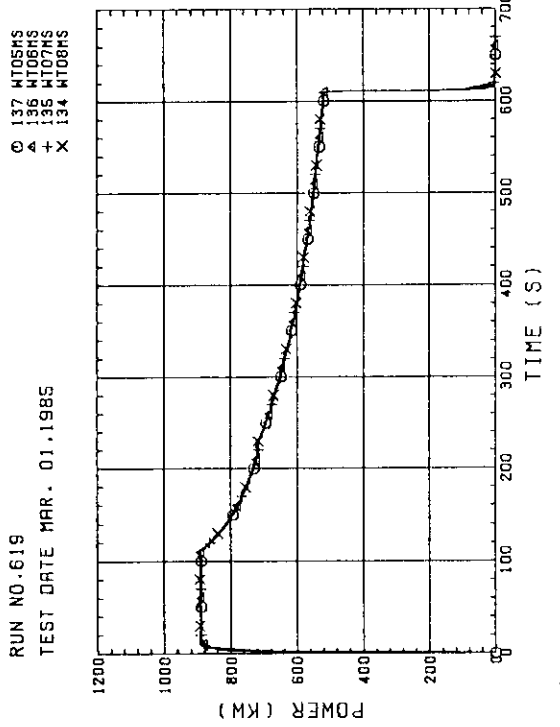
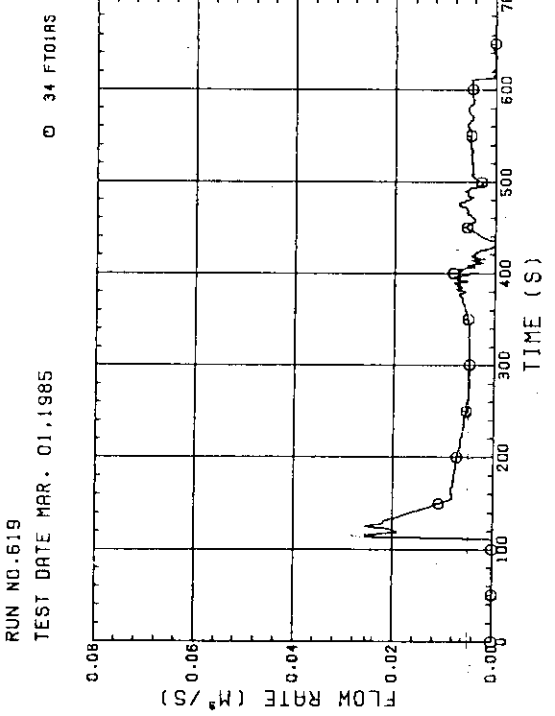


Fig. C-40 DIFFERENTIAL PRESSURE, STEAM/WATER SEPARATOR -  
CONTAINMENT TANK-II

Fig. C-41 DIFFERENTIAL PRESSURE, CONTAINMENT TANK-I -  
CONTAINMENT TANK-IFig. C-42 DIFFERENTIAL PRESSURE OF BROKEN COLD LEG - PV SIDE.  
CONTAINMENT TANK-I - CONTAINMENT TANK-IFig. C-43 PRESSURE IN PV (J - TOP OF PV, D - CORE CENTER, A -  
CORE INLET, P - BELOW COLD LEG NOZZLE IN DOWNCOMER)Fig. C-44 PRESSURE AT TOP OF CONTAINMENT TANK-I AND CONTAINMENT  
TANK-II (F-CONTAINMENT TANK-I, B-CONTAINMENT TANK-II)

Fig. C-45 BUNDLE POWER  
(BUNDLE 1,2,3,4)Fig. C-46 BUNDLE POWER  
(BUNDLE 5,6,7,8)Fig. C-47 FLOW RATE OF ECC WATER  
(01-LOWER PLENUM,  
02-INTACT COLD LEG, 03-BROKEN COLD LEG)

## Appendix D Selected Data of Test S2-15

Fig. D-1 ~ D-8	Heater rod temperatures
Fig. D-9 ~ D-12	Non-heated rod temperatures
Fig. D-13 ~ D-16	Steam Temperatures
Fig. D-17 ~ D-18	Fluid temperatures just above end box tie plate
Fig. D-19 ~ D-20	Fluid temperatures at core inlet
Fig. D-21 ~ D024	Fluid temperatures in core
Fig. D-25 ~ D-26	Liquid levels above end box tie plate
Fig. D-27 ~ D-28	Liquid levels above UCSP
Fig. D-29	Liquid levels in hot leg
Fig. D-30 ~ D-31	Differential pressures across core full height
Fig. D-32 ~ D-33	Differential pressures across end box tie plate
Fig. D-34 ~ D-39	Horizontal differential pressures in core
Fig. D-40 ~ D-44	Differential pressures in primary loops
Fig. D-45 ~ D-46	Pressures in pressure vessel and containment tanks
Fig. D-47 ~ D-48	Bundle powers
Fig. D-49	ECC flow rates

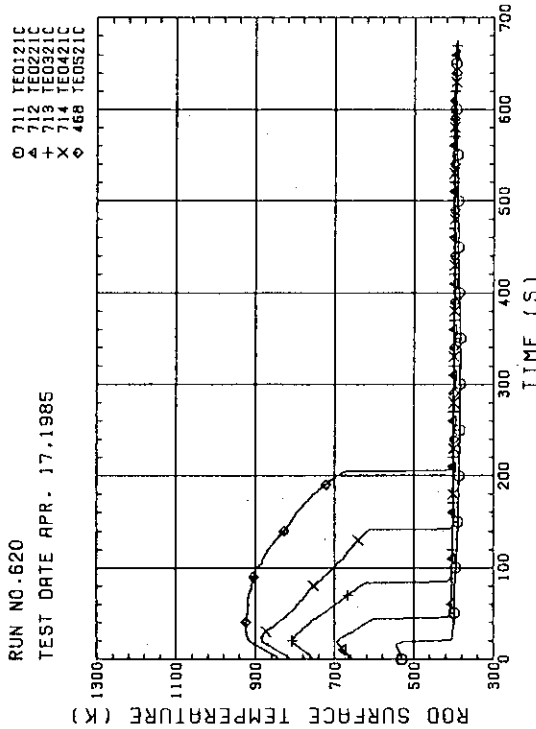


Fig. D-1 HEATER ROD TEMPERATURE  
(BUNDLE 2-1C, LOWER HALF)

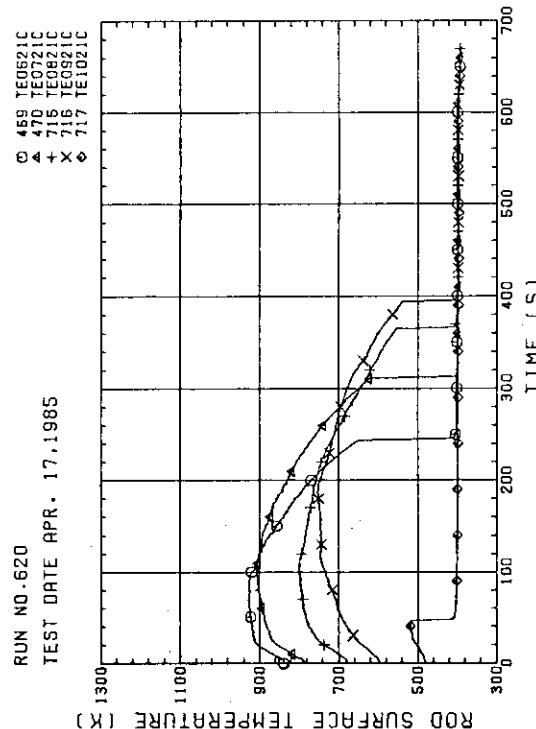


Fig. D-2 HEATER ROD TEMPERATURE  
(BUNDLE 2-1C, UPPER HALF)

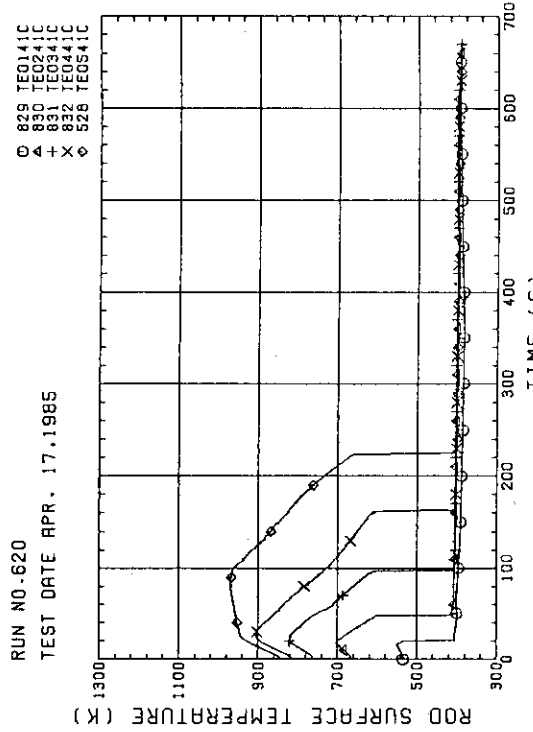


Fig. D-3 HEATER ROD TEMPERATURE  
(BUNDLE 4-1C, LOWER HALF)

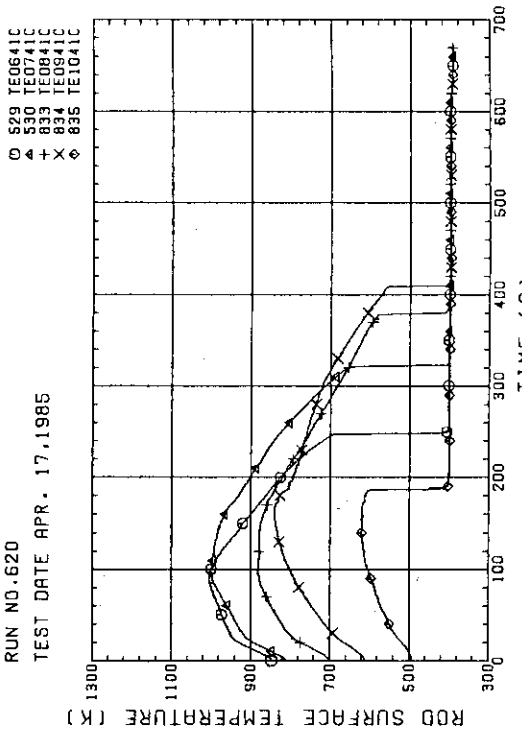
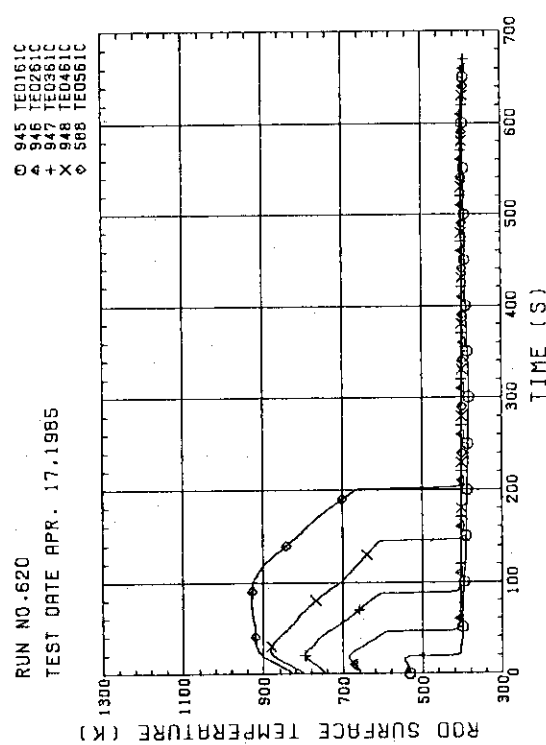
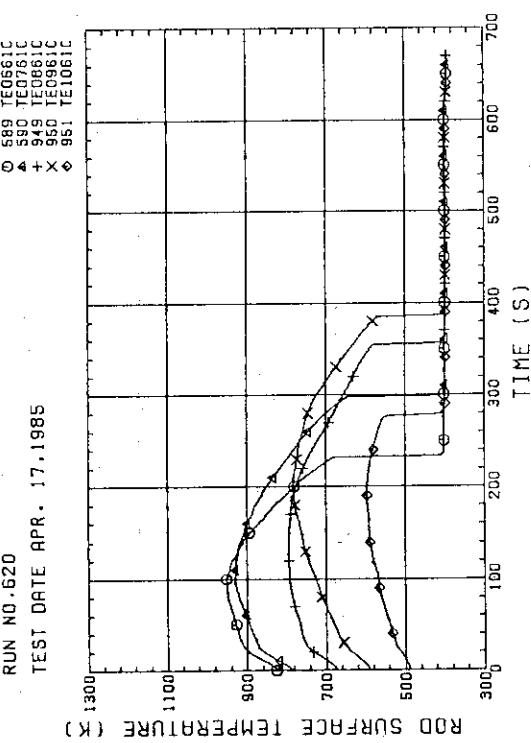
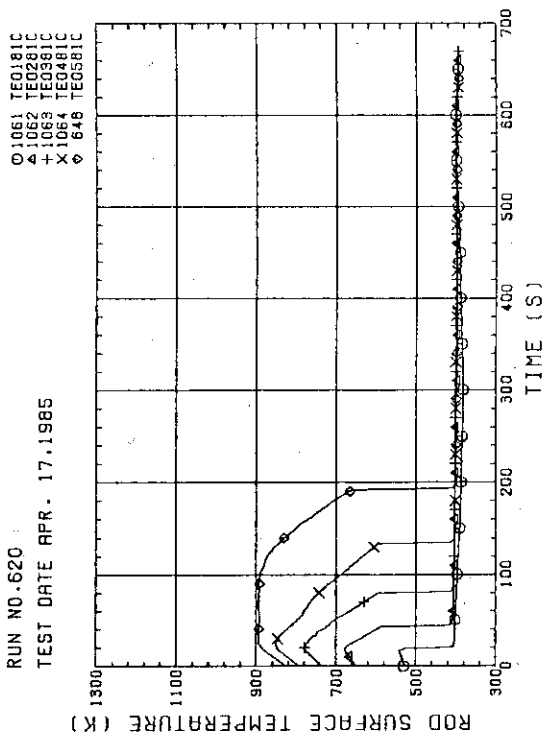
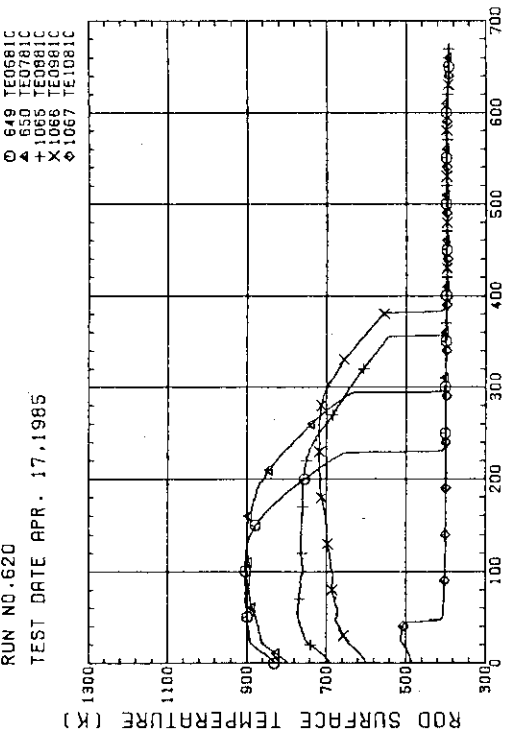
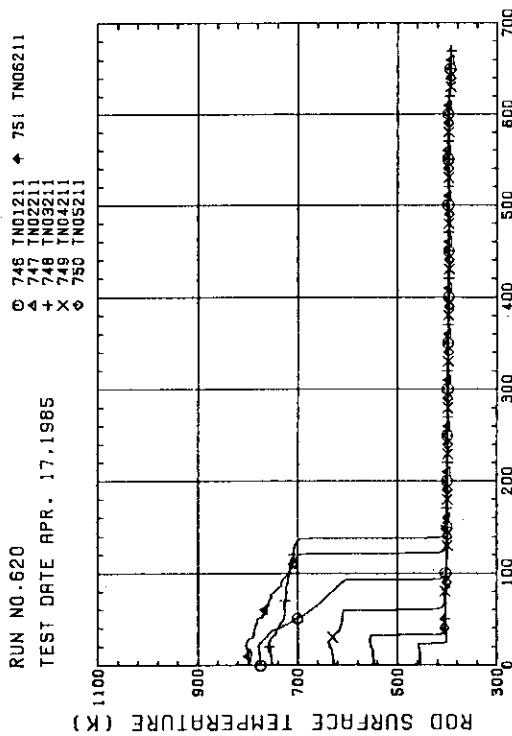
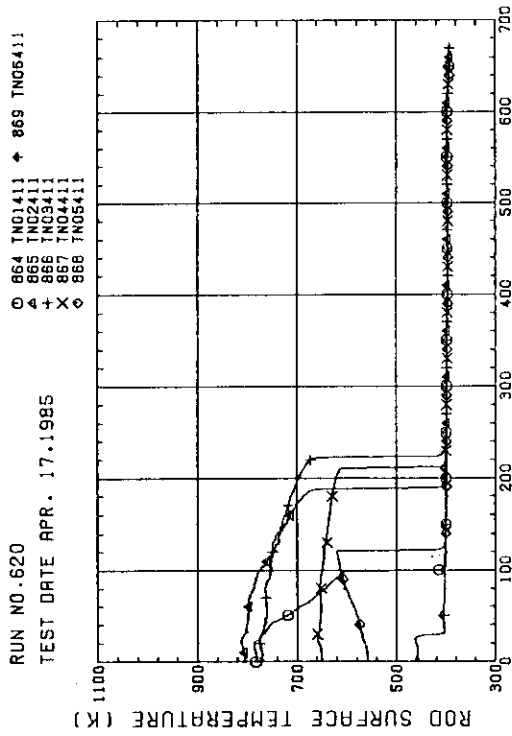
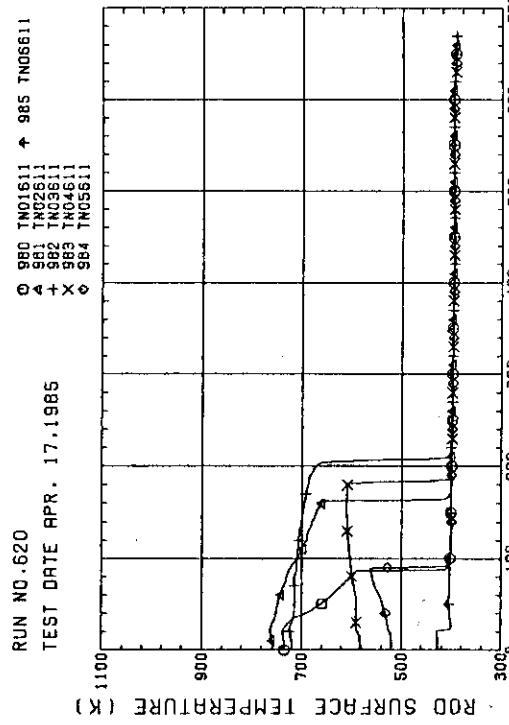
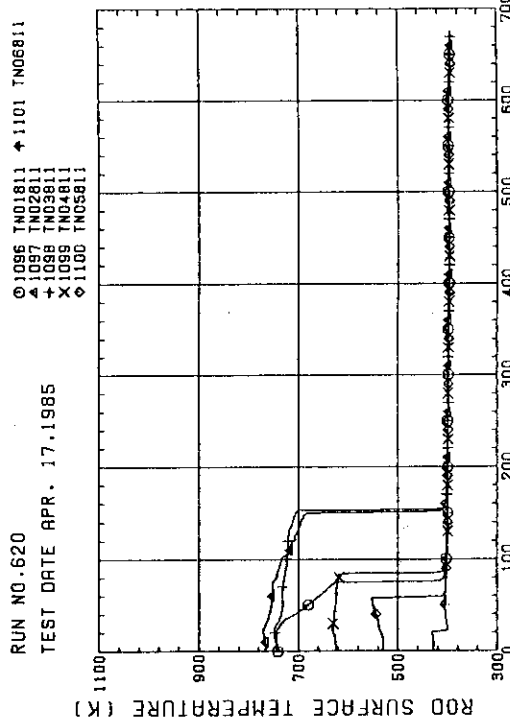


Fig. D-4 HEATER ROD TEMPERATURE  
(BUNDLE 4-1C, UPPER HALF)

Fig. D-5 HEATER ROD TEMPERATURE  
(BUNDLE 6-1C, LOWER HALF)Fig. D-6 HEATER ROD TEMPERATURE  
(BUNDLE 6-1C, UPPER HALF)Fig. D-7 HEATER ROD TEMPERATURE  
(BUNDLE 6-1C, LOWER HALF)Fig. D-8 HEATER ROD TEMPERATURE  
(BUNDLE 6-1C, UPPER HALF)

Fig. D-9 NON-HEATED ROD TEMPERATURE  
(BUNDLE 2-1)Fig. D-10 NON-HEATED ROD TEMPERATURE  
(BUNDLE 4-1)Fig. D-11 NON-HEATED ROD TEMPERATURE  
(BUNDLE 6-1)Fig. D-12 NON-HEATED ROD TEMPERATURE  
(BUNDLE 8-1)

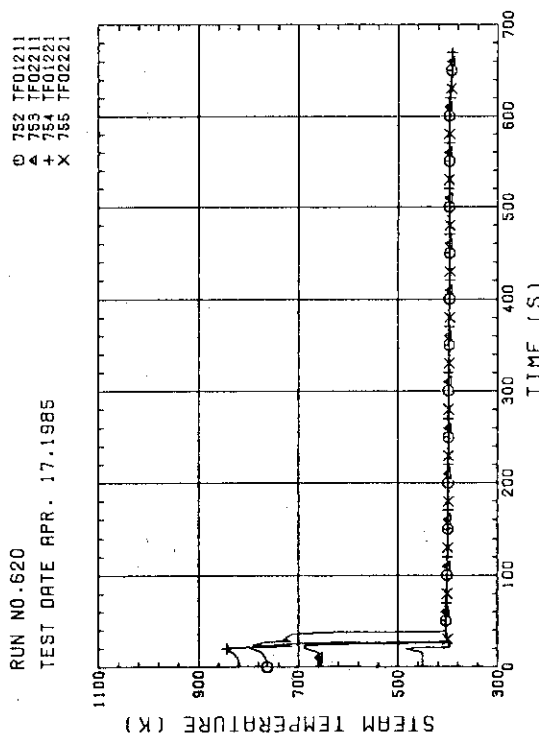


Fig. D-13 STEAM TEMPERATURE IN CORE, BUNDLE 2

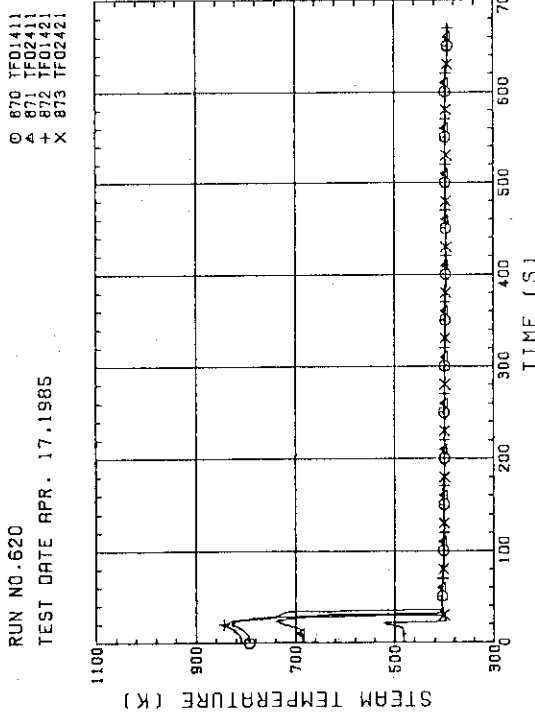


Fig. D-14 STEAM TEMPERATURE IN CORE, BUNDLE 4

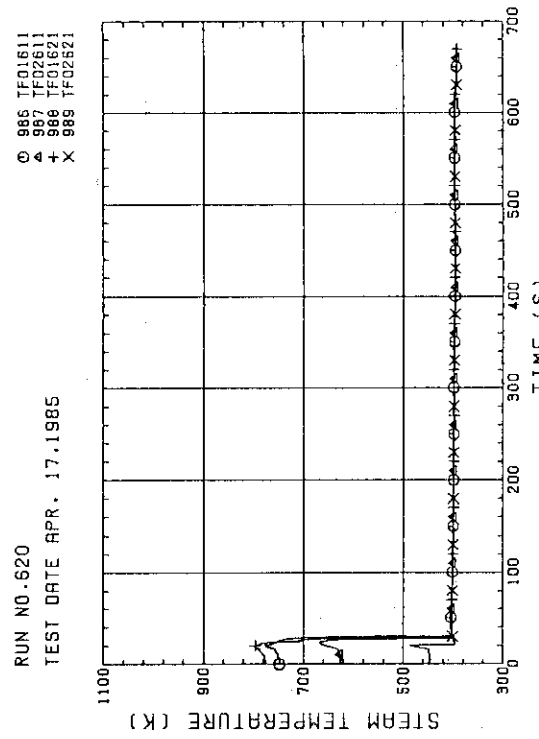


Fig. D-15 STEAM TEMPERATURE IN CORE, BUNDLE 6

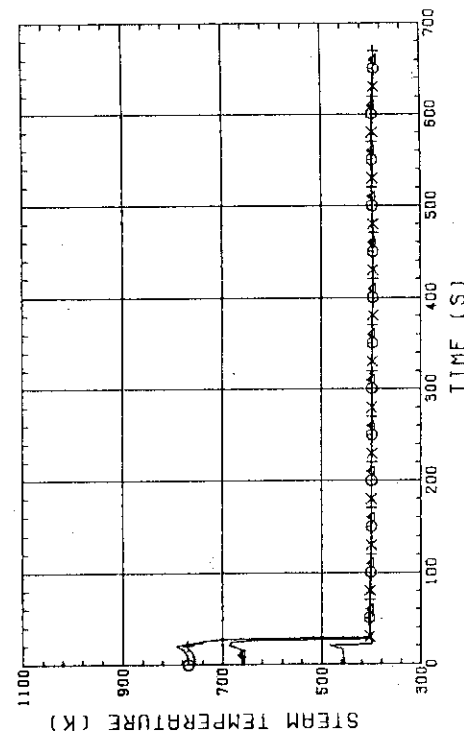


Fig. D-16 STEAM TEMPERATURE IN CORE, BUNDLE 8

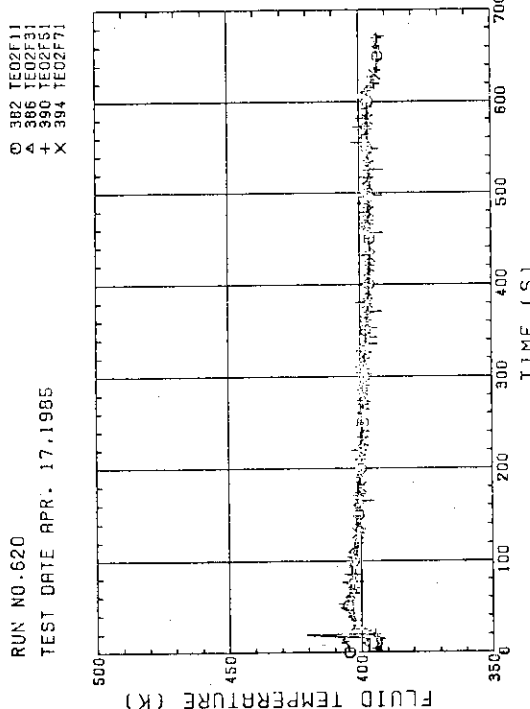


Fig. D-17 FLUID TEMPERATURE JUST ABOVE END BOX TIE PLATE (BUNDLE 1, 3, 5, 7, OPPOSITE SIDE OF COLD LEG, OUTER)

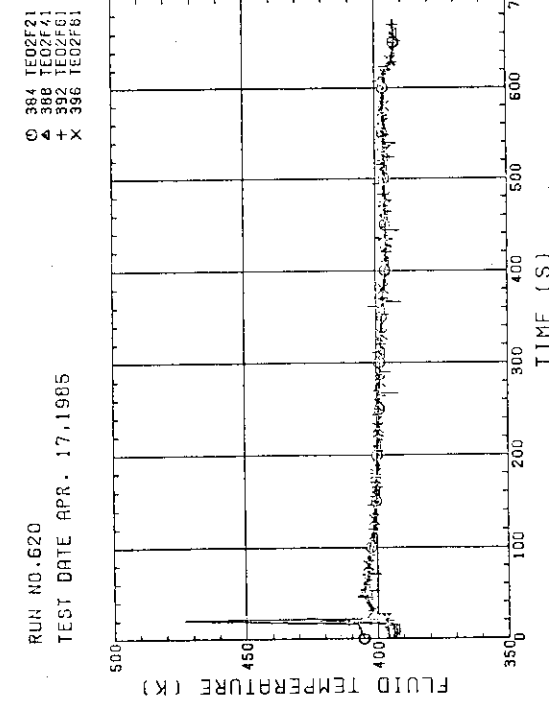


Fig. D-18 FLUID TEMPERATURE JUST ABOVE END BOX TIE PLATE (BUNDLE 2, 4, 6, 8, COLD LEG SIDE, INNER)

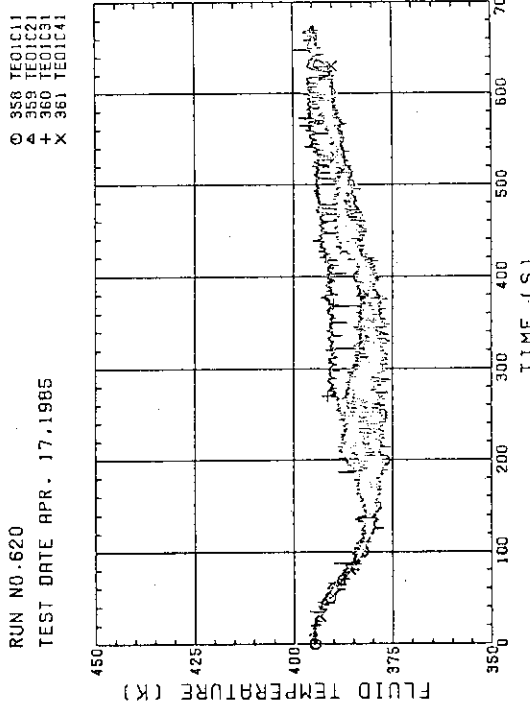


Fig. D-19 FLUID TEMPERATURE AT CORE INLET (BUNDLE 1, 2, 3, 4, 100MM BELOW HEATED PART)

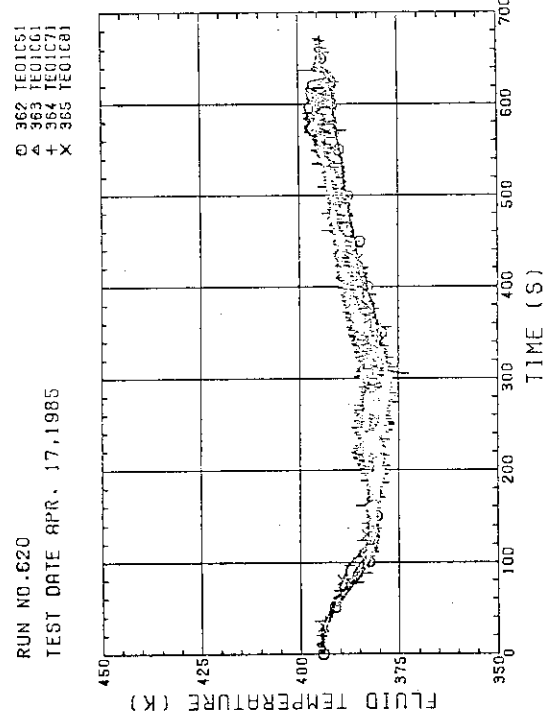
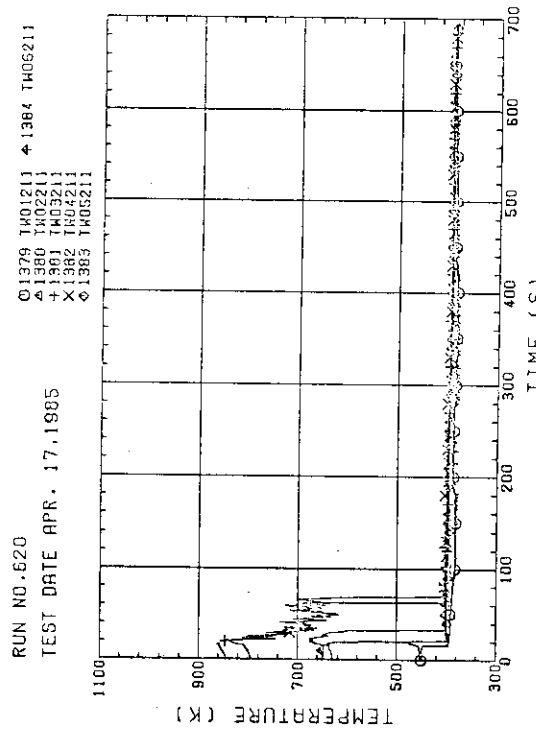
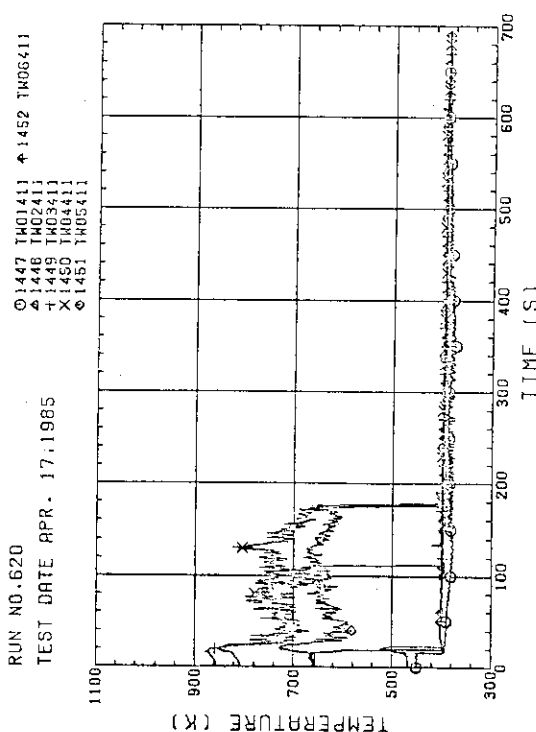
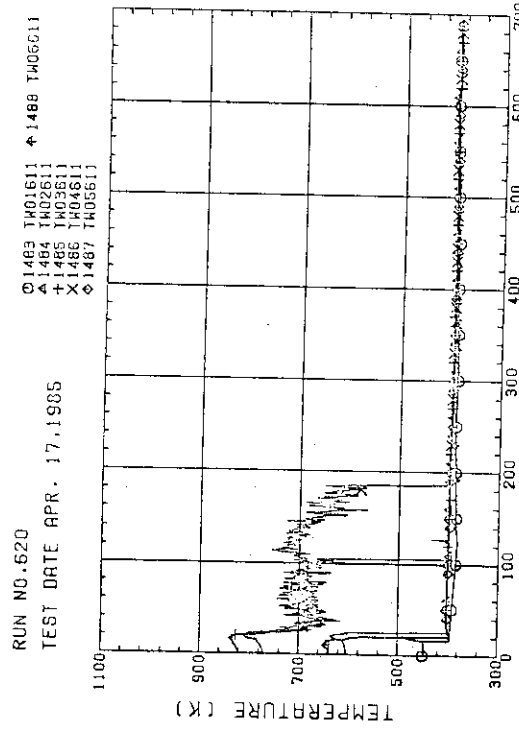
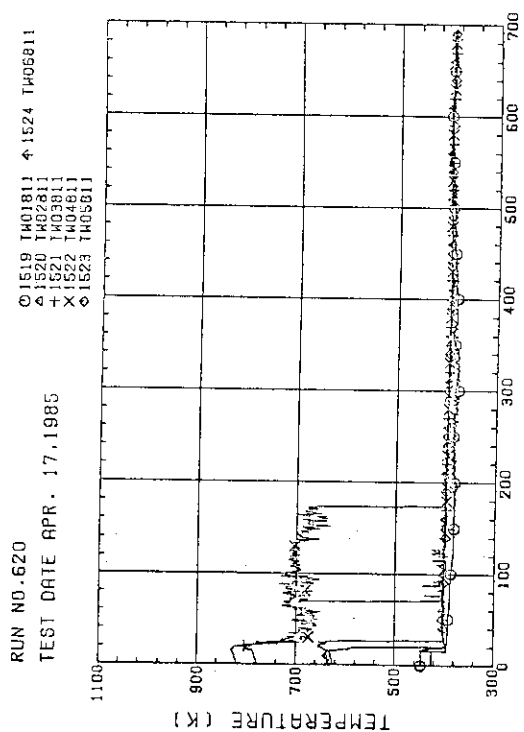
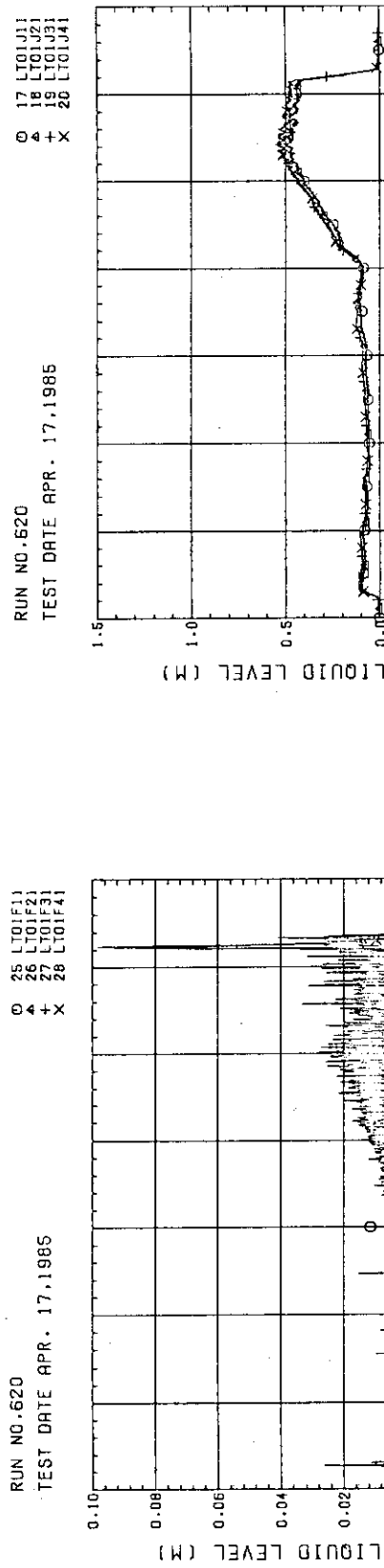
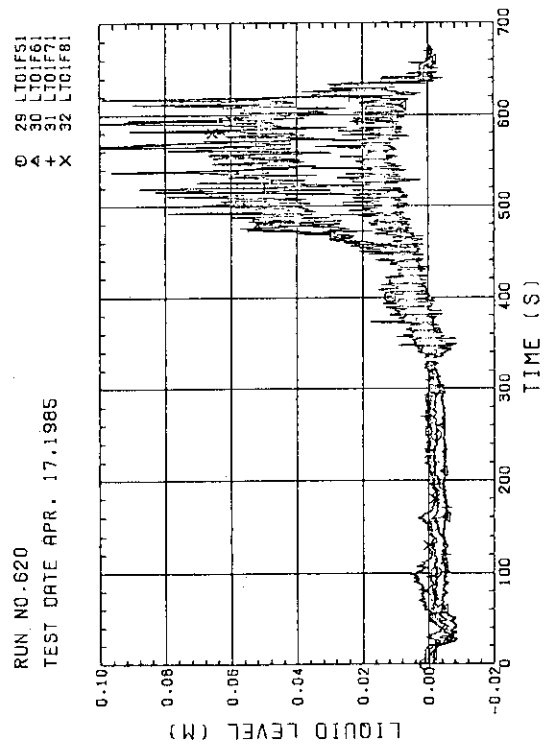
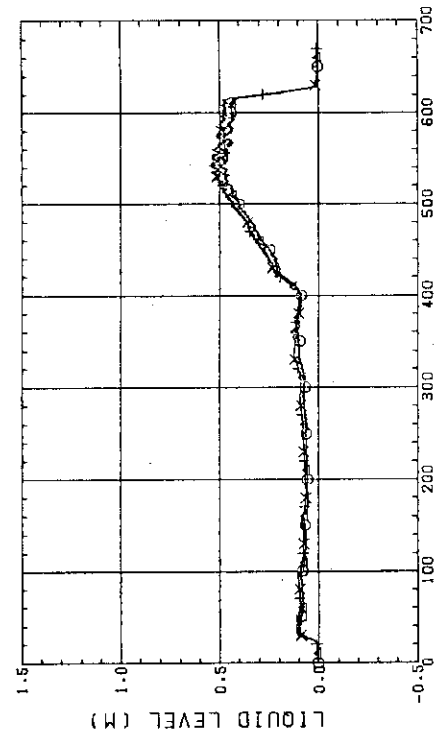
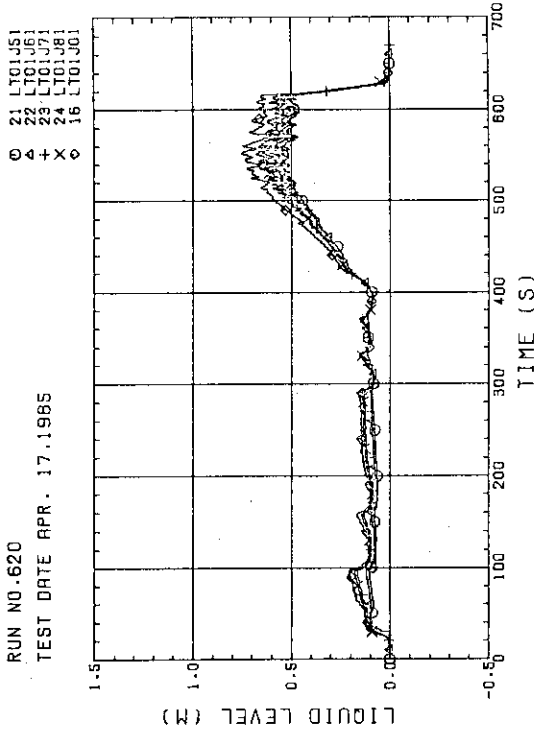


Fig. D-20 FLUID TEMPERATURE AT CORE INLET (BUNDLE 5, 6, 7, 8, 100MM BELOW HEATED PART)

Fig. D-21 TEMPERATURE FOR SPUTTERING DETECTION  
BUNDLE 2 , REGION 1 , TYPE 1Fig. D-22 TEMPERATURE FOR SPUTTERING DETECTION  
BUNDLE 4 , REGION 1 , TYPE 1Fig. D-23 TEMPERATURE FOR SPUTTERING DETECTION  
BUNDLE 6 , REGION 1 , TYPE 1Fig. D-24 TEMPERATURE FOR SPUTTERING DETECTION  
BUNDLE 8 , REGION 1 , TYPE 1

Fig. D-25 LIQUID LEVEL ABOVE END BOX TIE PLATE  
(BUNDLE 1,2,3,4)Fig. D-26 LIQUID LEVEL ABOVE END BOX TIE PLATE  
(BUNDLE 5,6,7,8)Fig. D-27 LIQUID LEVEL ABOVE UCSP  
(BUNDLE 1,2,3,4)Fig. D-28 LIQUID LEVEL ABOVE UCSP  
(BUNDLE 5,6,7,8 AND CORE BAFFLE)

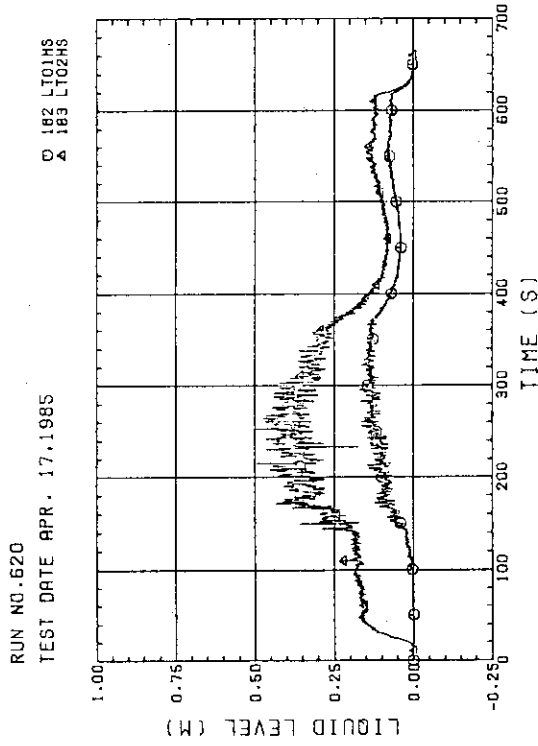


Fig. D-29 LIQUID LEVEL IN HOT LEG (O1HS - PV SIDE, O2HS - STEAM/WATER SEPARATOR SIDE)

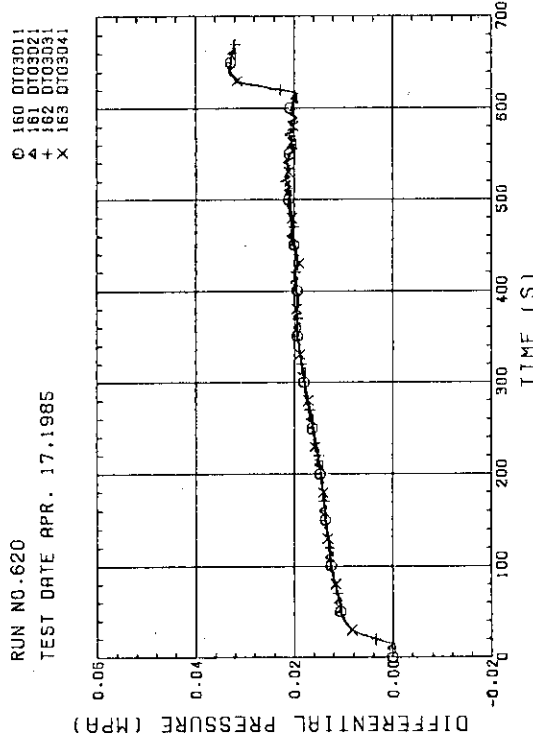


Fig. D-30 DIFFERENTIAL PRESSURE OF CORE FULL HEIGHT (BUNDLE 1,2,3,4)

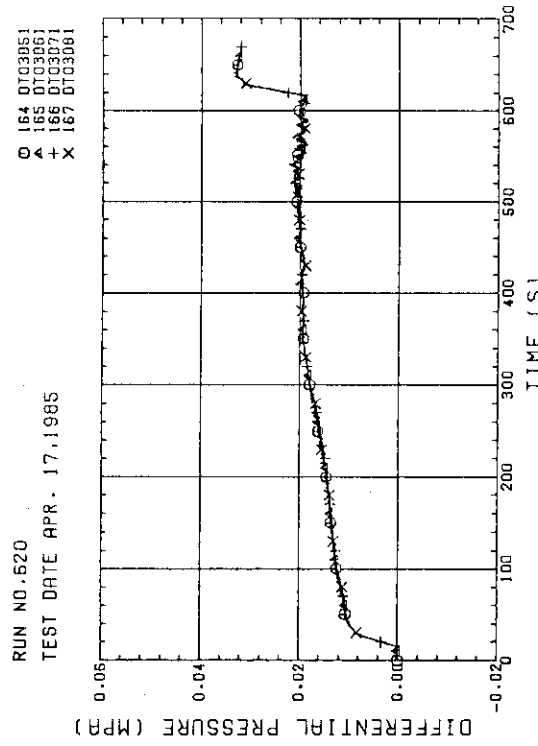


Fig. D-31 DIFFERENTIAL PRESSURE OF CORE FULL HEIGHT (BUNDLE 5,6,7,8)

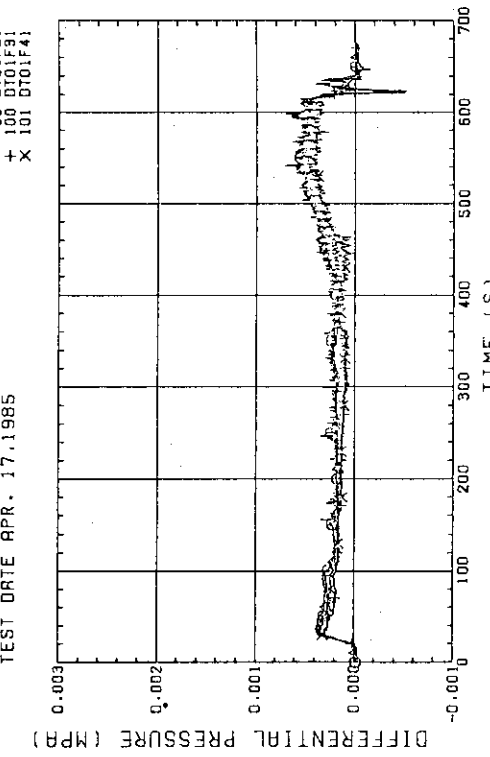


Fig. D-32 DIFFERENTIAL PRESSURE ACROSS END BOX TIE PLATE (BUNDLE 1,2,3,4)

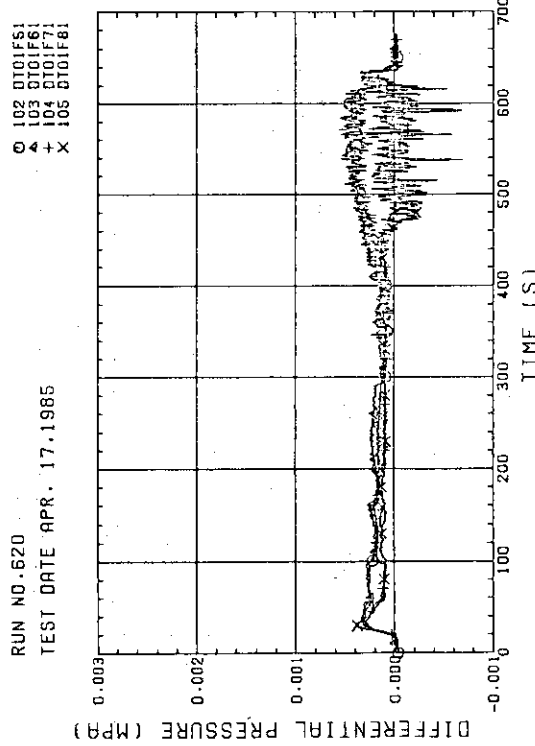


Fig. D-33 DIFFERENTIAL PRESSURE ACROSS END BOX TIE PLATE (BUNDLE 5,6,7,8)

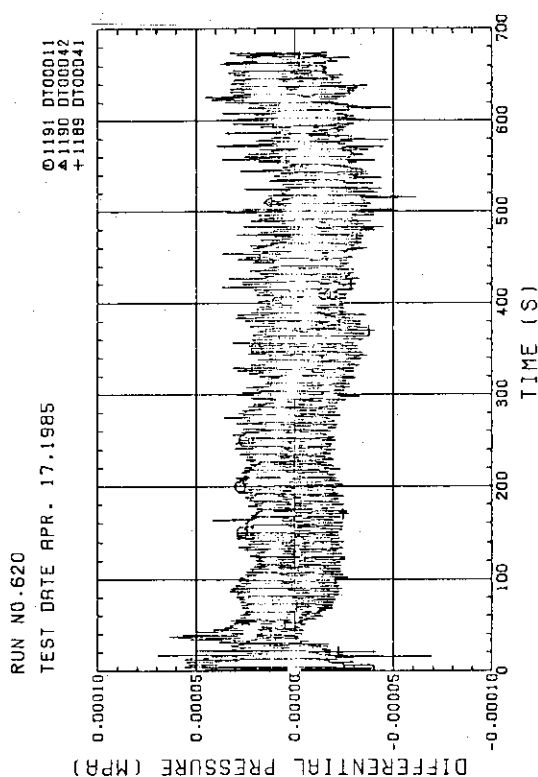


Fig. D-34 DIFFERENTIAL PRESSURE, HORIZONTAL AT -142 MM (11-BUNDLE 1-4, 42-BUNDLE 4-6, 41-BUNDLE 4-6)

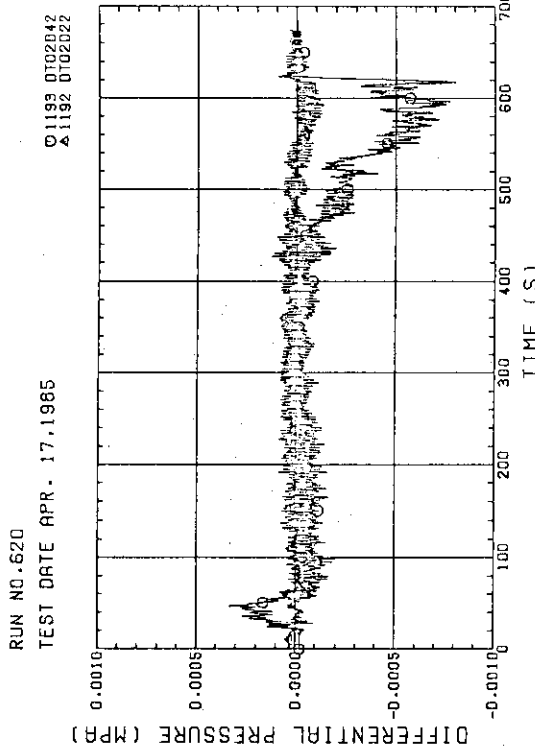


Fig. D-35 DIFFERENTIAL PRESSURE, HORIZONTAL AT 700 MM (42-BUNDLE 2-4, 22-BUNDLE 4-8)

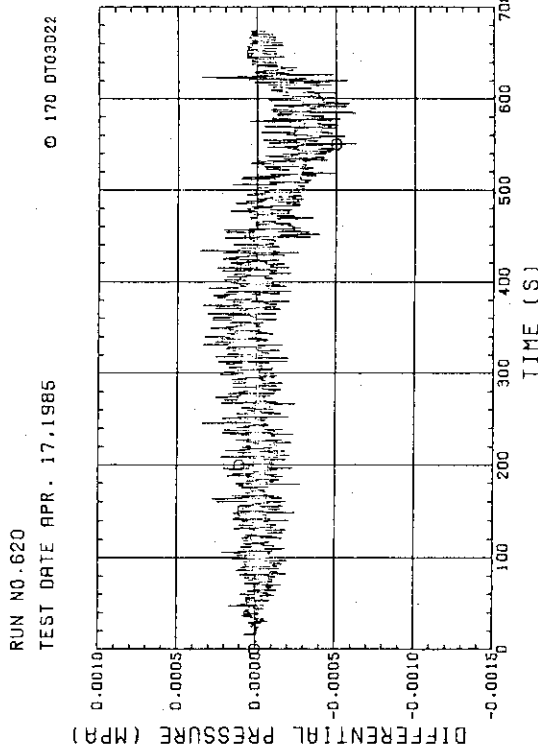


Fig. D-36 DIFFERENTIAL PRESSURE, HORIZONTAL AT 1365 MM (BUNDLE 2-4)

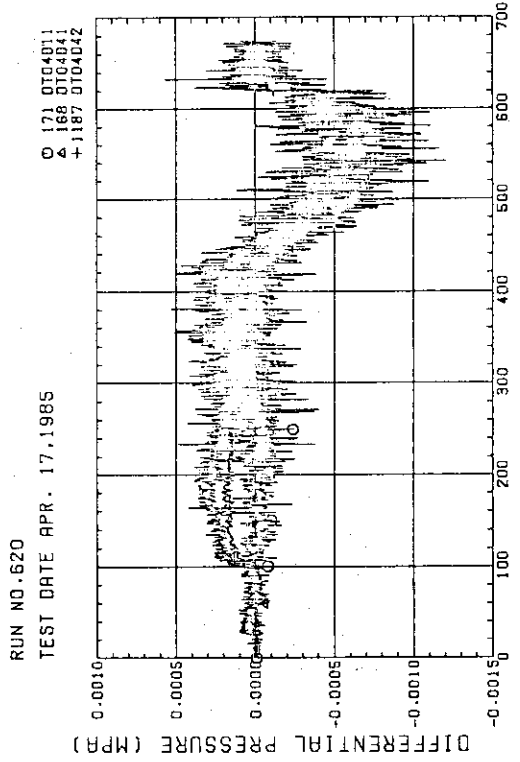


Fig. D-37 DIFFERENTIAL PRESSURE, HORIZONTAL AT 1905 MM  
(11-BUNDLE 1-4, 41-BUNDLE 4-8, 42-BUNDLE 4-6)

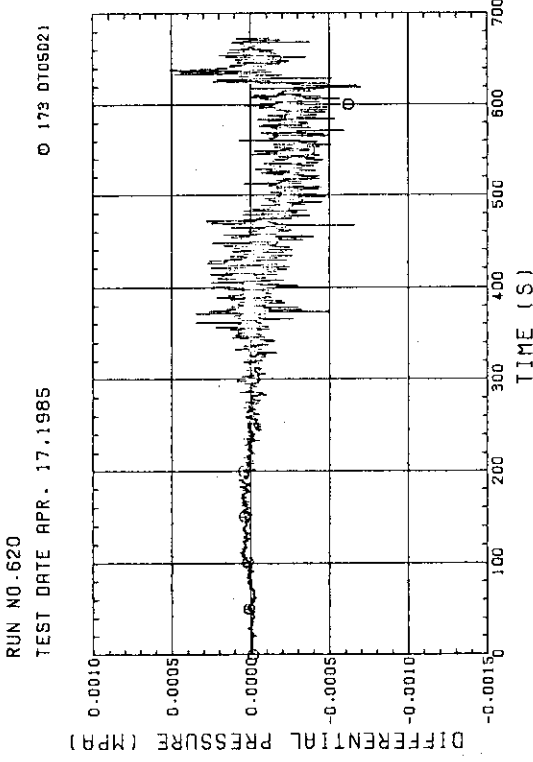


Fig. D-38 DIFFERENTIAL PRESSURE, HORIZONTAL AT 2570 MM  
(BUNDLE 2-4)

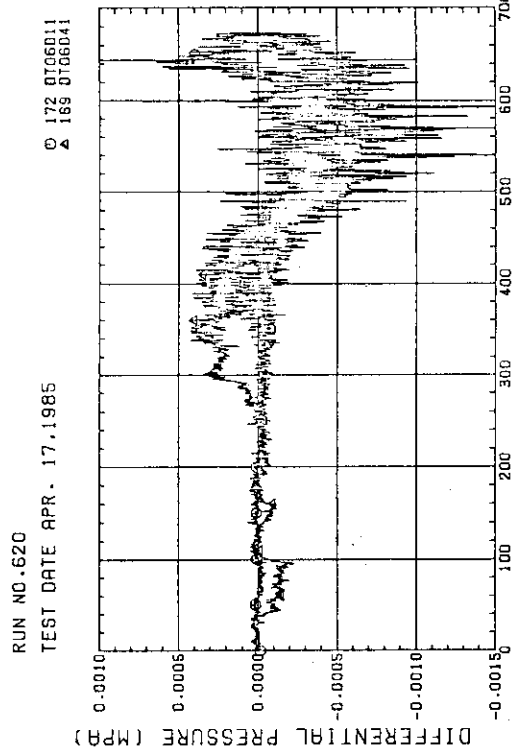


Fig. D-39 DIFFERENTIAL PRESSURE, HORIZONTAL AT 3235 MM  
(11-BUNDLE 1-4, 41-BUNDLE 4-8)

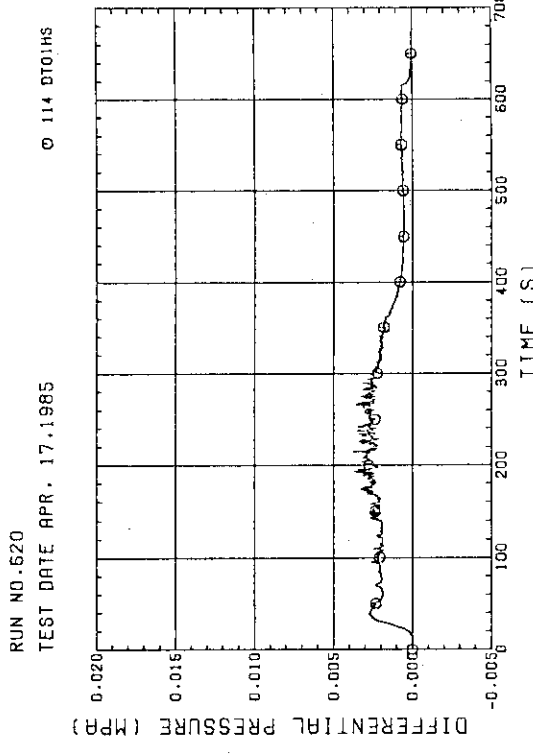


Fig. D-40 DIFFERENTIAL PRESSURE OF HOT LEG,  
HOT LEG INLET - STEAM/WATER SEPARATOR INLET

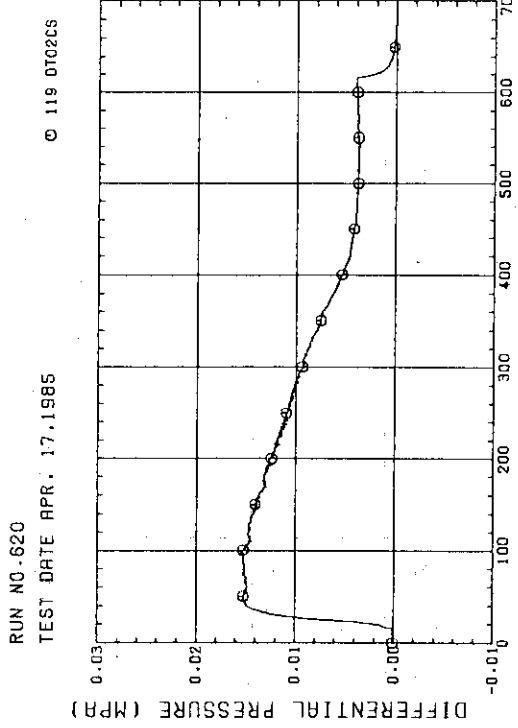
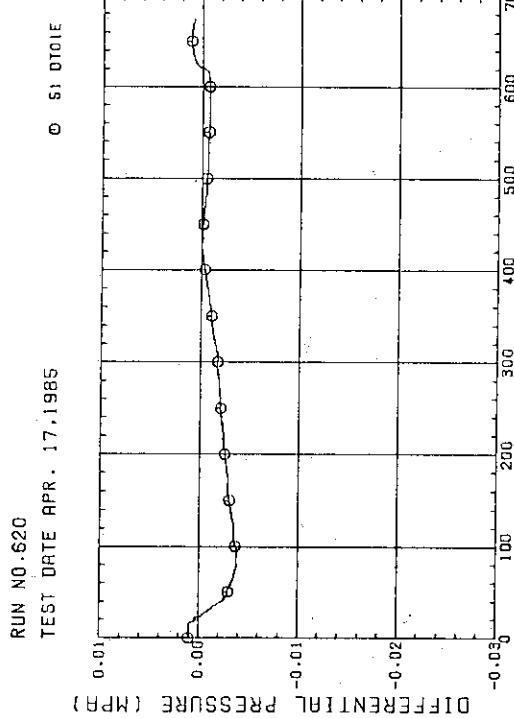
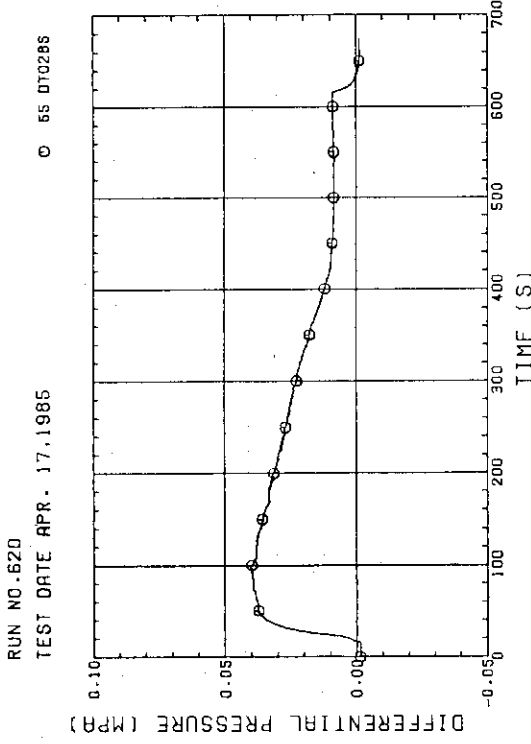
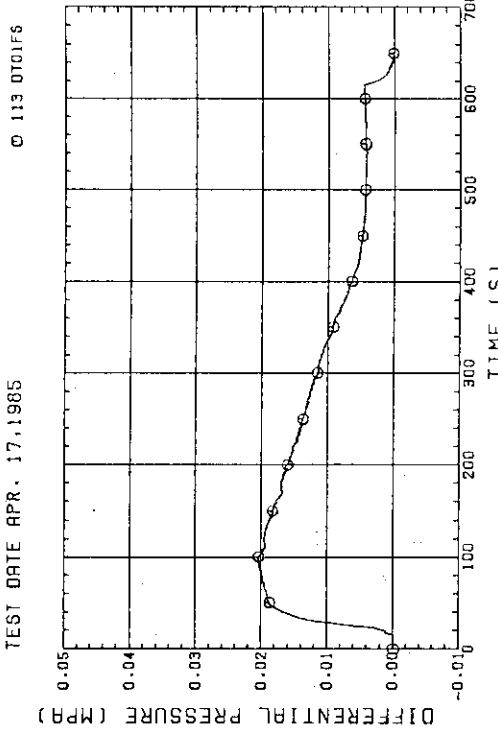


Fig. D-41 DIFFERENTIAL PRESSURE OF INTACT COLD LEG

Fig. D-43 DIFFERENTIAL PRESSURE, CONTAINMENT TANK-1 -  
CONFINEMENT TANK-1Fig. D-42 DIFFERENTIAL PRESSURE, STEAM/WATER SEPARATOR -  
CONFINEMENT TANK-1Fig. D-44 DIFFERENTIAL PRESSURE OF BROKEN COLD LEG - PV SIDE -  
DOWNCOMER - CONFINEMENT TANK-1Fig. D-44 DIFFERENTIAL PRESSURE OF BROKEN COLD LEG - PV SIDE -  
DOWNCOMER - CONFINEMENT TANK-1

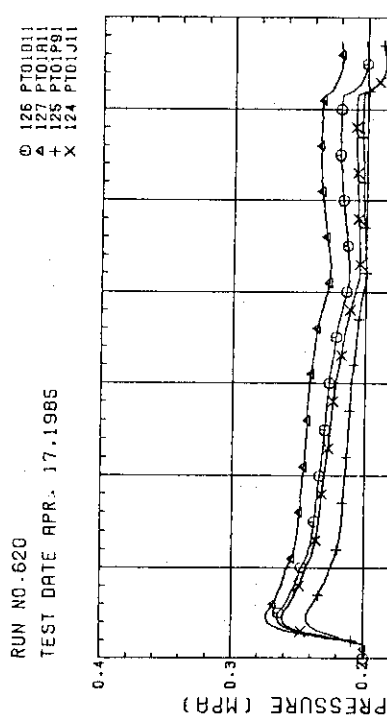


Fig. D-45 PRESSURE IN PV (J = TOP OF PV; D = CORE CENTER, A - CORE INLET; P = BELOW COLD LEG NOZZLE IN DOWNCOMER)

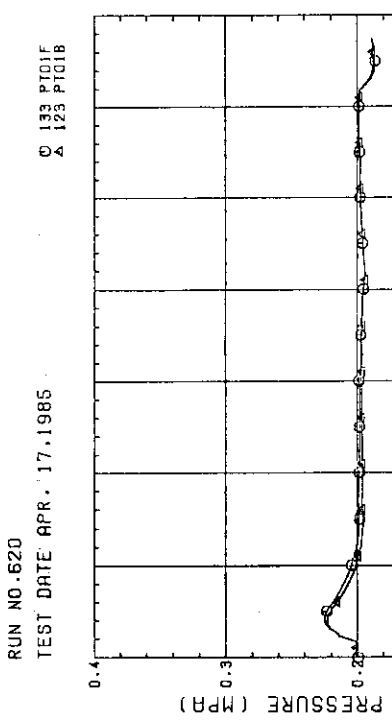


Fig. D-46 PRESSURE AT TOP OF CONTAINMENT TANK-I AND CONTAINMENT TANK-II (F = CONTAINMENT TANK-I, B = CONTAINMENT TANK-II)

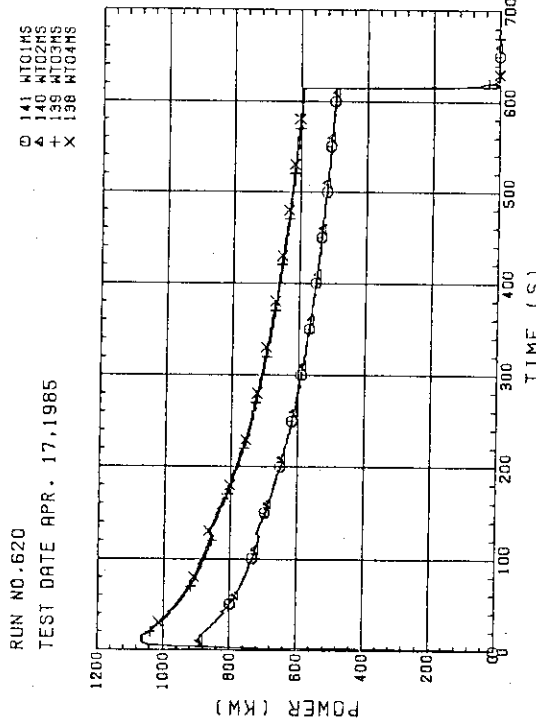


Fig. D-47 BUNDLE POWER (BUNDLE 1,2,3,4)

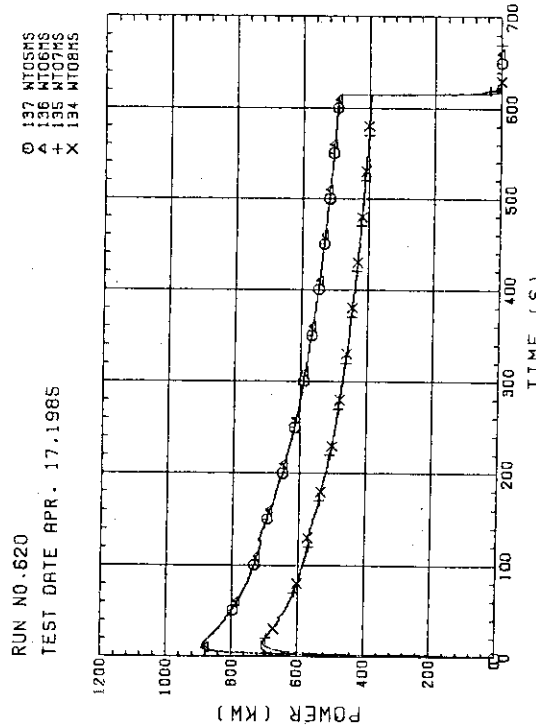
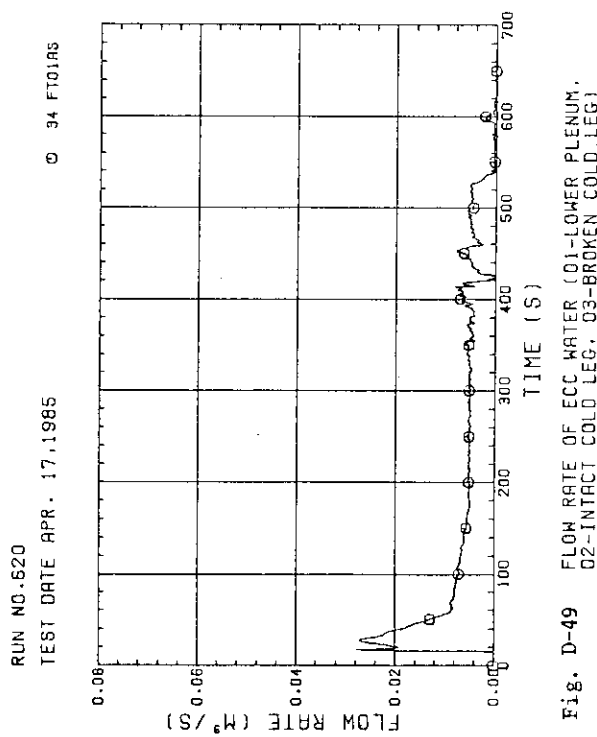


Fig. D-48 BUNDLE POWER (BUNDLE 5,6,7,8)



## Appendix E Selected Data of Test S2-21

Fig. E-1 ~ E-8	Heater rod temperatures
Fig. E-9 ~ E-12	Non-heated rod temperatures
Fig. E-13 ~ E-16	Steam temperatures
Fig. E-17 ~ E-18	Fluid temperatures just above end box tie plate
Fig. E-19 ~ E-20	Fluid temperatures at core inlet
Fig. E-21 ~ E-24	Fluid temperatures in core
Fig. E-25 ~ E-28	Liquid levels above end box tie plate
Fig. E-29	Liquid levels in hot leg
Fig. E-30 ~ E-31	Differential pressures across core full height
Fig. E-32 ~ E-33	Differential pressures across end box tie plate
Fig. E-34 ~ E-39	Horizontal differential pressures in core
Fig. E-40 ~ E-44	Differential pressures in primary loops
Fig. E-45 ~ E-46	Pressures in pressure vessel and containment tanks
Fig. E-47 ~ E-48	Bundle powers
Fig. E-49	ECC flow rates

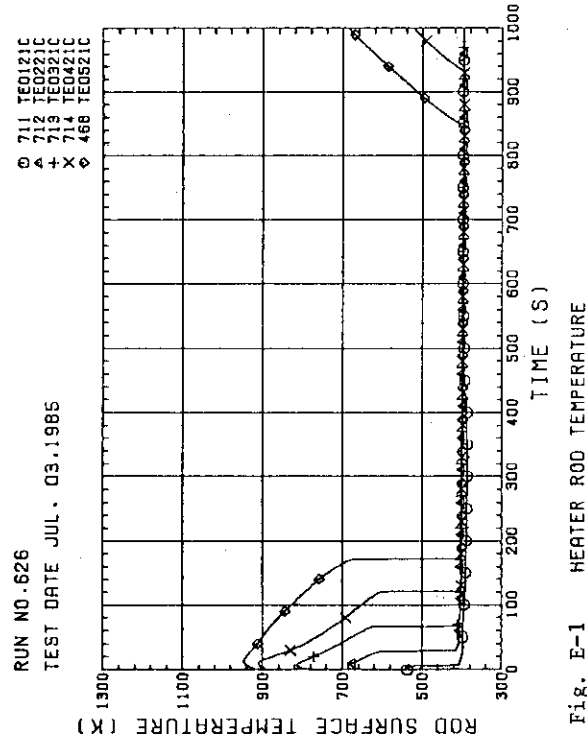


Fig. E-1 HEATER ROD TEMPERATURE (BUNDLE 2-1C, LOWER HALF)

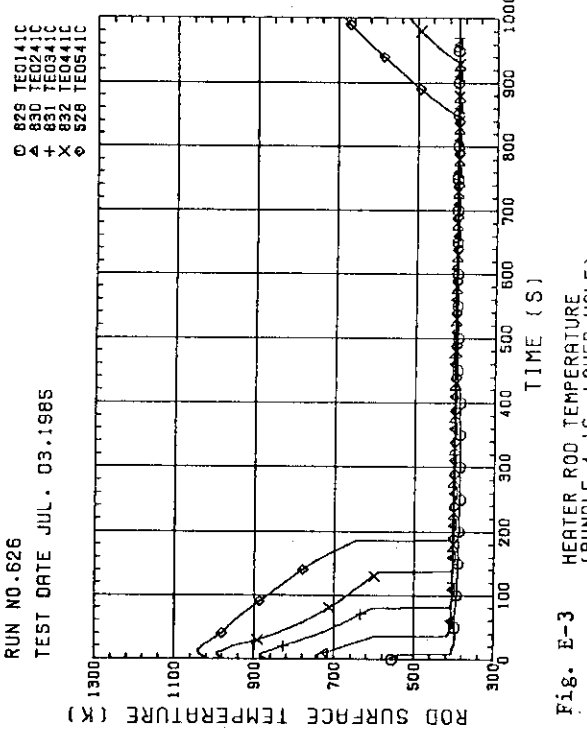


Fig. E-3 HEATER ROD TEMPERATURE (BUNDLE 4-1C, LOWER HALF)

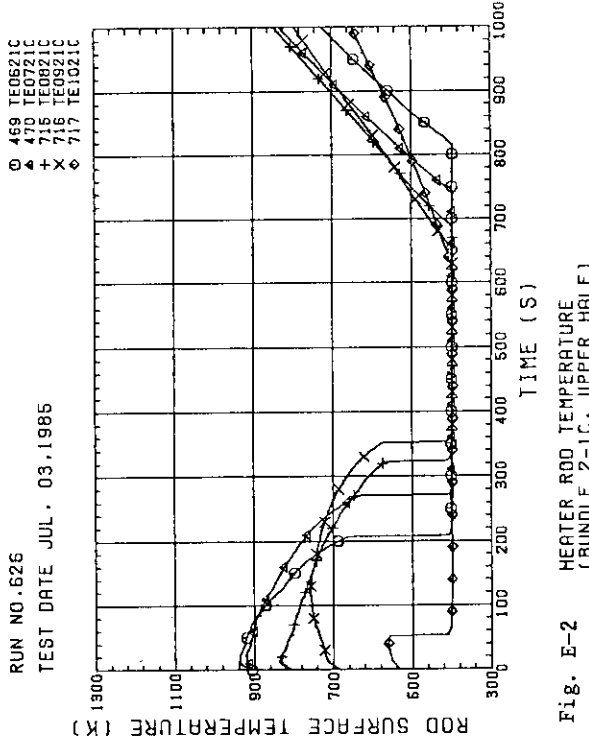


Fig. E-2 HEATER ROD TEMPERATURE (BUNDLE 2-1C, UPPER HALF)

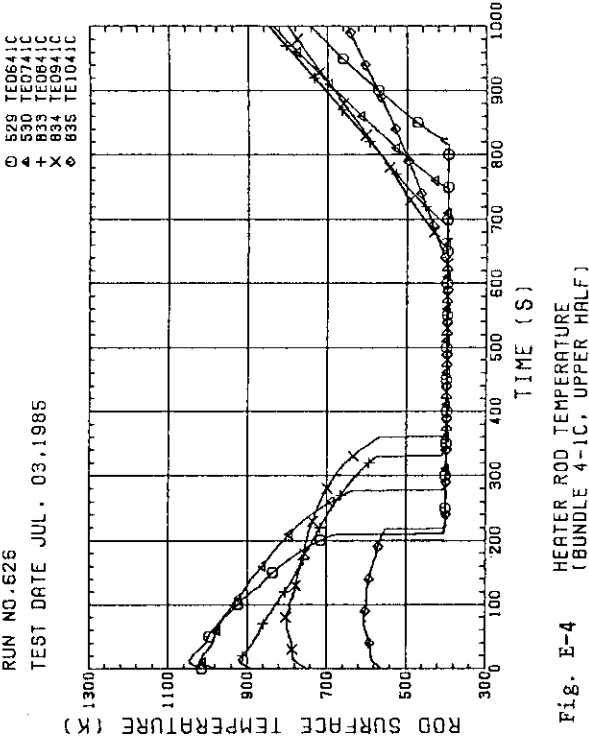
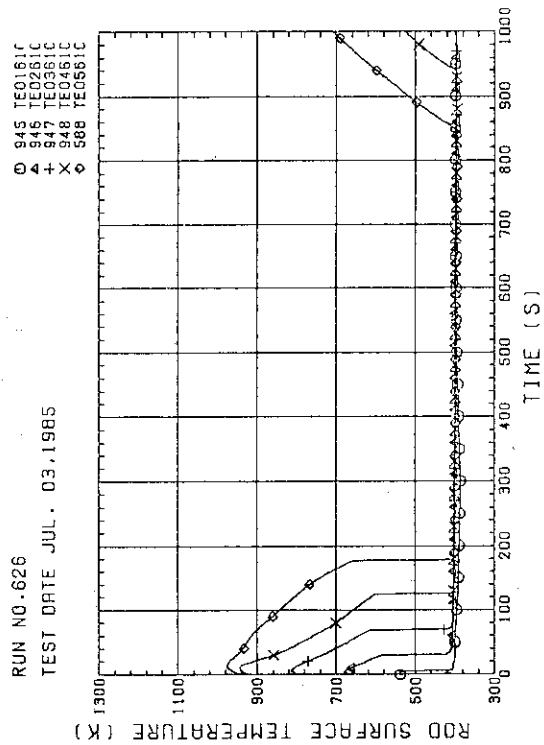
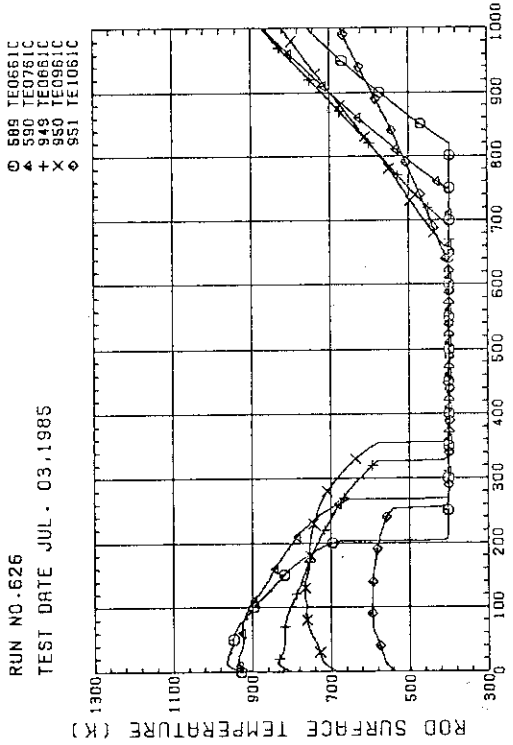
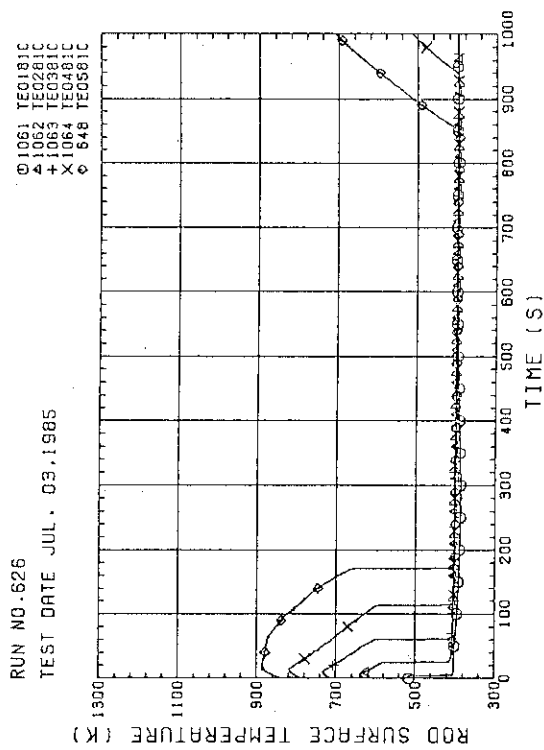
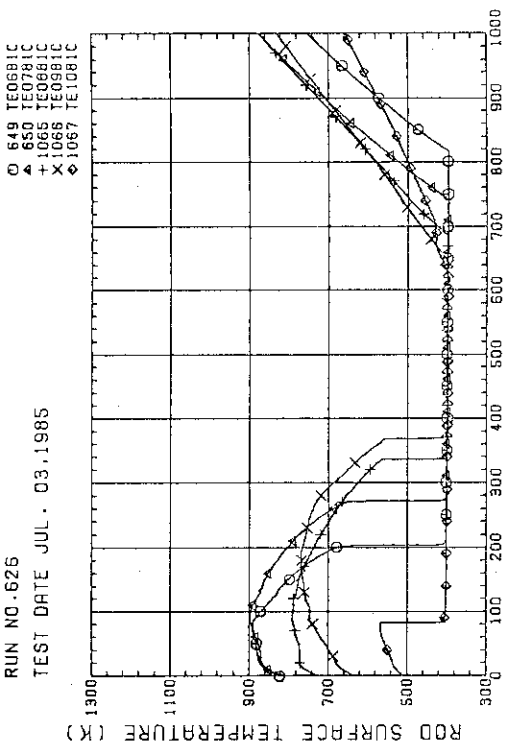


Fig. E-4 HEATER ROD TEMPERATURE (BUNDLE 4-1C, UPPER HALF)

Fig. E-5 HEATED ROD TEMPERATURE  
(BUNDLE 6-1C, LOWER HALF)Fig. E-6 HEATED ROD TEMPERATURE  
(BUNDLE 6-1C, UPPER HALF)Fig. E-7 HEATER ROD TEMPERATURE  
(BUNDLE 8-1C, LOWER HALF)Fig. E-8 HEATER ROD TEMPERATURE  
(BUNDLE 8-1C, UPPER HALF)

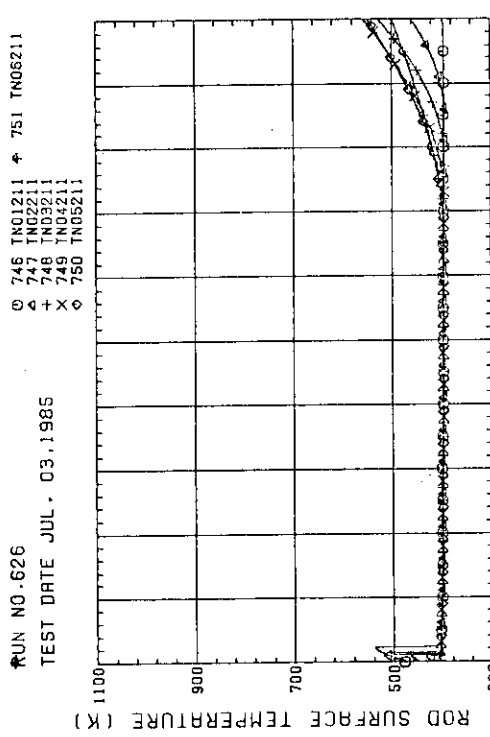


Fig. E-9 NON-HEATED ROD TEMPERATURE  
(BUNDLE 2-1)

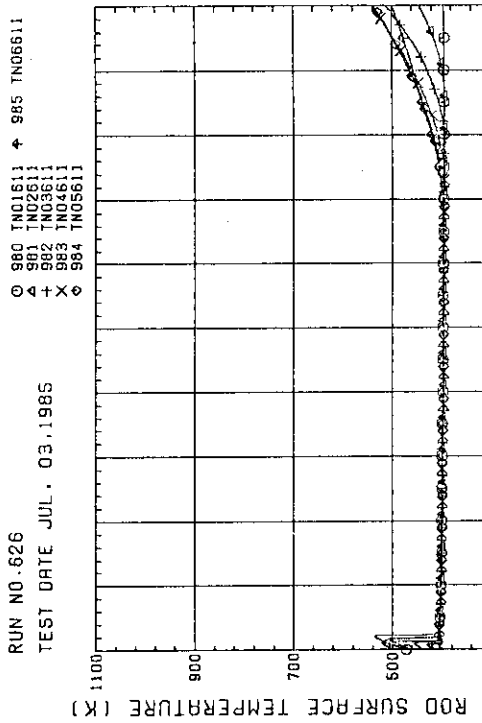


Fig. E-11 NON-HEATED ROD TEMPERATURE  
(BUNDLE 6-1)

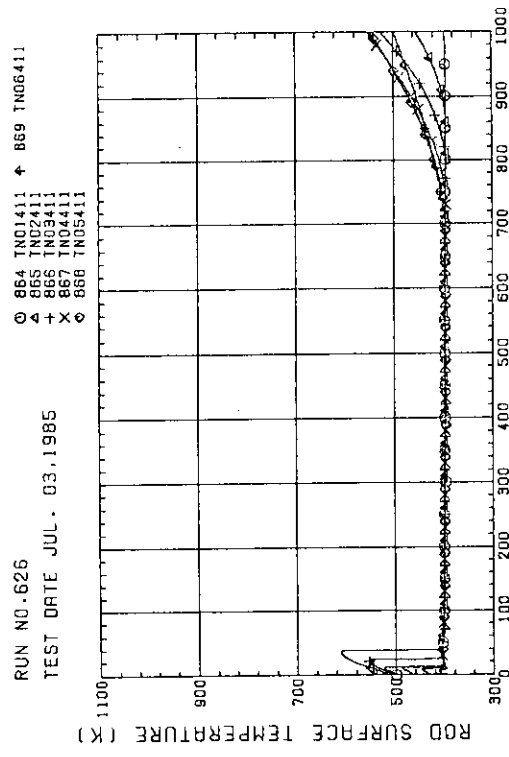


Fig. E-10 NON-HEATED ROD TEMPERATURE  
(BUNDLE 4-1)

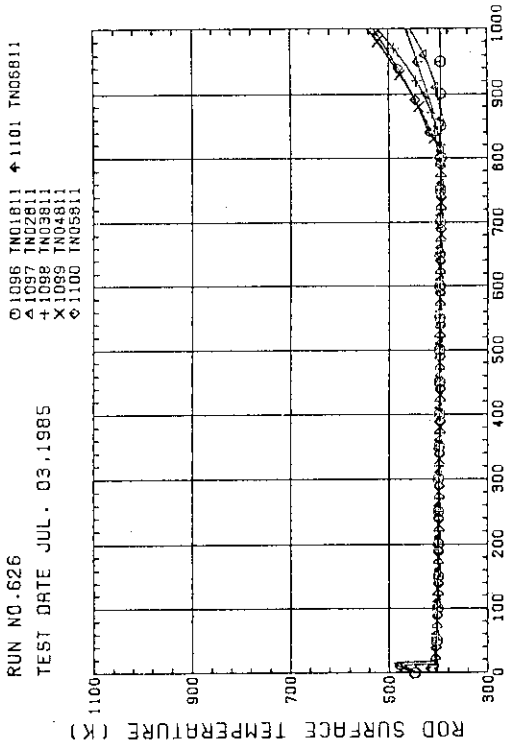


Fig. E-12 NON-HEATED ROD TEMPERATURE  
(BUNDLE 6-1)

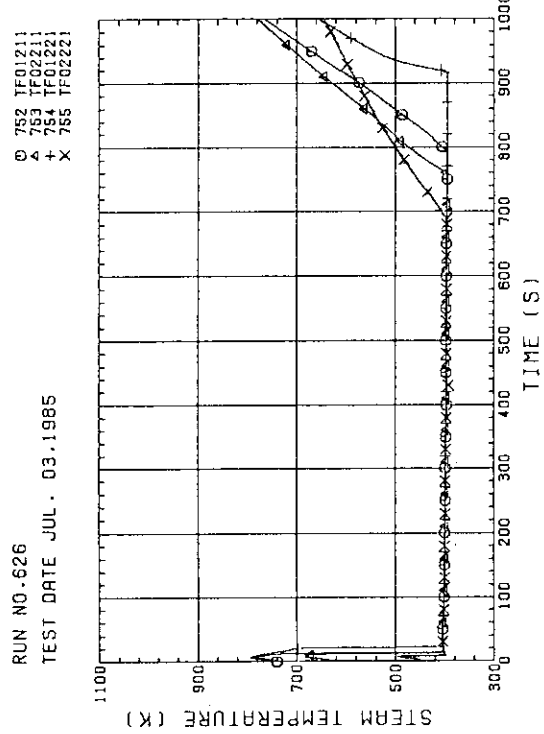


Fig. E-13 STEAM TEMPERATURE IN CORE, BUNDLE 2

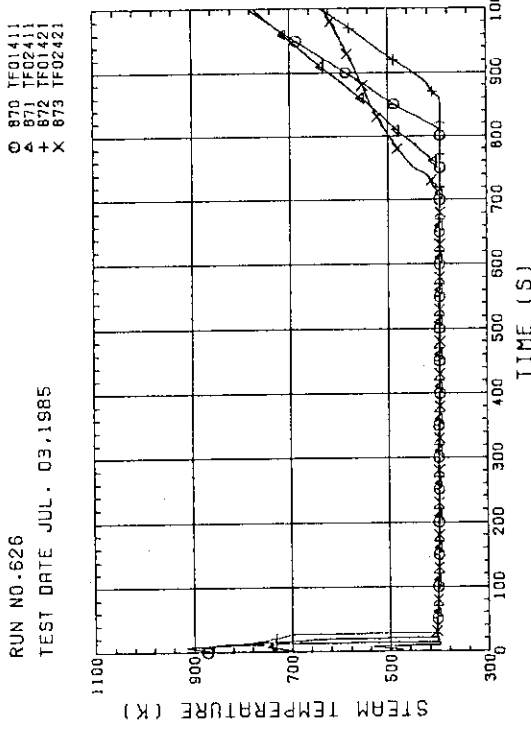


Fig. E-14 STEAM TEMPERATURE IN CORE, BUNDLE 4

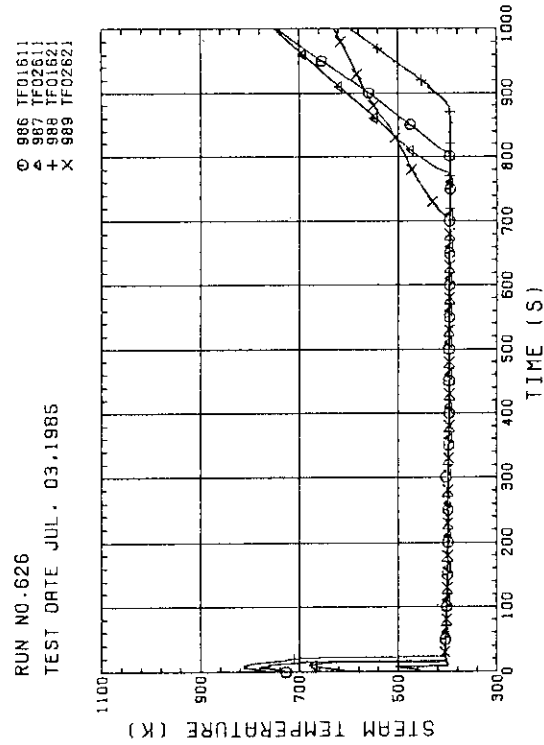


Fig. E-15 STEAM TEMPERATURE IN CORE, BUNDLE 6

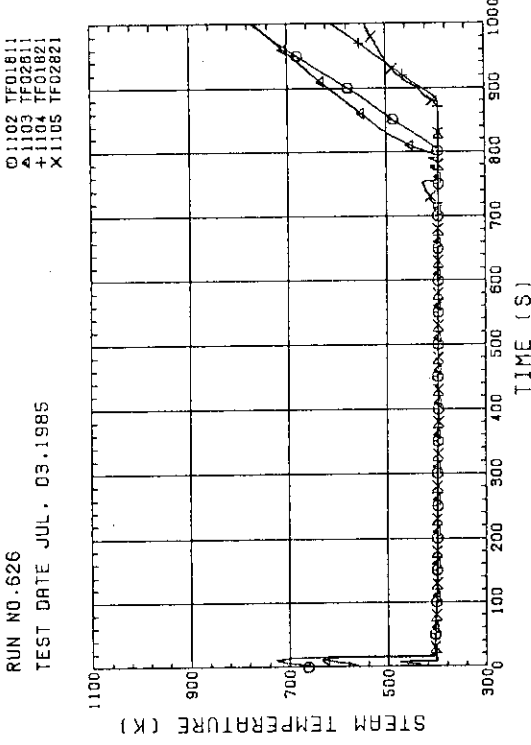
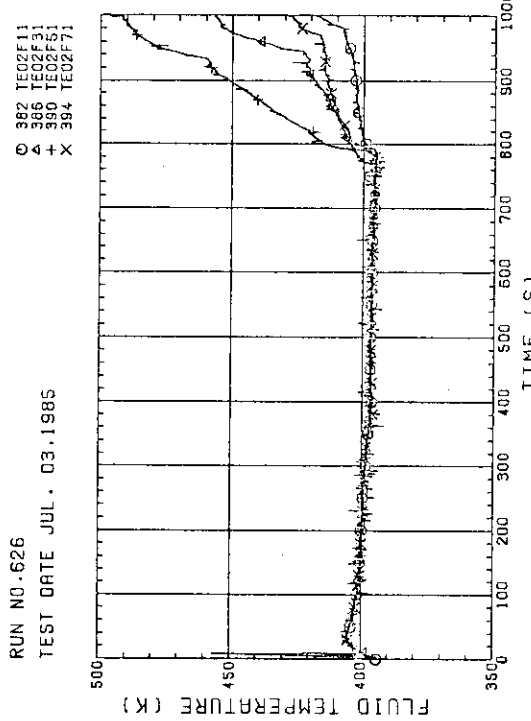
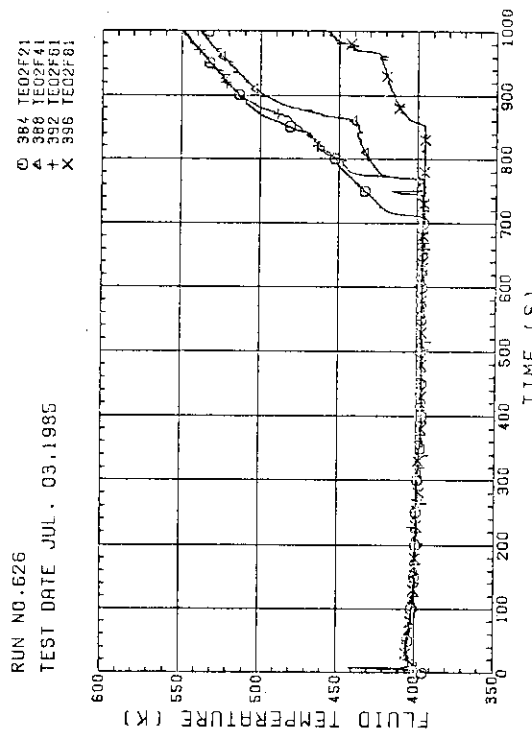
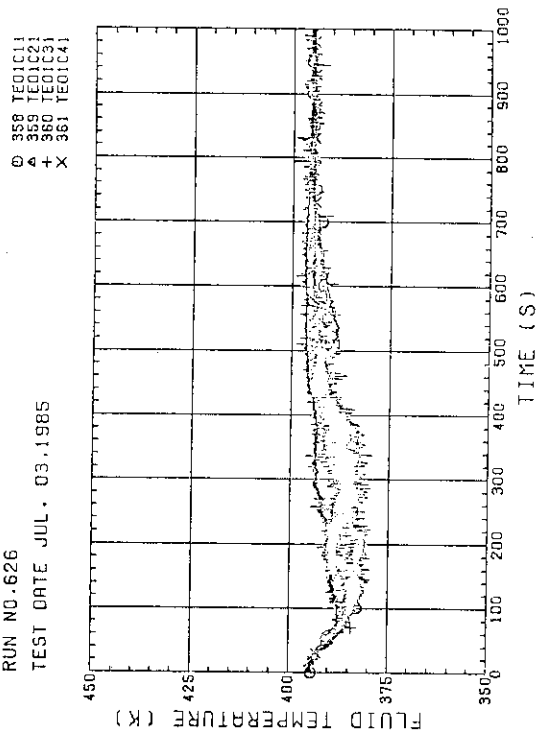
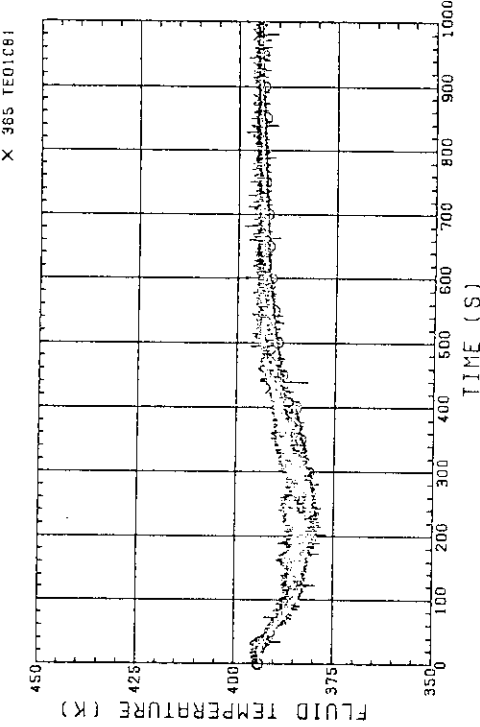
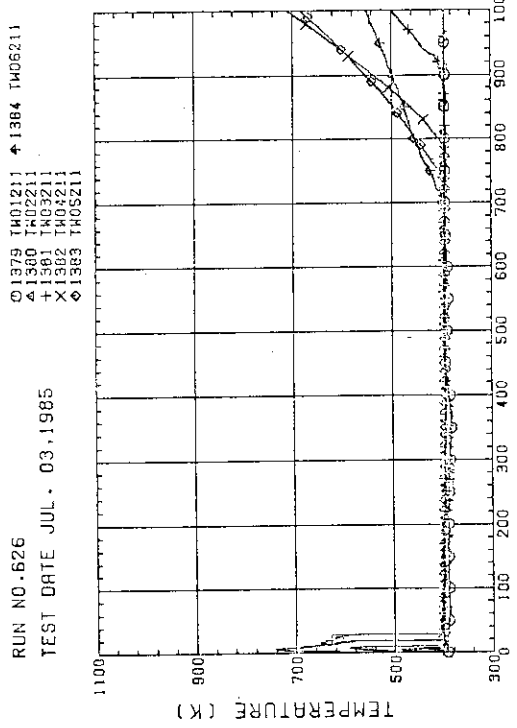
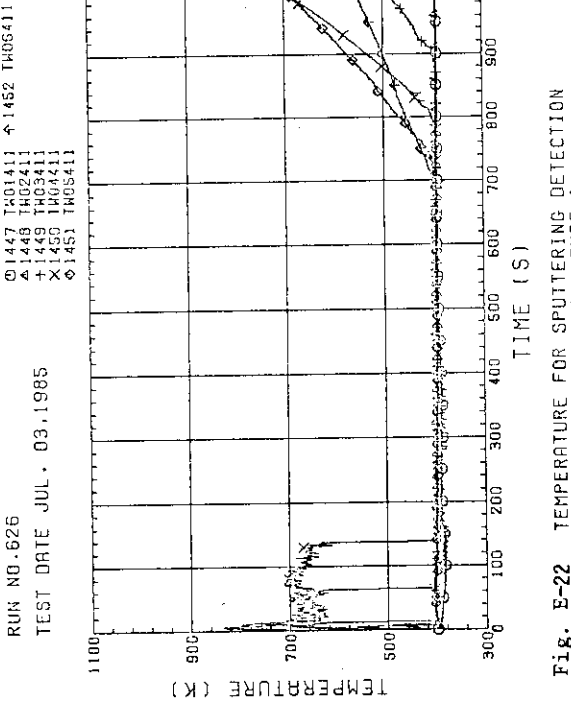
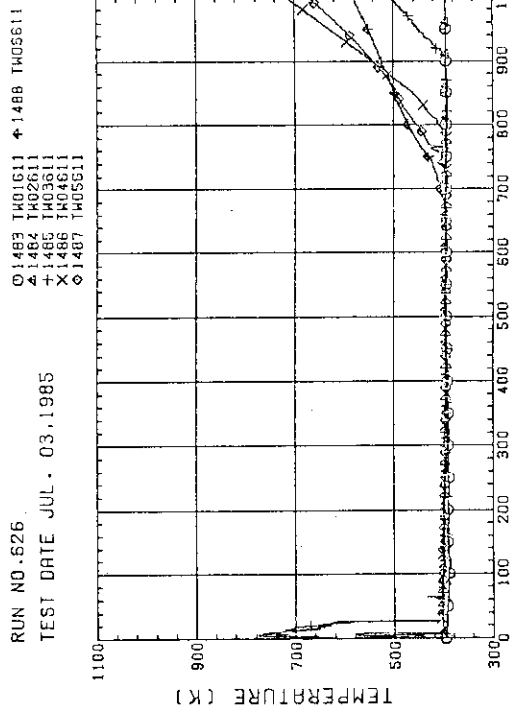
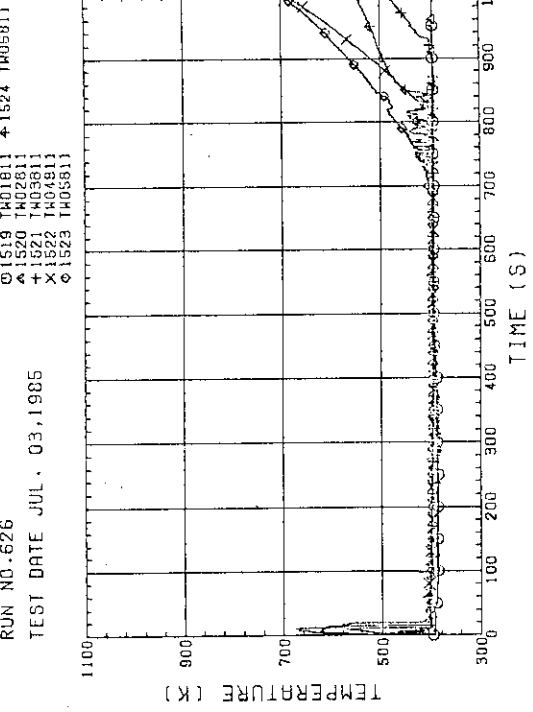
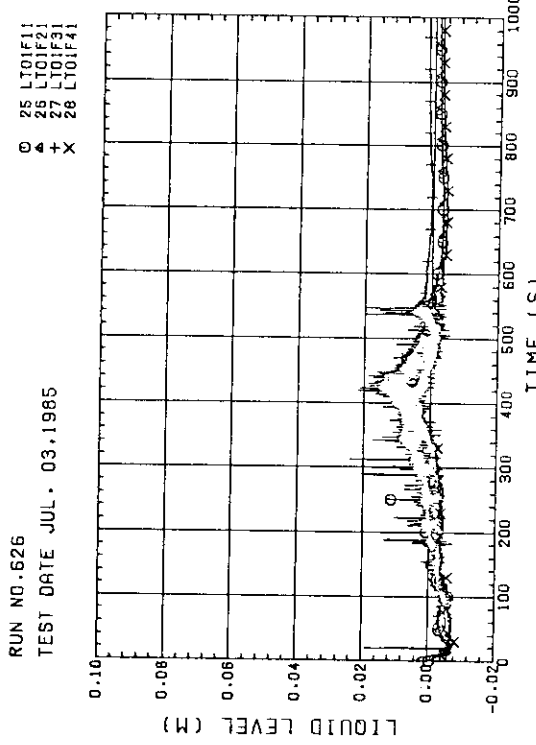
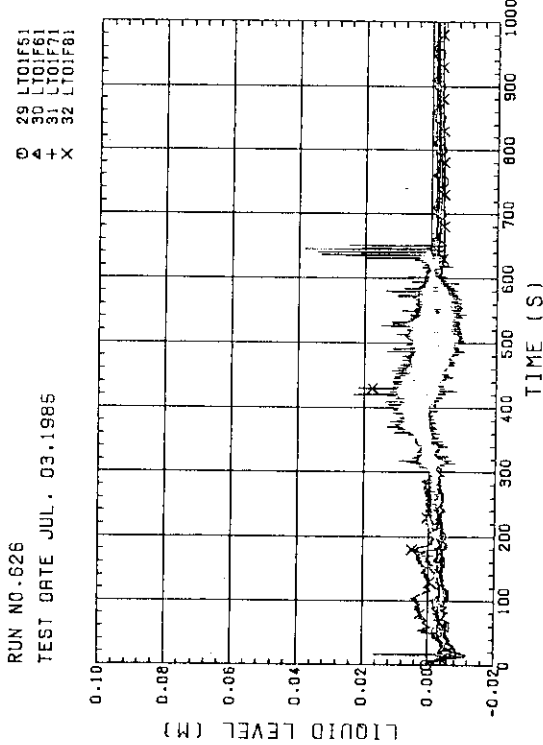
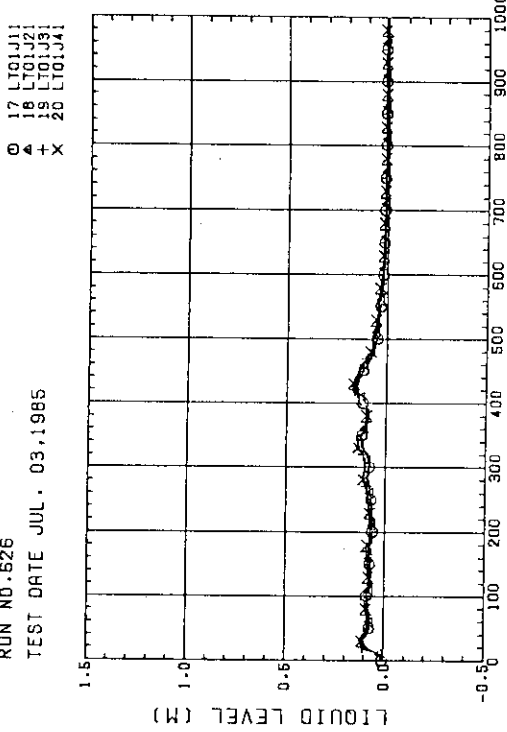
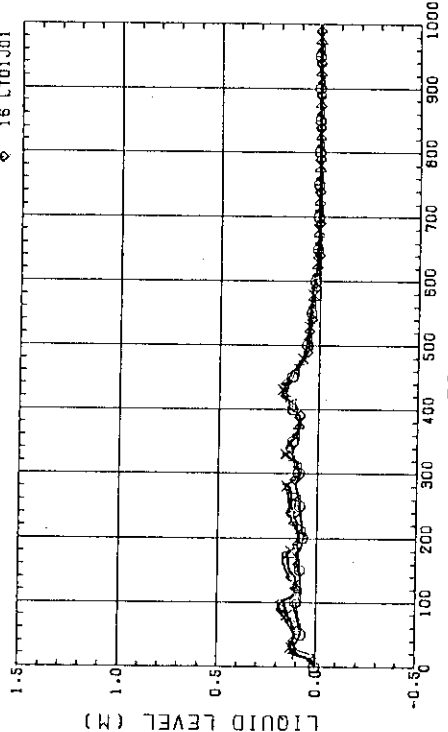


Fig. E-16 STEAM TEMPERATURE IN CORE, BUNDLE 8

Fig. E-17 FLUID TEMPERATURE JUST ABOVE END BOX TIE PLATE  
(BUNDLE 1,3,5,7, OPPOSITE SIDE OF COLD LEG, OUTER)Fig. E-18 FLUID TEMPERATURE JUST ABOVE END BOX TIE PLATE  
(BUNDLE 2,4,6,8, COLD LEG SIDE, INNER)Fig. E-19 FLUID TEMPERATURE AT CORE INLET  
(BUNDLE 1,2,3,4, 100MM BELOW HEATED PART)Fig. E-20 FLUID TEMPERATURE AT CORE INLET  
(BUNDLE 5,6,7,8, 100MM BELOW HEATED PART)

Fig. E-21 TEMPERATURE FOR SPUTTERING DETECTION  
BUNDLE 2 , REGION 1 , TYPE 1Fig. E-22 TEMPERATURE FOR SPUTTERING DETECTION  
BUNDLE 4 , REGION 1 , TYPE 1Fig. E-23 TEMPERATURE FOR SPUTTERING DETECTION  
BUNDLE 6 , REGION 1 , TYPE 1Fig. E-24 TEMPERATURE FOR SPUTTERING DETECTION  
BUNDLE 8 , REGION 1 , TYPE 1

Fig. E-25 LIQUID LEVEL ABOVE END BOX TIE PLATE  
(BUNDLE 1,2,3,4)Fig. E-26 LIQUID LEVEL ABOVE END BOX TIE PLATE  
(BUNDLE 5,6,7,8)Fig. E-27 LIQUID LEVEL ABOVE UCSP  
(BUNDLE 1,2,3,4)Fig. E-28 LIQUID LEVEL ABOVE UCSP  
(BUNDLE 5,6,7,8 AND CORE BAFFLE)

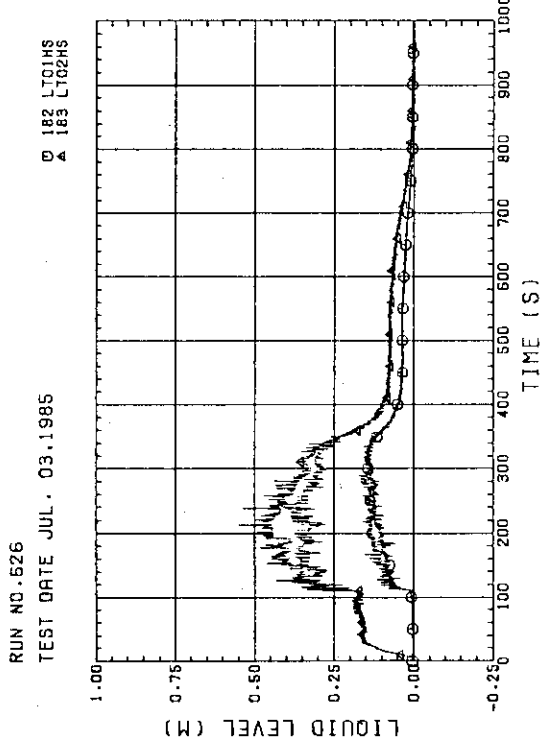


Fig. E-29 LIQUID LEVEL IN HOT LEG (LTO1HS - PV SIDE, LTO2HS - STEAM/WATER SEPARATOR SIDE)

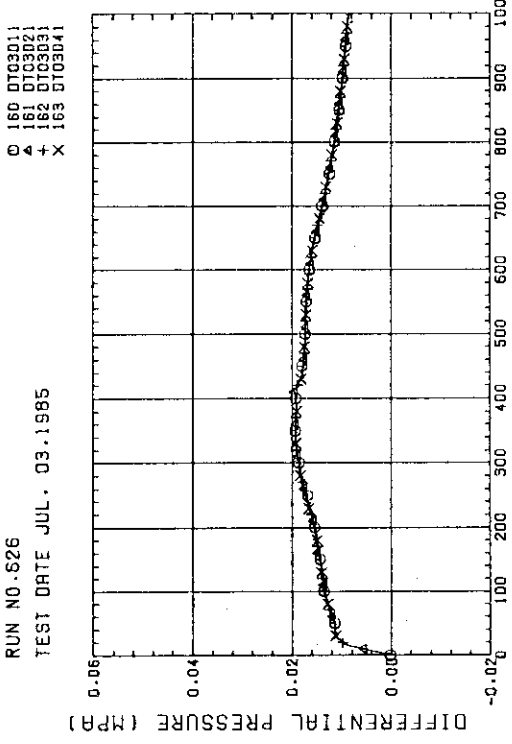


Fig. E-30 DIFFERENTIAL PRESSURE OF CORE FULL HEIGHT (BUNDLE 1,2,3,4)

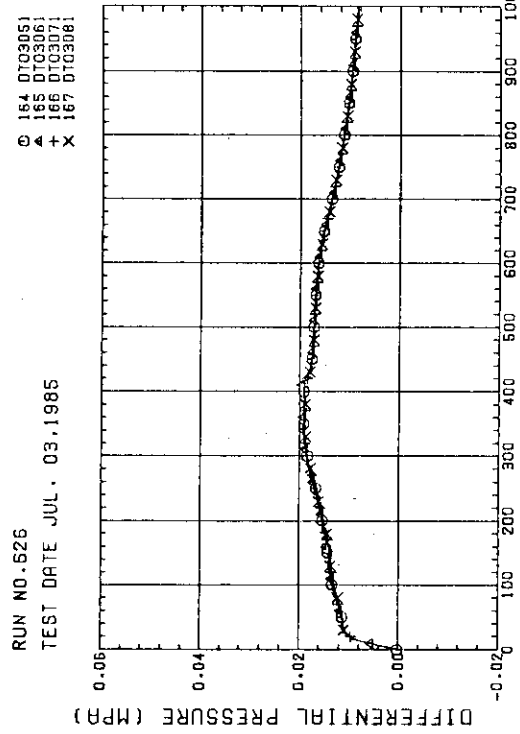


Fig. E-31 DIFFERENTIAL PRESSURE OF CORE FULL HEIGHT (BUNDLE 5,6,7,8)

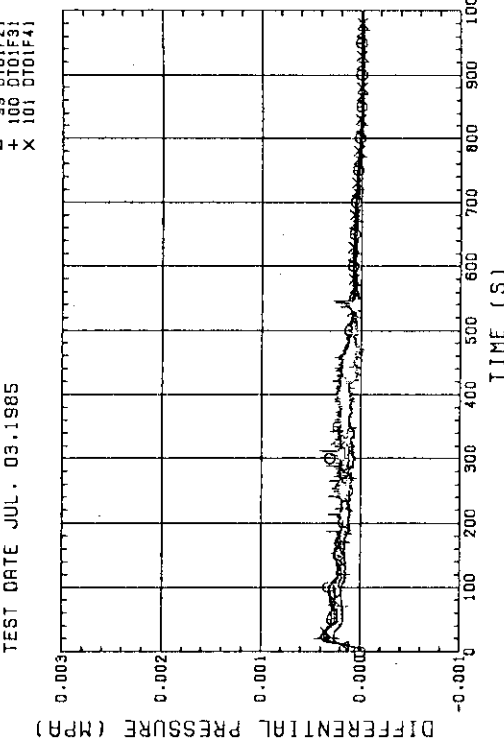


Fig. E-32 DIFFERENTIAL PRESSURE ACROSS END BOX TIE PLATE (BUNDLE 1,2,3,4)

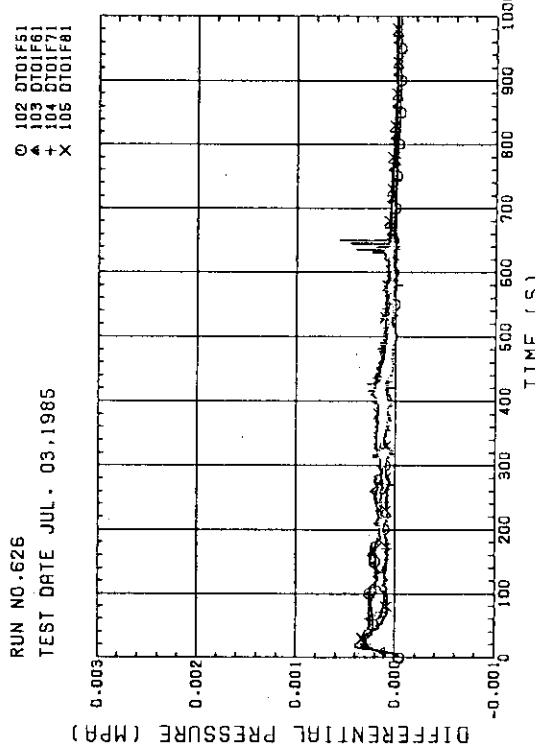


Fig. E-33 DIFFERENTIAL PRESSURE ACROSS END BOX TIE PLATE (BUNDLE 5, 6, 7, 8)

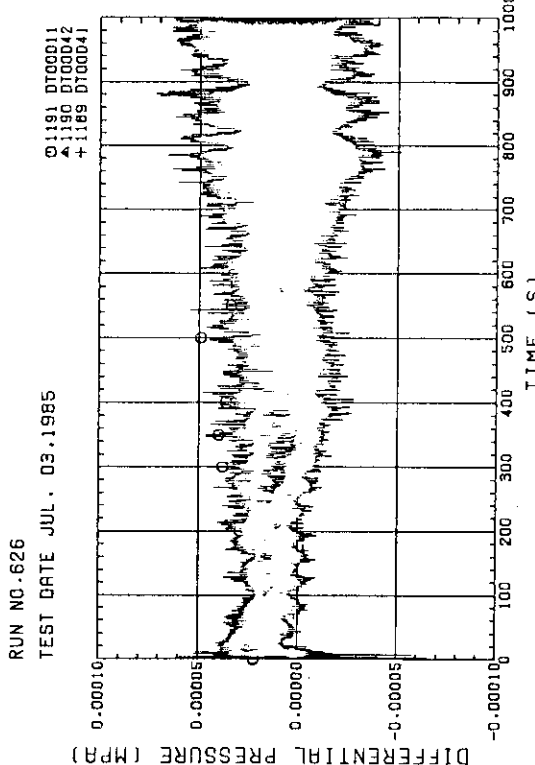


Fig. E-34 DIFFERENTIAL PRESSURE, HORIZONTAL RT -142 MM (11-BUNDLE 1-4, 42-BUNDLE 4-8, 41-BUNDLE 4-6)

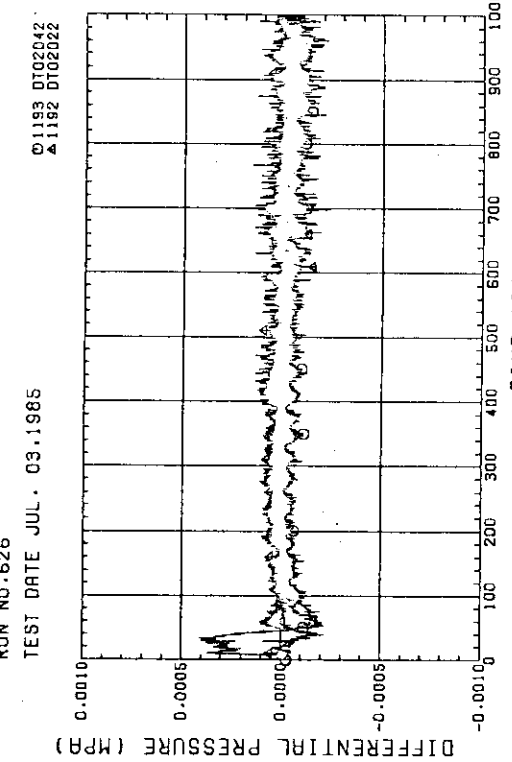


Fig. E-35 DIFFERENTIAL PRESSURE, HORIZONTAL AT 700 MM (42-BUNDLE 2-4, 22-BUNDLE 4-8)

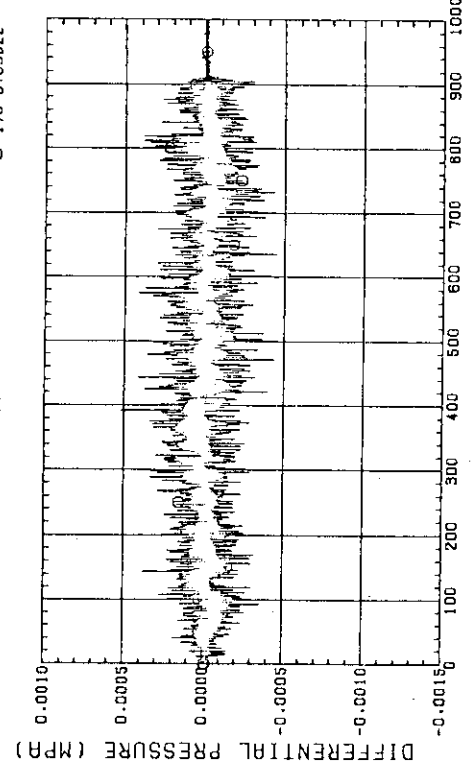


Fig. E-36 DIFFERENTIAL PRESSURE, HORIZONTAL AT 1365 MM (BUNDLE 2-4)

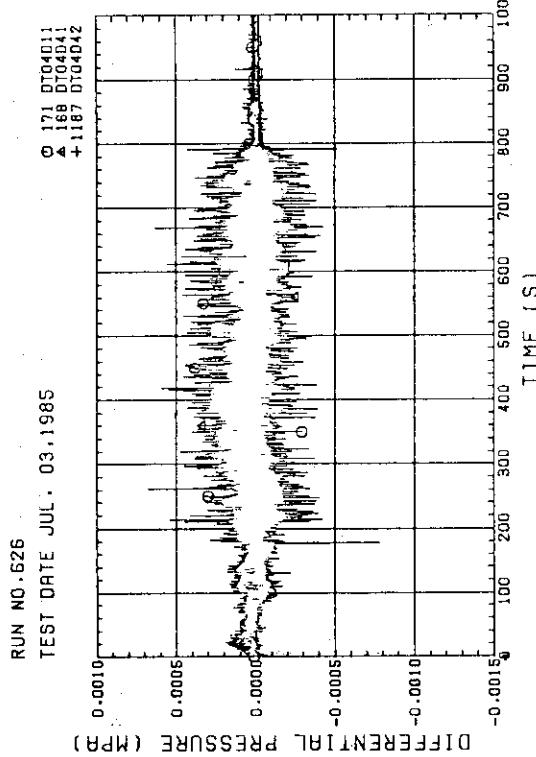


Fig. E-37 DIFFERENTIAL PRESSURE, HORIZONTAL AT 1905 MM  
(11-BUNDLE 1-4, 41-BUNDLE 4-6)

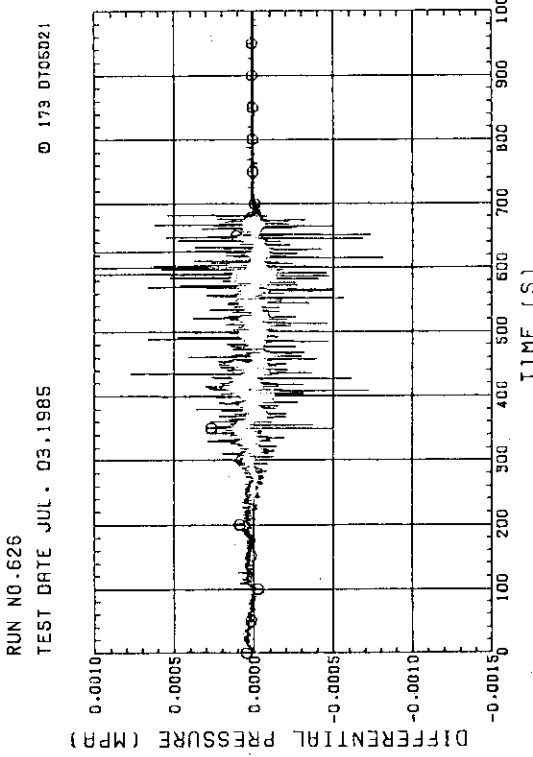


Fig. E-38 DIFFERENTIAL PRESSURE, HORIZONTAL AT 2570 MM  
(BUNDLE 2-4)

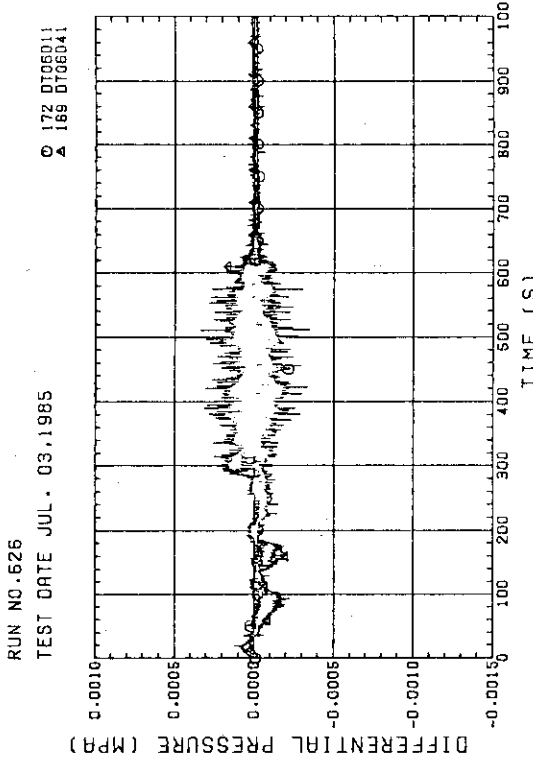


Fig. E-39 DIFFERENTIAL PRESSURE, HORIZONTAL AT 3235 MM  
(11-BUNDLE 1-4, 41-BUNDLE 4-8)

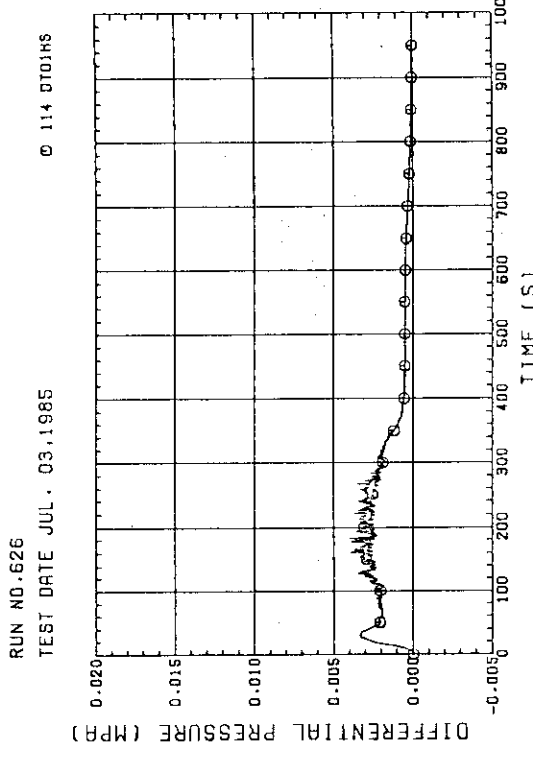


Fig. E-40 DIFFERENTIAL PRESSURE OF HOT LEG,  
HOT LEG INLET - STEAM/WATER SEPARATOR INLET

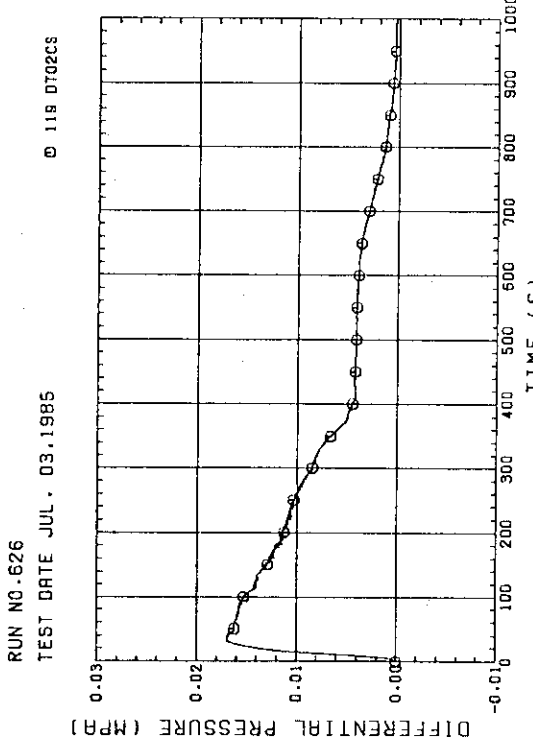
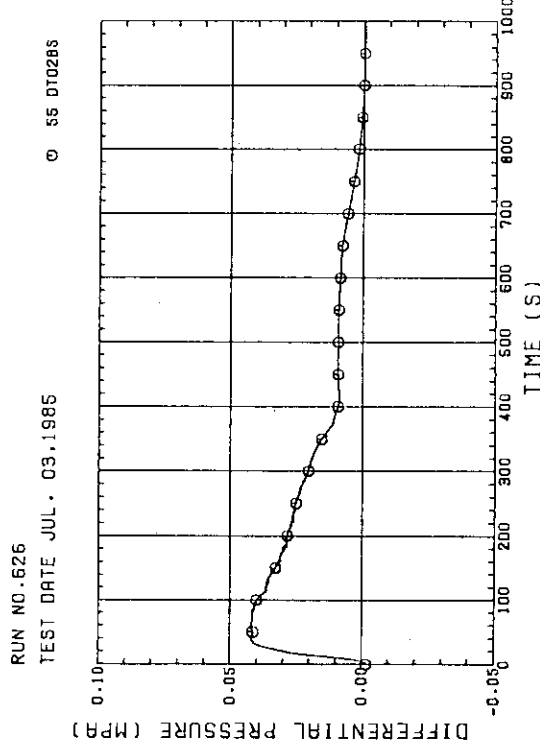
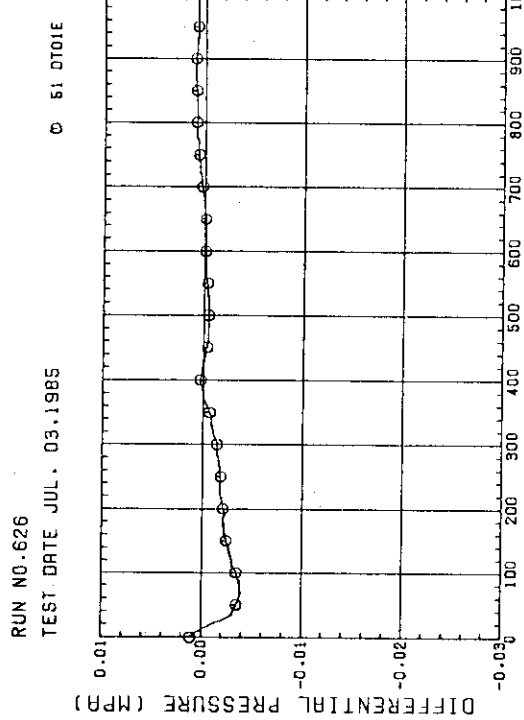
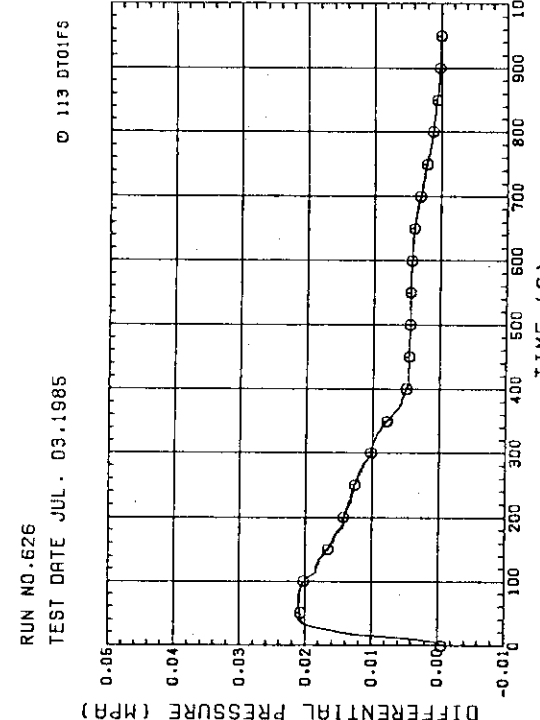


Fig. E-41 DIFFERENTIAL PRESSURE OF INTACT COLD LEG

Fig. E-42 DIFFERENTIAL PRESSURE OF STEAM/WATER SEPARATOR -  
CONTAINMENT TANK-IIFig. E-43 DIFFERENTIAL PRESSURE, CONTAINMENT TANK-II -  
CONTAINMENT TANK-IFig. E-44 DIFFERENTIAL PRESSURE OF BROKEN COLD LEG - PV SIDE -  
DOWNCOMER - CONTAINMENT TANK-II

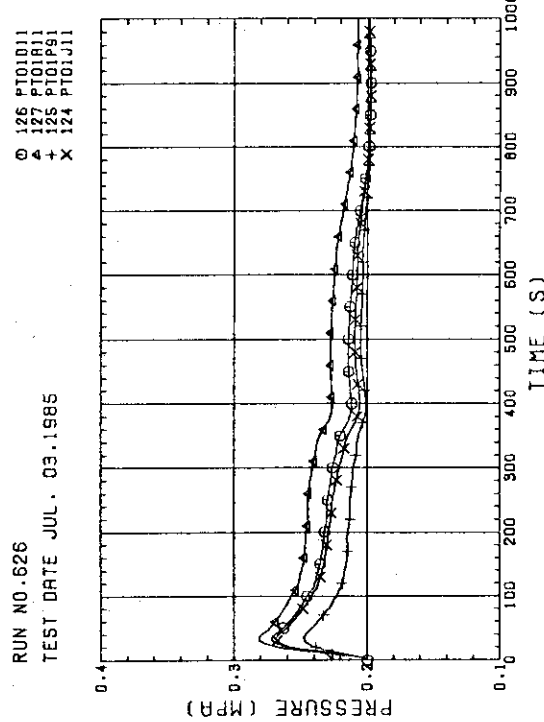


Fig. E-45 PRESSURE IN PV (J - TOP OF PV, D - CORE CENTER, A - CORE INLET, P - BELOW COLD LEG NOZZLE IN DOMINICER)

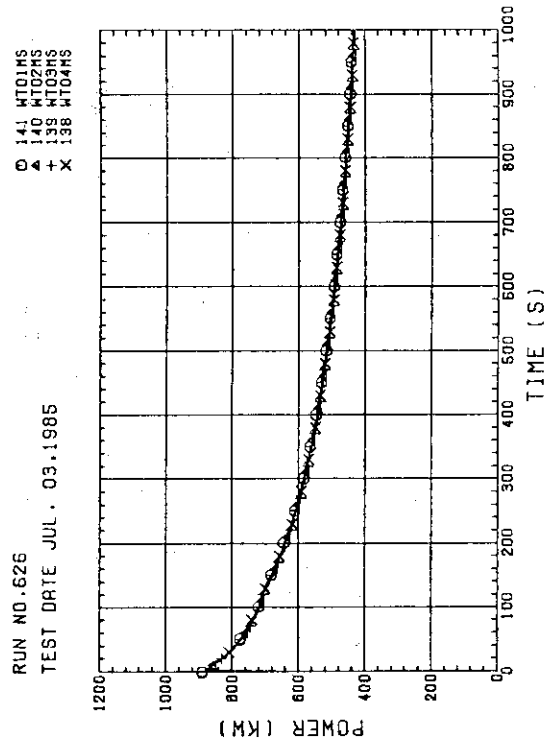


Fig. E-47 BUNDLE POWER (BUNDLE 1,2,3,4)

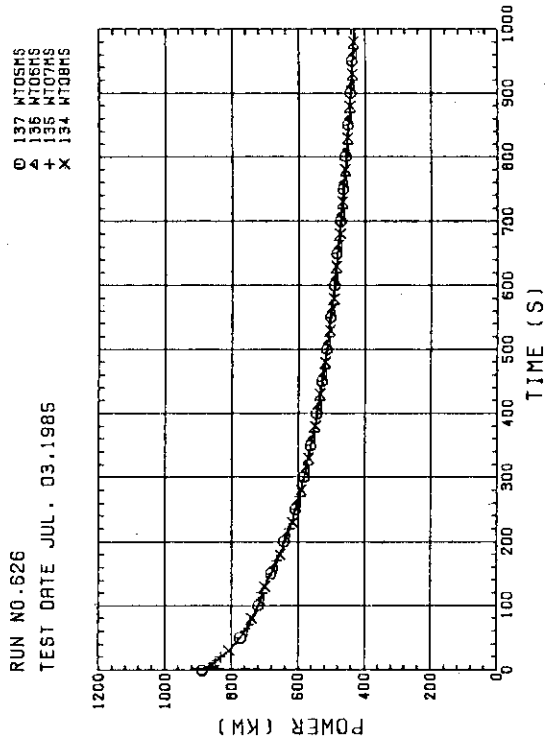


Fig. E-48 BUNDLE POWER (BUNDLE 5,6,7,8)

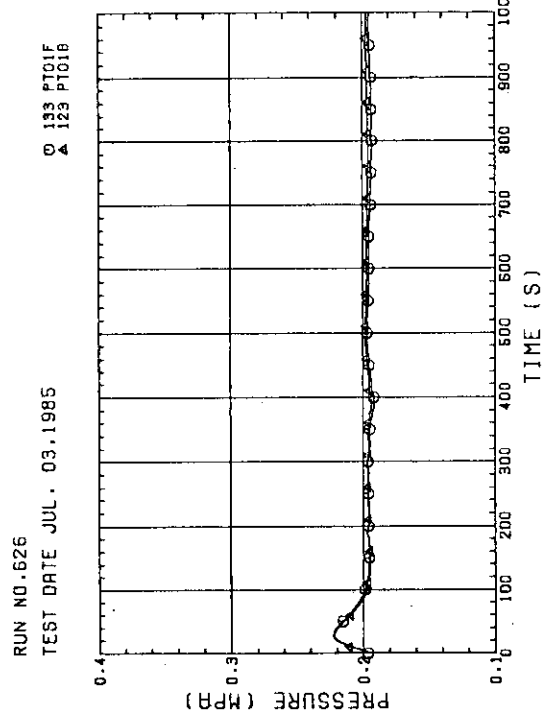
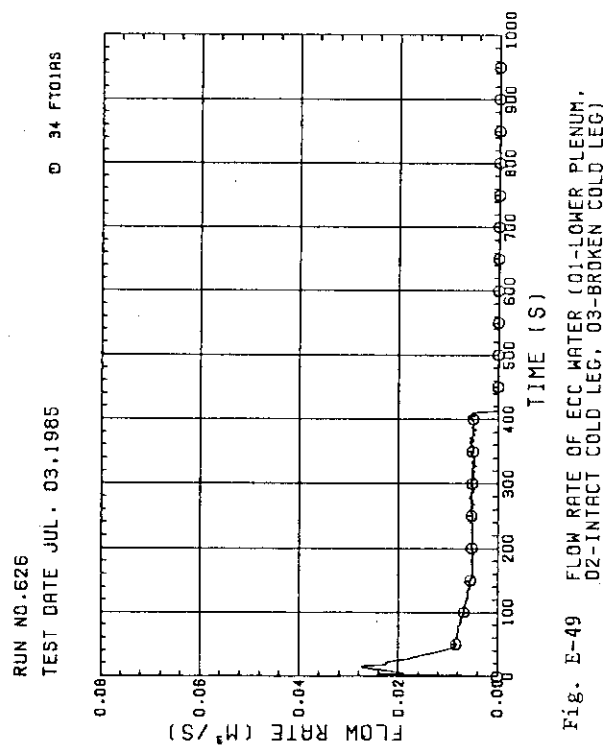


Fig. E-46 PRESSURE AT TOP OF CONTAINMENT TANK-I AND CONTAINMENT TANK-II (F - CONTAINMENT TANK-I, B - CONTAINMENT TANK-II)



Appendix F Comparison between TRAC Post-test Analysis and Test Data  
of Test S2-12

List of figures in Appendix F

Fig. F-1 - F-40	Heater rod temperatures
Fig. F-41 - F-64	Water temperatures in core
Fig. F-65 - F-72	Steam temperature in core
Fig. F-73 - F-76	Vertical differential pressures across core lower half
Fig. F-77 - F-80	Vertical differential pressures across core upper half
Fig. F-81 - F-84	Vertical differential pressures across core full height
Fig. F-85 - F-102	Void fractions in core
Fig. F-103	Liquid level in core baffle
Fig. F-104 - F-111	Liquid levels in upper plenum
Fig. F-112	Liquid level in lower plenum
Fig. F-113 - F-116	Pressures in pressure vessel
Fig. F-117 - F-120	Differential pressures in primary loops
Fig. F-121 - F-124	Mass flow rates in primary loops
Fig. F-125 - F-126	Pressures in containment tanks
Fig. F-127	Liquid level in S/W separator
Fig. F-128 - F-132	Horizontal differential pressures in core

TRAC-PF1 post-test analysis results obtained by the Los Alamos National Laboratory (LANL) based on the 2D/3D Agreement are compared with the test results of Test S2-12. For the comparison plots in this Appendix, the TRAC results are identified by circle symbols and the SCTF results by triangular symbols. Comments on the comparison results are presented as follows :

(1) Heater rod temperature (Figs. F-1 - F-40)

The heater rod temperatures predicted by TRAC qualitatively agree with the SCTF results except at the upper part of the core. TRAC tends to overpredict the turnaround temperature except at the upper part of the core in all bundles. The calculated quench time is also in good

agreement with the test data at almost all elevations except at the upper part of the core.

(2) Water temperatures in core (Figs. F-41 - F-64)

The water temperatures in the core predicted by TRAC exhibit the saturation temperature, while the measured temperatures are affected by the superheated steam temperatures except at the bottom of heated part. At the later period, the measured water temperatures agree with the calculated temperatures.

(3) Steam temperatures in core (Fig. F-65 - F-72)

The measured steam temperature sometimes shows much lower temperature than the calculated temperature as shown in Figs. E-66 and E-68 and the measured temperature decreases to the saturation temperature at much earlier time than the calculated temperature. These are due to the fact that the superheated steam probes used for the steam temperature measurement might be wetted by water droplets. Superheat data before the quench of the probes show almost reasonable agreement with the TRAC calculation as shown in Figs. F-65, F-67 and F-70.

(4) Vertical differential pressures in core (Figs. F-73 - F-84)

TRAC overpredicts the differential pressure across the lower half of the core and underpredicts the differential pressure across the upper half of the core. The calculated differential pressures across the core full height agree well with the test data except during the initial 40 s after the beginning of bottom reflood. During that period, TRAC underpredicts the differential pressure. In general, the calculated vertical differential pressures in the core show oscillatory behavior, whereas no significant oscillations are observed in the SCTF results.

(5) Void fractions in core (Figs. F-85 - F-102)

The calculated void fraction remains almost unity before the occurrence of quench and then decreases rapidly, while the measured void fraction gradually decreases with time from the beginning of reflood.

(6) Liquid level in core baffle (Fig. F-103)

The initial increasing of the liquid level in the core baffle is well predicted by TRAC. Thereafter, TRAC slightly overpredicts the liquid level.

(7) Liquid levels in upper plenum (Figs. F-104 - F-111)

TRAC underpredicts the liquid level in the upper plenum above all bundles. The measured liquid levels in the upper plenum begin to increase just after the beginning of reflood, while the predicted values

indicate no increases until about 300 s after the beginning of reflood.

(8) Liquid level in lower plenum (Fig. F-112)

The initial liquid level in the TRAC calculation is slightly lower than the measured initial value.

(9) Pressures in pressure vessel (Fig. F-113 - F-116)

TRAC slightly underestimates the pressures in the core, the upper plenum, the lower plenum and the downcomer during the initial 40 s after the beginning of reflood. At the later period, TRAC tends to overpredict the pressures.

(10) Differential pressures in primary loop (Fig. F-117 - F-120)

The differential pressure between the upper plenum and the steam/water separator predicted by TRAC is smaller than the SCTF result especially at the later period. The differential pressures between the steam/water separator and the downcomer and between the downcomer and the containment tank-I are overpredicted by TRAC except during the initial 30 s. The calculated differential pressure between the steam/water separator and the containment tank-II is much lower than the test result.

(11) Mass flow rate in primary loops (Fig. F-121 - F-124)

TRAC underpredicts the mass flow rate in the hot leg. The mass flow rates in the intact cold leg and in the broken cold legs are overpredicted by TRAC except during the initial 30 s.

(12) Pressures in containment tanks (Figs. F-125 and F-126)

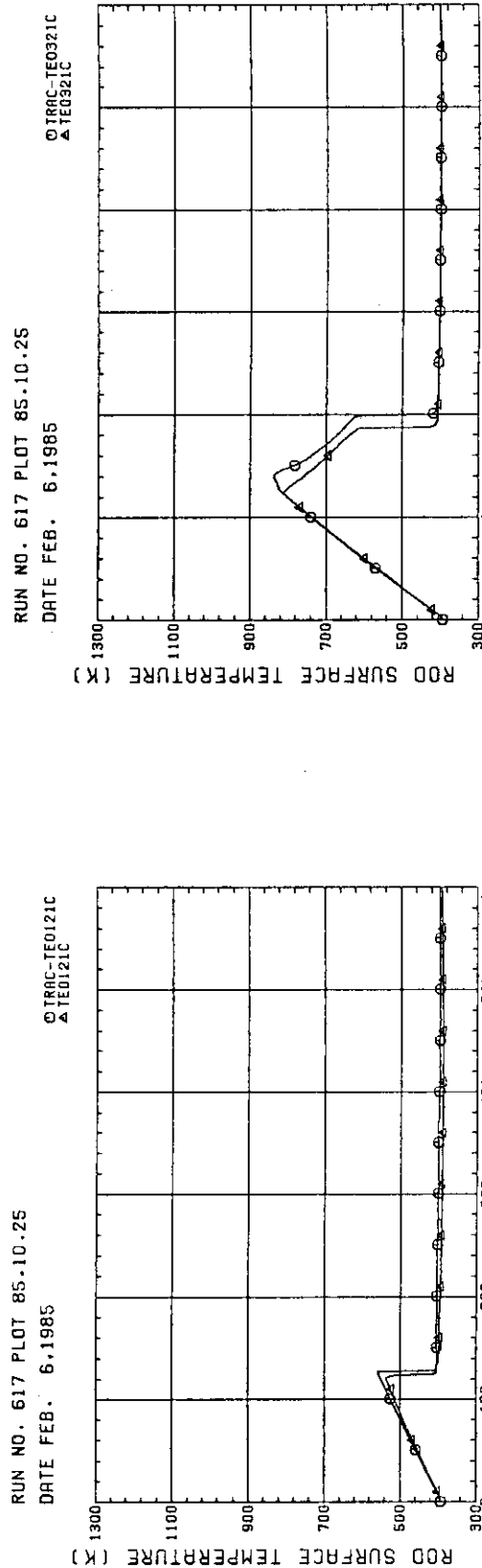
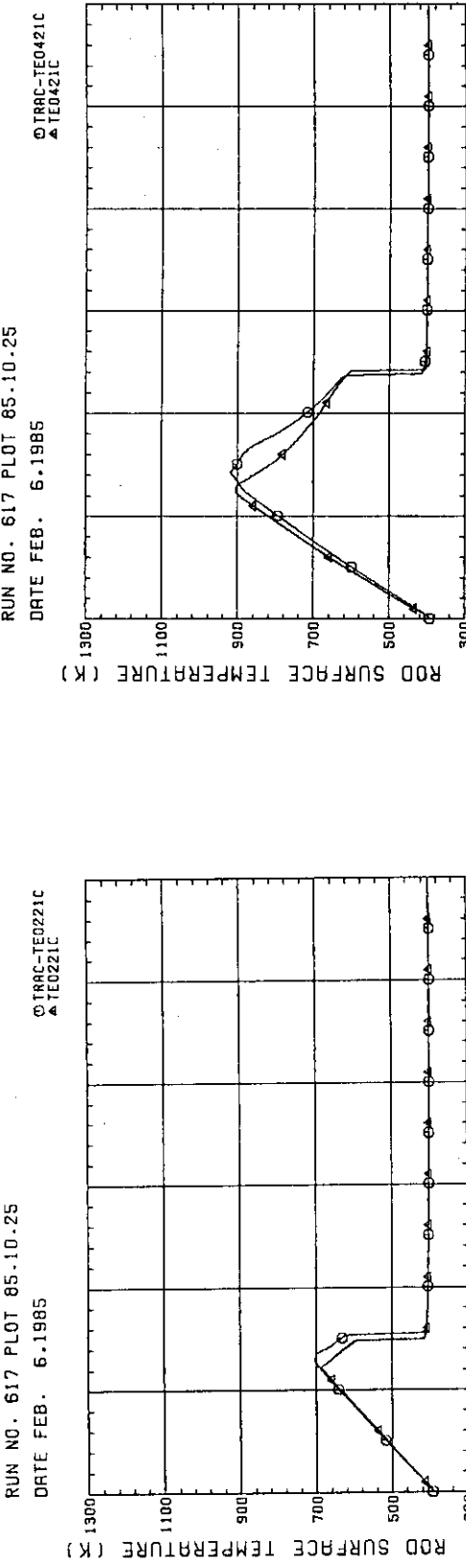
Since the measured pressure transients in the containment tank-I were used in the TRAC analysis as the boundary condition, the TRAC and SCTF results agree well with each other.

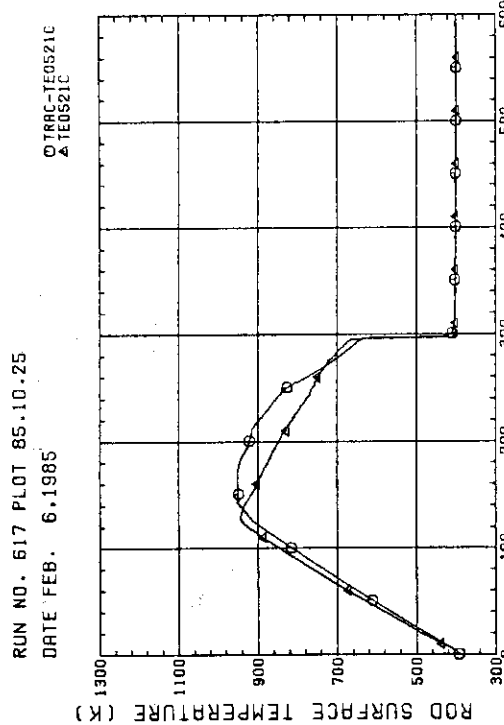
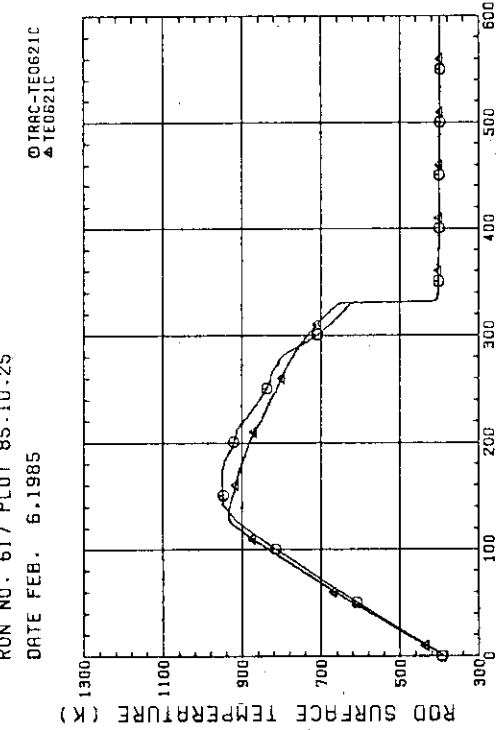
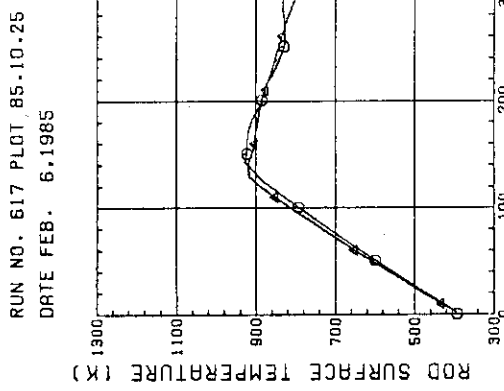
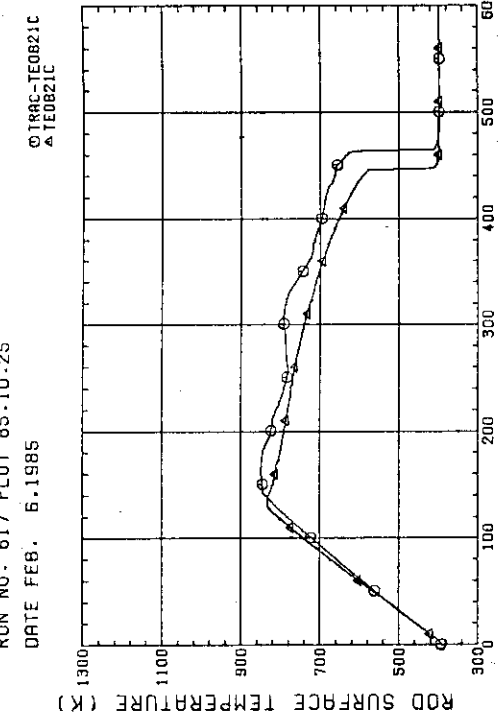
(13) Liquid level in steam/water separator (Fig. F-127)

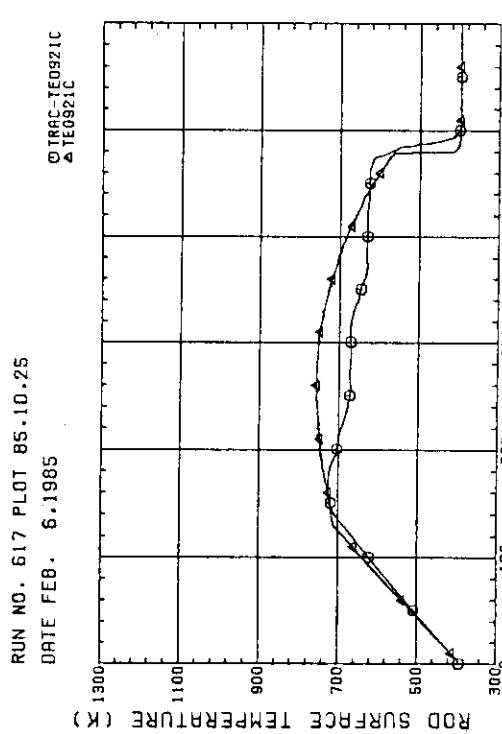
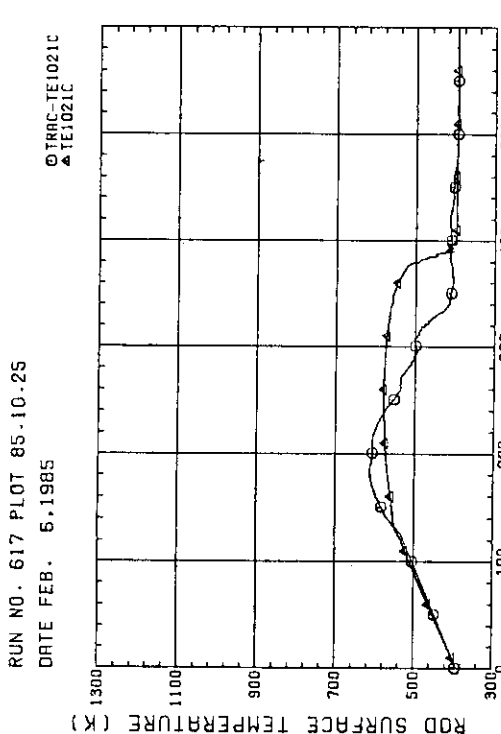
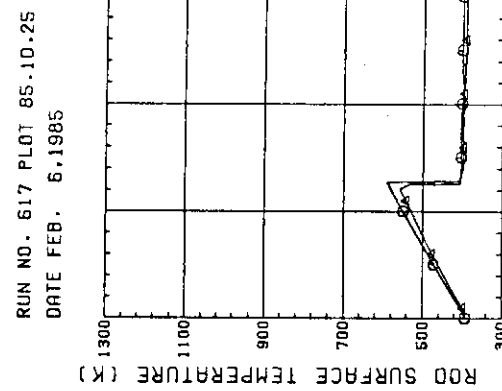
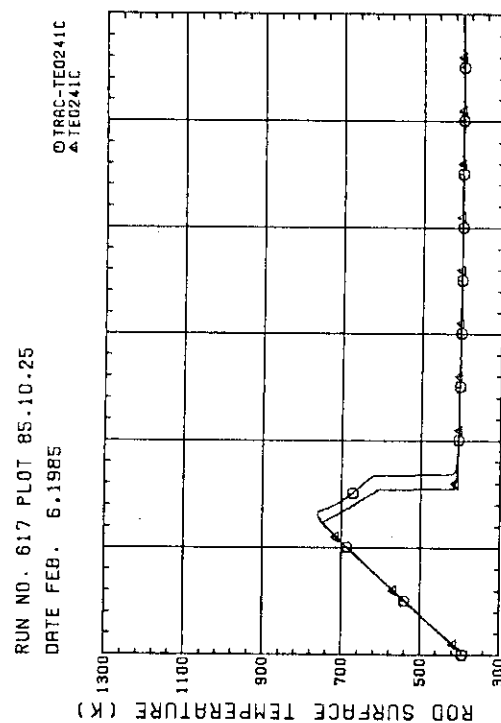
The increasing rate of the liquid level in the steam/water separator is underpredicted by TRAC.

(14) Horizontal differential pressures in core (Figs. F-128 - F-132)

Both the measured and calculated horizontal differential pressures between bundles 4 and 6 and between bundles 4 and 8 at elevation of 1.905 m show positive value. However, the TRAC results indicate negative differential pressure between bundles 1 and 4 at 1.905 m and between bundles 2 and 4 at 2.57 m, while the corresponding test results show approximately zero differential pressures.

Fig. F-1 HEATER ROD TEMPERATURE  
(BUNDLE 2 H=1827MM)Fig. F-2 HEATER ROD TEMPERATURE  
(BUNDLE 2 H=2237MM)Fig. F-3 HEATER ROD TEMPERATURE  
(BUNDLE 2 H=2667MM)Fig. F-4 HEATER ROD TEMPERATURE  
(BUNDLE 2 H=3097MM)

Fig. F-5 HEATER ROD TEMPERATURE  
(BUNDLE 2 H=3452MM)Fig. F-6 HEATER ROD TEMPERATURE  
(BUNDLE 2 H=3622MM)Fig. F-7 HEATER ROD TEMPERATURE  
(BUNDLE 2 H=4047MM)Fig. F-8 HEATER ROD TEMPERATURE  
(BUNDLE 2 H=4477MM)

Fig. F-9 HEATER ROD TEMPERATURE  
(BUNDLE 2 H=4907MM)Fig. F-10 HEATER ROD TEMPERATURE  
(BUNDLE 2 H=5337MM)Fig. F-11 HEATER ROD TEMPERATURE  
(BUNDLE 4 H=1827MM)Fig. F-12 HEATER ROD TEMPERATURE  
(BUNDLE 4 H=2237MM)

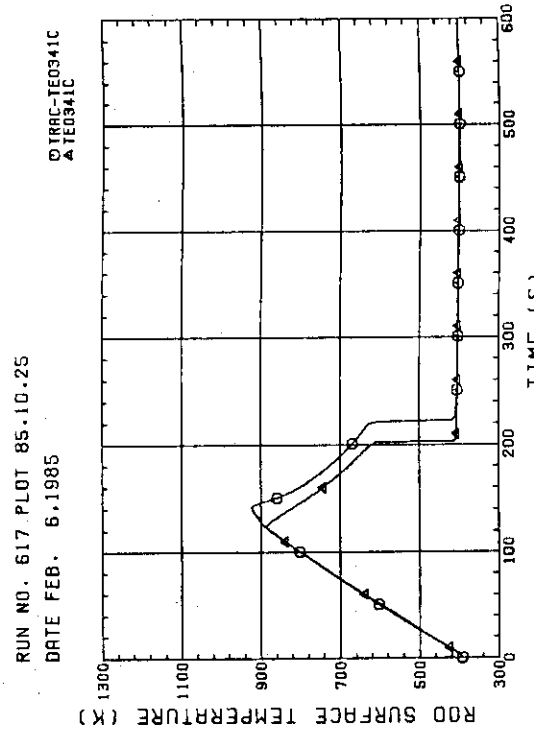


Fig. F-13 HEATER ROD TEMPERATURE (BUNDLE 4 H=2667MM)

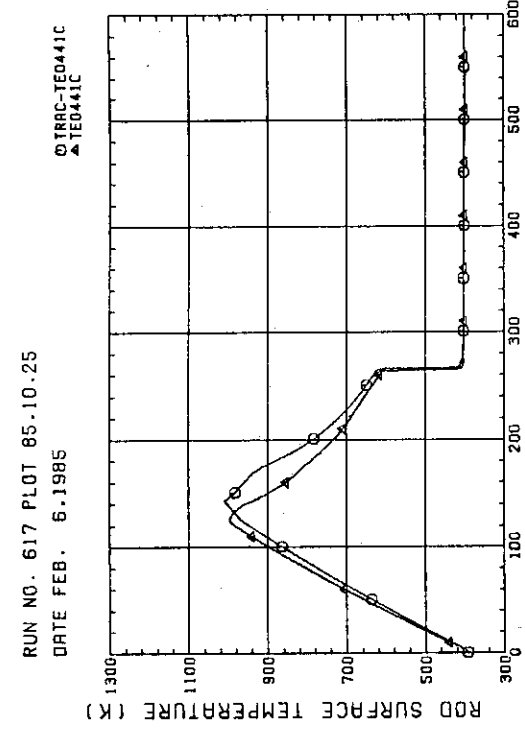


Fig. F-14 HEATER ROD TEMPERATURE (BUNDLE 4 H=3097MM)

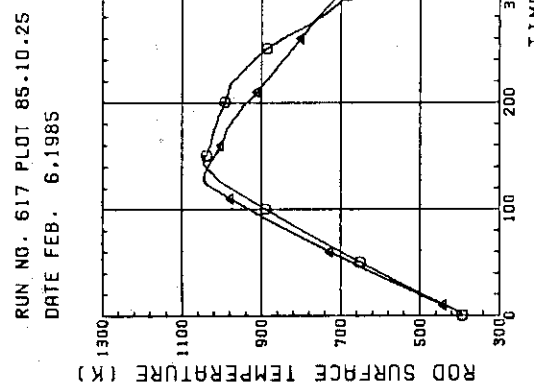


Fig. F-15 HEATER ROD TEMPERATURE (BUNDLE 4 H=3452MM)

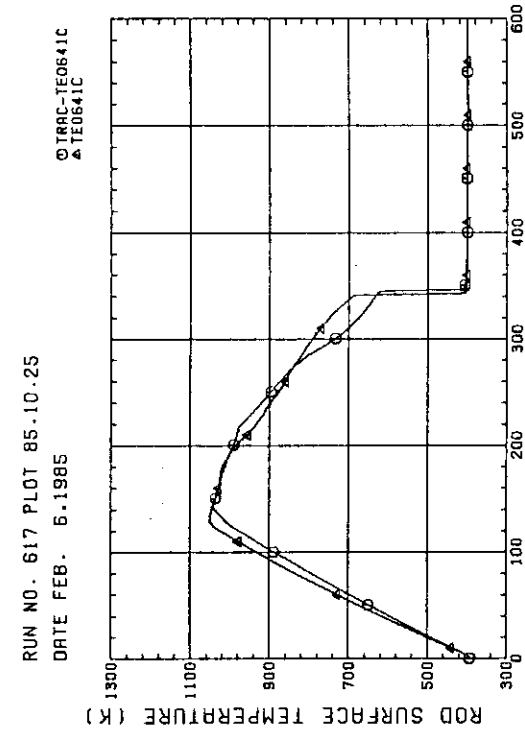


Fig. F-16 HEATER ROD TEMPERATURE (BUNDLE 4 H=3622MM)

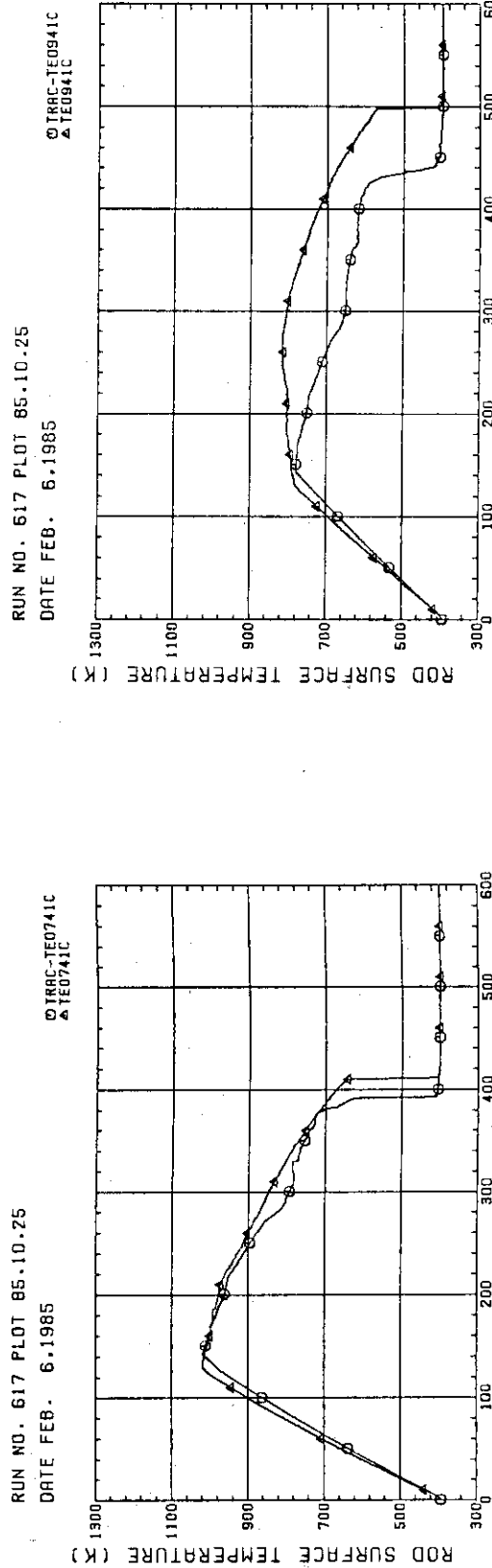


Fig. F-17 HEATER ROD TEMPERATURE  
(BUNDLE 4 H=4047MM)

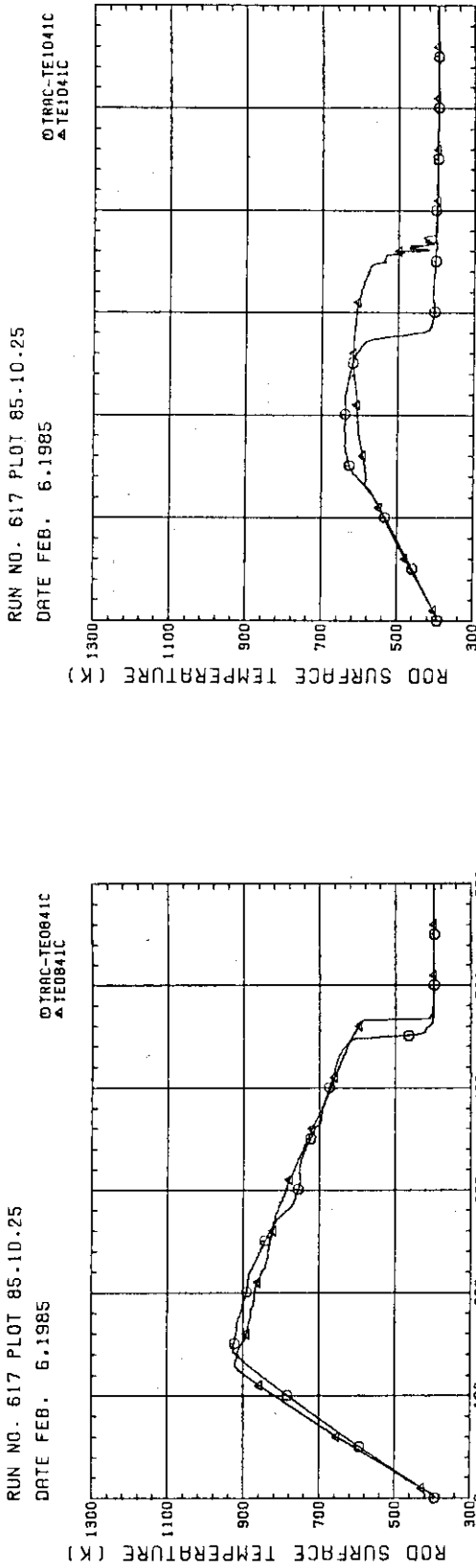


Fig. F-18 HEATER ROD TEMPERATURE  
(BUNDLE 4 H=4477MM)

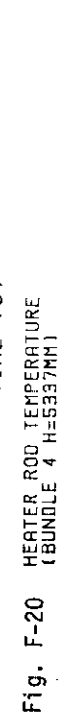


Fig. F-19 HEATER ROD TEMPERATURE  
(BUNDLE 4 H=4907MM)

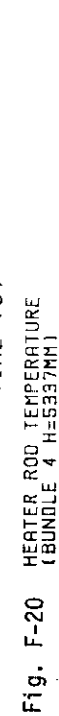
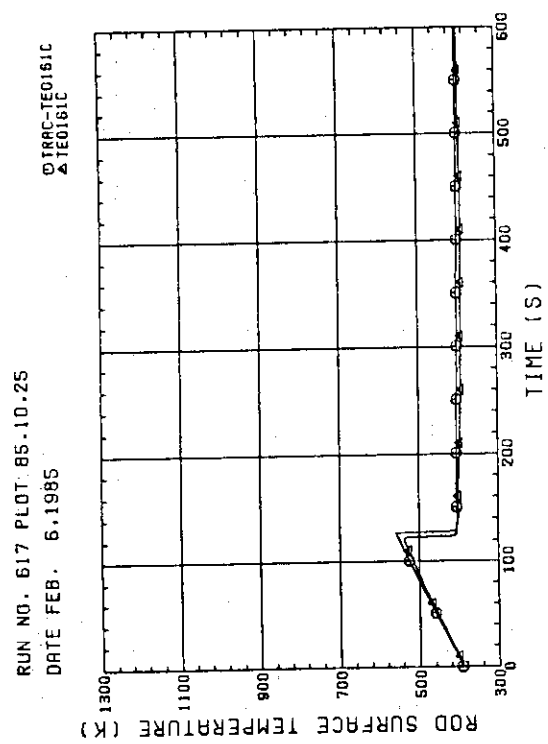
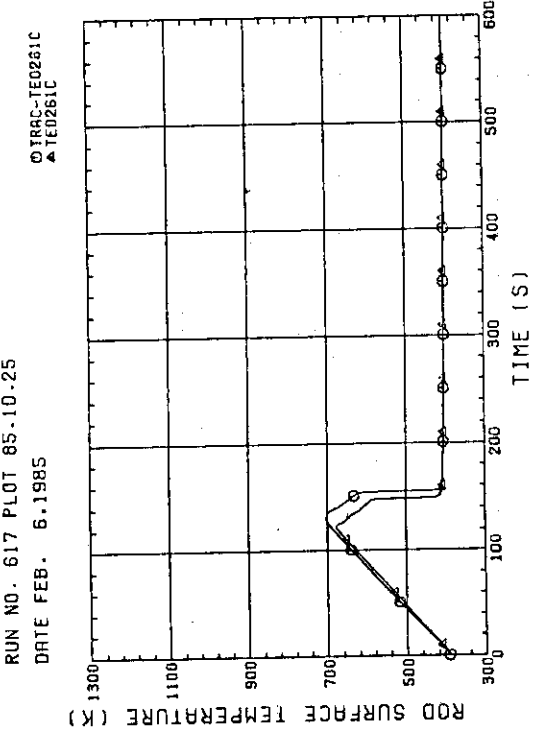
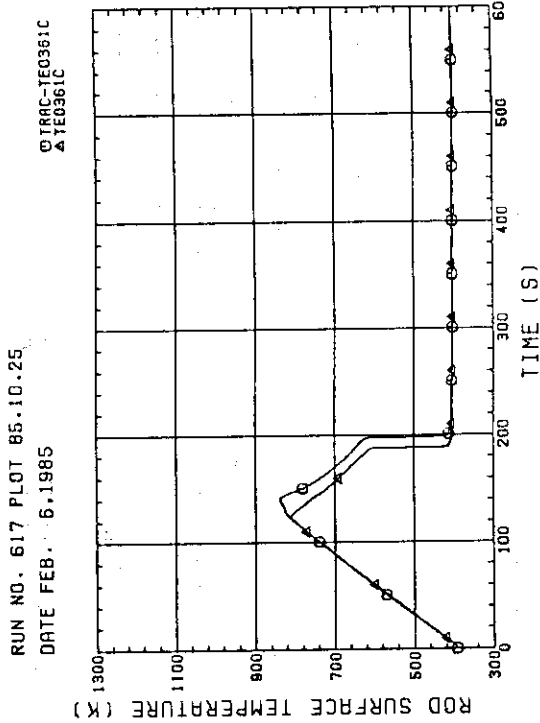
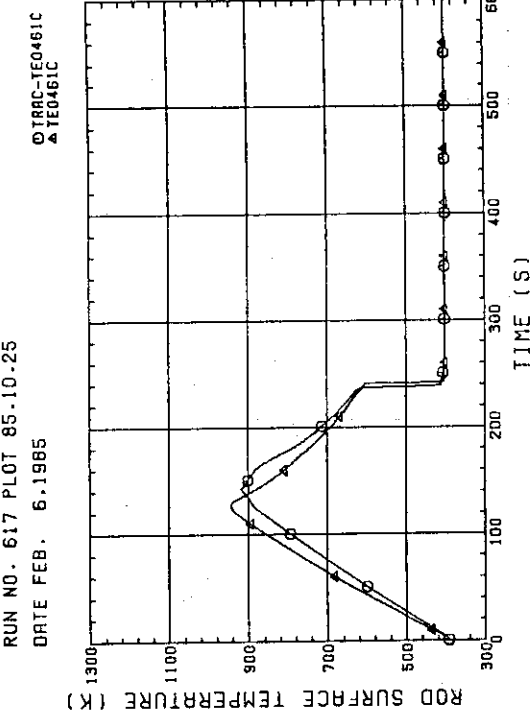


Fig. F-20 HEATER ROD TEMPERATURE  
(BUNDLE 4 H=5337MM)

Fig. F-21 HEATER ROD TEMPERATURE  
(BUNDLE 6 H=1827MM)Fig. F-22 HEATER ROD TEMPERATURE  
(BUNDLE 6 H=2237MM)Fig. F-23 HEATER ROD TEMPERATURE  
(BUNDLE 6 H=2667MM)Fig. F-24 HEATER ROD TEMPERATURE  
(BUNDLE 6 H=3097MM)

RUN NO. 617 PLOT 85.10.25  
DATE FEB. 6.1985

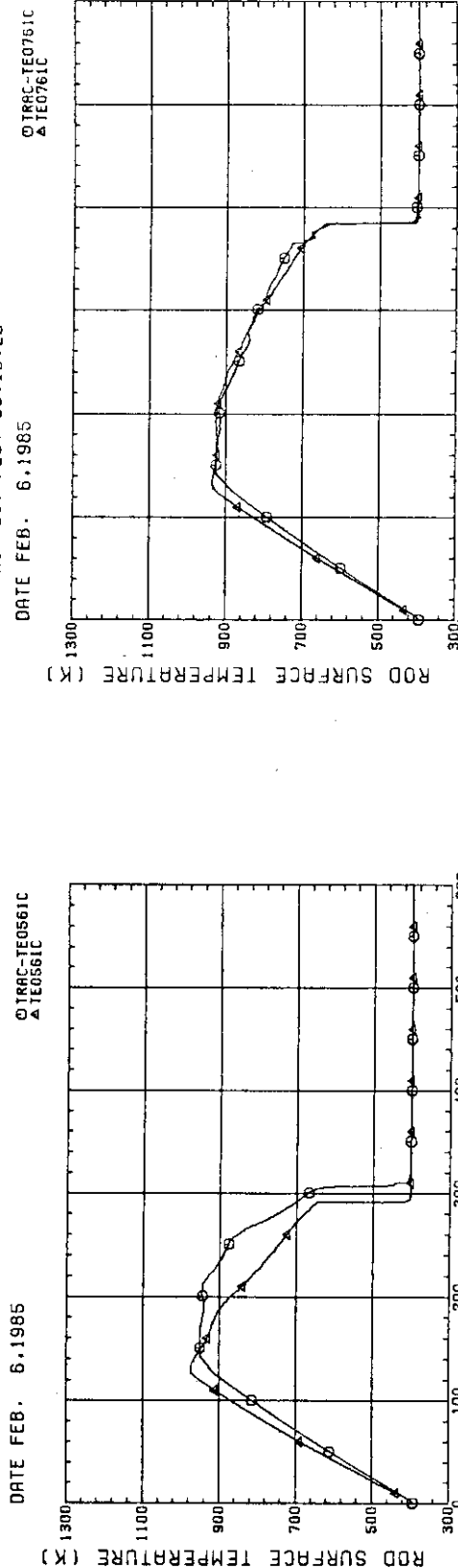


Fig. F-25 HEATER ROD TEMPERATURE  
(BUNDLE 6 H=3452MM)

RUN NO. 617 PLOT 85.10.25  
DATE FEB. 6.1985

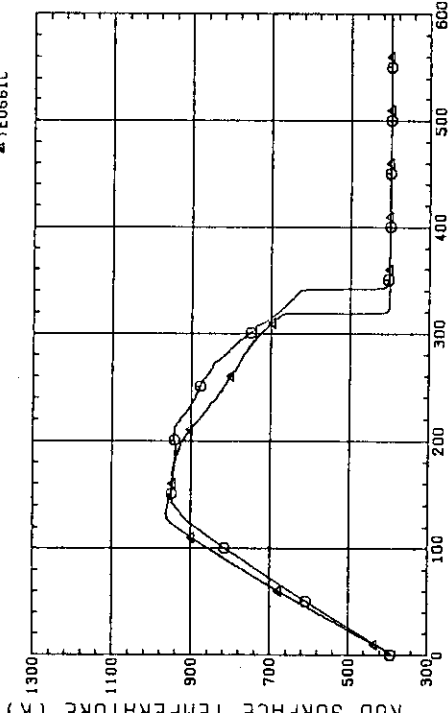


Fig. F-26 HEATER ROD TEMPERATURE  
(BUNDLE 6 H=3622MM)

RUN NO. 617 PLOT 85.10.25  
DATE FEB. 6.1985

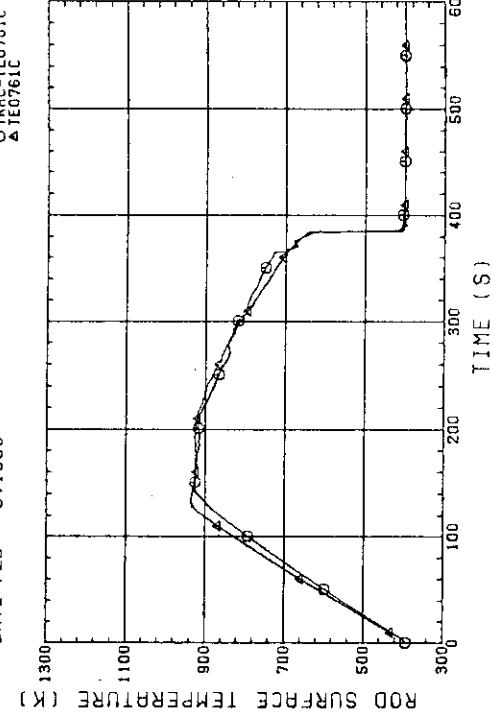


Fig. F-27 HEATER ROD TEMPERATURE  
(BUNDLE 6 H=4047MM)

RUN NO. 617 PLOT 85.10.25  
DATE FEB. 6.1985

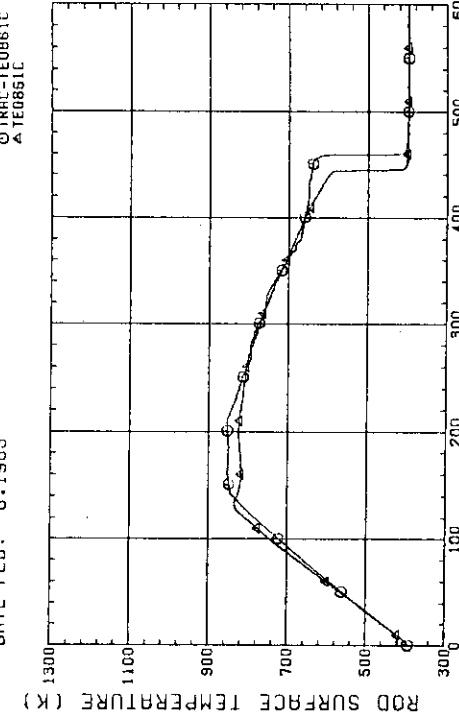
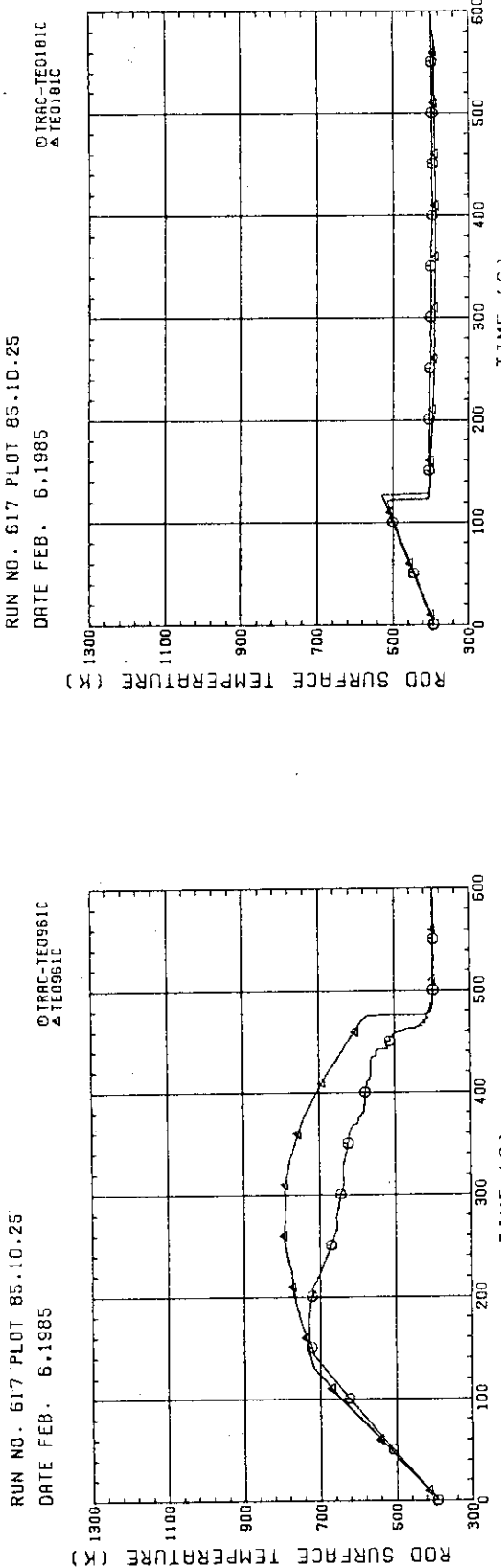
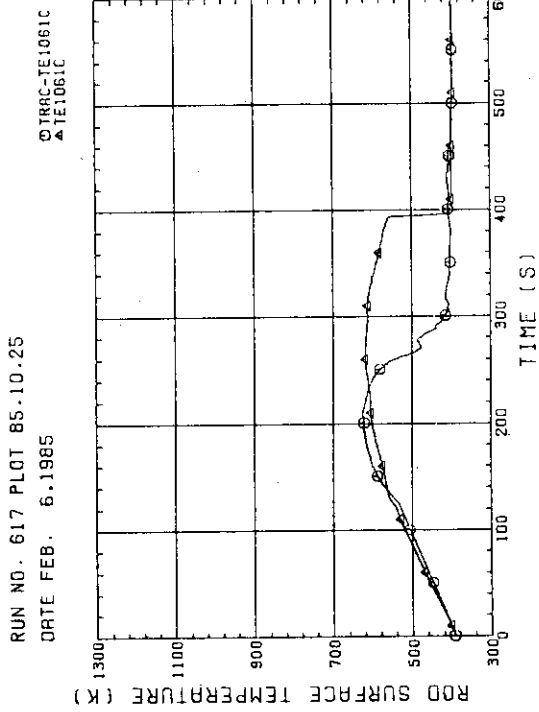
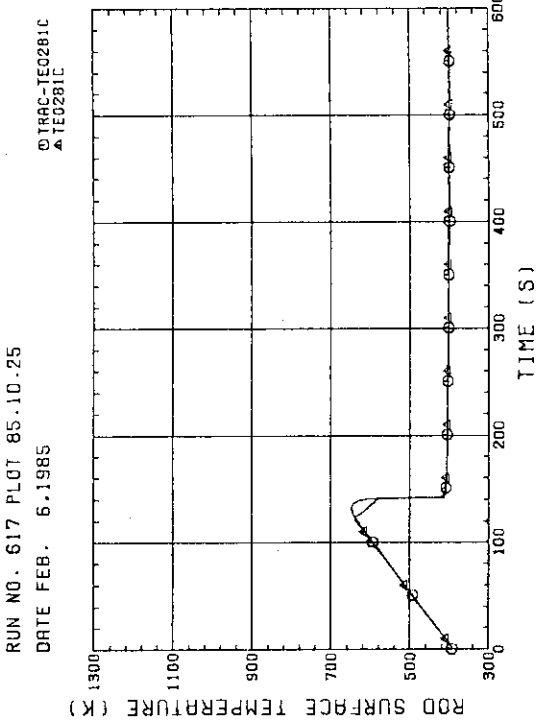
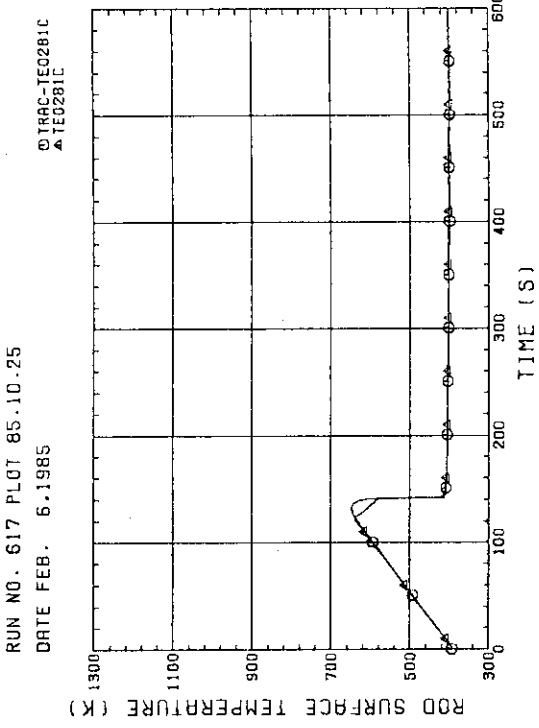


Fig. F-28 HEATER ROD TEMPERATURE  
(BUNDLE 6 H=4477MM)

Fig. F-29 HEATER ROD TEMPERATURE  
(BUNDLE 6 H=4907mm)Fig. F-30 HEATER ROD TEMPERATURE  
(BUNDLE 6 H=5337mm)Fig. F-31 HEATER ROD TEMPERATURE  
(BUNDLE 8 H=1827mm)Fig. F-32 HEATER ROD TEMPERATURE  
(BUNDLE 8 H=2237mm)

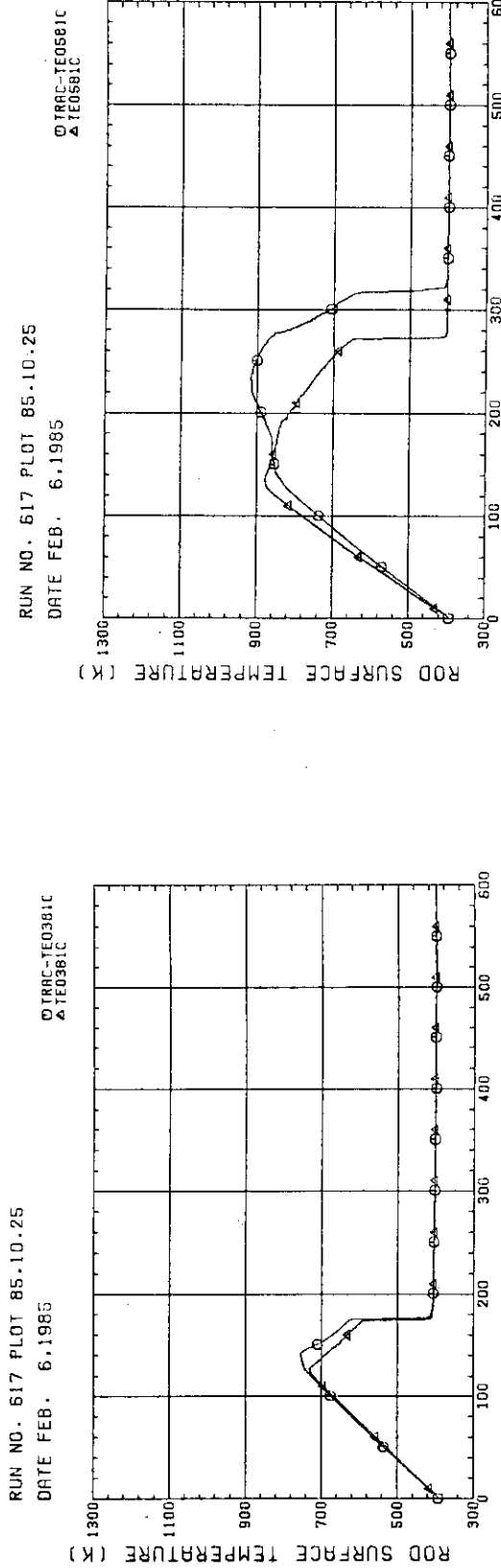


Fig. F-33 HEATER ROD TEMPERATURE (BUNDLE 8 H=266.7MM)

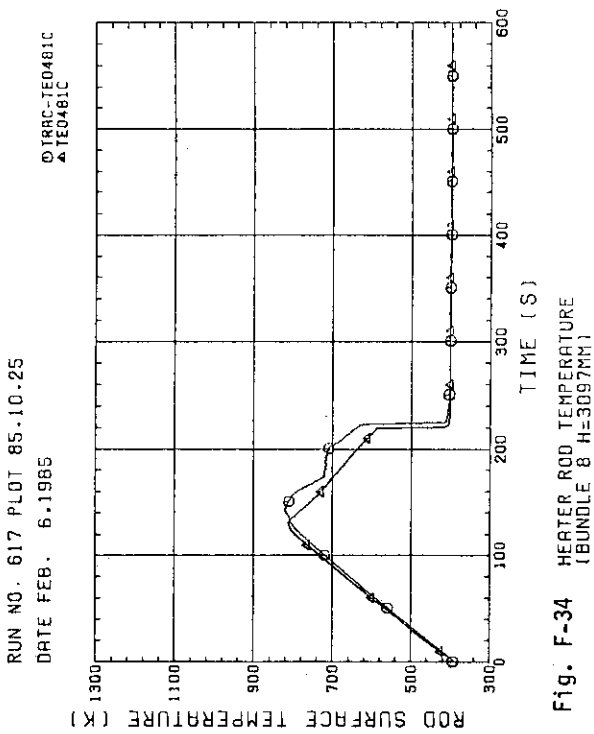


Fig. F-34 HEATER ROD TEMPERATURE (BUNDLE 8 H=309.7MM)

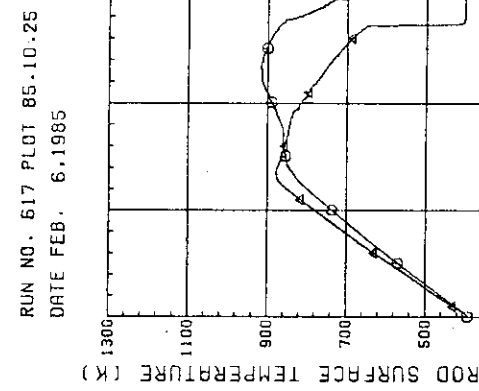


Fig. F-35 HEATER ROD TEMPERATURE (BUNDLE 8 H=345.2MM)

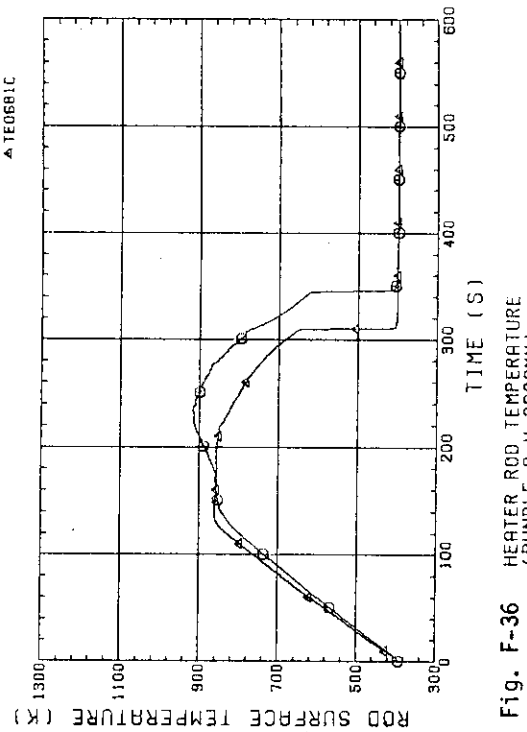


Fig. F-36 HEATER ROD TEMPERATURE (BUNDLE 8 H=362.0MM)

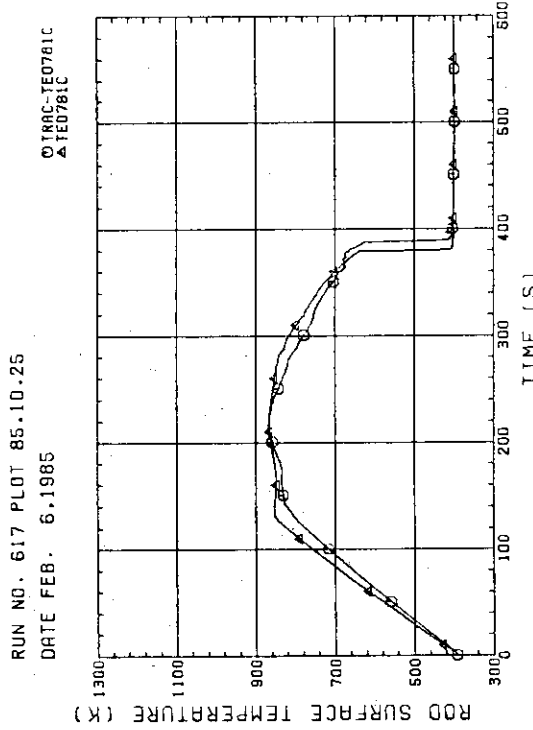


Fig. F-37 HEATER ROD TEMPERATURE  
(BUNDLE 8 H=404.7MM)

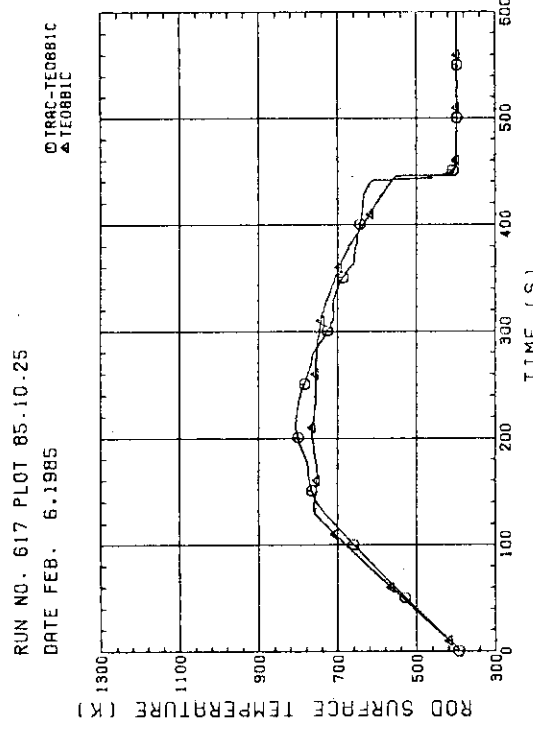


Fig. F-38 HEATER ROD TEMPERATURE  
(BUNDLE 8 H=533.3MM)

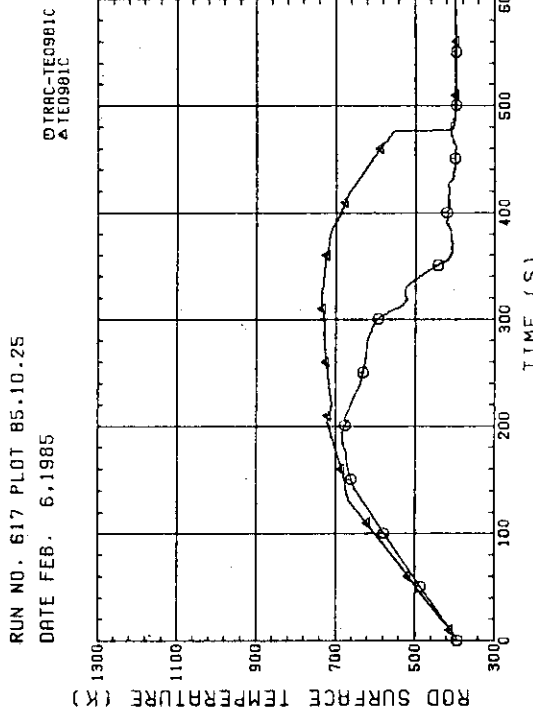


Fig. F-39 HEATER ROD TEMPERATURE  
(BUNDLE 8 H=507.7MM)

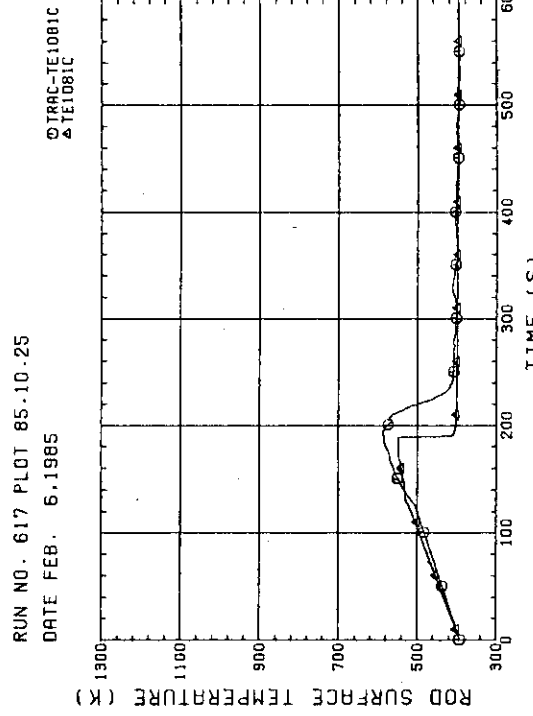


Fig. F-40 HEATER ROD TEMPERATURE  
(BUNDLE 8 H=447.7MM)

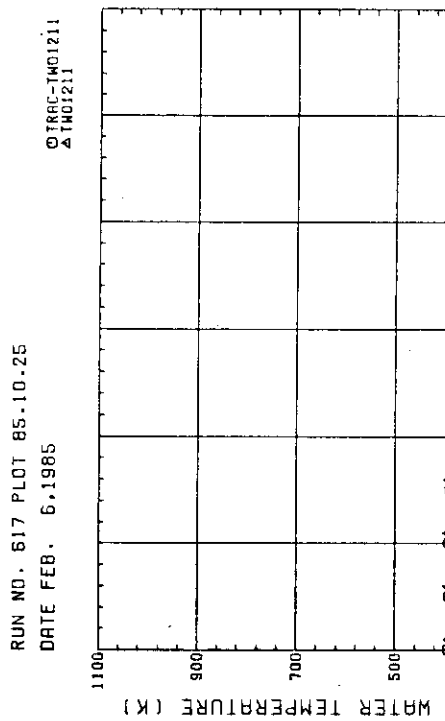


Fig. F-41 WATER TEMPERATURE (BUNDLE 2 H= 0mm)

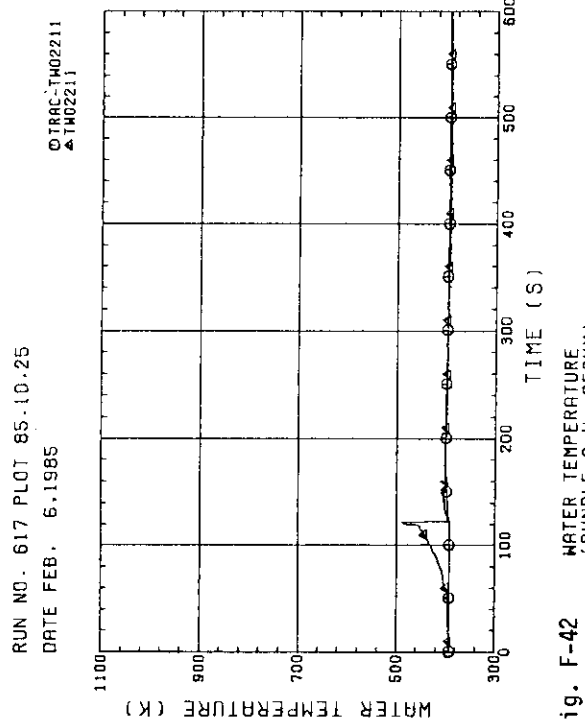


Fig. F-42 WATER TEMPERATURE (BUNDLE 2 H= 950mm)

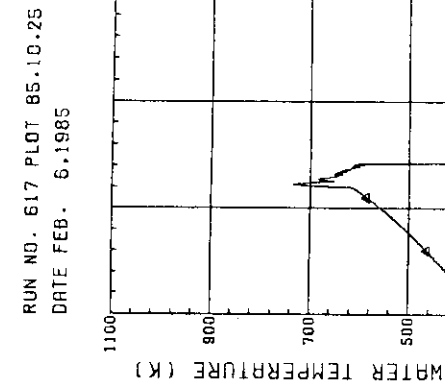


Fig. F-43 WATER TEMPERATURE (BUNDLE 2 H= 1735mm)

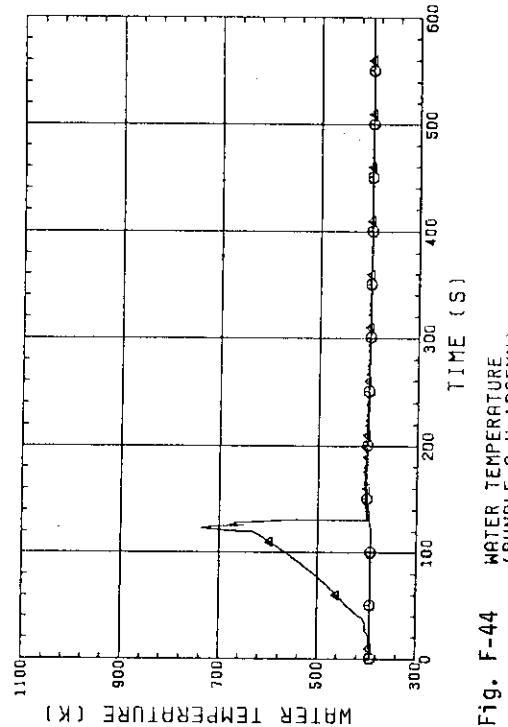
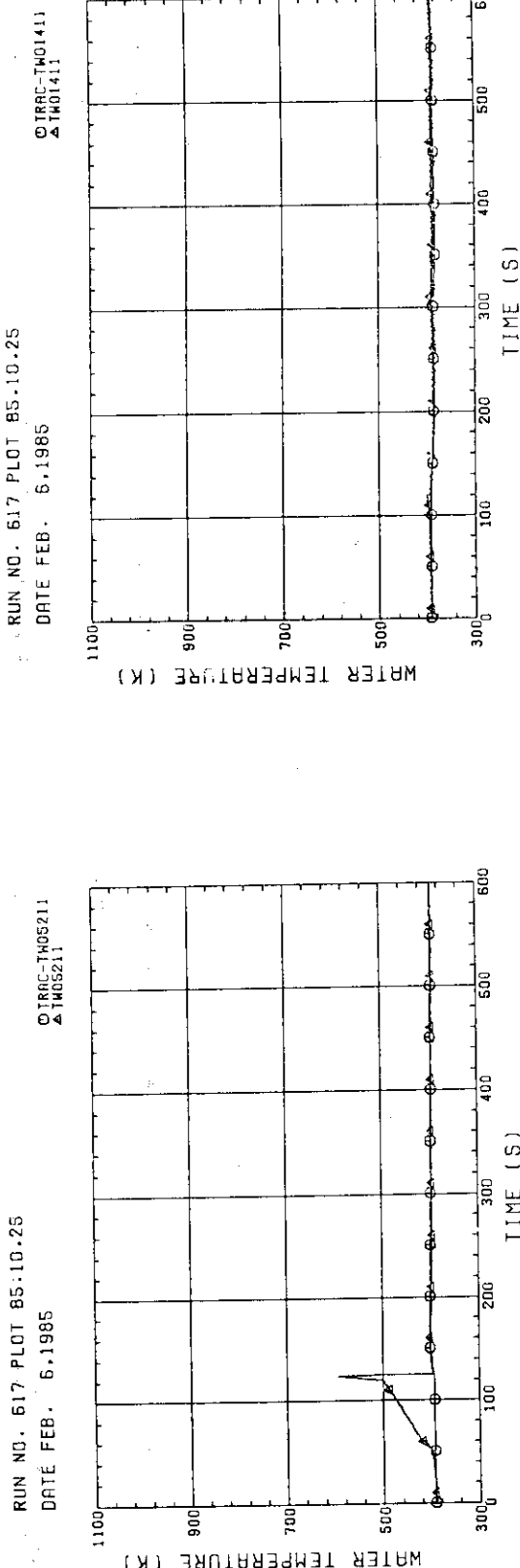
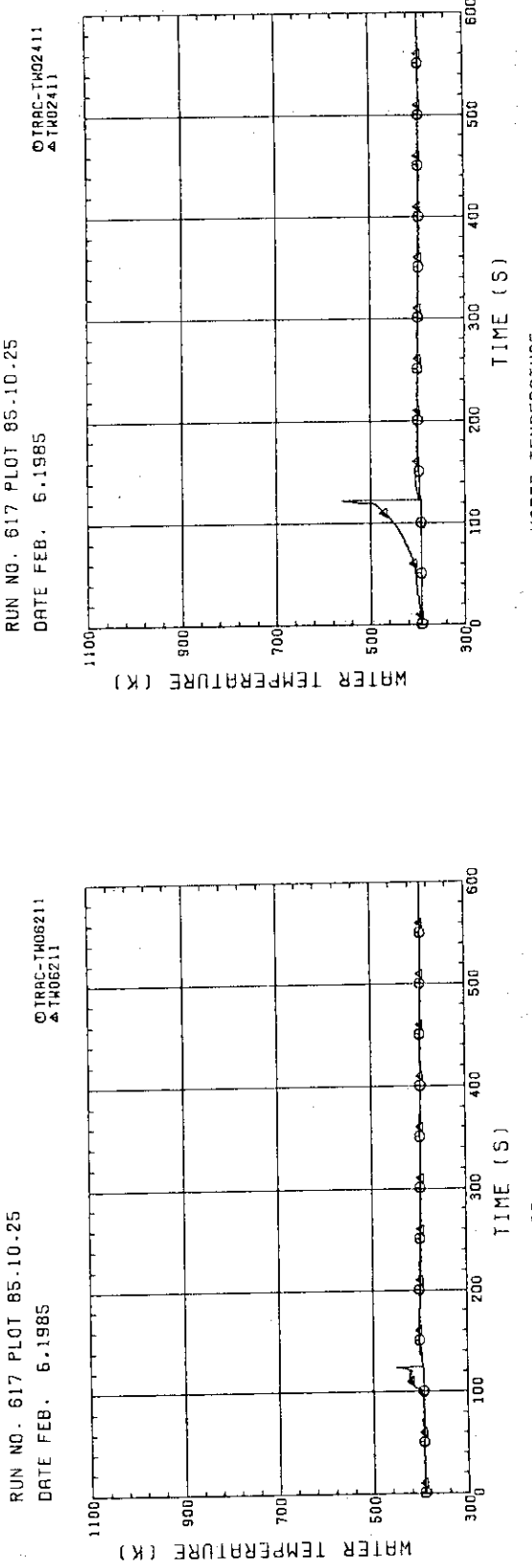
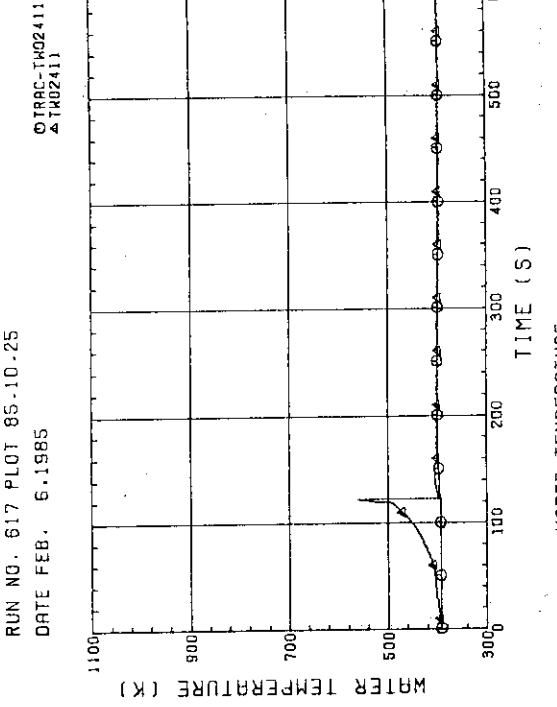


Fig. F-44 WATER TEMPERATURE (BUNDLE 2 H= 1900mm)

Fig. F-45 WATER TEMPERATURE  
(BUNDLE 2 H=2760MM)Fig. F-46 WATER TEMPERATURE  
(BUNDLE 2 H=3660MM)Fig. F-47 WATER TEMPERATURE  
(BUNDLE 4 H= 3MM)Fig. F-48 WATER TEMPERATURE  
(BUNDLE 4 H= 950MM)

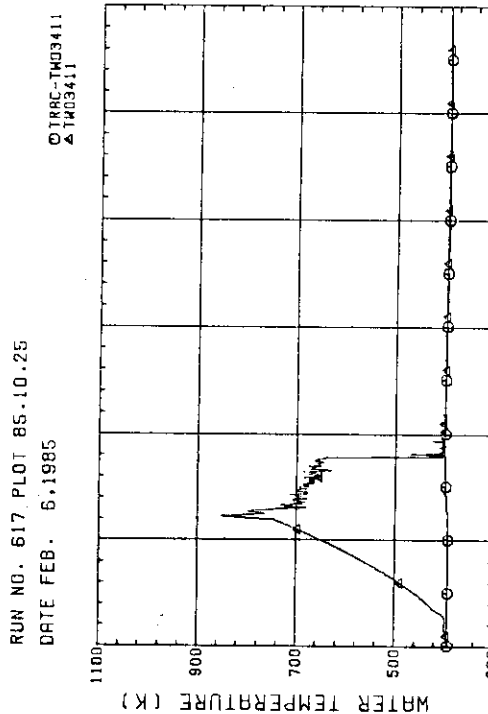


Fig. F-49 WATER TEMPERATURE (BUNDLE 4 H=1735MM)

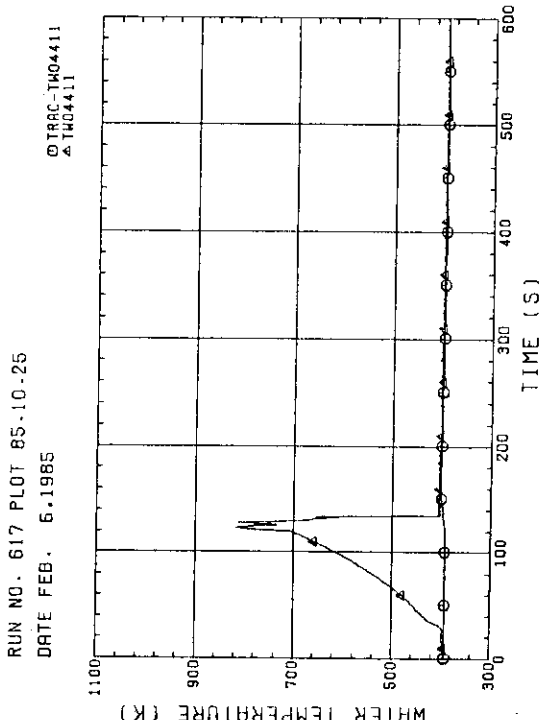


Fig. F-50 WATER TEMPERATURE (BUNDLE 4 H=1905MM)

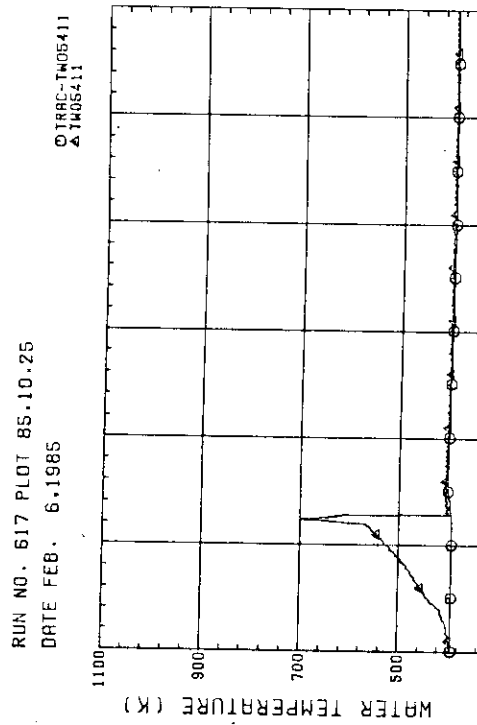


Fig. F-51 WATER TEMPERATURE (BUNDLE 4 H=2760MM)

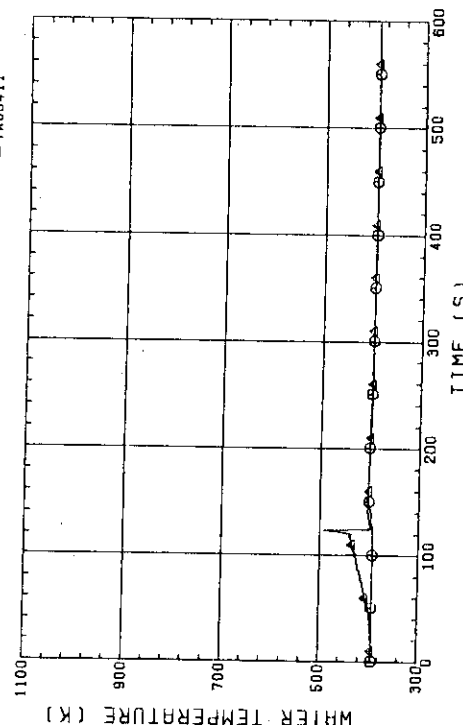


Fig. F-52 WATER TEMPERATURE (BUNDLE 4 H=3660MM)

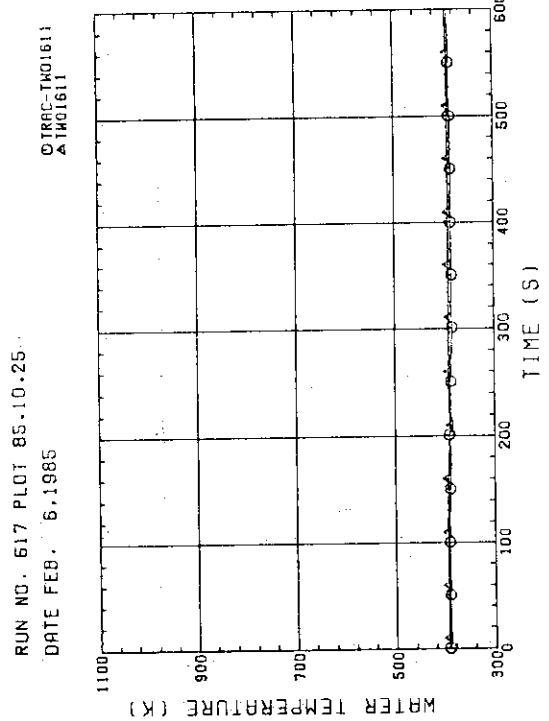


Fig. F-53 WATER TEMPERATURE (BUNDLE 6 H= 0MM)

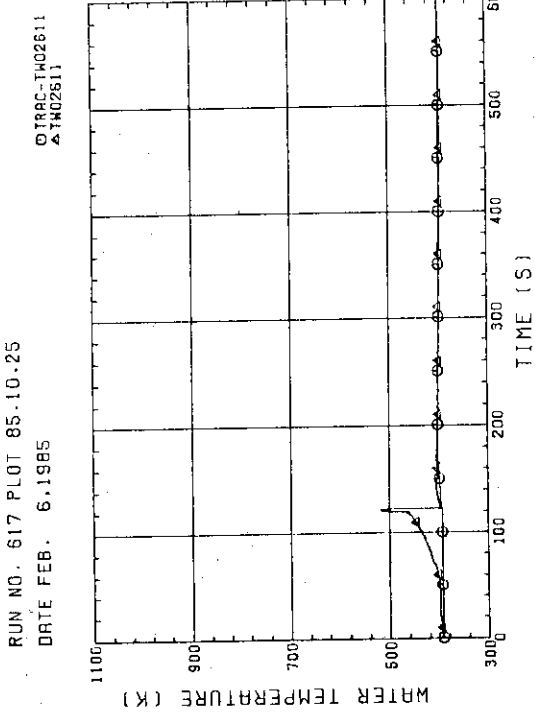


Fig. F-54 WATER TEMPERATURE (BUNDLE 6 H= 950MM)

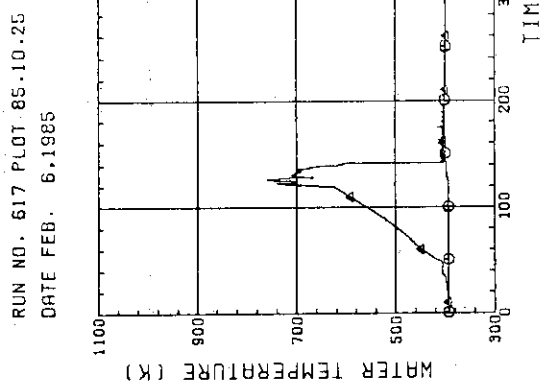


Fig. F-53 WATER TEMPERATURE (BUNDLE 6 H= 0MM)

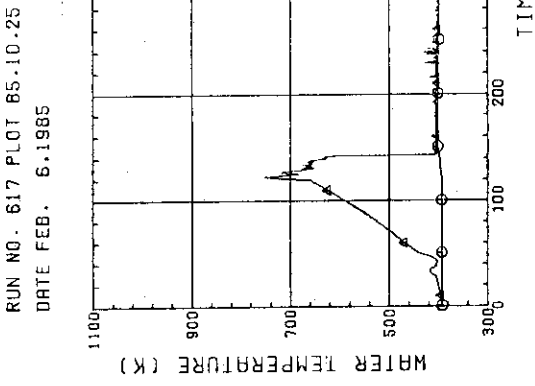


Fig. F-55 WATER TEMPERATURE (BUNDLE 6 H= 1735MM)

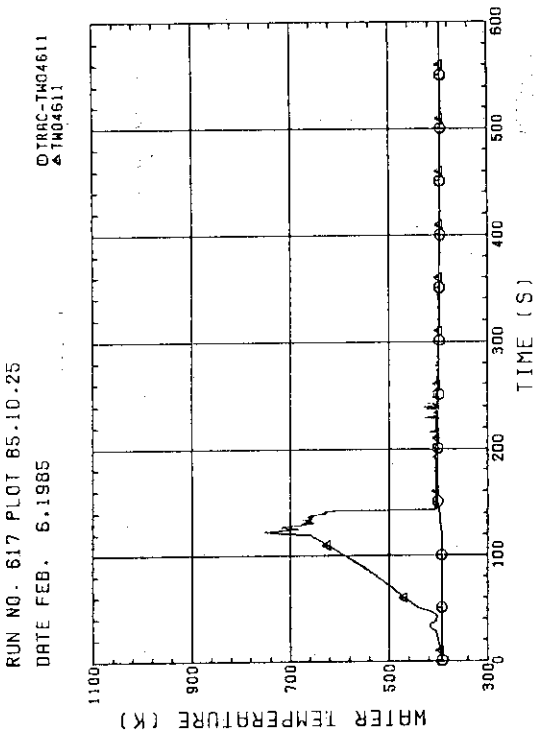
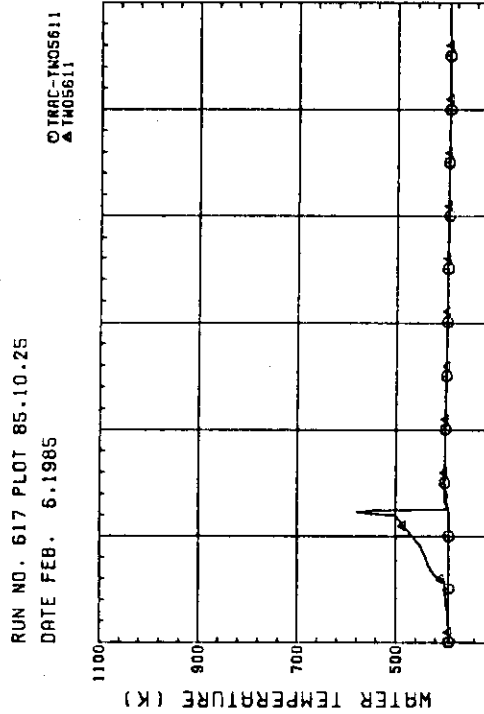
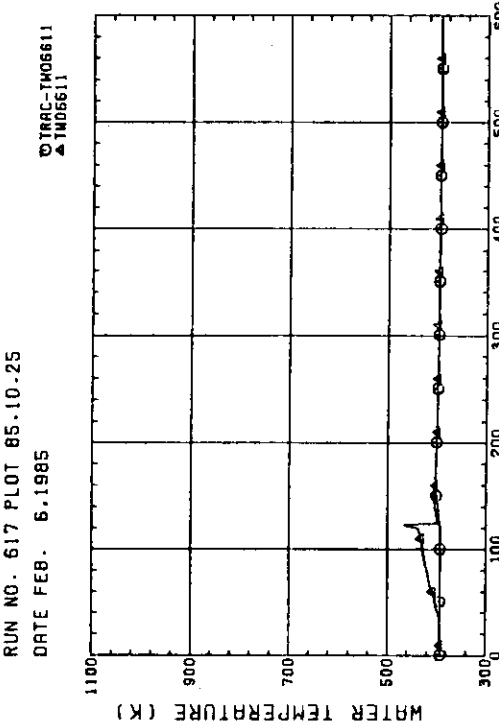
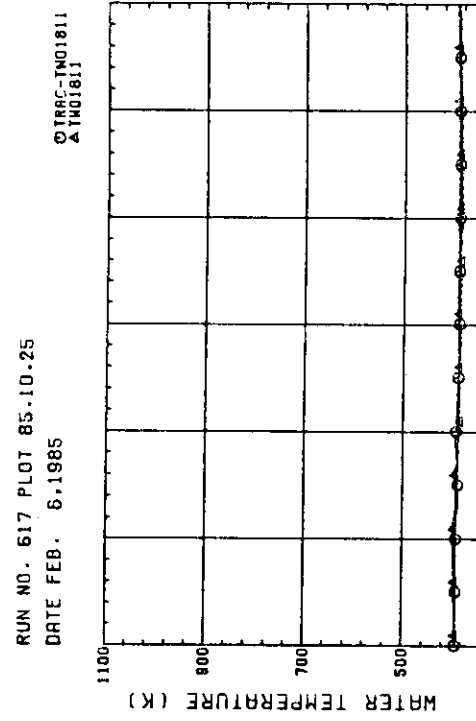
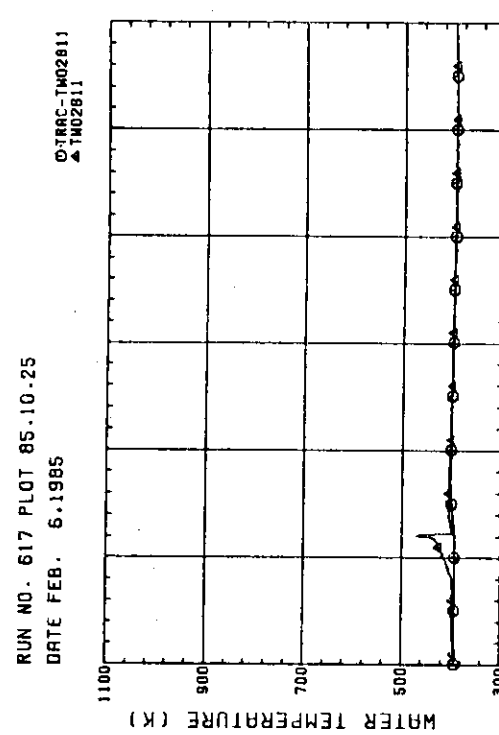


Fig. F-56 WATER TEMPERATURE (BUNDLE 6 H= 1905MM)

Fig. F-57 WATER TEMPERATURE  
(BUNDLE 6 H=2760MM)Fig. F-58 WATER TEMPERATURE  
(BUNDLE 6 H=3660MM)Fig. F-59 WATER TEMPERATURE  
(BUNDLE 8 H= 0MM)Fig. F-60 WATER TEMPERATURE  
(BUNDLE 8 H= 950MM)

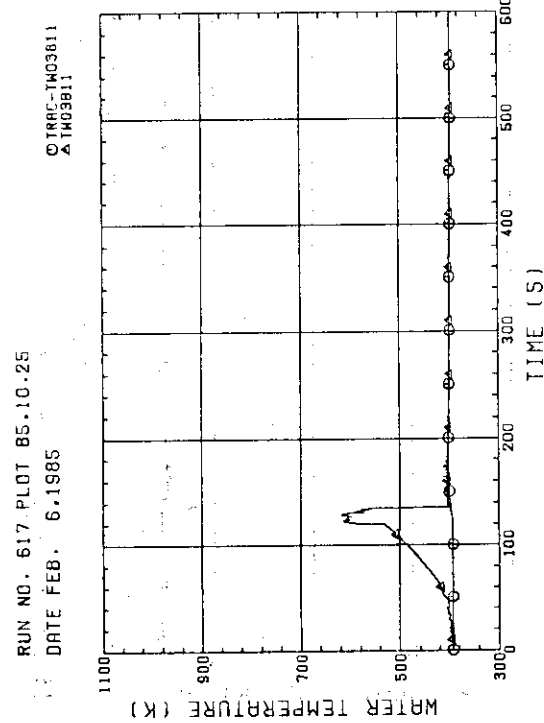


Fig. F-61 WATER TEMPERATURE (BUNDLE 8 H=1735MM)

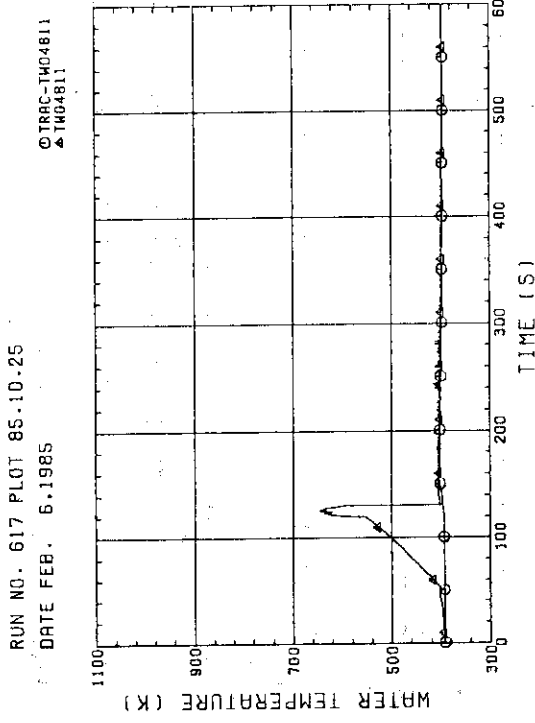


Fig. F-62 WATER TEMPERATURE (BUNDLE 8 H=1905MM)

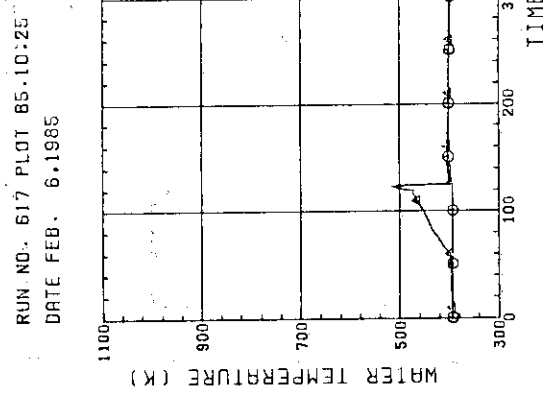


Fig. F-63 WATER TEMPERATURE (BUNDLE 8 H=2760MM)

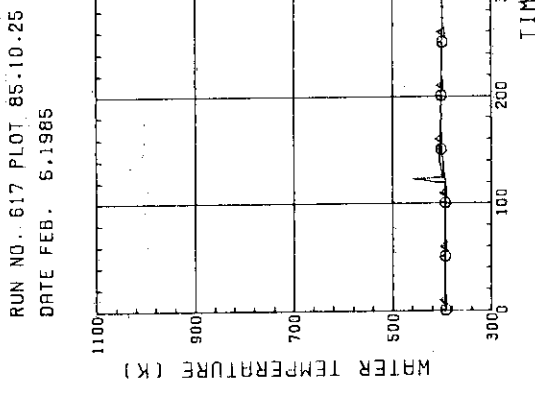


Fig. F-64 WATER TEMPERATURE (BUNDLE 8 H=3660MM)

RUN NO. 617 PLOT 85.10.25  
 DATE FEB. 6.1985  
 ◉ TRAC-TF01121  
 ▲ TF01321

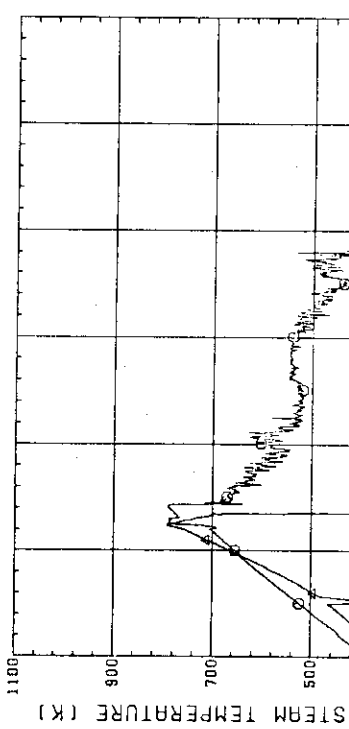


Fig. F-65 STEAM TEMPERATURE  
 (BUNDLE 1 H=1915MM)

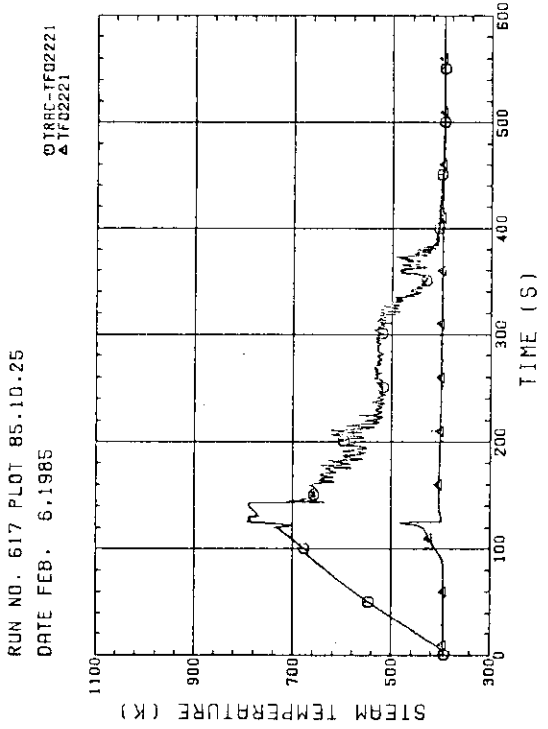


Fig. F-66 STEAM TEMPERATURE  
 (BUNDLE 2 H=1915MM)

RUN NO. 617 PLOT 85.10.25  
 DATE FEB. 6.1985  
 ◉ TRAC-TF01121  
 ▲ TF01321

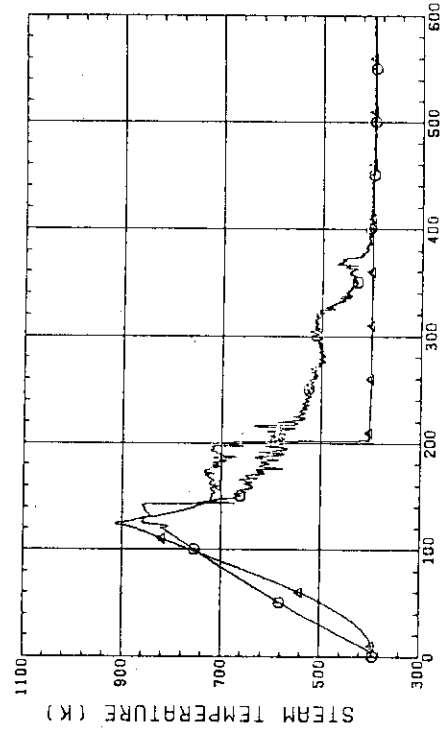


Fig. F-67 STEAM TEMPERATURE  
 (BUNDLE 3 H=1915MM)

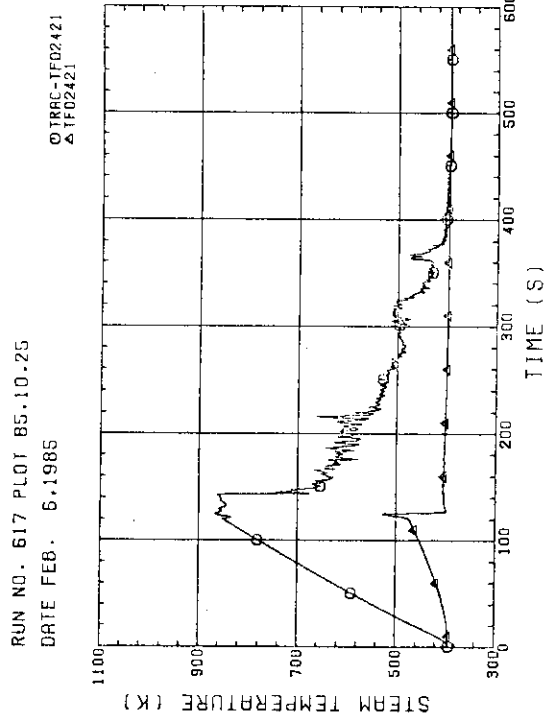
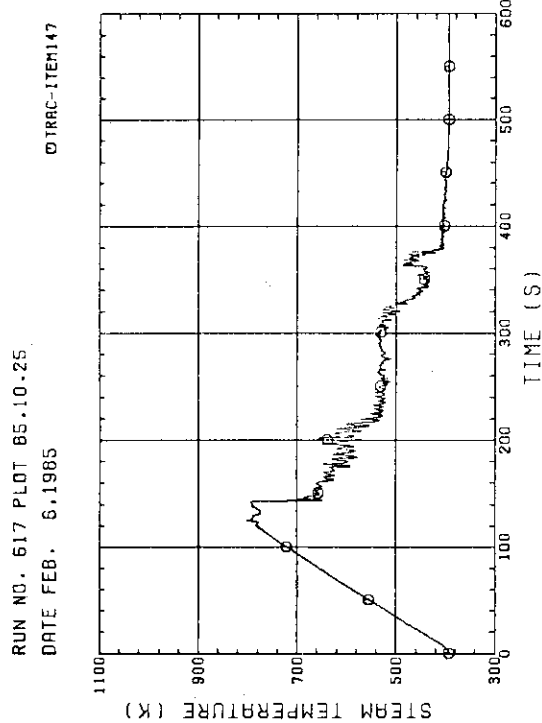
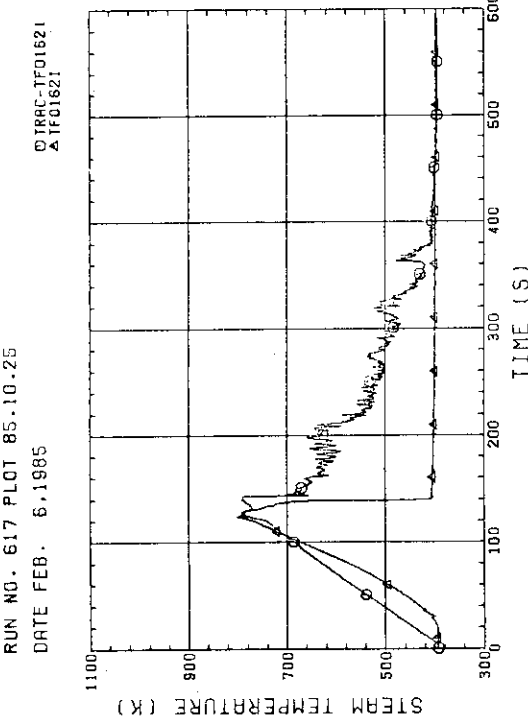
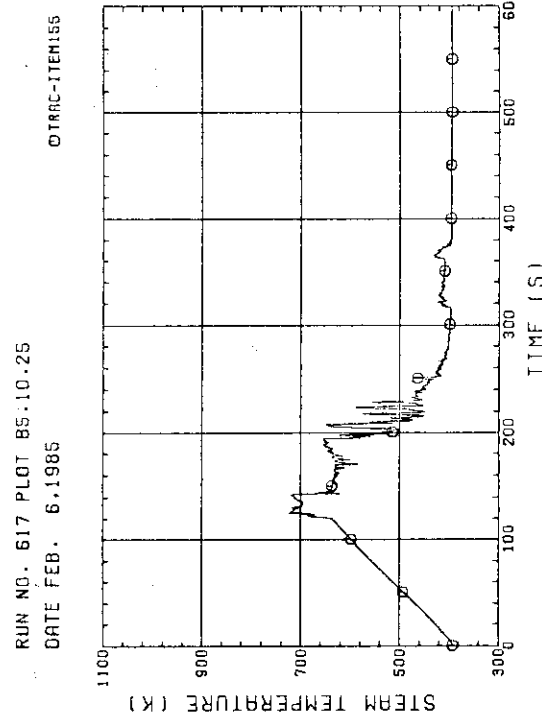
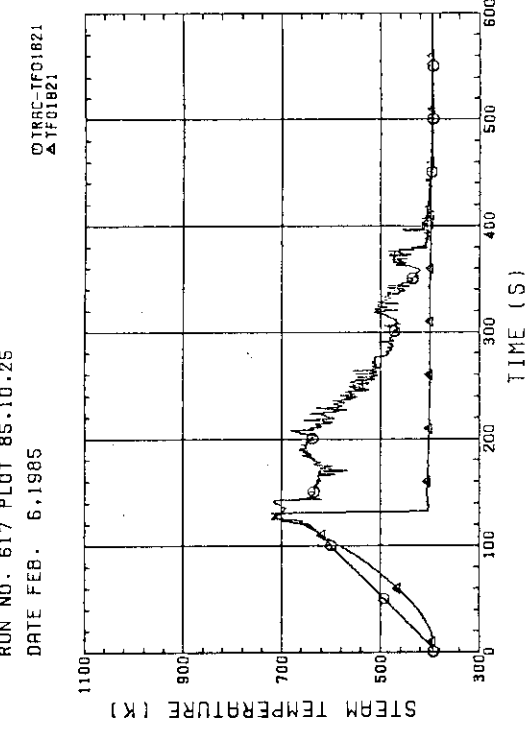


Fig. F-68 STEAM TEMPERATURE  
 (BUNDLE 4 H=1915MM)

Fig. F-69 STEAM TEMPERATURE  
(BUNDLE 5 H=1915MM)Fig. F-70 STEAM TEMPERATURE  
(BUNDLE 6 H=1915MM)Fig. F-71 STEAM TEMPERATURE  
(BUNDLE 7 H=1915MM)Fig. F-72 STEAM TEMPERATURE  
(BUNDLE 8 H=1915MM)

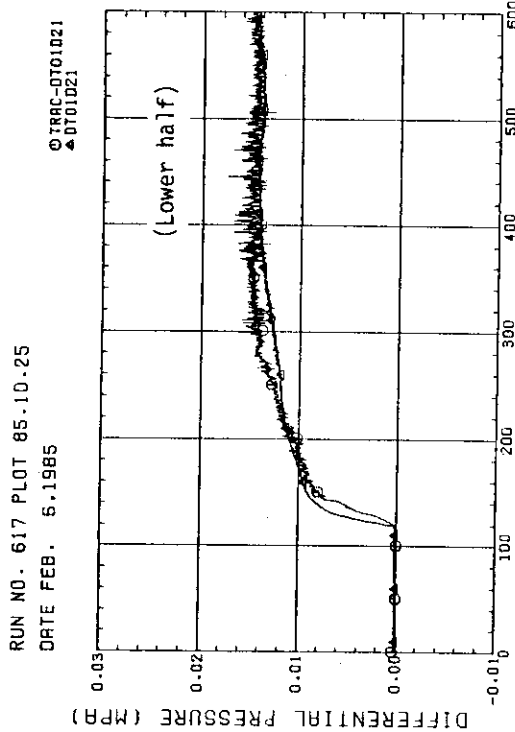


Fig. F-73 VERTICAL DIFFERENTIAL PRESSURE (BUNDLE 2)

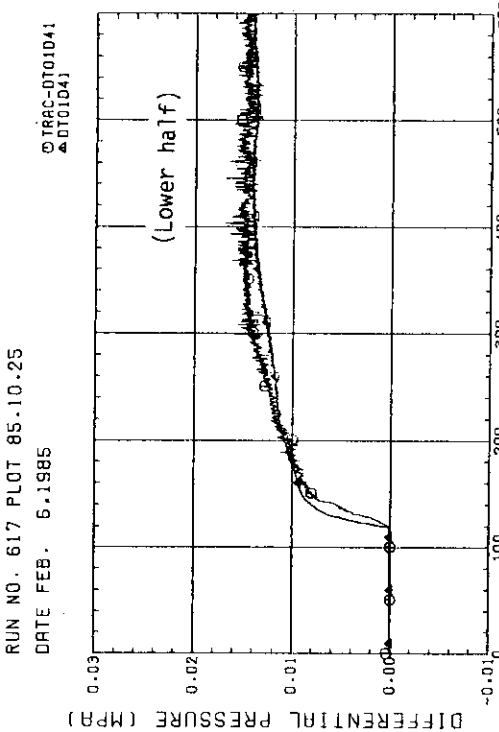


Fig. F-74 VERTICAL DIFFERENTIAL PRESSURE (BUNDLE 4)

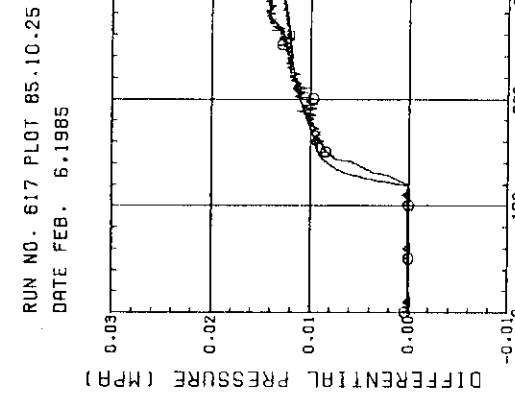


Fig. F-75 VERTICAL DIFFERENTIAL PRESSURE (BUNDLE 6)

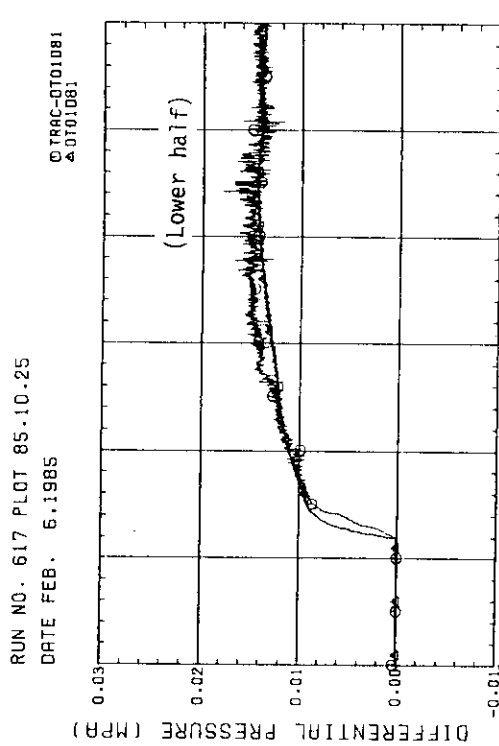


Fig. F-76 VERTICAL DIFFERENTIAL PRESSURE (BUNDLE 8)

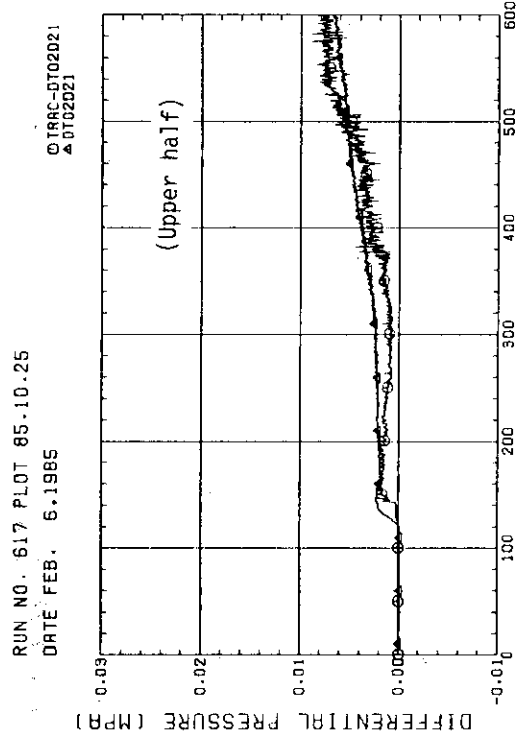


Fig. F-77 VERTICAL DIFFERENTIAL PRESSURE (BUNDLE 2)

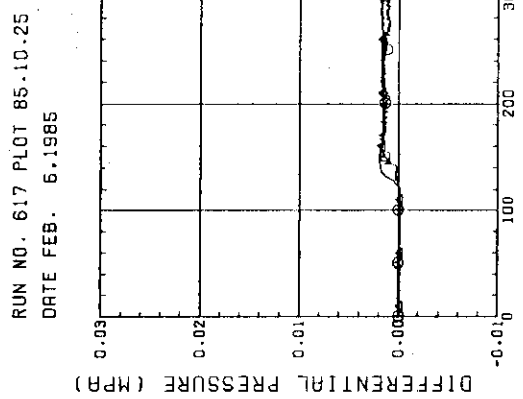


Fig. F-79 VERTICAL DIFFERENTIAL PRESSURE (BUNDLE 6)

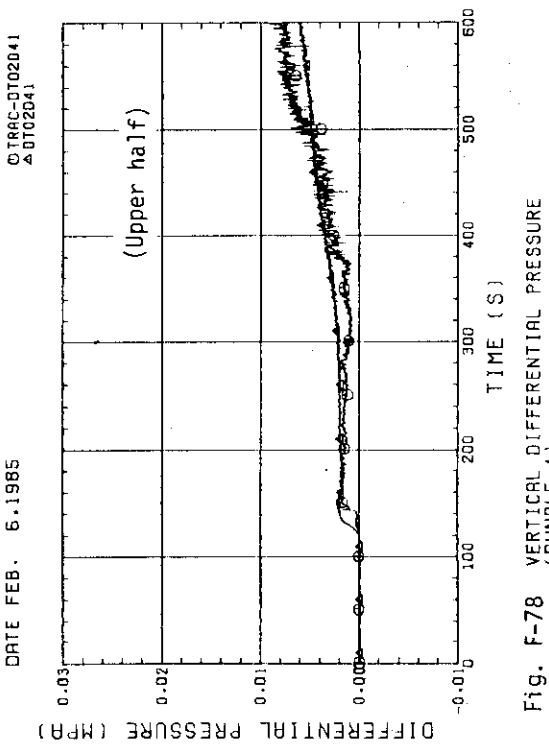


Fig. F-78 VERTICAL DIFFERENTIAL PRESSURE (BUNDLE 4)

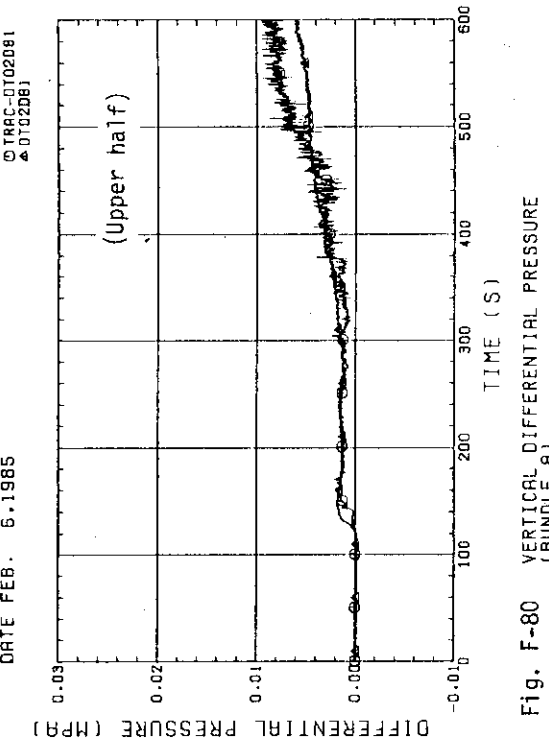


Fig. F-80 VERTICAL DIFFERENTIAL PRESSURE (BUNDLE 8)

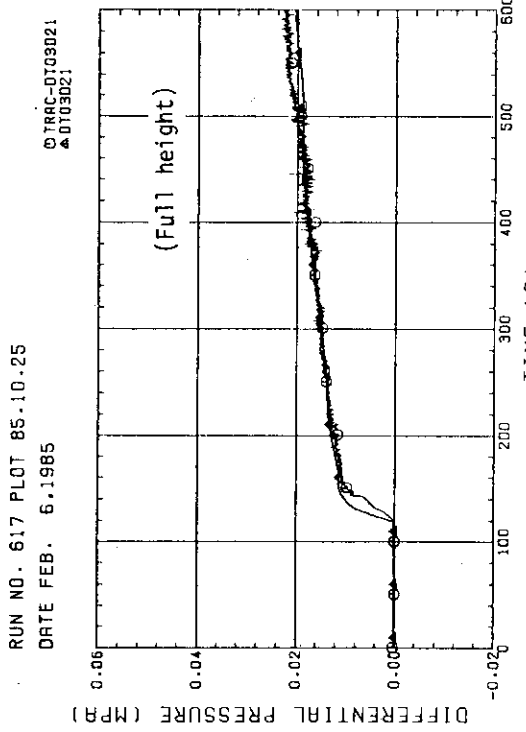


Fig. F-81 VERTICAL DIFFERENTIAL PRESSURE (BUNDLE 2)

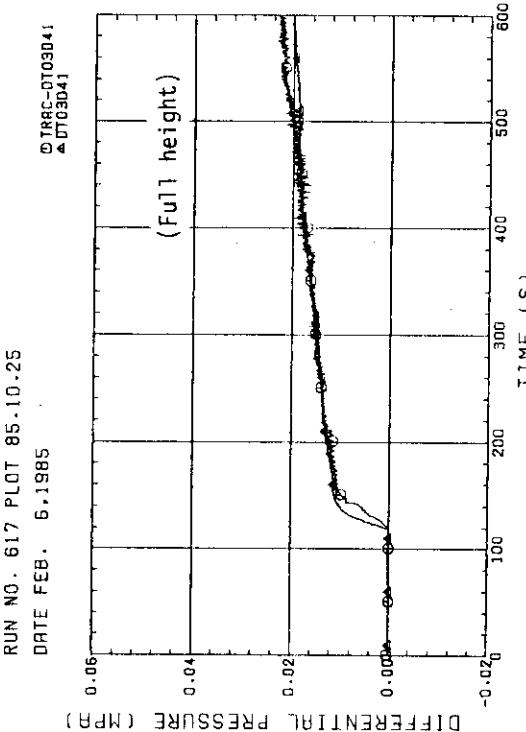


Fig. F-82 VERTICAL DIFFERENTIAL PRESSURE (BUNDLE 4)

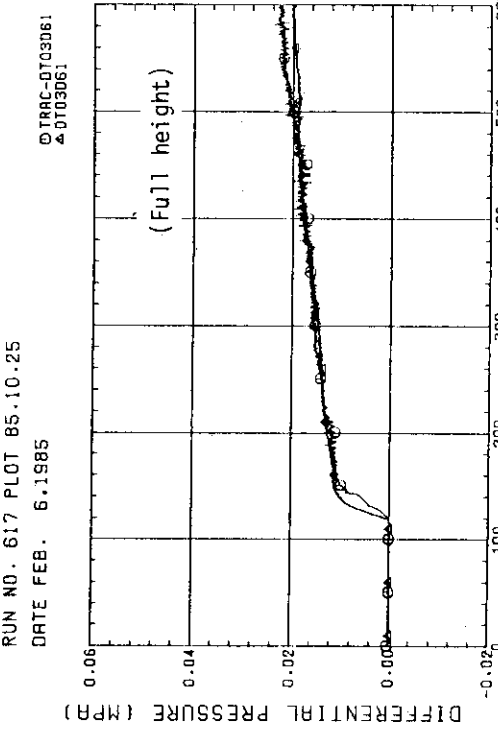


Fig. F-83 VERTICAL DIFFERENTIAL PRESSURE (BUNDLE 6)

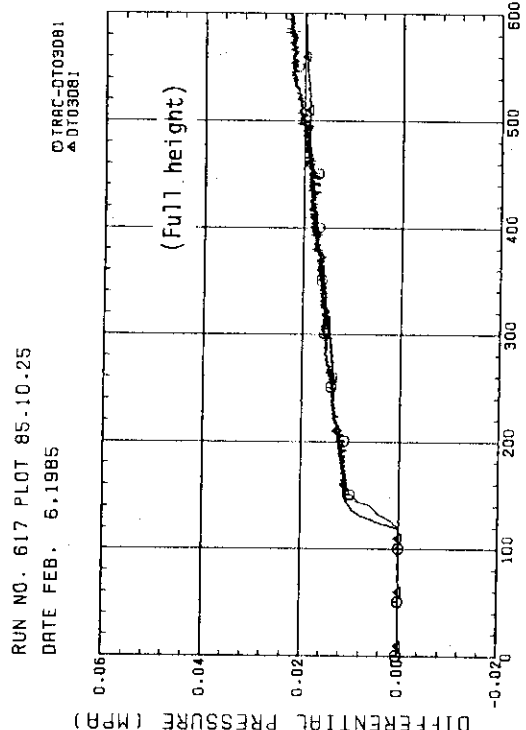


Fig. F-84 VERTICAL DIFFERENTIAL PRESSURE (BUNDLE 8)

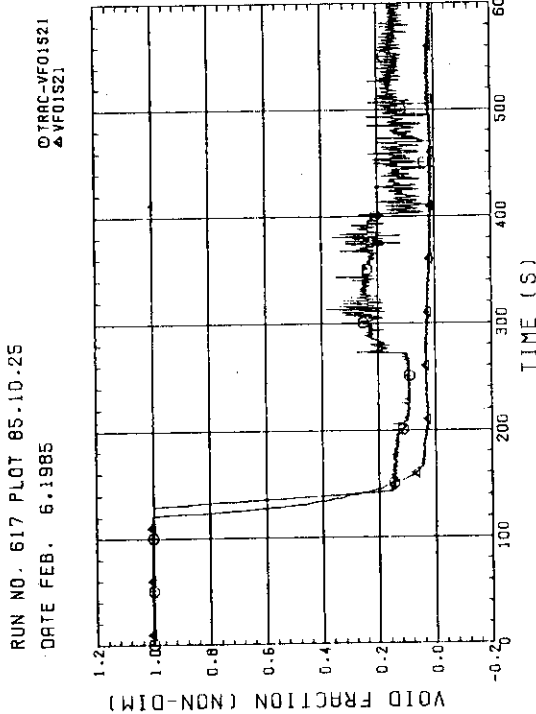


Fig. F-85 VOID FRACTION (BUNDLE 2)

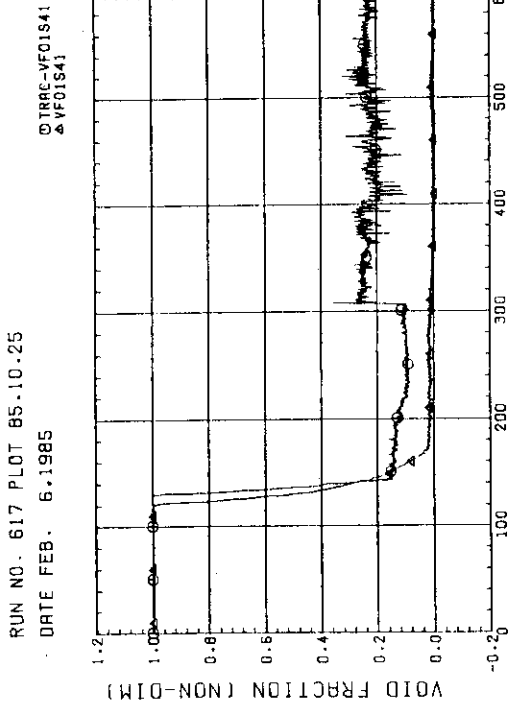


Fig. F-86 VOID FRACTION (BUNDLE 4)

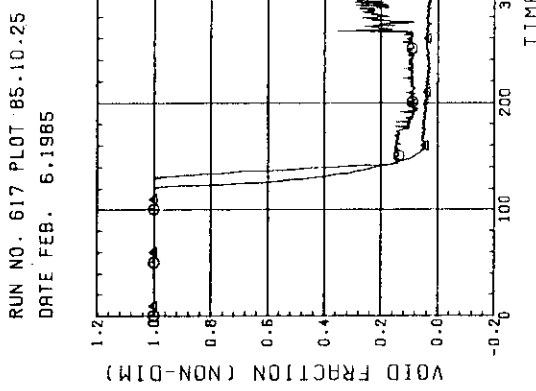


Fig. F-87 VOID FRACTION (BUNDLE 8)

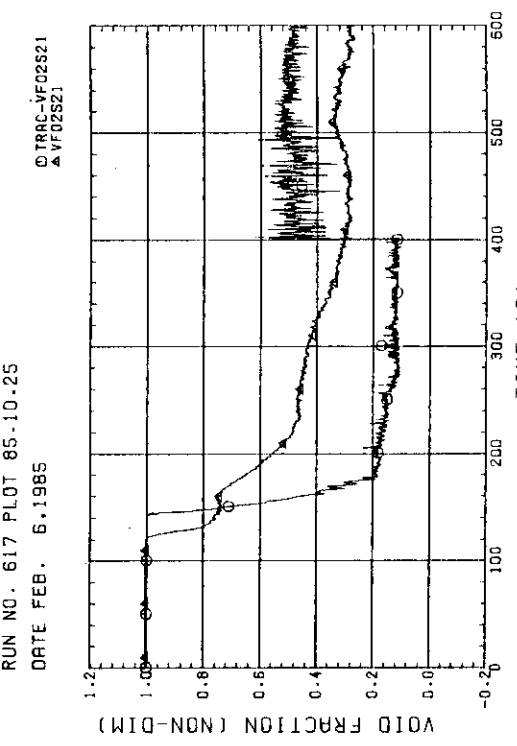


Fig. F-88 VOID FRACTION (BUNDLE 2)

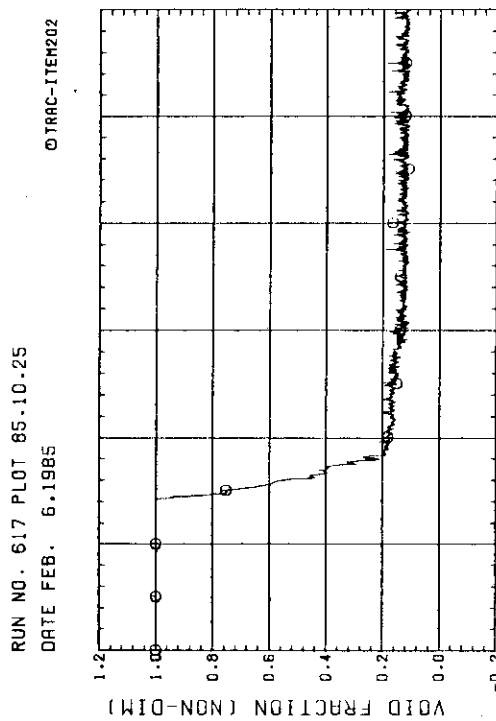


Fig. F-89 VOID FRACTION (BUNDLE 4)

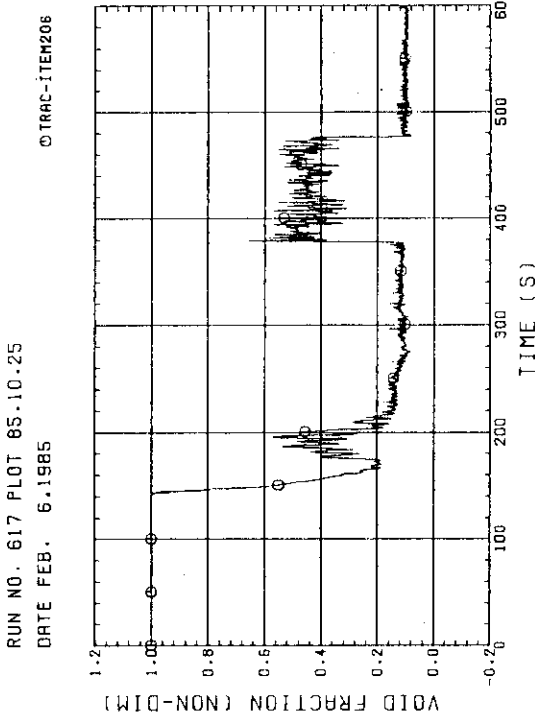


Fig. F-90 VOID FRACTION (BUNDLE 8)

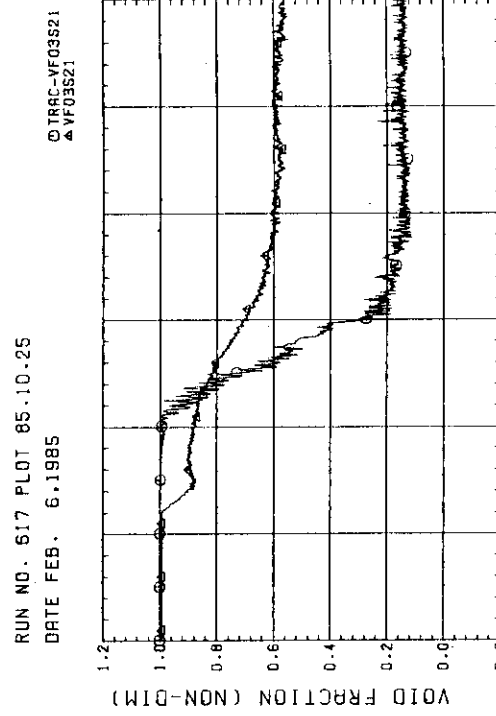


Fig. F-91 VOID FRACTION (BUNDLE 2)

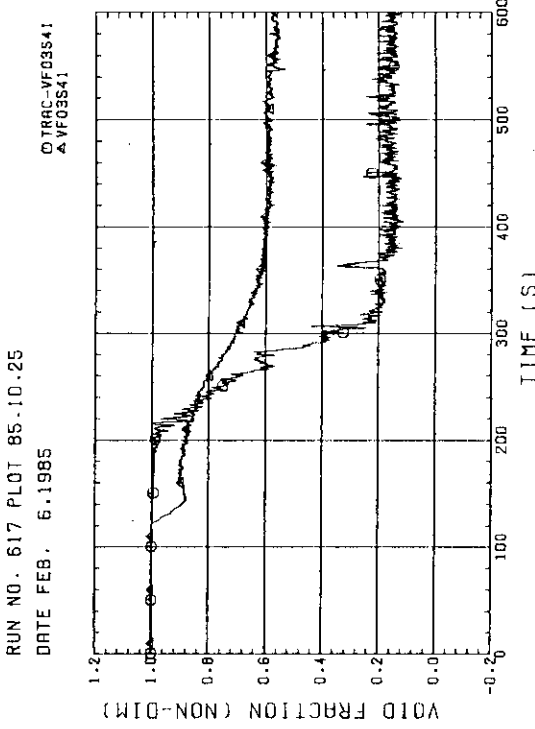


Fig. F-92 VOID FRACTION (BUNDLE 4)

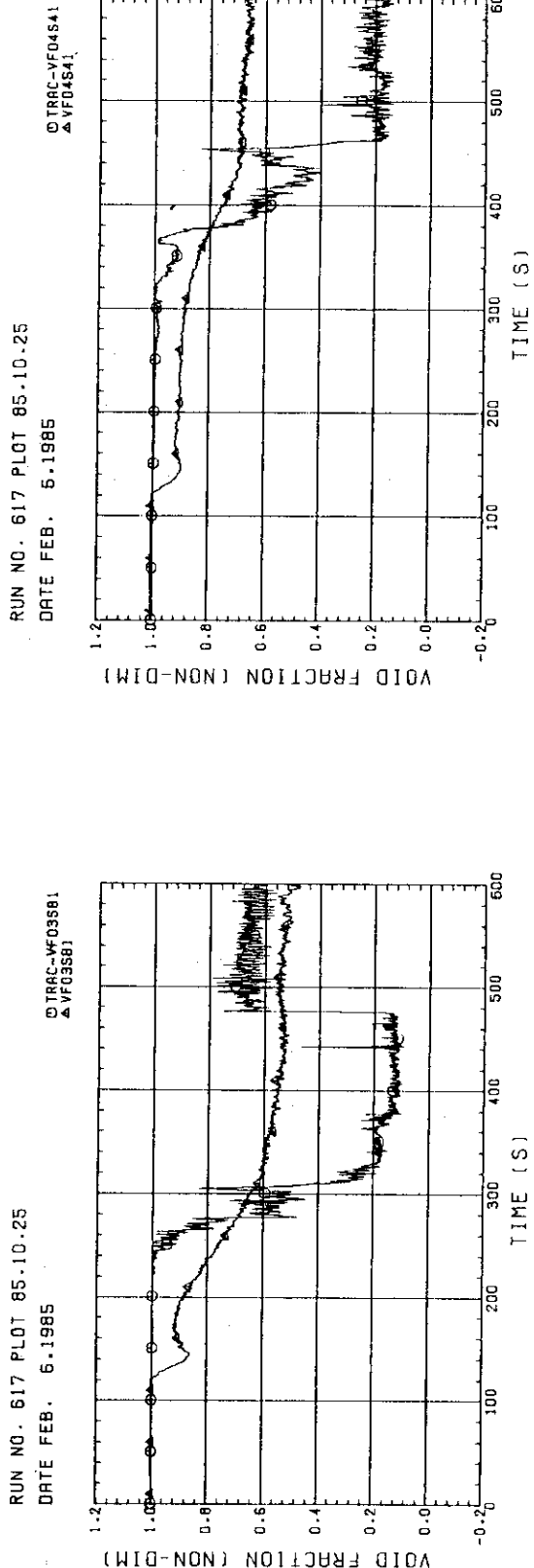


Fig. F-93 VOID FRACTION (BUNDLE 8)

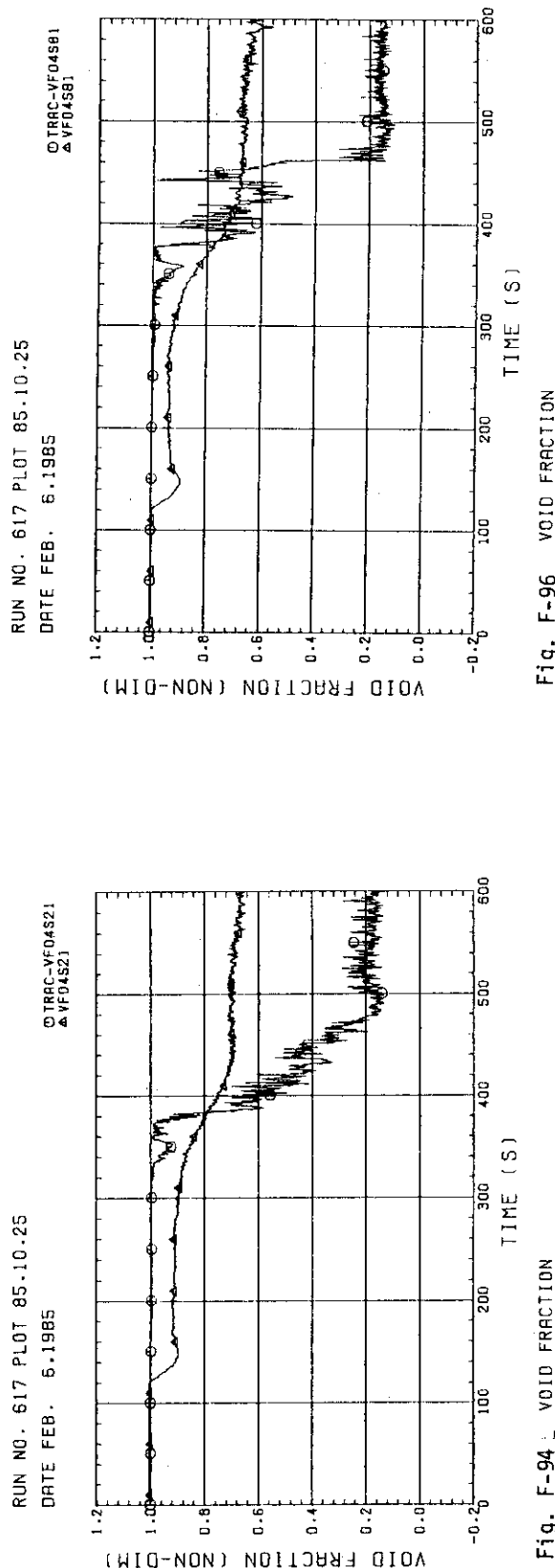


Fig. F-94 VOID FRACTION (BUNDLE 2)

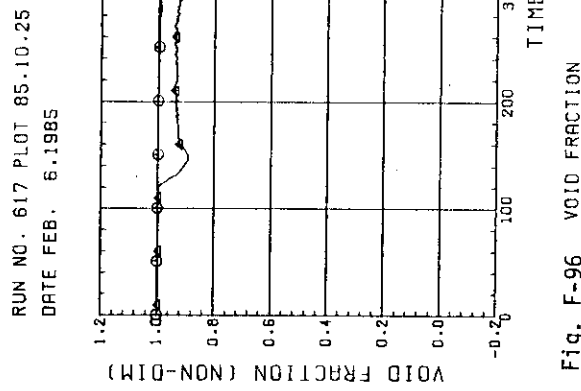


Fig. F-95 VOID FRACTION (BUNDLE 4)

Fig. F-95 VOID FRACTION (NON-DIM)

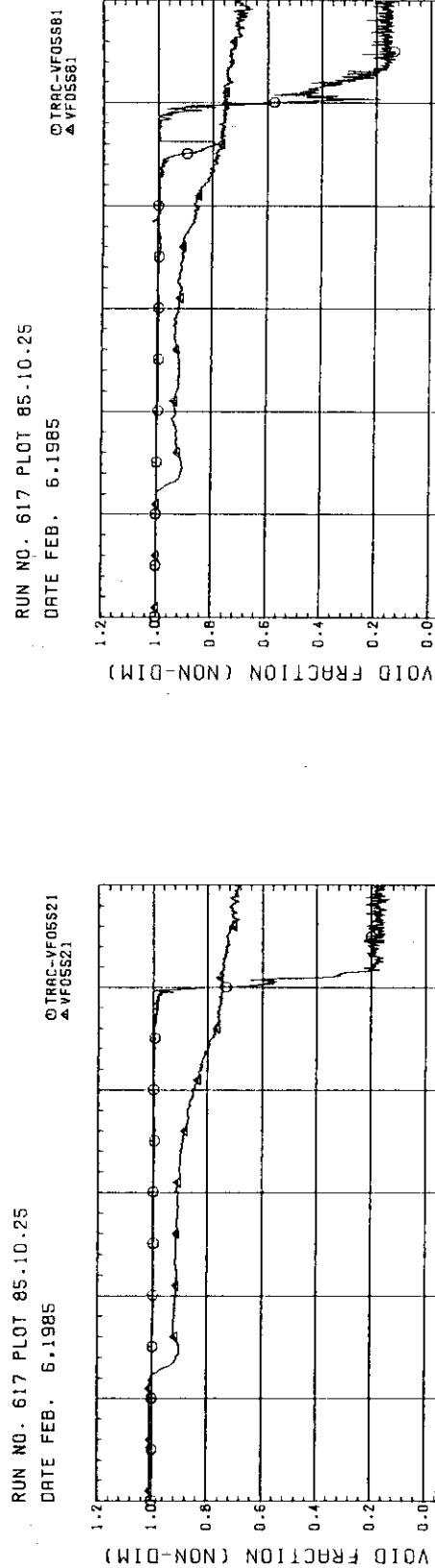


Fig. F-97 VOID FRACTION (BUNDLE 2)

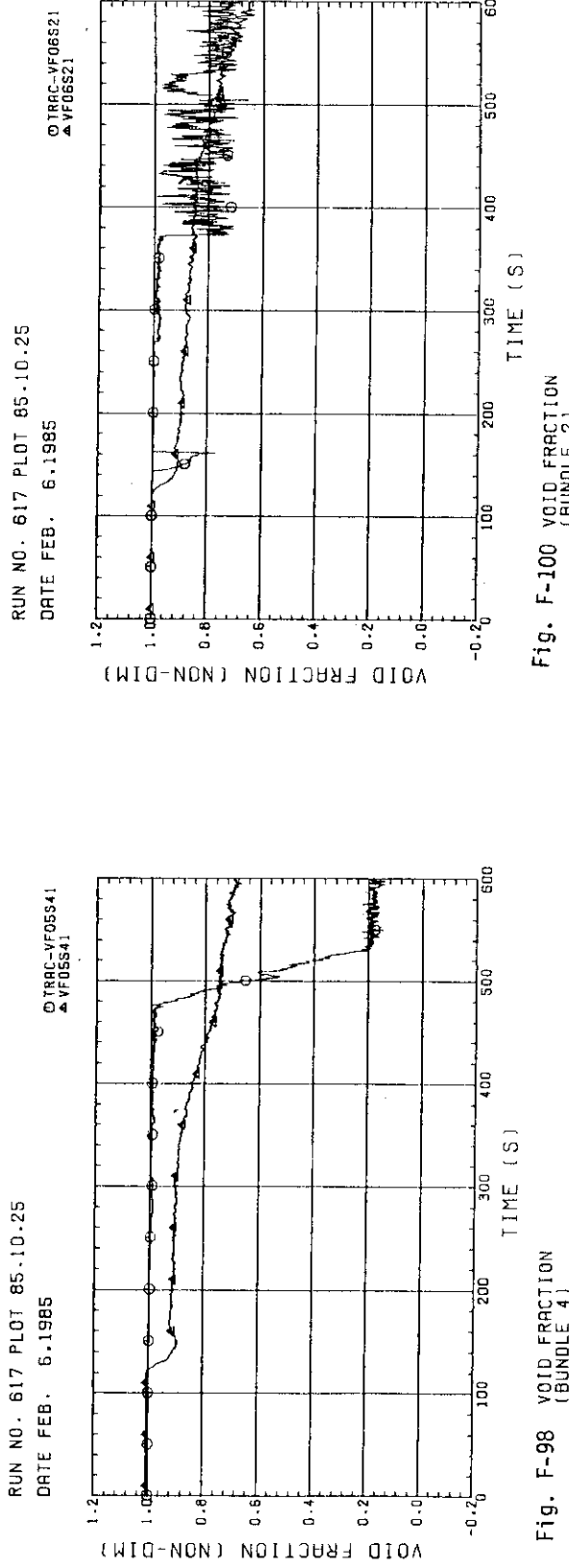


Fig. F-98 VOID FRACTION (BUNDLE 4)

Fig. F-99 VOID FRACTION (BUNDLE 8)

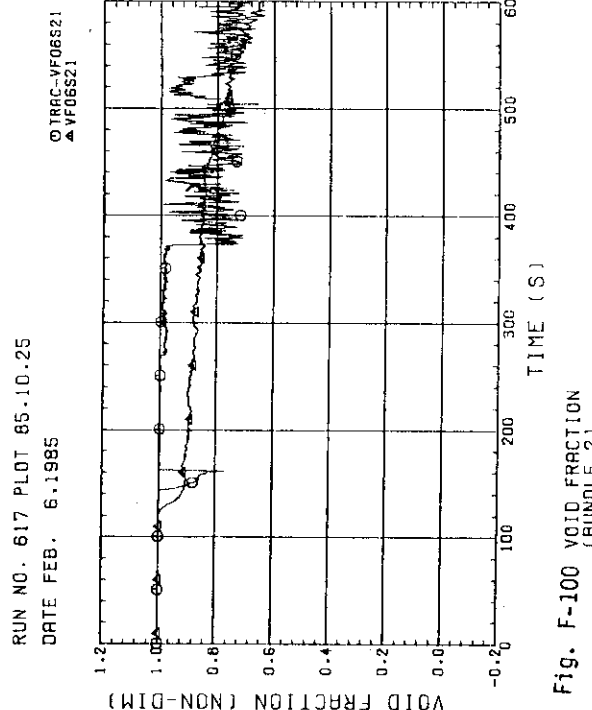


Fig. F-100 VOID FRACTION (BUNDLE 2)

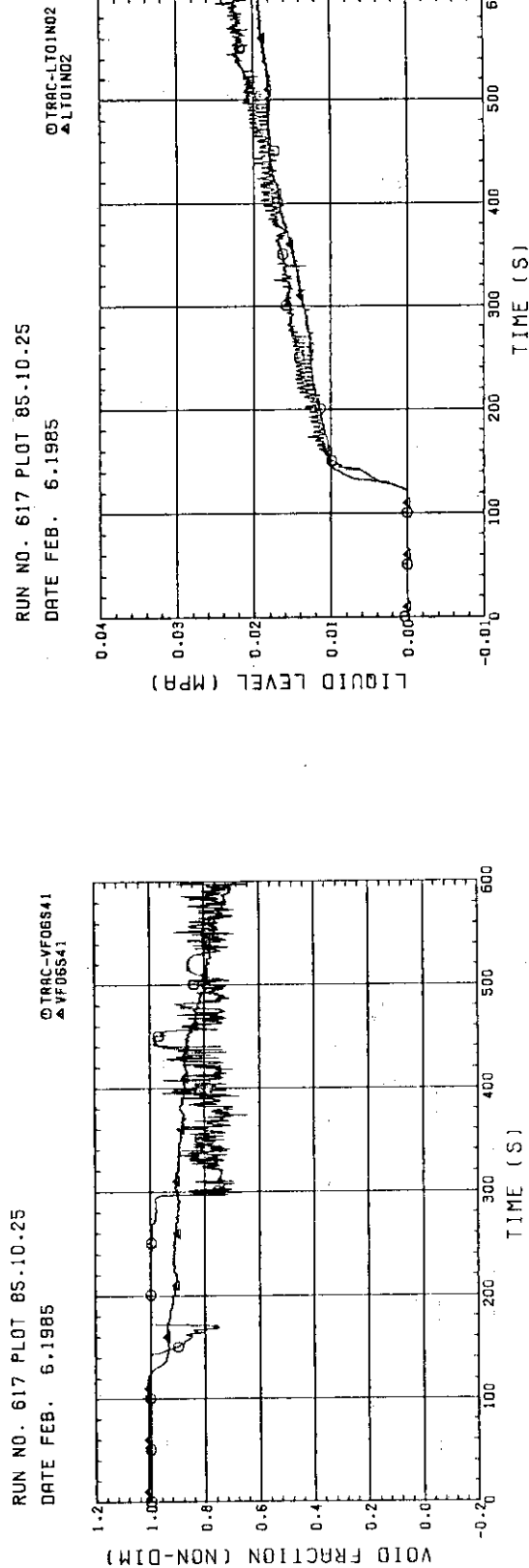


Fig. F-101 VOID FRACTION (BUNDLE 4)

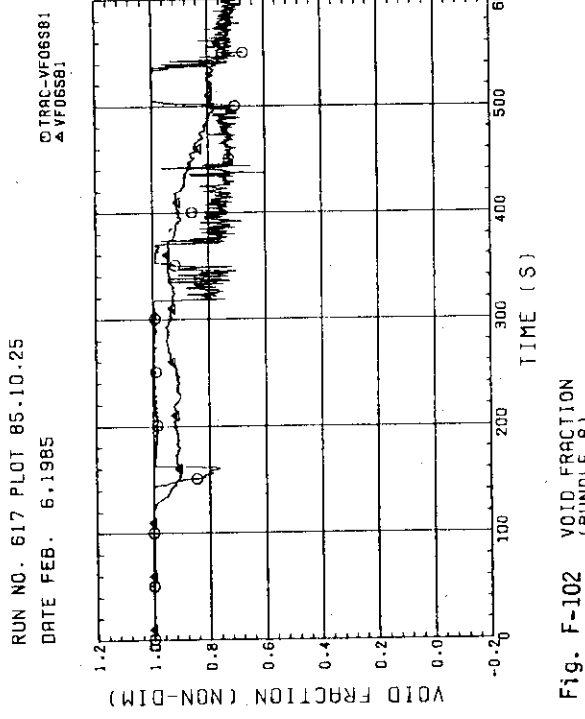


Fig. F-102 VOID FRACTION (BUNDLE 8)

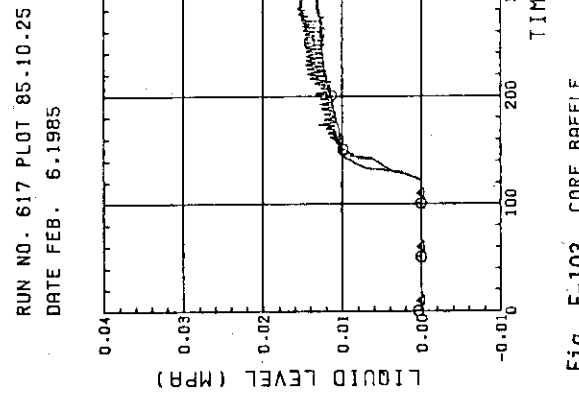


Fig. F-103 CORE BAFFLE FULL HT

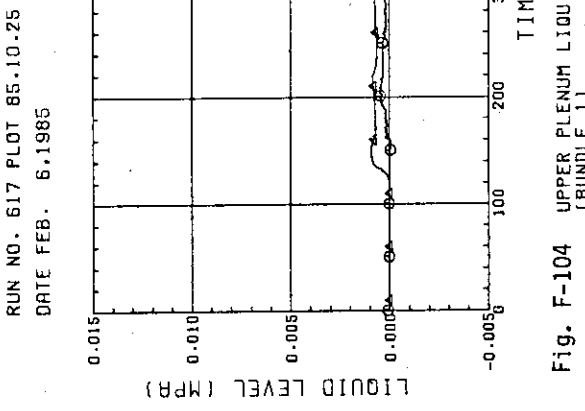


Fig. F-104 UPPER PLENUM LIQUID LEVEL (BUNDLE 1)

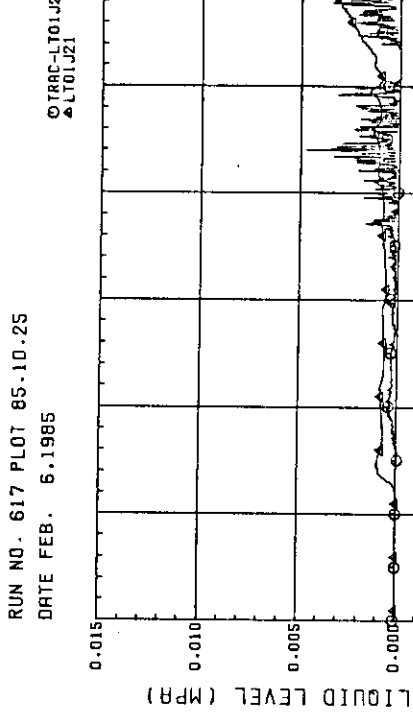


Fig. F-105 UPPER PLENUM LIQUID LEVEL (BUNDLE 2)

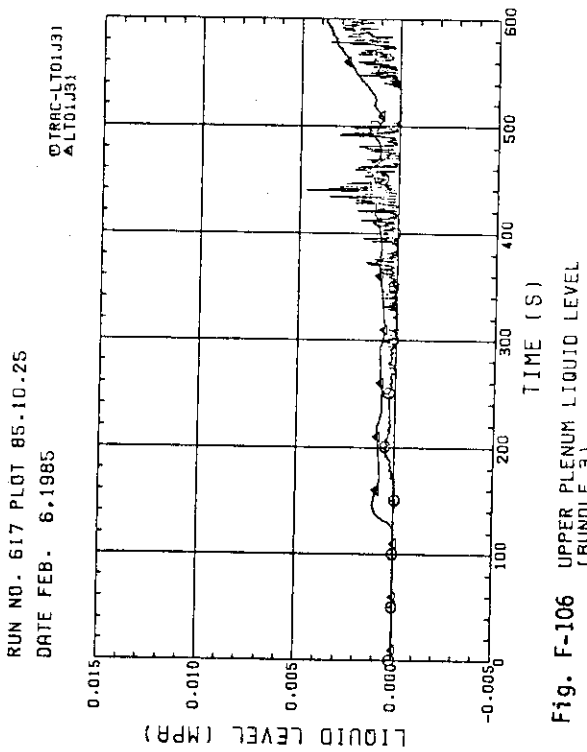


Fig. F-106 UPPER PLENUM LIQUID LEVEL (BUNDLE 3)

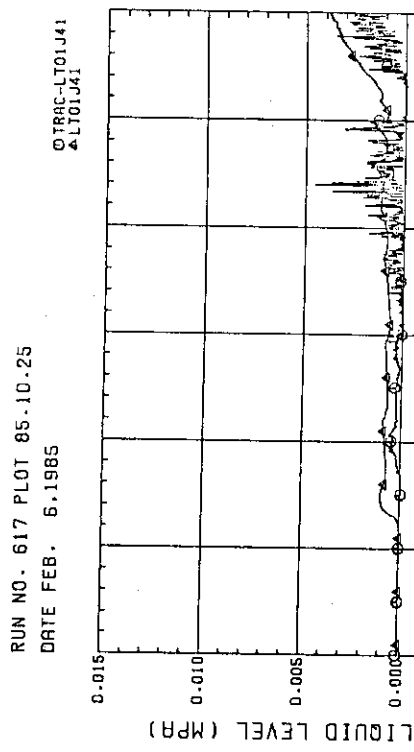


Fig. F-107 UPPER PLENUM LIQUID LEVEL (BUNDLE 4)

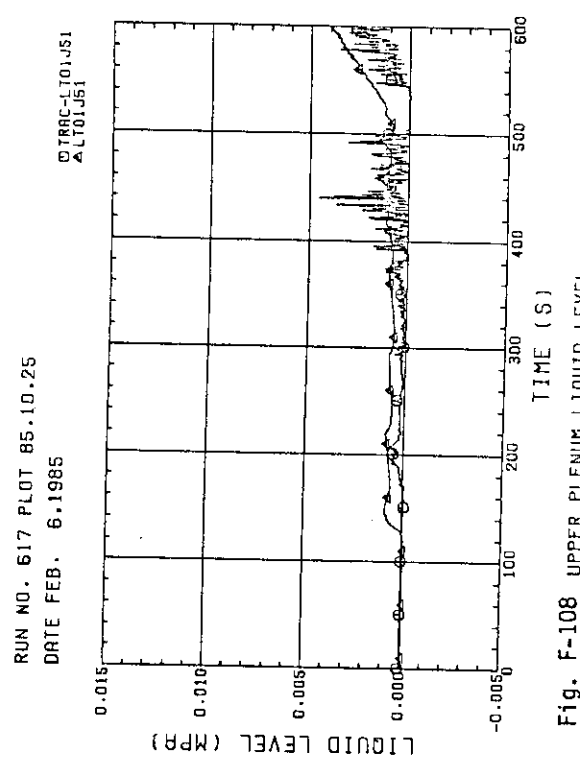
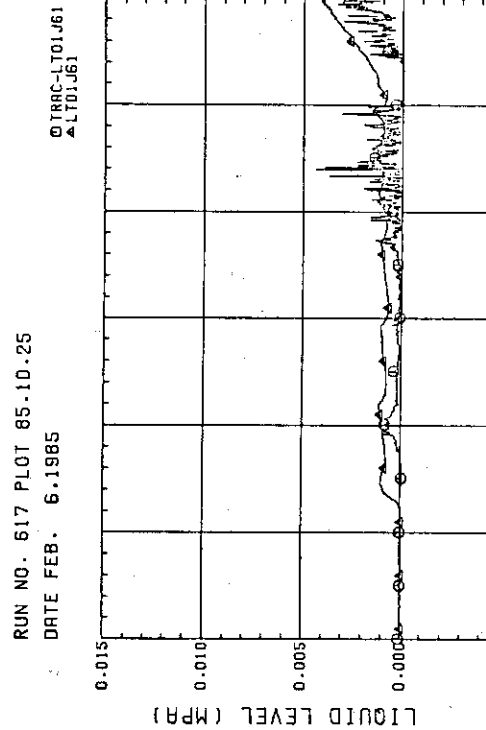
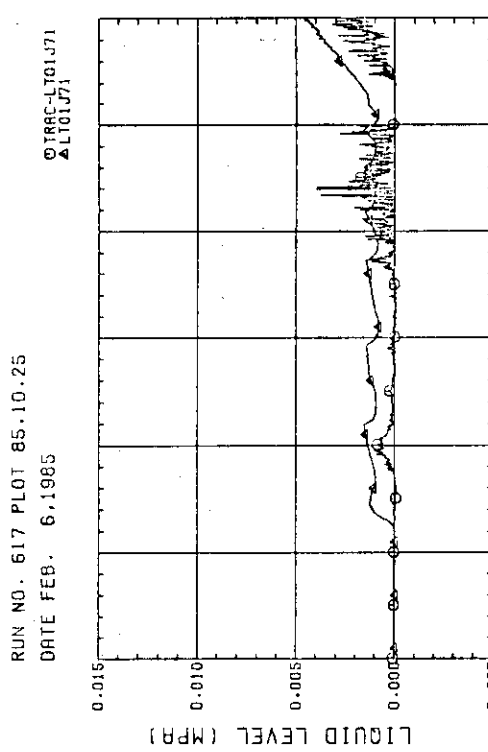
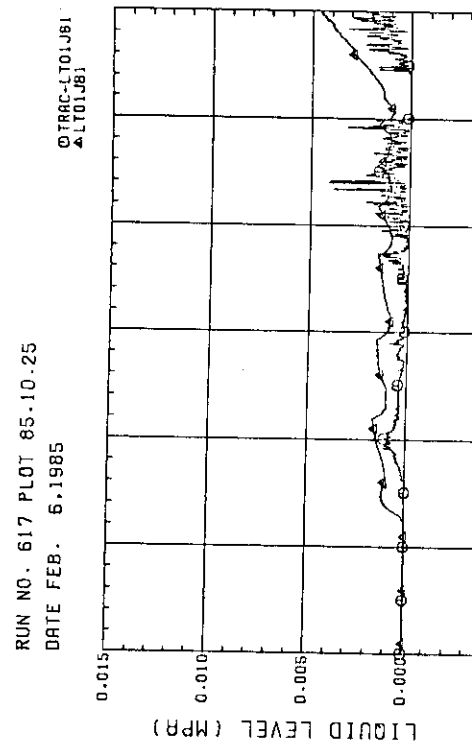
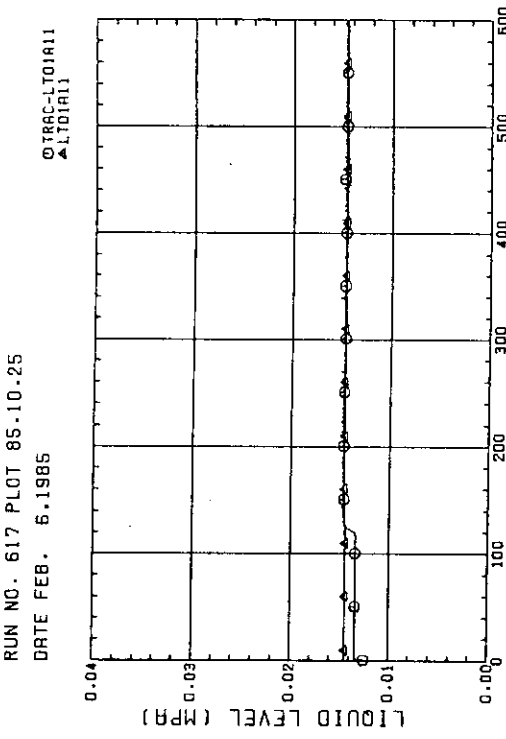


Fig. F-108 UPPER PLENUM LIQUID LEVEL (BUNDLE 5)

Fig. F-109 UPPER PLENUM LIQUID LEVEL  
(BUNDLE 6)Fig. F-110 UPPER PLENUM LIQUID LEVEL  
(BUNDLE 7)Fig. F-111 UPPER PLENUM LIQUID LEVEL  
(BUNDLE 8)Fig. F-112 LOWER PLENUM LIQUID LEVEL  
(TOTAL)

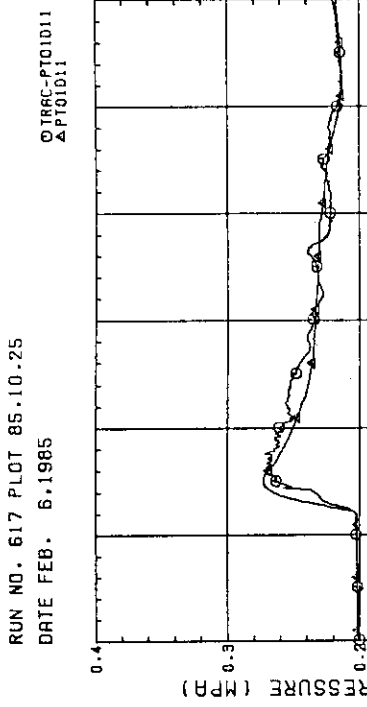


Fig. F-113 PRESSURE (CORE)

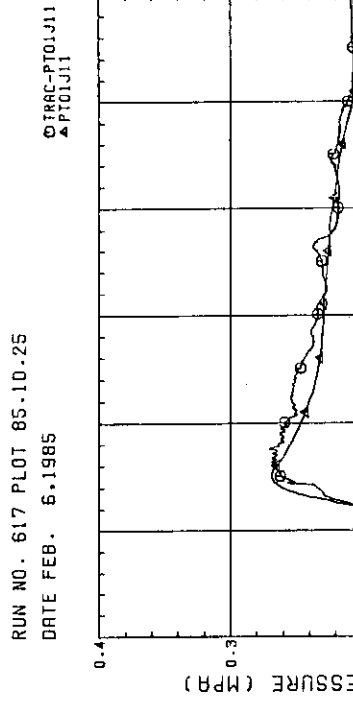


Fig. F-114 PRESSURE (UPPER PLenum)

RUN NO. 617 PLOT 85.10.25  
DATE FEB. 6.1985

© TRAC-PT01A11  
▲ PT01A11

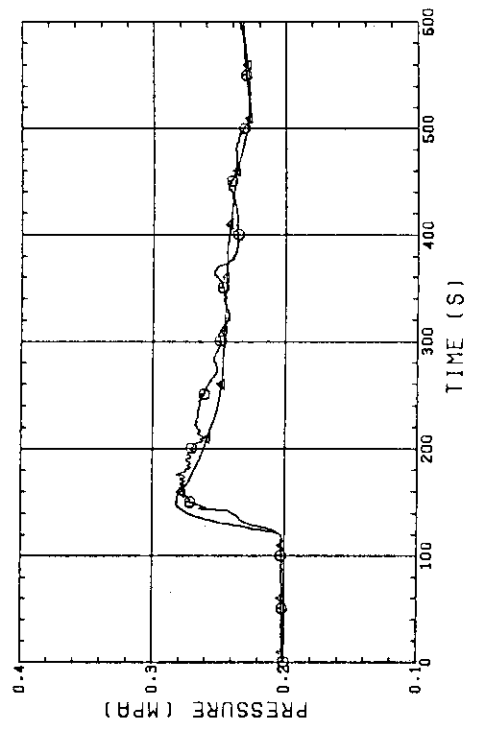


Fig. F-115 PRESSURE (LOWER PLenum)

RUN NO. 617 PLOT 85.10.25  
DATE FEB. 6.1985

© TRAC-PT01P91  
▲ PT01P91

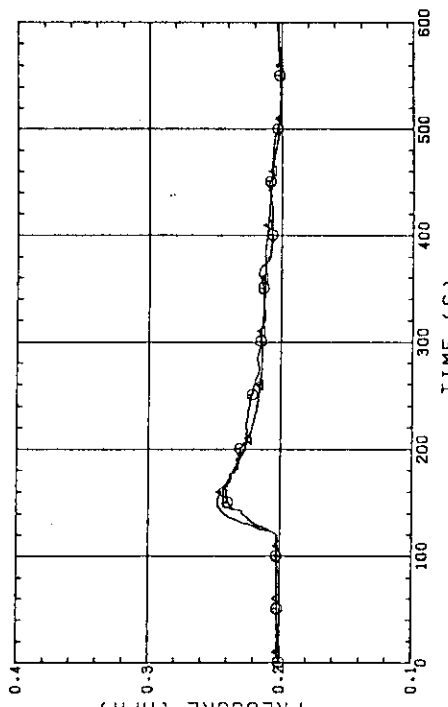
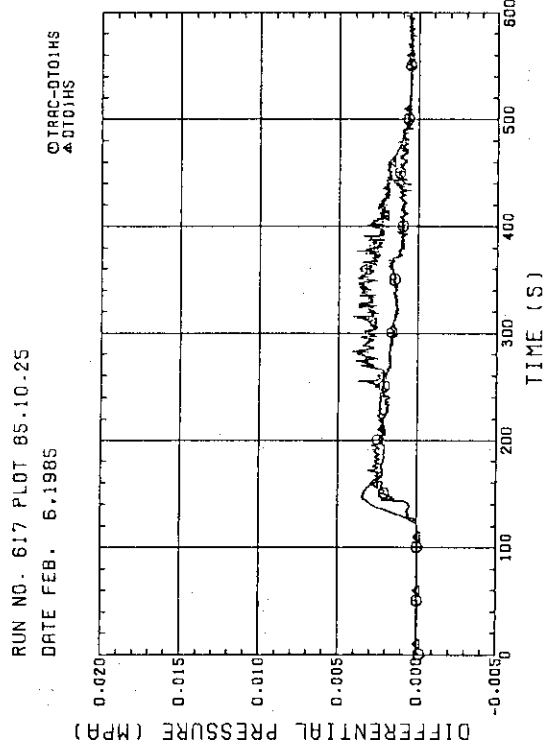
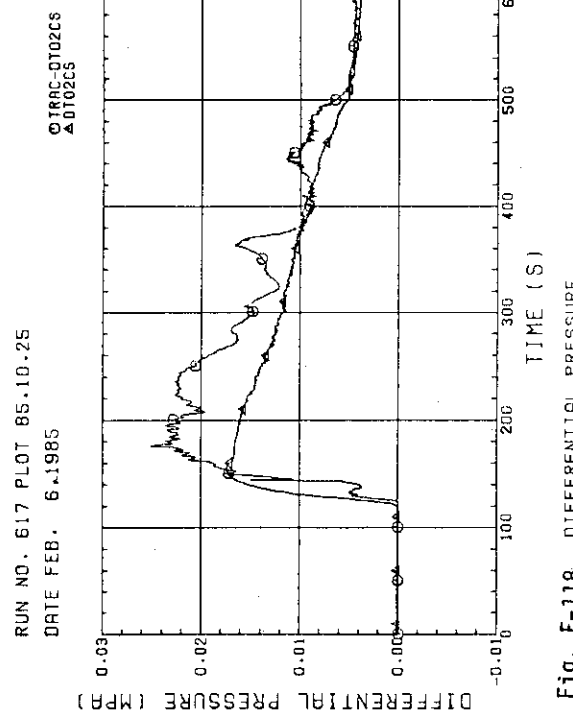
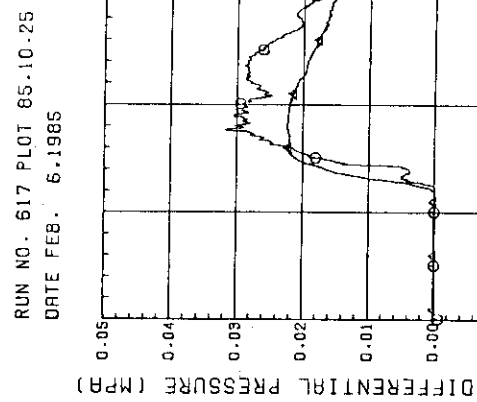
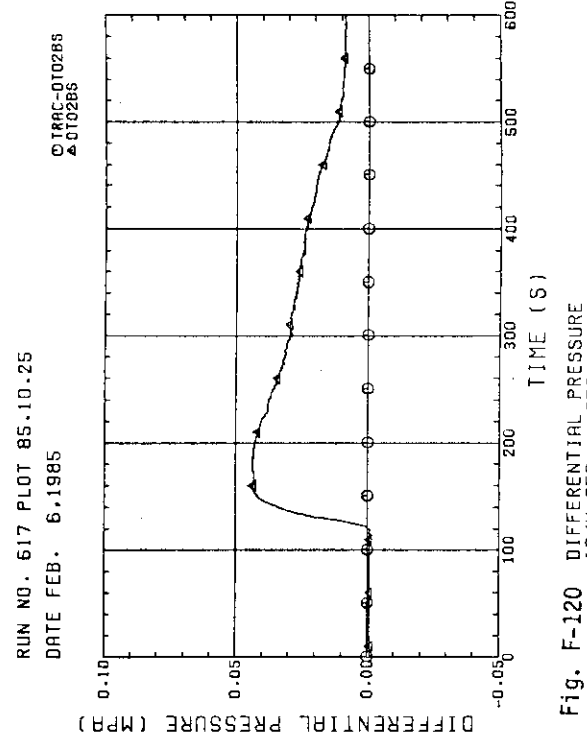


Fig. F-116 PRESSURE (DOWNCOMER)

Fig. F-117 DIFFERENTIAL PRESSURE  
(UP - S/W SEP.)Fig. F-118 DIFFERENTIAL PRESSURE  
(S/W SEP. - DC)Fig. F-119 DIFFERENTIAL PRESSURE  
(DC - CT1)Fig. F-120 DIFFERENTIAL PRESSURE  
(S/W SEP. - CT2)

RUN NO. 617 PLOT 85.10.25  
DATE FEB. 6, 1985

RUN NO. 617 PLOT 85.10.25  
DATE FEB. 6, 1985

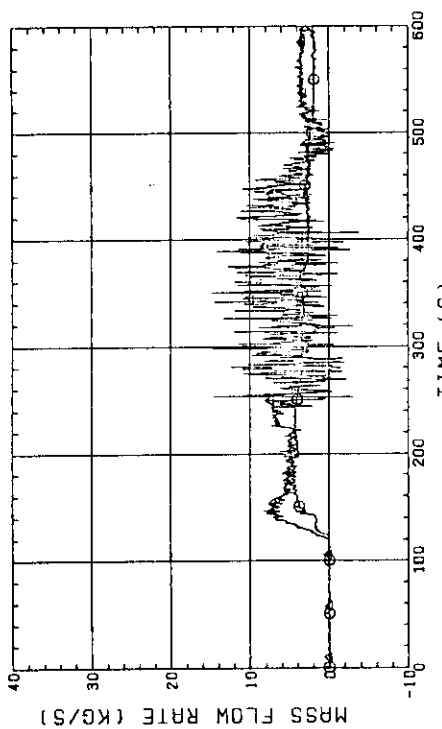


Fig. F-121 MASS FLOW RATE  
(HOT LEG)

RUN NO. 617 PLOT 85.10.25  
DATE FEB. 6, 1985

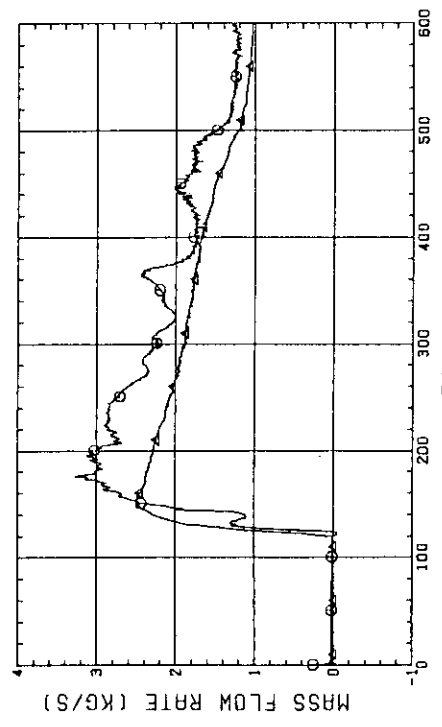


Fig. F-122 MASS FLOW RATE  
(ECC TO S/W)

RUN NO. 617 PLOT 85.10.25  
DATE FEB. 6, 1985

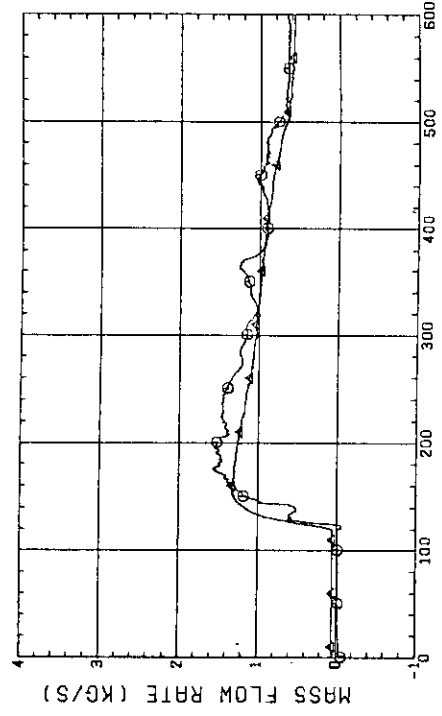


Fig. F-123 MASS FLOW RATE  
(BCL - S/W SIDE)

RUN NO. 617 PLOT 85.10.25  
DATE FEB. 6, 1985

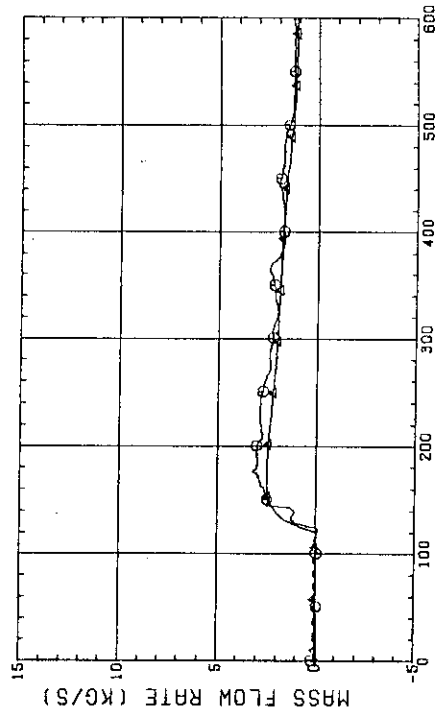


Fig. F-124 MASS FLOW RATE  
(BCL - PV SIDE)

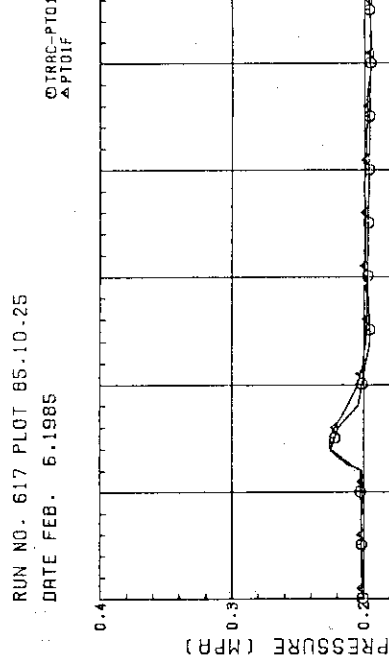


Fig. F-125 PRESSURE (CT1)

RUN NO. 617 PLOT 85.10.25  
DATE FEB. 6.1985  
©TRAC-PT01B  
▲PT01B

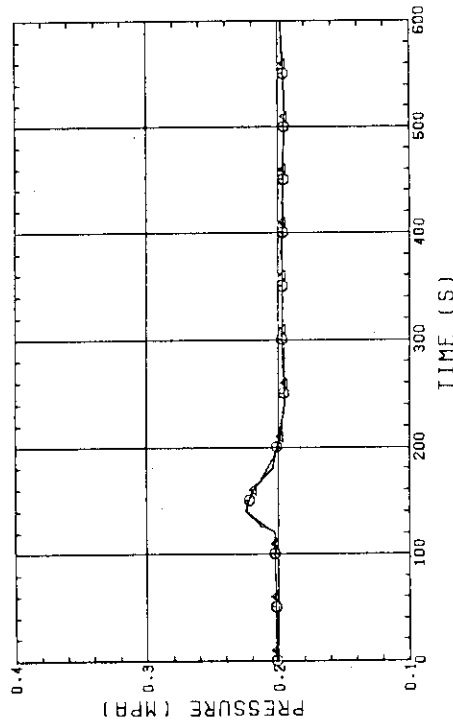


Fig. F-126 PRESSURE (CT2)

RUN NO. 617 PLOT 85.10.25  
DATE FEB. 6.1985  
©TRAC-PT01F  
▲PT01G5

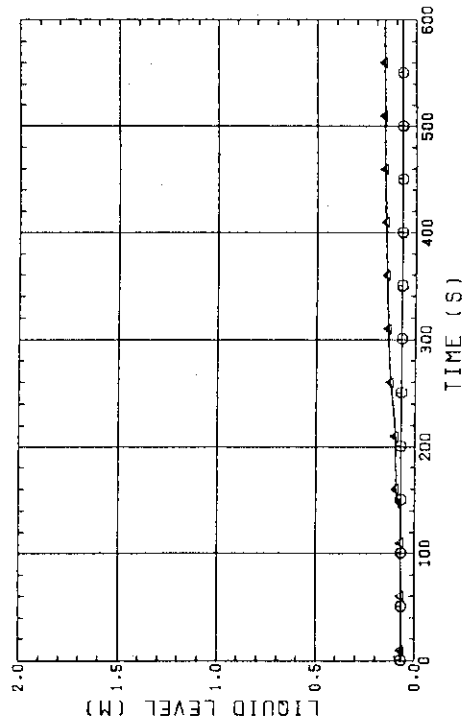


Fig. F-127 LIQUID LEVEL (S/W SEPARATOR)

RUN NO. 617 PLOT 85.10.25  
DATE FEB. 6.1985  
©TRAC-HD04B24  
▲D103022

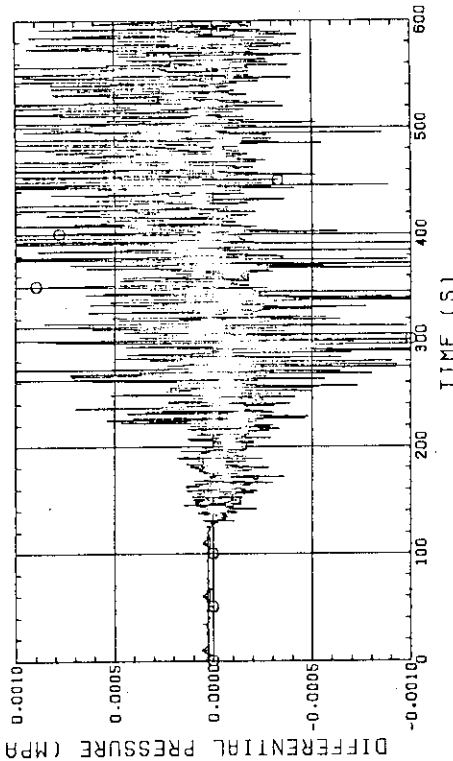
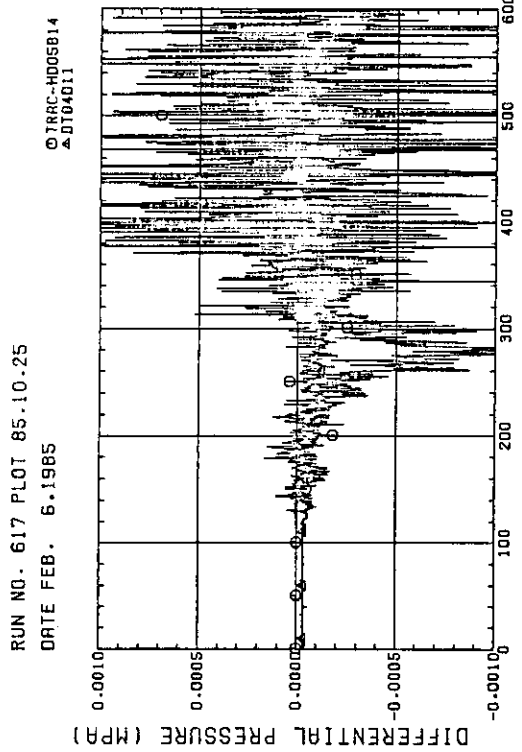
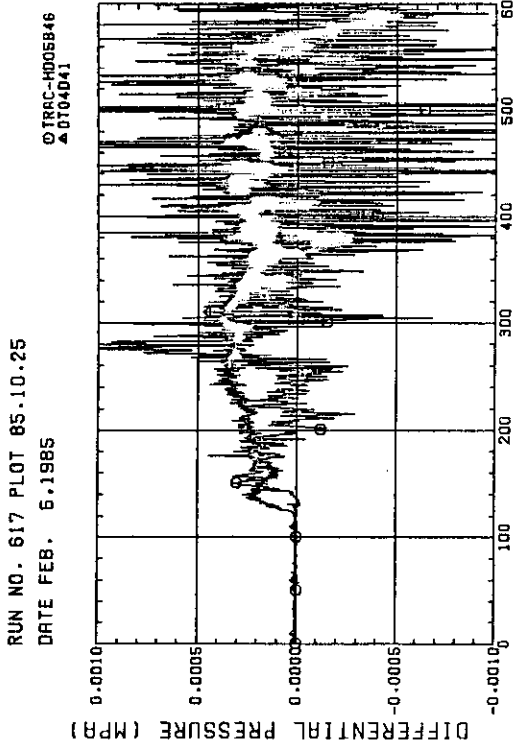
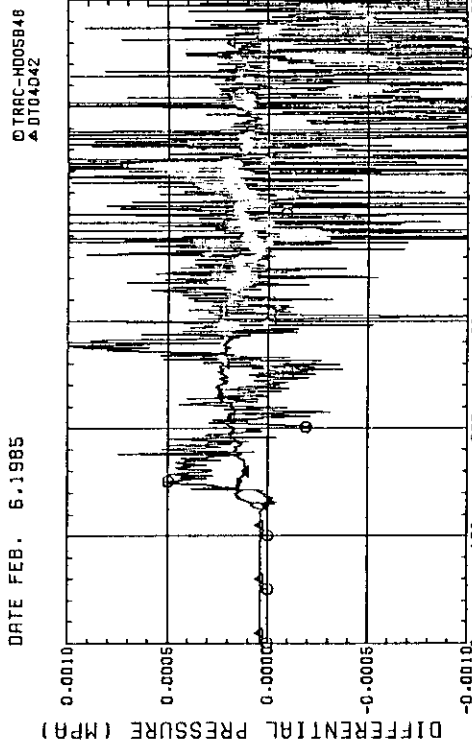
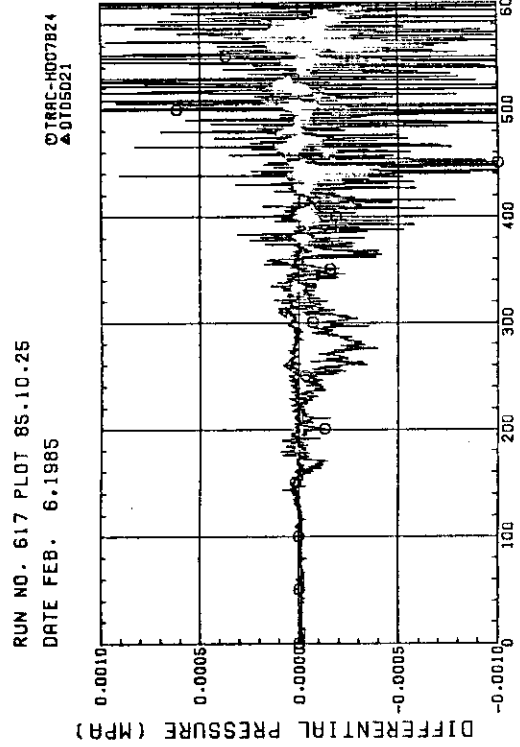


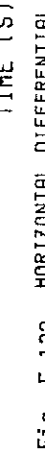
Fig. F-128 HORIZONTAL DIFFERENTIAL PRESSURE (ELEV. 1.365M , BUNDLE 2 - 4)

Fig. F-129 HORIZONTAL DIFFERENTIAL PRESSURE  
(ELEV. 1.905M • BUNDLE 1 - 4)Fig. F-130 HORIZONTAL DIFFERENTIAL PRESSURE  
(ELEV. 1.905M • BUNDLE 4 - 6)

RUN NO. 617 PLOT 85.10.25  
DATE FEB. 6.1985

Fig. F-127 HORIZONTAL DIFFERENTIAL PRESSURE  
(ELEV. 1.905M • BUNDLE 4 - 8)Fig. F-131 HORIZONTAL DIFFERENTIAL PRESSURE  
(ELEV. 1.905M • BUNDLE 4 - 8)

RUN NO. 617 PLOT 85.10.25  
DATE FEB. 6.1985

Fig. F-132 HORIZONTAL DIFFERENTIAL PRESSURE  
(ELEV. 2.57M • BUNDLE 2 - 4)